Studies on the role of the M1 protein in MHV-68 infection of a natural host

Thesis submitted in accordance with the requirements of the University of Liverpool for the degree of Doctor in Philosophy by

Rita Inês Barros da Silva Papoula-Pereira

June 2013

Abstract

Viruses are highly adapted to their evolved hosts and have developed mechanisms to improve their ability to infect them[1, 2] including targeting host chemokines and/or their function[2-4]. When herpesviruses infect animals other than their natural host, the disease outcome is frequently different. Laboratory mouse strains (*Mus musculus*) have not been identified as natural hosts to MHV-68 in the wild[5]. In this study, a natural host to MHV-68, the wood mouse (*Apodemus sylvaticus*)[5], was used to study the infection.

The aim of this study was to ascertain the role of the MHV-68 *M1* gene product in infection, in particular during the pathogenesis elicited by infection. Little is known regarding its function. It is known that M1 is a secreted protein and it is not essential for latency establishment. In laboratory mouse strains, M1 suppresses reactivation from latency[6]. This M1 activity appears to be IFN-γ dependent and results in the activation of $V\beta4^+CD8^+$ T cells[6-8]. Literature suggests that the M1 protein shares functional similarities with the chemokine-binding proteins resulting from the closely related genes, M3 and M4[9].

In order to determine the effect of M1 expression in MHV-68 infection of a natural host, the wood mouse, *in vivo* experiments were performed using vM1stop virus and its genetically repaired counterpart, vM1rev virus. In the wood mouse M1 expression was found not to be essential for latency establishment or lytic replication. M1 expression led to the maintenance of alternatively activated macrophages in the lung and the regulation of cytokine expression by airway, and alveolar epithelial cells and macrophages. M1 expression was seen together with a significant decrease in the mainly pro-inflammatory cytokines TNF-α and MIP1-α, and in the growth factor HGF. Furthermore, M1 expression was associated with significant increase in the expression of the anti-inflammatory cytokine CCSP by Clara cells present in the airways. This cytokine expression profile favours an anti-inflammatory response and could explain the more severe pathogenesis seen in the absence of the M1.

This study demonstrated that the expression of M1 in the BALB/c mouse is much reduced compared to the wood mouse. This indicates that the role of the M1 is more significant in the natural host. There was no increase in IFN-γ expression in the wood mouse infection indicating that the previously described IFN-γ mediated M1 role is unlikely to be present in the wood mouse.

LIST OF CONTENTS

LIST OF FIGURES

List of Tables

Acknowledgements

I would like to thank my supervisors, Prof. Anja Kipar and Prof. James Stewart for their availability, guidance, expertise, support and encouragement and most of all for providing me the opportunity and conditions necessary to do this work.

I would also like to thank Dr. Bernadette Dutia, University of Edinburgh for kindly supplying the vM1stop, vM1rev and LHΔMHV-68 viruses.

During this project I have had the pleasure to work with members of the Department of Medical Microbiology and the Department of Veterinary Pathology of the University of Liverpool and I wish thank all of them for their support and assistance. These include members of the MHV-68 group: Dave, Helen, Elaine, Bahram, Vicky, Bruno and Gail and the staff of the Veterinary Laboratory Services: Val, Marie, Sean, Mark and Adam that performed the histology and immunohistology. Thanks to Sue Jopson and John Waters for their assistance in the animal husbandry, infection and sample collection. I would like to thank Marion Pope for her eternal availability and patience when I was looking for the mysterious virus and her technical expertise in electron microscopy. I would also like to thank my colleagues Dr. Phil Jones and Dr. Eleni Michalopoulou for their support often in detriment of their own wellbeing.

I would like to thank my Liverpool family that kept reminding me where the goal posts were and prevented me from disbelieving it: Dee, Siobhan, Gareth, Giovanni, Alex, Lee, Joana and Sonia.

I owe my deepest gratitude to those that for better or for worse have always stood by me through this period, my family, Mike and Chris and last but not least, my mother, the most beautiful and brave woman in the world, my main source of inspiration, strength and perseverance to whom I dedicate this thesis.

To my father:

"I carry your heart with me (I carry it in my heart)
I am never without it (anywhere I go you go, my dear;
and whatever is done by only me
is your doing, my darling)"
E. E. Cummings

List of abbreviations

ATF: activating transcription factor
APC: antigen presenting cells
BAL: bronchioalveolar lavage
Bcl-2: B cell lymphoma protein
BL: Burkitt's lymphoma
CCSP: Clara cell secretory protein
CCR C-C motif receptor
CK chemokines
CNS: central nervous system
DC: dendritic cells
DNA: deoxyribonucleic acid
ds: double stranded
E: early
EBV: Epstein-Barr virus
EGFR: epidermal growth factor receptor
EM transmission electron microscopy
ERK: extracellular signal-regulated kinase
eNO: endothelial nitric oxide synthase
FADD: Fas receptor associated death domain
FasR: Fas receptor
g: relative centrifugal force (gravity)
GFP: green fluorescent protein
GPCR: G-protein coupled receptor
HE: haematoxylin and eosin
HHV: *Human herpesvirus*
HGF: hepatocyte growth factor
HPAI: high pathogenicity avian influenza
h.p.i.: hours post infection
HRSV: *Human respiratory syncytial virus*
HVS: herpesvirus saimiri
ICAM: intercellular adhesion molecule
IFN: interferon
IFNγ-/-: interferon γ knock out
IFNγR: interferon γ receptor
IFNγR-/-: interferon gamma receptor knock out
ICAM: intracellular adhesion molecule
IE: immediate early
Ig: immunoglobulin
IL: interleukin
IM: Infectious mononucleosis
iNO: inducible nitric oxide synthase
IP-10: IFN-inducible protein 10
IRAK: interleukin-1 receptor-associated kinase
IRF: interferon regulatory factor
IKKε: IκB kinase
Jak: Janus kinase
JNK: c-Jun N-terminal kinase
kb: kilobase

kDa: kiloDalton
KO: knock out
KS: Kaposi's sarcoma
KSHV: Kaposi's sarcoma-associated herpesvirus
L: late
LANA: latency associated nuclear antigen
LMP: latent membrane protein
LPAI: low pathogenicity avian influenza
LPS: lipopolysaccharide
M2: alternatively activated macrophages
MAb: monoclonal antibody
MAPK: mitogen activated protein kinase
MCD: multicentric Castleman's disease
MCF: malignant catarrhal fever
MCP: monocyte chemoattractant protein
MHC: major histocompatibility complex
MHV: murine herpesvirus
MIP: macrophage-inflammatory protein
MEK: MAP kinase kinase
MuHV: *Murid herpesvirus*
NLR: NOD-like receptors
NFκB: nuclear factor kappa-light-chain-enhancer of activated B cells
NO: nitric oxide
ORF: open reading frame
PAb: polyclonal antibody
PAS: Periodic acid Schiff reaction
PEL: primary effusion lymphoma
PFU: plaque forming units
pi: post infection
PKA: protein kinase
PKR: dsRNA activated kinase R
PRR: pattern recognition receptor
p_{53}: tumour protein 53
RANTES: regulated upon activation, normal T cell expressed and secreted
Ras: rat sarcoma protein
RLR: RIG-1 like receptors
RIP: receptor interaction protein
RTA: replication and transcription activator
RTK: receptor tyrosine kinase
RNA: ribonucleic acid
ss: single stranded
STAT: signal transducer and activator of transcription
SCID: severe combined immunodeficiency
SEM: standard error of the mean
TAP: transporter associated with antigen processing
TBK: TANK binding kinase
TGF: transforming growth factor
TEM: transmission electron microscopy
TLR: toll like receptor
TNF: tumour necrosis factor

VCAM: vascular cell adhesion molecule
VEGF: vascular endothelial growth factor
vtRNA: viral transfer RNA
wt: wild type
ZO1: *zona occludens*
-/-: double knock out

1. Introduction

Viruses are non cellular microorganisms which are unable to replicate outside living cells[10]. They are omnipresent on the planet[10, 11]. Some viruses are widespread such as the gammaherpesvirus, Epstein Barr virus (EBV) which infects approximately 90% of the world's population[12]. There is evidence that viruses evolved alongside their hosts and developed mechanisms to improve their ability to infect these[1, 2]. These include the acquisition of genes and genetic functions of host origin, by targeting host chemokines and their function [2-4]. When herpesviruses infect animals other than the natural host, the disease outcome is frequently different. For example, ovine herpesvirus type 2 (OvHV2) and alcelaphine herpes virus 1 (AlHV-1) persist sub-clinically in their natural host, sheep and wildebeest respectively. However, these infections can be fatal when heterologous species such as cattle are infected, leading to malignant catarrhal fever (MCF)[13]. Murid herpesvirus 68 (MHV-68) the virus of interest in this study is most commonly studied in laboratory mouse strains. However, these mice (*Mus musculus*) have not been identified as natural hosts to MHV-68 infection in the wild [5]. In this study, a natural host to MHV-68, the wood mouse (*Apodemus sylvaticus*)[5], was used to study the infection.

MHV-68 is a gammaherpesviruses. Herpesviruses show high sequence conservation[14-17] and consequently share biological properties. These shared properties include viral protein interaction with host cells. Gammaherpesviruses are host specific and include human infecting EBV and Kaposi's sarcoma associated herpesvirus (KSHV)[18]. The host specificity and the fact that these viruses infect humans make infection studies unfeasible. The disease syndromes seen in humans due to EBV and KSHV infection are not fully replicated in the infection of non human primates[19]. In order to investigate gammaherpesvirus pathogenesis it is most adequate to examine these in their natural hosts and the alternatives would be to study herpesvirus saimiri (HVS) or MHV-68 infection[20-26]. MHV-68, unlike other gammaherpesviruses, can be easily replicated *in vitro* and is a natural pathogen of free living rodents[19, 27]. These features make MHV-68 a very useful tool in the study of gammaherpesvirus infection in a natural host[28, 29]. The natural route of infection of MHV-68 is thought to be intranasal which leads to an acute pneumonia[28]. This was the method used to infect the animals in this study.

The aim of this study was to ascertain the role of the MHV-68 *M1* gene product in infection, in particular in the pathogenesis elicited by infection. Little is known regarding its function. It is known that M1 is a secreted protein and it is not essential for

latency establishment. In laboratory mouse strains, M1 suppresses reactivation from latency[6]. This M1 activity appears to be IFN-γ dependent and results in the activation of $V\beta4^+CD8^+$ T cells[6-8]. The recent literature suggests that the M1 protein shares functional similarities with the chemokine-binding proteins resulting from the closely related genes, M3 and M4[9].

In order to bring the study and the methods used into perspective, the present introductory chapter reviews general immune responses to viral infection and the general features of herpesviruses including MHV-68. In the immune responses review, special emphasis is laid on responses seen in the respiratory system as this is the main site where pathological changes are seen following infection with MHV-68. Cytokine secretion will also be discussed as cytokines are suspected to be the main target of the M1 protein.

1.1 The immune system and viral infection

The immune system consists of a complex system of strategies to impede invasion by foreign organisms or proliferation of altered cells and thus avoid disease[30-32]. This system can be divided into innate and adaptive immunity (Figure 1.1). Innate immunity entails those effects which are immediate and do not take into account any previous exposure to the invading pathogen. Components of the innate system include the physical barrier created by cells, complement activation, cytotoxicity by Natural killer (NK) cells and phagocytosis by antigen presenting cells (APC)[31]. Adaptive immunity is employed when the host has been primed previously to the invading pathogen and provides a more specific response mediated by B and T cells[31, 33]. The distinction between the two types of immunity is not clear cut and several components are part of both, such as Toll-like Receptor (TLRs) and Interferon (IFN) signalling[31, 33]. The recognition of pathogens is mostly through TLR present on cellular surfaces. APC prime T cells to the antigens through major histocompatibility complex (MHC) Class II molecules[34]. MHC molecules are cell surface presentation molecules. There are two types of MHC, MHC Class I and MHC Class II. MHC Class I molecules are ubiquitous in cells and class II molecules are expressed mostly by APC cells such as B-cells, monocytes/macrophages and dendritic cells (DC). MHC Class II molecules can also be expressed in non APC cells in the presence of cytokines such as IFN-γ[35, 36]. MHC Class I molecules present antigen to cytotoxic T cells (CTLs)/$CD8^+$ T T-cell[37]. Once

activated, the CD8+ T cells undergo clonal expansion, to generate more cells that can complex with antigen[30, 37]. Interference with MHC presentation disables antigen detection and thus decreases $CD8^+$ T cells activation[38-40]. When $CD8^+$ T cells are activated, they release cytotoxic perforin, and granulysin and the apoptosis inducer, granzyme, all leading to cell death[37]. In MHV-68 infection, expression of K3, a early lytic protein, leads to the ubiquination of MHC class I proteins[40-42] and the transporter associated with antigen processing (TAP)[42, 43] in infected cells. As a result of ubiquination, proteins are degraded through a proteosome-dependent mechanism. K3 also inhibits the expression of endogenous p53 in lytically infected cells[38-40]. HHV-8 expresses K3 similarly to MHV-68, and also K5 which acts on the intercellular adhesion molecules (ICAM) and CD86. In HHV-8, ubiquination of MHC class I results in the diversion of molecules into the Tsg101-endocytic pathway and ultimate lisosomal digestion[38-40]. MHC Class II molecules present processed antigen to helper T-cells/$CD4^+$ T cells. The antigen presented by MHC Class II molecules is mostly exogenous to the cell presenting it and results from phagocytosis by the APC cells[30, 36]. Phagocytosis induces maturation of DC and maturation leads to gradual loss of the phagocytic ability and increases the expression of MHC Class II molecules[44]. With maturation there is also increased expression of cytokines such as those modulating T and B cells[31, 45, 46]. Viruses including MHV-68 inhibit maturation of bone marrow derived immature DC from transgenic mice with BALB/c background[47]. MHV-68 infection of mature DC leads to the establishment of latent infection[47, 48]. With DC maturation, C-C motif receptor 7 (CCR7) expression occurs, which modulates migration of DC to lymph nodes where they present the antigen on their surface and prime naive T cells[49, 50].

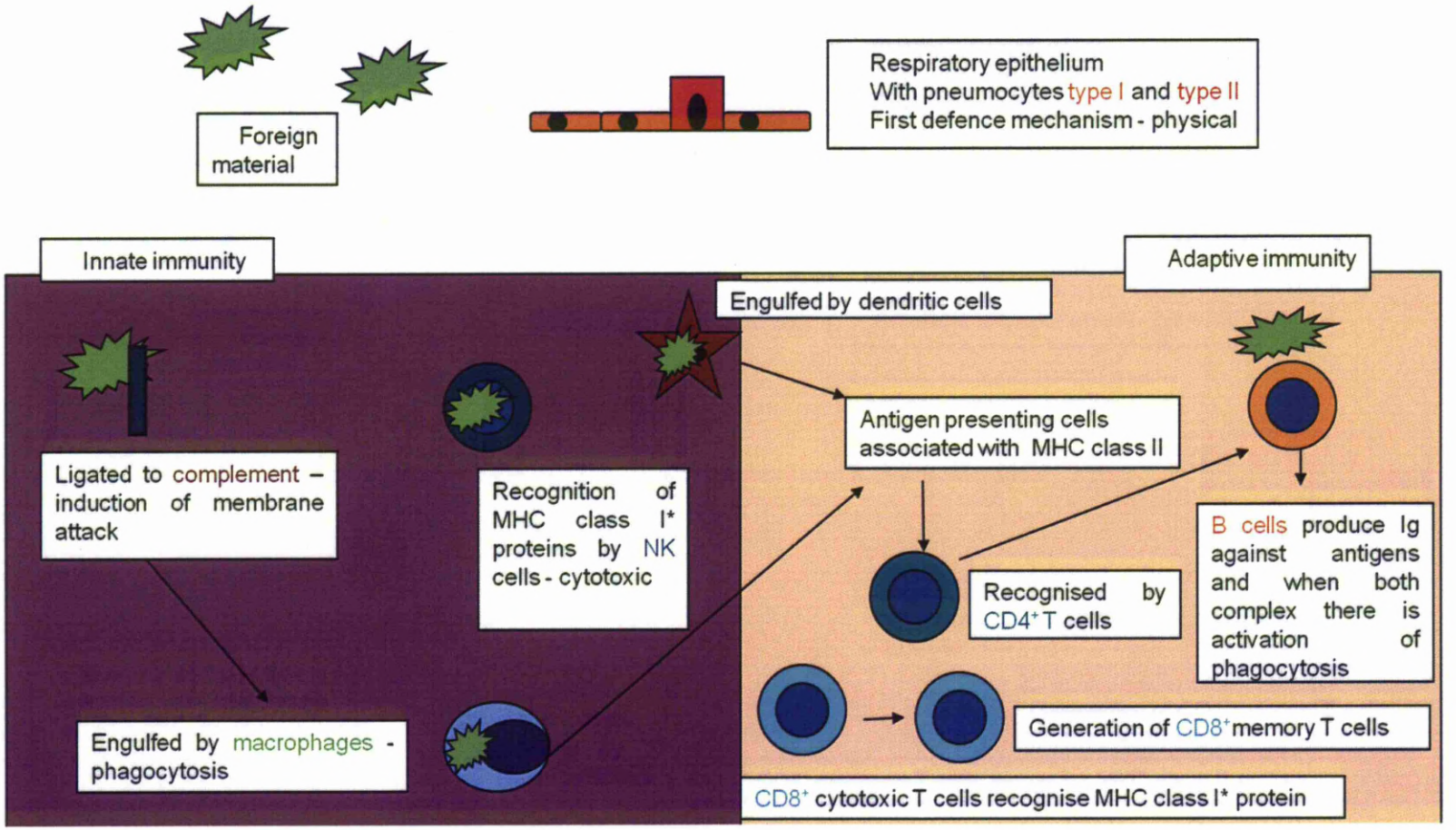

Figure 1.1 Schematic representation of innate and adaptive immunity.
The physical barrier represented is as applies to the lung.

1.1.1 The respiratory tract

1.1.1.1 The airways

The airways are composed of pseudostratified columnar ciliated cells and mucin producing goblet cells, which form a physical barrier against external particles, including viruses[51-54]. The mucociliary escalator is responsible for the removal of almost 90% of inhaled exogenous material and allows the exchange of nutrients, gases and water. Mucus is produced by epithelial goblet cells and subepithelial glands, and is composed mainly of mucins and, to a lesser extent, other substances such as immunoglobulins. Mucus is beneficial for the response against viruses but if present in excess can cause obstruction of the airway. Viruses can target mucin production as a means of entry to the host cell[51-55]

Airway epithelial cells comprised of clara cells and respiratory epithelial cells form a well "knitted", mostly impermeable barrier, due to tight intercellular junctions (tight junctions, adherens junctions, gap junctions and desmosomes)[55]. These junctions function as physical binders and take part in intercellular chemical communication[55]. The physical "wall" they form is of major importance because it hinders viral access to basolateral membrane receptors on the epithelial cells. Cells possess numerous pattern recognition receptors (PRRs). These receptors, upon the detection of pathogens, initiate cellular pathways. Receptors can be present extracellularly or intracellularly and include TLR, NOD-like receptors (NLRs) and RIG-I like receptors (RLRs)[56]. TLRs implicated in viral recognition are the endosome bound TLR3, TLR7, TLR8 and TLR9. They can induce activation of enzymes, such as mitogen-activated protein (MAP) kinases and transcription factors such as NF-κB and interferon regulatory factors 3 and 7 (IRF3 and IRF7). The NF-κB is a cytosolic protein complex which controls DNA transcription. Following TLR activation, epithelial cells respond to viral infection by inducing secretion of substances such as cytokines and chemokines[51]. One of the most potent anti-viral chemokines produced upon TRL activation is Type I Interferon (IFN) [57]. IFN Type I (further described in Section 1.1.2.1) effects include inhibition of viral replication[57-59] and of cellular immunoproteosomes[60]. Secretion of cytokines by airway epithelial cells is generally seen at the basolateral surface, an example being the secretion of MIP1-α and TNF-α in Influenza A infection [55]. The purpose of basolateral secretion is thought to be modulation of inflammatory cell migration into areas adjacent to the airways[55]. *In vivo* work using tracheal tissue from guinea pigs and rats has

determined that cellular migration occurs in the airways within the first 12 to 24 hours and proliferating changes are initiated 15 to 24 hours post stimulus [61].

1.1.1.2 The lung

The lung parenchyma enables the exchange of noxious gases, such as CO_2 present in the host's blood with O_2 present in the atmosphere. Gas exchange takes place in the pulmonary alveoli. Most (~90%) of the alveolar surface is covered by the spindloid-like (flattened and long) pneumocytes type I, responsible for the gas exchange. The remaining space is occupied by the surfactant producing and cuboidal, type II pneumocytes. Once there is an immune challenge, type I and type II pneumocytes can activate PKR, NF-κB pathways and WNT signalling[51] and trigger cytokine cascades leading to migration of inflammatory cells[55]. If the noxious incident induces irreversible cell damage, this results in necrosis/apoptosis. The slender type I pneumocytes are the cell type most susceptible to injury. However there is also targeting of type II pneumocytes by pathogens including viruses. In H5N1 infection of human *ex-vivo* pulmonary cells viral RNA interacts with cellular receptors and secondarily modulates cytokine expression and metabolism in type II pneumocytes[62].

Apoptosis is the ATP-dependent programmed cell death which is induced by caspases, proteolytic enzymes that degrade cellular proteins. Caspase activation can follow the extrinsic pathway through ligand binding to tumour necrosis factor receptor (TNFR) or Fas receptor. Apoptosis can also be induced following the intrinsic pathway by an intracellular effector, such as p53 or members of the Bcl protein family[63]. Bcl-2, Bcl-x_L and Bcl-w exhibit anti-apoptotic potential and the proteins which bind to Bcl-2, Bax, Bak and Bok exhibit pro-apoptotic potential[64, 65]. Morphologically, apoptosis is characterized by individual cell shrinkage, chromatin condensation and nuclear fragmentation. The cellular components are released into cell membrane enclosed vesicles which are phagocytosed, but there is no induction of an inflammatory response[64, 66].

Necrosis is cell death following a chemical or physical injury to the cell. Traditionally it was considered not to be ATP-dependent, but research has found that necrosis can also be a type of programmed cell death with ATP consumption, referred to as necroptosis[67]. Receptor interaction protein (RIP 1) plays a major role in this pathway. Morphologically, necrosis is characterized by organelle swelling and plasma

membrane rupture. The release of cellular components into the environment elicits an inflammatory response, resulting frequently in the death of neighbouring cells. Unlike in apoptosis, protein synthesis still occurs during necrosis. Likely this represents a host response to viruses to signal APC to mount the adequate immune response[68].

Regeneration of the denuded alveolar surface is mainly by proliferation of type II pneumocytes which leads to thickening of the blood-air barrier and partial impairment of gas exchange[62]. As regeneration progresses the type II pneumocytes differentiate into type I pneumocytes. In rats type I pneumocytes have also been shown to possess this proliferative ability[69]. In mice there is evidence for the presence of other stem cells niches in the lung besides type II pneumocytes[70].

1.1.2 Cytokines

Cytokines are inter-cellular signalling molecules and exert functions through binding to specific cellular receptors. The effect of cytokines is varied and includes induction of growth, cellular functions including cytotoxicity, cellular migration or secretion of other cytokines[30, 32, 36, 71]. Viruses evolve alongside their hosts and viruses such as poxviruses and herpesviruses evade the immune system by targeting cytokine effects and influence intracellular signalling by the host[3, 4]. The present evidence is that viruses evolved and introduced secretion of these proteins into their replication process in order to increase their ability to infect and persist in the host[72, 73]. By increasing the migration of the adequate cell type, viruses increase the availability of target cells. By decreasing certain cells types that would identify virally infected cells, viruses evade viral clearance.

1.1.2.1 Chemokines

Chemokines (CKs) are grouped into four classes depending on the N-terminus: CXC (α), CC (β), CX_3C (γ) and C (δ). CKs bind to G-protein coupled receptors (GPCR) on cell surfaces and can modulate leukocyte migration and activation by binding to these receptors[74, 75]. To further increase cellular migration to specific sites, CKs interact with glycosaminoglycans (GAGs) on the endothelium or matrix[76, 77]. The GAG-CK complex acts as an attractant for leukocytes, via receptors complementary to the secreted CK. Furthermore, chemokines produced by perivascular inflammatory cells such as macrophages, can be released into the circulation through transcytosis and

induce migration of intravascular cells to the sites of infection[78]. CKs also induce activation of mitogen activated protein kinases (MAPKs), such as Janus-N-terminal kinase 1 and 2, extracellular signal regulator kinase 1 and 2 (ERK1, ERK2) and p38[79].

The strategies employed by viruses to alter CK action include mimicking CKs or their receptors and binding to the CKs themselves[80]. The aim of viral CK targeting is mainly to modulate migration of immune cells to sites of infection[3, 74, 75, 79]. The MHV-68 *M3* gene, encodes for M3/vCKBP3 which binds to a broad range of chemokines and impairs their function[9, 81]. In the absence of M3 there is an increase in RANTES, MIP-1α, and MIP-3β, all associated with T cell activation. In the wood mouse, M3 drives the B cell dominated inflammatory response and iBALT formation[9]. In MHV-68 infection, B cells are the main cell type where latent replication occurs[28, 82]. Therefore it is of benefit to the virus to increase the availability of B cells which is achieved partly by preventing T cell activation[9]. In HSV-1 and HSV-2 infection, a viral secreted protein, glycoprotein G (gG), has been found to bind to chemokines through their glycosaminoglycan domain. This binding has been shown to increase inflammatory cell migration through GPRC signalling and phosphorylation of MAPKs[79]. KSHV encodes for viral proteins some of which are homologous to cellular proteins in the human host (Table 1.1)[73, 83]. Most of these proteins are produced during lytic replication[84]. KSHV encoded proteins include vMIP1 and vMIP2 which are homologues of human MIP-1 and MIP-2 and are implicated in the establishment of both the sarcoma and lymphoma associated with infection[85]. Also in KSHV, the open reading frame (ORF) 74 encodes for vGPCR, a viral chemokine receptor that has been shown to be associated with the development of the KS and to have an angiogenic potential[86].

ORF	Gene product	Function
K2	vIL-6	Activation of gp130, B cell growth factor and angiogenesis
K6	vCCL1	CCR5 and CCR8 agonist, chemotaxis of Th2 cells and monocytes, angiogenesis
K4	vCCL2	CCR3 and CCR8 agonist, chemotaxis of Th2 cells and monocytes, angiogenesis
K4.1	vCCL3	CCR4 agonist, chemotaxis of Th2 cells, induction of VEGF-A, angiogenesis
K7	vIAP	Inhibition of apoptosis, downregulation of vGPRC expression
ORF 16	vBcl-2	Inhibition of viral and BAX mediated apoptosis
K9	vIRF1	Cellular transformation, inhibition of p300, p53, TGF-β and type I IFN
K11.5	vIRF2	Inhibition of Fas mediated apoptosis, inhibition of type I IFN and NF-κB
K10.6	vIRF3	Inhibition of p53, NF-κB and Fas mediated apoptosis
ORF 74	vGPCR	Transformation, inducer of VEGF secretion

Table 1.1 KSHV encoded proteins sharing homology with human proteins

1.1.2.2 Interferons

Interferon (IFN) synthesis occurs following various signals, primarily Interferon regulatory factors (IRFs) but also nuclear factor kappa-light-chain-enhancer of activated B cells (NF-$_k$B) and activation transcription factor 2 (ATF2). When IFNs are bound to their receptors, the Jak-STAT pathway is initiated which results in the formation of activated STAT1/2-IRF-9 complex that localises in the nucleus[51]. The complex is composed of a receptor, Janus kinase (JAK) and signal transducer and activator of transcription (STAT). This complex regulates gene expression for a variety of genes, including p53 (a pro-apoptotic protein)[87] and antiviral proteins, such as dsRNA-activated kinase R (PKR)[88]. One effect of PKR is protein phosphorylation of translation initiation factor (eIF-2). This impedes mRNA translation of both host and viral genes and thus is of highest importance in anti-viral defence mechanisms[89]. PKR also induces nitric oxide production via a Fas-dependent pathway[90]. HSV-1 virion degradation has been shown to occur following PKR activation. However, this degradation can be blocked by ICP34.5, a HSV-1 viral product[91]. Once signal transduction occurs, the receptor-ligand undergoes endosomal digestion[92].

Type I IFNs include IFN-α and IFN-β. IFN-α can be produced by virus-infected leukocytes and epithelial cells. Type I IFNs are of major relevance in the host anti-viral

response since they induce the host cell to express different proteins which interfere with the viral replication, protein synthesis or trafficking processes [51]. IFN-α and IFN-β have been shown to induce DC mediated differentiation of B cells into plasma cells and clonal expansion of memory T cells[93, 94]. In Influenza A infection, abrogation of type I IFN signalling has been associated with a decreased expression of cytokines[55]. The expression of IFN-α and IFN-β is mainly regulated by IRF3 and IRF7[51]. KSHV LANA proteins have been found to bind to the IFN-β promoter and thus compete with IRF3, resulting in decreased expression of IFN-β[95]. IFN expression is not always of benefit to viral evasion. In human primary airway epithelial cells from patients with chronic obstructive pulmonary disease (COPD), there is an increase in susceptibility to rhinovirus infection despite an increase in IFN expression following infection[96].

IFN-γ is the only known type II interferon and it is mainly produced by activated T, NK, B and dendritic cells as well as monocytes/macrophages. Its secretion can be induced by interleukin (IL)-12 and IL-18 and decreased by IL-4, transforming growth factor-β (TGF-β) and glucocorticoids[92, 97]. The IFN-γ receptor is present on most cells. An important role in the immune response induced by IFN-γ is the induction of the expression of MHC Class I and II molecules[92, 97]. By modulating the synthesis of these molecules IFN-γ plays a fundamental role in the host recognition of viral antigens and the response to these[31]. In MHV-68 infection significant upregulation of IFN-γ secretion is seen in latent infectio [98]. IFN-γ has been identified as key in controlling reactivation[99, 100] through its interaction with ORF50 promoters[101]. ORF 50 encodes for replication and transcription factor (RTA). The IFN-γ effect is cell type specific. IFN-γ treatment of cells harvested from MHV-68 infected mice leads to a decrease in viral reactivation frequency and cytopathic effect in macrophage dominated but not in B cell dominated populations[82]. IFN-γ upregulation in MHV-68 infection has been associated with resistance to secondary infections[98].

1.1.2.3 TNF-α

Tumour necrosis factor α (TNF-α) is a proinflammatory cytokine, known to be a strong inducer of cellular apoptosis[102-105] proliferation and differentiation[106, 107]. TNF-α is mainly produced by macrophages and monocytes. However, TNF-α is also expressed by cells such as $CD8^+$ T cells, microglia, epithelial cells and smooth muscle cells[108]. TNF-α can exist in two forms: either as a membrane bound (mTNF-α) or a soluble form

[109]. TNF-α binds to two cellular receptors: TNFR1/p55 and TNFR2/p75. These receptors are predominantly membrane bound. TNFR1 is present in a wide spectrum of cells whereas TNFR2 is present in lymphocytes, epithelial cells[110] endothelial cells, cardiomyocytes, and some neuronal cells[111]. Endoepithelial cells are epithelial cells dervived from the endoderm and include respiratory epithelial cells. Binding of TNF-α to TNFR1 or TNFR2 activates downstream pathways and/or leads to detachment of the membrane bound receptors into solution[112]. Contrary to what is seen in TNFR1, the TNFR2 family lacks a death domain. TNFR1 activation generally leads to inflammation and apoptosis and this receptor has been shown to be essential in secondary lymphoid follicle formation[113-115]. TNFR2 activation on the other hand, generally leads to cell activation, proliferation, and migration[116, 117]. The downstream pathway activated by TNF-α binding depending also on the strength of the signal and the existing conditions (i.e. the presence of other cytokines, targeted cell types). Binding of mTNF-α will lead mainly to apoptosis and anergy of the surrounding cells. On the other hand, the binding of the soluble form mostly induces cytokine expression. Apoptosis at times, is convenient since programmed cell death enables the host to destroy the inciting intracellular stimulus i.e. virus, alongside the targeted cell whilst necrosis does not. TNF-α induces apoptosis through various mechanisms including activation of the proapoptotic Fas pathway and/or decreasing cellular resistance to Fas-dependent apoptosis[102] or inhibition of Bcl-2[102][. Other TNF-α mediated apoptosis induction mechanisms include, activation of caspase 3 and increased expression of cytokines secreted by macrophages (TNF-α, MIP-1α, MIP-2 and IL-6)[112, 118]. IFN-γ has been reported as potentiating the TNF-α anti-apoptotic effect[102]. Other effects associated with TNF-α include enhancement of pulmonary epithelial cell permeability through the decrease in expression of *zona occludens* (ZO1 - part of the tight junction complex) and/or functional opening of the tight junction barrier[112].

1.1.2.4 TGF-β

TGF-β known functions include chemotaxis of fibroblasts and induction of apoptosis[119]. In the lungs of mice, TGF-β has been reported to promote DNA repair in type II pneumocytes[120] and promote differentiation of progenitor bronchiolar cells[121]. Various cells including fibroblasts, macrophages, regulatory T cells and epithelial cells produce TGF-β.

In MHV-68 infection there is an increase in TGF-β expression by alveolar fibroblasts, alveolar macrophages and latently-infected pneumocytes[122]. In the latently infected pneumocytes, the increase in TGF-β was seen alongside increases in expression of TNF-α and IFN-γ[122]. In MHV-68 infection of aged (15-18 months) mice, fibroblasts showed an increased expression in TGF-β receptors[123]. However, instead of pro-apoptotic potential these cells showed resistance to apoptosis independent of the viral titre[123]. TGF-β mediated resistance to apoptosis in human primary lung fibroblasts has been associated with an increase in plasminogen activator inhibitor 1 (PAI-1)[124]. TGF-β expression in mouse primary bronchiolar-alveolar cell lines (composed mostly of type II pneumocytes and fewer Clara cells) and pulmonary fibroblasts has been reported to be increased by TNF-α[125-127]. This TNF-α induced increase in TGF-β expression was also observed in RAW 624 cells (murine macrophage cell line) co-cultured with A549 cells (human lung adenocarcinoma cell line) and was related to activation of the NF-κB pathway[128]. TGF-β increased expression led to the transformation of A549 cells from epithelial to a mesenchymal phenotype[128].

1.1.2.5 MIP1-α and MIP1-β

MIP-1α (aka CCL3) and MIP1-β (aka CCL4) are highly homologous and bind to CCR5 receptors, existent in T cells, natural killer cells (NK), dendritic cells and monocytes. Similarly, RANTES also binds to CCR5. HIV virus is known to be a ligand for CCR5, thus these three chemokines are important in the impairment of HIV virus replication. MIP-1α and MIP1-β are produced by macrophages, epithelial cells (including pneumocytes), lymphocytes and platelets. They are chemoattractants for monocytes and a vast array of inflammatory cells, including T cells, NK cells and dendritic cells. They have been associated with lymphocytic migration to the nasal mucosa and their expression is particularly significant in the nasal and bronchial epithelium of influenza infected mice. Activation of CCR5 enhances $CD8^+$ T cell responses to tumours, via regulation of T helper cells (T_H)/$CD4^+$T cells[129]. Activation of CCR5 also mediates the egress of thymic regulatory T cells (Treg)[130]. Additionally, MIP1-α binds to CCR3 and CCR1 receptors and MIP1-β binds to CCR8 receptors[131]. T helper 1 (Th1) cells exhibit CCR5 receptors whilst T helper 2 (Th2) cells exhibit CCR3 and CCR8 receptors[132].

MIP1-α is thought to have a more efficient chemoattractant/activating capacity for B and Th1 cells, the latter leading to an increment in IFN-γ. It has also been associated with increased cytotoxicity of $CD8^+$ T cells in mucosal (nasal, vaginal) and immune (serum extracted) murine cells. It has long been implicated in host immune response to viruses in the lung. In equine herpesvirus type 1 (EHV-1) infection of mice with BL/6 background, MIP1-α was found to decrease viral replication, enhance lymphocyte migration and the pneumonia observed. In rabies infection an increase in MIP1-α is seen associated with an increase in dendritic and B cells[133, 134]. This results in a increase in neutralizing antibodies at the site of inoculation, lymph nodes and in the blood and less extensive pathological changes in the brain[133, 134]. In RSV infection, MIP1-α expression by macrophages and $CD8^+$T cells is increased. The impairment of MIP1-α expression in RSV infection, leads to a decrease in T cell recruitment but does not have an effect on NK cell kinetics[135] .

1.1.2.6 Interleukin 10

Interleukin 10 (IL-10) belongs to the IL-10 cytokine family, which is thought to have developed prior to the adaptive immune system response and is related to the IFN family. It is of major importance in epithelial maintenance and its main actions aim at dampening inflammation by inhibiting expression of other pro-inflammatory cytokines and inducing a response towards healing[136]. IL-10 binds to IL-10R1 and IL-10R2. IL-10R1 is mainly present in leucocytes and IL-10R2 in cells from epithelial cell rich tissues[137]. It is one of the main cytokines produced by B cells, Th2 lymphocytes and alternatively activated macrophages and one of its effects is suppression of Th1 cytokine expression[138]. Upon TGF-β and IL-6 presence, IL-10 expression in Treg cells (Th17) is induced via extracellular signal-regulated kinases (ERK) activation and the transcription factor, cMAF[139]. The MAPK/ERK pathway is a cell membrane-nucleus communication system. It is activated upon surface receptor binding. This is followed by sequential phosphorylation of cellular proteins and ultimately affects DNA by for example regulation of protein secretion. ERK activation of IL-10 expression occurs to lesser extent in Th1 cells alongside IFN-γ production. The expression of IL-10 in Th1 cells is probably a self-regulating process which acts to decrease the inflammatory changes induced by the other pro-inflammatory cytokines produced by these cells[138, 140].

1.1.3 Nitric oxide

Nitric oxide (NO) is an endogenous nitrogen-based free radical. NO is cytotoxic and cytostatic via its interaction with oxygen radicals. NO is the product of nitric oxide synthase (NOS). There are three main types of NOS, namely iNOS (inducible), nNOS (neuronal) and eNOS (endothelial). iNOS is not expressed in cells under normal physiological conditions, but only when there is an inflammatory stimulus[141]. Whereas nNOS and eNOS are constitutively expressed. iNOS and nNOS are both present in soluble forms whilst eNOS is membrane bound. Furthermore, these enzymes differ in their function, eNOS and nNOS function is dependent on Ca^{2+} concentrations and is intermittent, whilst iNOS function is Ca^{2+} independent and persistently active[141] once the enzyme is expressed. iNOS is known to be expressed in macrophages, dendritic cells, endothelial cells, epithelial cells and neutrophils[142]. CBA/J mice infected intranasally with HSV-1 developed severe pneumonia. However, when these mice were treated with NG-monomethyl-l-arginine, a NOS inhibitor, the severity of the pneumonia was very much decreased. This decrease in severity of pathological changes in the presence of NOS inhibitor occurred despite the viral titres being 17 times higher in lung tissue. These findings indicate that the severe pneumonia seen with HSV-1 infection was not a direct effect of the virus but of NO produced as a result of the viral infection [143]. The induction of NOS is thought to be by PKR, which is activated by the virus intermediate replication stage of dsRNA[144].

There are two pathways of macrophage activation, classical and alternative. Classical activation of macrophages (M1) occurs mostly upon stimulation by Th1 cytokines (mainly IFN-γ, IL-6, IL-12 and TNF-α)[145, 146]. M1 express iNOS which converts arginine into NO. On the contrary, alternative activation of macrophages (M2) occurs mostly upon stimulation by Th2 CKs (mainly IL-13 and IL-4)[145, 146]. M2 express arginase which also uses arginine as a substrate and converts it into urea and ornithidine. Urea and ornithidine will produce polyamines and proline which induce proliferation and collagen production respectively. The CKs produced by M1 macrophages inhibit M2 macrophage proliferation, and vice versa, by blocking the specific arginine metabolism at the translational level[145-148].

Migration of macrophages to affected tissues occurs generally within the first 24 hours of the intitial incident[146].

1.1.4 Summary of signalling pathways

A summary of the main cellular pathways referred to throughout this thesis is represented in Figure 1.2.

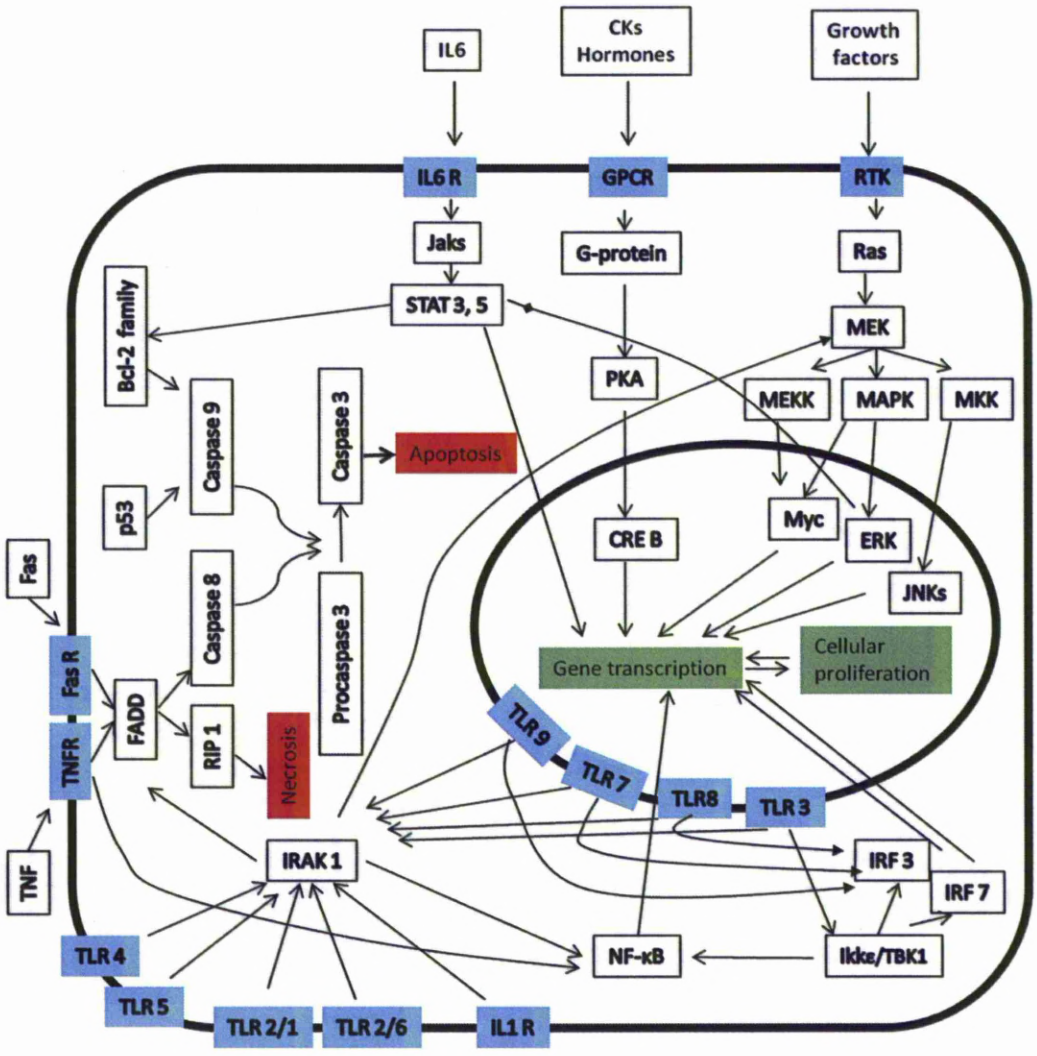

Figure 1.2 Schematic representation of cellular signalling pathways referred to throughout this thesis.

Signalling pathways are extremely complex and in this representation, for purpose of clarity, not all effects are shown. Abbreviations: ERK - extracellular signal-regulated kinase; FasR - Fas receptor; FADD - Fas receptor associated death domain; IL-6 - interleukin-6; JNK mediators and/ - c-Jun N-terminal kinase; MAPK - mitogen-activated protein kinases; RIP1 - receptor interaction protein; TNFα, tumour necrosis factor a; TNF-R - tumour necrosis factor receptor; IL1R – interleukin 1receptor; TLR: Toll like receptor; IRAK: interleukin-1 receptor-associated kinase 4; p53 - tumour protein 53; Bcl-2 – B cell lymphoma protein; STAT - signal transducer and activator of transcription Jak –Janus kinase; PKA – protein kinase A; RTK – receptor tyrosine kinase; GPCR - G-protein coupled receptors; CK – Chemokines; Ras – rat sarcoma protein; MAPK - microtubule-associated protein kinase; MKK – a.k.a. MAP3K, MAP kinase kinase kinase; IRF - Interferon regulatory factors; IKKε - IκB kinase; TBK – TANK binding kinase

1.2 Herpesviruses

1.2.1 Taxonomy

Since 1966, the taxonomy of viruses has been established by the International Committee on Taxonomy of Viruses (ICTV)[11]. Viruses are classified by the use of the hierarchical levels of Order, Family, Subfamily, Genus, and Species[11]. These divisions are made based predominantly on the morphology of viruses[149] and thus indicate their evolutionary relationships. The Herpesvirales order includes three families: the Herpesviridae, the Alloherpesviridae and the Malacoherpesviridae (Table 1.2)[150]. The current nomenclature uses the family or subfamily of the host that the virus infects and the order it was found in such family or subfamily. Sequence homology between the different families of viruses consists of a common gene, encoding a putative ATPase subunit of a DNA-packaging terminase[11, 151, 152].

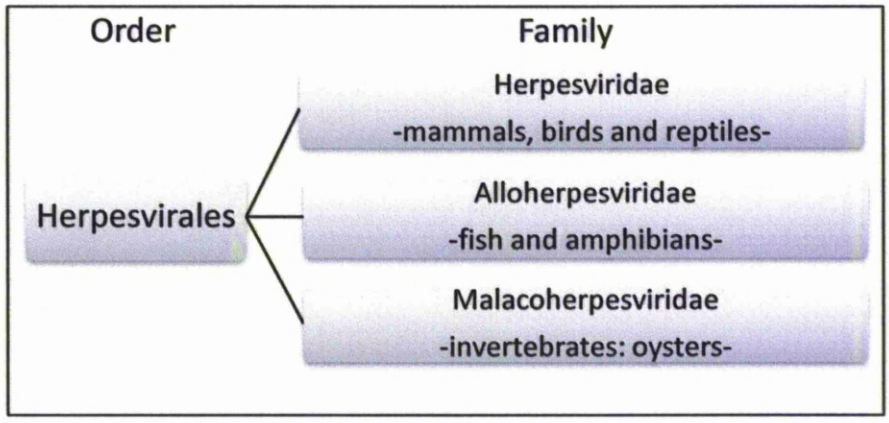

Table 1.2 Taxons of the *Herpesvirales* order and their host range [150].

1.2.2 The *Herpesviridae* family

Herpesviridae infect a broad spectrum of species including mammals, birds and reptiles. Members of the Herpesviridae family show a high degree of sequence conservation[14-17]. Even when sequence conservation is not present it has been found that there is often conservation of viral protein interaction and/or their role in the different viral species[153]. Viruses within the Herpesviridae family share the same basic morphology and structures: genome, nucleocapsid, tegument and envelope[16, 149, 150]. The genome consists of double stranded DNA (dsDNA) and is 120 to 230 kilobases in size [154]. It encodes 70 to 170 open reading frames, this being for most enzymes and genes

needed for viral replication and viral evasion of the immune system[154]. The structure of the genome in herpesviruses allows the division of these into six groups based on the presence and location of repeat sequences (Table 1.3). The capsid is icosahedral and is composed of 162 capsomers enclosing the genome[154]. It integrates four structural proteins: the major capsid protein, triplex-1 protein, triplex-2 protein and a small capsid protein[155]. The tegument is a layer of proteinaceous material surrounding the capsid. MHV-68 is the virus of interest in this study and will be further discussed ahead. The tegument in MHV-68 has unique features when compared to the other herpesviruses. In MHV-68, the tegument consists of an outer layer that does not completely encircle the inner layer (Figure 1.3)[156]. This feature enables contact between the inner layer and the envelope[156]. The morphology of the outer layer could account for the different morphologies of virions encountered [156]. The envelope in herpesviruses is the outermost layer and forms a lipid bilayer made up of viral encoded glycoprotein spikes and host-cell derived lipids[16, 149, 150]. The glycoprotein spikes are involved in multiple functions including virus attachment, fusion and entry. The tegument and envelope protect the DNA from nucleolytic or chemical attack by the host[16, 149, 150, 155]. *Herpesviridae* share biological properties such as the ability to remain latent in the host cell, this can occur when viral DNA covalently ligates to the host DNA and is maintained as episomal DNA [157]. The virus, whilst incorporated into the host DNA, utilises the hosts cellular machinery for its own replication[157]. In latent replication only a subset of the viral genome is expressed[16, 149]. Latency allows virus survival in successively dividing cells whilst maintaining its ability to fully replicate upon reactivation[4, 149, 150]. Full replication with production of infectious virions results in cell lysis[16, 149]. Viruses in this family have a very narrow host range and in the case of the mammal infecting gammaherpesvirus, are thought to have developed in parallel with their host[18]. These viruses are highly adapted to their host and generally only exert mild pathological changes except in the very young, foetuses, immunosuppressed or aberrant hosts[150]. Some of these viruses are widespread such as the Epstein Barr virus (EBV) which infects approximately 90% of the human population[12].

The herpesvirus family is further classified into four subfamilies, alpha, beta, gamma (Table 1.3) and one unassigned species[150]. Disease expression amongst subfamilies is highly variable, mainly due to the different cell specificity and replication rates of these viruses[2].

Group	Terminal repeat sequences	Example
A	Identical terminal repeats at either end of genome	EHV-2
B	Terminal repeats that repeat several times within the genome	MHV-68
C	Terminal repeats that repeat several times and additional internal repeat sequences throughout genome	EBV
D	Terminal repeat which is inverted and repeated within the genome	VZV
E	Terminal repeats are inverted and positioned adjacently on either end	HSV
F	No terminal repeats	TSHV

Table 1.3 Herpesvirus group divisions based on the presence and location of genomic terminal repeats.

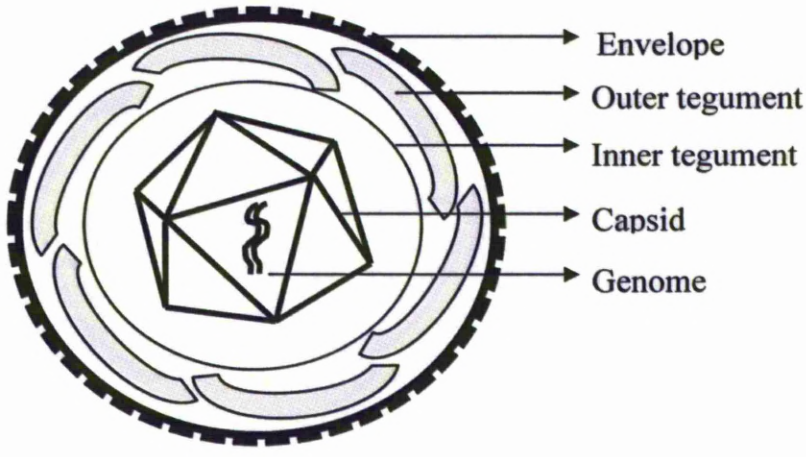

Figure 1.3 Schematic representation of the MHV-68 virion.

Alphaherpesvirinae	Betaherpesvirinae	Gammaherpesvirirnae
• Iltovirus •Gallid herpesvirus 1 •Psittacid herpesvirus 1 • Mardivirus •Columbid herpesvirus 1 •Gallid herpesvirus 2 •Gallid herpesvirus 3 •Meleagrid herpesvirus 1 • Simplexvirus •Ateline herpesvirus 1 •Bovine herpesvirus 2 •Cercopithecine herpesvirus 2 •Human herpesvirus 1 (HSV-1) •Human herpesvirus 2 (HSV-2) •Macacine herpesvirus 1 •Macropolid herpesvirus 1 •Macropolid herpesvirus 2 •Papiine herpesvirus 2 •Saimiriine herpesvirus 1 • Varicellovirus •Bovine herpesvirus 1 •Bovine herpesvirus 5 •Bubaline herpesvirus 1 •Canid herpesvirus 1 •Caprine herpesvirus 1 •Cercopithecine herpesvirus 9 •Cervid herpesvirus 1 •Cervid herpesvirus 2 •Equid herpesvirus 1 •Equid herpesvirus 3 •Equid herpesvirus 4 •Equid herpesvirus 8 •Equid herpesvirus 9 •Felid herpesvirus 1 •Human herpesvirus 3 •Phocid herpesvirus 1 •Suid herpesvirus 1 • Unassigned •Chelonid herpesvirus 5 •Chelonid herpesvirus 5	•Cytomegalovirus •Cercopithecine herpesvirus 5 •Human herpesvirus 5 (CMV) •Macacine herpesvirus 3 •Panine herpesvirus 2 •Muromegalovirus •Murid herpesvirus 1 •Murid herpesvirus 2 •Proboscivirus •Elephantid herpesvirus 1 •Roseolovirus •Human herpesvirus 6 •Human herpesvirus 7 •Unassigned •Caviid herpesvirus 2 •Suid herpesvirus 1 •Tupaiid herpesvirus 1	• Lymphocryptovirus •Callitrichine herpesvirus 3 •Cercopithecine herpesvirus 14 •Gorilline herpesvirus 1 •Human herpesvirus 4 (EBV) •Macacine herpesvirus 4 •Panine herpesvirus 1 •Papiine herpesvirus 1 •Pongine herpesvirus 2 • Macavirus •Acelaphine herpesvirus 1 •Acelaphine herpesvirus 2 •Bovine herpesvirus 6 •Caprine herpesvirus 2 •Hippotragine herpesvirus 1 •Ovine herpesvirus 2 •Suid herpesvirus 3 •Suid herpesvirus 4 •Suid herpesvirus 5 • Percavirus •Equid herpesvirus 2 •Equid herpesvirus 5 •Mustelid herpesvirus 1 • Rhadinovirus •Ateline herpesvirus 2 •Ateline herpesvirus 3 •Bovine herpesvirus 4 •Human herpesvirus 8 (KSHV) •Macacine herpesvirus 5 •**Murid herpesvirus 4 (MHV-68)** •Saimiriine herpesvirus 2 • Unassigned •Equid herpesvirus 7 •Phocid herpesvirus 2 •Sanguinine herpesvirus 1

Table 1.4 Herpesviridae sub-families with respective genuses and species[150].
Species acronyms are occasionally shown in brackets. MHV-68, the virus of interest in this study, is highlighted in bold.

1.2.2.1 Alphaherpesviruses

Alphaherpesviruses have the widest host range of animal species and cell types of the Herpesviridae family[150]. The hosts include humans, various ungulate and avian species, seals and turtles. Alphaherpesviruses are characterized by a short replication cycle, between 16 and 18 h[4], which leads to early cell death and high infectivity[158]. The target host cells are mostly nerves and the spread of the virus infection occurs via intraxonal transmission[4]. Latency is established predominantly in sensory ganglia[149, 159, 160]. Herpes simplex-1 (HSV-1), HSV-2 and Varicella-Zoster virus (VZV) are examples of this subfamily.

1.2.2.2 Betaherpesvirus

Betaherpesviruses are more host specific than alphaherpesviruses[150] but are still capable of infecting a variety of cell types[4]. They are characterized by a longer replication cycle than alphaherpesvirus. CMV replication usually takes between 48 and 72 hours[4]. This longer replication time leads to cell death later than in alphaherpesviruses, being several days post-infection[159-161]. Latency can be established in various tissues, including secretory glands, lymphoreticular tissues and kidneys[16, 149]. Similarly to gammaherpesviruses, reactivation occurs when immunosuppression is present[16]. Cytomegalovirus (CMV) and Human Herpes virus- 6 (HHV-6) are examples of this sub-family[15-17].

1.2.2.3 Gammaherpesvirus

Gammaherpesviruses are the most host specific of all the three sub-families and are subdivided into four genera. These genera include: the γ1-herpesviruses (lymphocryptoviruses), which affects only primates and the γ2-herpesviruses (rhadinoviruses) which are known to have a wider host range of mammal species[18]. The *Macavirus* and *Percavirus* (artiodactyls, perissodactil and carnivore viruses) exhibit an internal structure which resembles the *lymhocriptovirus* clade[162]. MHV-68, the virus of interest in this study belongs to the γ2-herpesviruses subfamily. Despite rodent and primate γ2-gammaherpesvirus being thought to have diverged in evolutionary terms approximately 60 million years ago[163] sequence homology is quite considerable. MHV-68 genome possesses 80 open reading frames (ORFs) and these are often homologous with those of other gammaherpesvirus such as KSHV, EBV and Herpesvirus Saimiiri

(HVS) (Figure 1.4). Homologous genes most frequently encode for factors related to viral replication or structural components of the virion particle[2, 163]. Non homologous genes normally are related to latency establishment and/or transformation of infected cells[163]. MHV-68 exhibits genes unique to its sequence in the left end of the genome consisting of eight vtRNA-like genes and M1 to M11 genes[164]. M1 gene is the gene of interest in this thesis. Unlike other gammaherpesviruses, MHV-68 can be easily replicated *in vitro* thus facilitating research into its function[25, 26].

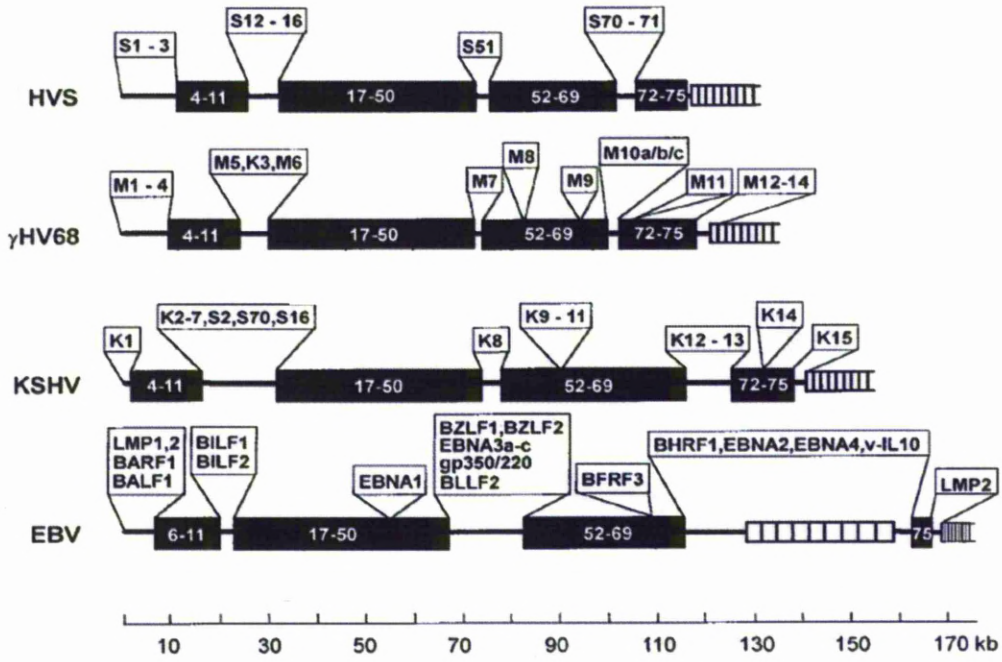

Figure 1.4 Alignment of HVS, MHV-68, KSHV and EBV genomes
Taken from[163].
In the HVS genome, attribution of ORF numbers is based on their sequential position. In the remaining genomes attribution of ORF numbers is based on collinear and nucleotide/functional homology of these and the HVS genome. Conserved sequences are shown in black boxes. Unique genes are shown in the white boxes and in this figure MHV-68 is represented by γHV68.

Gammaherpesviruses are characterized by an initial lytic phase of high replication. This is followed, in immunocompetent animals, by a latent phase of continuous and low level replication mainly in lymphoid tissue[159, 160, 165]. In latency there is tethering of the viral genome to the hosts chromosome, with only a subset of genes being transcribed. During latency intermittent reactivation with low level lytic replication also occurs. In the presence of an immunosuppression episode, lytic

replication is reinitiated[15-17, 159, 160]. It is not fully understood why some cells enter latency rather than the lytic cycle but it is suspected to be due to failure in the expression of immediate early transcribed (IE) genes[166]. In MHV-68, ORF 73 is an IE gene essential to reactivation but not to lytic replication. ORF 73 encodes for latency associated nuclear antigen (LANA) which is involved in viral episome maintenance during latent replication in MHV-68, HVS and KSHV. In KSHV and MHV-68 LANA proteins bind to viral genome terminal repeats, tethering the viral genome to the host mitotic chromosomes, enabling viral persistence in daughter cells[167-170]. LANA proteins also inhibit the activation and propagation of cellular tumour-suppressing protein, p53[171]. p53 is a DNA-binding protein that regulates DNA transcription of various genes[172]. Normally, in the presence of DNA errors p53 expression is increased and can induce either cellular repair or apoptosis[172]. In herpesvirus infections such as VZV and MHV-68 infection, p53 enhances viral lytic gene expression instead of being a cellular regulator[173]. The presence of LANA proteins and their inhibitory effect on p53, decreases cellular injury and enables latent virus maintenance[171]. LANA proteins also target pRb, oncogenic β-catenin and c-Myc pathways as alternative ways of promoting the survival of infected cells[174-178]. In order to halt viral lytic transcription, LANA proteins inhibit the transcription of RTA[179]. RTA is encoded by ORF 50 and induces lytic replication [180, 181]. Contrary to LANA, RTA does not exert a negative effect on LANA expression and instead binds to the ORF 73 promoter and induces LANA expression[182]. RTA induces expression of different genes by binding to their promoter, M3 in MHV-68 being one of these[183]. RTA location in the viral genome and its function as viral lytic replication inducer is common between gammaherpesviruses[163, 184]. In EBV infection besides RTA as a viral transactivators, there is also ZTA. In EBV lytic replication the reactivation process results from the interaction between RTA and ZTA[185-189].

1.2.2.3.1 Gammaherpesvirus and oncogenesis

Some gammaherpesviruses are associated with oncogenic transformation and lymphoid cells are the main cell types to show such change[18, 159, 160, 165, 190, 191].

Oncogenic transformation of B cells has been seen associated with EBV infection and occurs both *in vitro* and *in vivo*. Infected humans develop in a small percentage of cases, Burkitt's lymphoma[160]. The oncogenic potential in EBV infection, has been

related in part to Epstein Barr nuclear antigen 1(EBNA1) which binds to the latency associated origin of replication, oriP[18]. EBV has also been associated with carcinomas such as nasopharyngeal carcinoma[192].

KSHV infection of immunosupressed human patients has been associated with Kaposi's sarcoma (KS), primary effusion lymphoma (PEL) and multicentric Castleman's disease (MCD)[193]. KS is a spindle cell neoplasm with significant neoangiogenesis as a feature. KS can present in four different clinical forms, classic, endemic, latrogenic or AIDS associated. In the case of classic KS, it occurs most frequently in elderly men from Mediterranean and Eastern European countries. The endemic form is mostly seen in African children. This suggests that a genetic predisposition or local infectious agent increases the likelihood of developing KS[84]. In PEL, the neoplastic cells are B cells exhibiting the cluster of differentiation 30 (CD30) and CD138 indicating that expansion of these cells occurred at a late stage of cellular differentiation[86, 194-198]. MCD is characterised by a multicentric lymphoid and vascular proliferation mostly in germinal centres of lymphoid tissue[84]. In KSHV, the gene product of K13, vFLIP has been linked to apoptosis resistance in B cells. Resistance to apoptosis often predisposes to uncontrolled cell growth and likely contributes to the lymphoproliferative disorder. This resistance to apoptosis was indicated as being through enhanced expression of RelB, a subunit of NF-κB. vFLIP also led to inhibition of c-Myc and p27 rise following blockage of anti-IgM. C-Myc and p27, are known growth arrest and apoptosis inducers[199].

HVS infects New World primates and leads to T cell proliferation[200] that can be occasionally fatal[201]. Oncogenic potential has been related in part to HVS tyrosine kinase-interacting protein (Tip) both *in vitro* and *in vivo*. Evidence suggests Tip induced transformation of T-cell is through Tip activity on signal transducer and activator of transcription 6 interleukin 4 induced (STAT6)[202]. STAT 6 is an inducer of Th2 cell polarization[203, 204].

1.2.2.3.2 Gammaherpesvirus and pulmonary fibrosis

Idiopathic pulmonary fibrosis (IPF) is a condition seen in humans and is characterized by progressive and irreversible interstitial fibrosis in the lung. IPF is frequently accompanied by arterial hypertension due to thickening of arterial walls[205-207]. The aetiology of IPF has not fully been determined but herpesviruses, in particular

EBV to lesser extent KSHV and the betaherpesvirus HHV-7 and HHV-5 are often detected in the lungs of IPF patients[208-210]. Equine nodular fibrosis is a uncommon entity described in horses which features extensive interstitial fibrosis in a nodular to coalescing pattern. There have been several reports associating equid herpesvirus 5 (EHV-5) with equine nodular fibrosis[211, 212]. MHV-68 infection has been used as a laboratory model to study pathogenesis of IPF since similar lesions are observed in the chronic infection of CD1[208] or IFNγR$^{-/-}$ mice[209, 210]. In human patients with IPF and MHV-68 infected CD1 and IFNγR$^{-/-}$ mice with evident interstitial fibrosis, there is an increase in the expression of the pro-fibrotic cytokine, TGF-β[208, 210, 213]. When IFNγR$^{-/-}$ mice were infected with a MHV-68 virus expressing a mutant dominant inhibitor of the NFκB signaling pathway, in latent infection there was a decrease in viral load and absence of vasculitis and fibrosis. This was seen together with a decrease in the expression of integrin αvβ6, a transmembrane receptor associated with TGF-β activation and decrease in the expression of arginase, an enzyme used as a marker for alternative activation of macrophages[210]. Alternative activation of macrophages with no change to classical activation of macrophage was also related to splenic fibrosis in the chronic MHV-68 infection of IFN-γ R$^{-/-}$ mice[209]. Alternative activation of macrophages occurs mainly upon stimulation by Th2 CKs[145, 146]. Additionally in MHV-68 infection of IFN-γ R$^{-/-}$ mice if CD4^{+} T cells and CD8^{+} T cells are extracted prior to infection, there is no onset of the fibrosis, indicating the role of these cells in the induction of fibrosis[214-216].

1.2.2.3.3 Gammaherpesvirus and neurotropism

Gammaherpesviruses are generally lymphotropic but viruses such as EBV and KSHV have been detected in the brains of both asymptomatic and immunosuppressed humans[217-225]. EBV infection is only occasionally accompanied by neurological disease[219, 226]. However, neurologic complications are often the cause of death in humans with infectious mononucleosis, a syndrome of EBV infection[219, 227]. Viral replication in the brain has been recognized but it is not certain if this is restricted to the infiltrating lymphocytes[217, 228]. EBV associated neuropathogenesis has been related to

immune-mediated mechanisms resulting in demyelination of white matter rather than effects on the gray matter as commonly observed in typically neurotropic viruses[229].

Meningitis following intranasal MHV-68 infection has been described in BALB/c mice newborn[231] or with a deletion in type-I interferon receptor gene[230]. MHV-68 is able to persist in the central nervous system (CNS) during the infection of laboratory mouse strains[232]. In 4-5 weeks and 9-10 weeks old BALB/c infected intracerebrally with MHV-68, lytic replication was detected in astrocytes and to lesser extent in neuronal and glial cells[227]. The highest mortality was observed in 4-5 weeks old mice and the authors hypothesised this to be related to a higher increase in the expression of TNF-α, IL-1β and IL-6 in this age group. The literature available suggests that MHV-68 shows neurotropism despite the absence of obvious neuropathogenesis in immunocompetent animals.

1.2.3 Cell infection

Most of the literature available on herpesvirus entry, assembly and egress has been obtained through the study of Herpes simplex virus (HSV) infection[233].

1.2.3.1 Binding to the cell surface

Like most viruses, the first step in the herpesvirus infection is binding to the cell surface[14, 15, 17]. Binding occurs mainly by ligation of viral envelope glycoproteins to heparan sulphate on the cell surface[234]. However, this process is non-essential and in some cases reversible[16, 149]. Binding potentiates infectivity by concentrating virions on the cell surface and so enables better access of the virions to cell entry receptors[16, 149].

Following binding, the virus enters the cell either by endocytic vesicles or by fusion with the plasma membrane. Fusion leads to loss of the envelope, making this ligation irreversible[16, 149]. In Varicella Zoster virus (VZV) infection the mechanism of viral entry is dependent on the targeted host cell, being through endocytosis in endothelial and epithelial cells[235, 236] and through membrane fusion in fibroblasts[236]. In *Herpesviridae* binding to the cell surface is mainly mediated by the core fusion machinery: Glycoprotein B (gB), gH and gL[237-239] which is conserved throughout the family[240]. However other glycoproteins have been identified as viral ligands, including gD in HSV-1 [241, 242] and gp42 in EBV[243] explaining in part the different cell and tissue tropism[159, 160]. In the case of EBV, the glycoproteins used for binding to cells lead to

their sequestration and so the produced virions will not express them. Consequently, virions produced by infected B cells infect epithelial cells more readily and virions produced by infected epithelial cells infect B lymphocytes more efficiently[239, 243].

1.2.3.2 Virus entry into the cell

During the fusion process, there is loss of the virion envelope and exposure of the tegument proteins. The released proteins are known to interfere with cellular mechanisms at various levels, either by priming the host cell for synthesis of viral components (VP16 in HSV-1), virion–host shut off (SOX in KSHV) or immediate-early gene transactivators[244-246]. In KSHV the release of proteins includes RTA with its expression being detected at 2 h post infection (p.i.)[247-249]. The progression of replication into latent or lytic cycle is dependent on the proteins present.

1.2.3.3 Viral assembly

Once inside the cell, the virus translocates to the nucleus within microtubules[250, 251] and then enters through nuclear pores[4], releasing the capsid which remains perinuclear. When virus particles are intranuclear, viral genome replication is initiated either as a subset (latent replication) or completely (lytic replication).

During lytic replication, gene transcription and consequent protein synthesis occurs in a staggered manner. Consequently, genes are classified as immediate early (IE) or α, early (E) or β and late (L) or γ[149, 160]. IE genes are the first to be expressed in lytic replication and generally correspond to genes modulating the cellular machinery for viral replication and activating transcription of downstream genes[149, 154]. Such genes, in KSHV and MHV-68, include ORF 50 encoding for RTA. E gene products are related to DNA replication and control cellular activities[84, 149, 154]. In KSHV, E protein is vIL-6 that induces B cell proliferation as does the human IL-6. Also in KSHV, Kaposin an early gene, has been identified as inducing cellular transformation[252, 253]. L proteins are related to production of structural components[149, 154]. Genome replication occurs in the nucleus and results in formation of concatemeric molecules that need to be assembled into a unit-length genome. This process is mediated by a dodecameric portal complex (pUL6)[244]. The capsid proteins are synthesised and released in the cytoplasm. In order for the capsid to be packed with the viral DNA, the proteins have to migrate to the

nucleus where they assemble into preformed capsids[254]. The packed capsid then acquires an initial layer of tegument while in the nucleus[149].

1.2.3.4 Viral egress

Viral egress is thought to be by sequential de-envelopment and re-envelopment as the viral particles travel through the cell (Figure 1.5). The primary envelopment occurs at the inner nuclear membrane. However, this envelope is lost once the virus translocates into the cytoplasm, through the outer nuclear membrane (de-envelopment)[149, 244]. Secondary envelopment is thought to occur when viral particles bud into Golgi-apparatus derived vesicles that afterwards fuse with the extracellular membrane and release the virus into the extracellular matrix[244, 255]. This is supported by the finding that there are differences in morphology and protein composition between enveloped virions that present perinuclearly (immature virions) or extracellularly (mature virions) [244, 255].

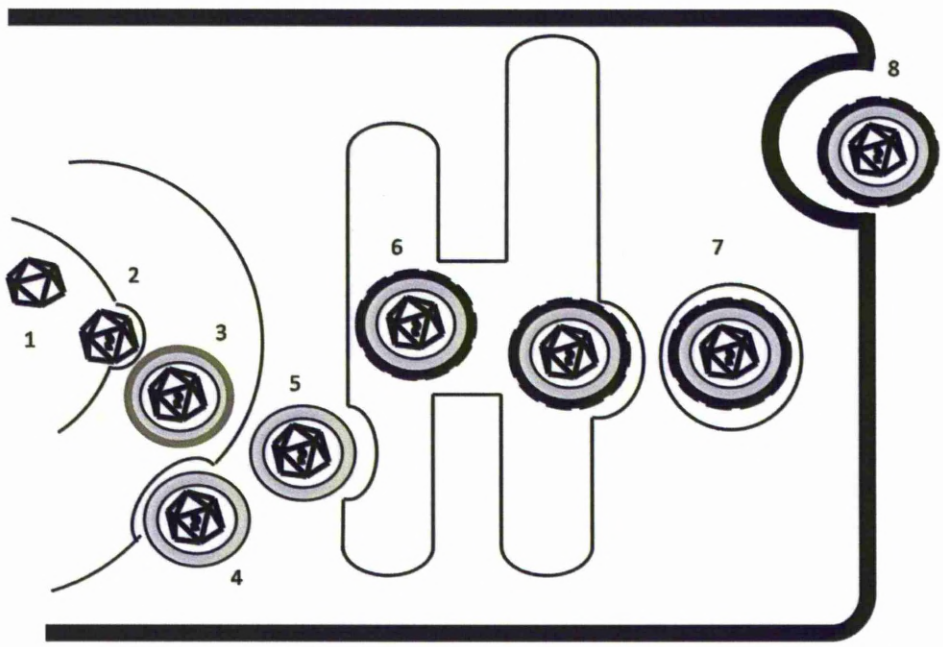

Figure 1.5 Schematic representation of viral egress.
1) Empty capsid in the nucleus. 2) Filled capsid (capsid and genome) as it fuses with the inner nuclear membrane (primary envelopment). 3) Primarily enveloped virus as it migrates between inner and outer leaflet of nuclear membrane. 4) Loss of primary envelopment as virus translocates into the cytoplasm, through the outer nuclear membrane (de-envelopment). 5) Secondary envelopment when viral particles bud into Golgi-apparatus. 6) Enveloped and tegumented viral particles migrating through Golgi apparatus. 7) Enveloped

viral particles fuse with the extracellular membrane. 8) Release of virion into extracellular space

1.3 MHV-68

To date, several acronyms are used to refer to the MHV-68 virus, including murine gammaherpesvirus, murine gammaherpesvirus type 4 strain 68, gammaherpesvirus 68 and Murid herpesvirus type 4[150].

MHV-68 is a natural pathogen of free living rodents[19, 27]. It was first isolated in Slovakia, from *Myodes glareolus*, the bank vole, and *Apodemus flavicollis*, yellow-necked field mice captured in Slovakia during a study on the ecology of arboviruses[20, 27]. Along with MHV-68, four more murid herpesviruses were isolated (strains 60, 72, 76 and 78). An epidemiological study in the UK revealed *Apodemus sylvaticus*, the wood mouse, as the natural host of MHV-68[19]. Contrary to what was found in Slovakia, MHV-68 infection was not detected in bank voles in the UK[256]. Further serological and molecular studies have led to the conclusion that MHV-68 does not naturally infect free-living *Mus musculus*[164].

The natural route of infection of MHV-68 is thought to be intranasal[28] although neonatal transmission is also suspected[257]. A recent study using luciferase imaging reported sexual transmission of MHV-68 in BALB/c mice. In this study genital excretion and latent infection by MHV-68 was detected at the external border of the vagina in females that had been infected intranasally. The viral excretion was dependent on oestrogen levels and efficiently infected males following intercourse. However this excretion site did not lead to horizontal of other females nor vertical transmission to offspring. In the males, virus was seen to replicate in the penis epithelium and corpus cavernosum prior to viral seeding of local lymph nodes and spleen[258].

Experimental studies are performed mainly by using the intranasal route[28, 170, 215, 259]. Intraperitoneal, subcutaneous, intravenous and oral routes of infection are also used in infection studies but less frequently[256, 260-263]. Like other gammaherpesviruses MHV-68 is capable of establishing latent replication in the infected host (Figure 1.6).

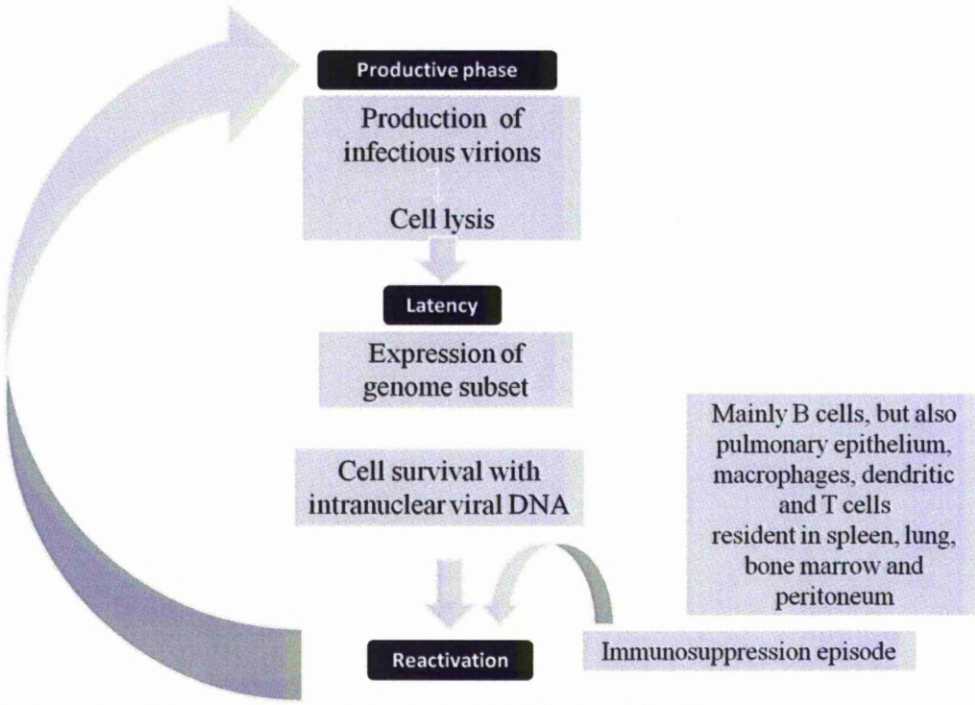

Figure 1.6 Schematic representation of MHV-68 replication.

MHV-68 binds to the host cell heparan sulphate proteoglycans, which occurs initially through gB/gL or gp70[240, 264]. This results in the displacement of the viral glycoprotein gp150 and further heparan-sulphate independent binding[264, 265]. Cell entry occurs through endocytic vesicles and release of the encapsulated viral particle into the cytoplasm by membrane fusion[266, 267].

1.3.1 MHV-68 pathogenesis based on the laboratory mouse model

Following intranasal infection, high level viral lytic replication occurs in the pulmonary epithelium and mononuclear cells, mainly in macrophages (Figure 1.7). During acute replication there is an acute interstitial pneumonia. The pneumonia is characterised by a moderate to severe increase in interstitial cellularity due to moderate to severe infiltration by macrophages and lymphocytes, and there is abundant necrotic debris accumulation. Peribronchiolar and perivascular cuffing is also seen during acute infection which is mainly T cell dominated[154]. The pneumonia is usually cleared around day 10 p.i.[268] but latently infected cells can still be detected by *in situ* hybridization after this period[269].

Through lymphatic drainage, the virus spreads further to the local lymph nodes, the mediastinal lymph nodes. Once in the mediastinal lymph nodes, MHV-68 infects B

lymphocytes, macrophages and dendritic cells[34]. MHV-68 haematogenous spread also occurs during acute infection and virus can be detected in this phase in adrenal glands and heart[25, 270, 271].

Next, further dissemination of infectious virus occurs in the spleen. As in the lymph node, infection of lymphocytes, macrophages and dendritic cells occurs in the spleen[270, 272-276]. Secondary splenic and peripheral mononucleosis develops [276], similar to what occurs in EBV[277]. By the second to third week following infection, there is a transient splenomegaly and adenopathy, associated with a peak in latently infectious cells[278]. In general, after 28 days splenomegaly is no longer observed[154]. The virus then remains latent mostly in B cells of germinal centres and upon an immunosuppressive episode, reactivation occurs with initiation of lytic replication (Figure 1.7). The reactivation mechanism is not fully determined. Studies have found however that the immediate-early gene transcription necessary for reactivation is triggered by hypoxia and chemicals such as phorbol esters and sodium butyrate can induce it[279-286].

If an intraperitoneal route of infection is used there is a different cellular tropism. Lytic infection that follows the intraperitoneal route is established mostly in B cells, while latent infection is observed mostly in macrophages[256].

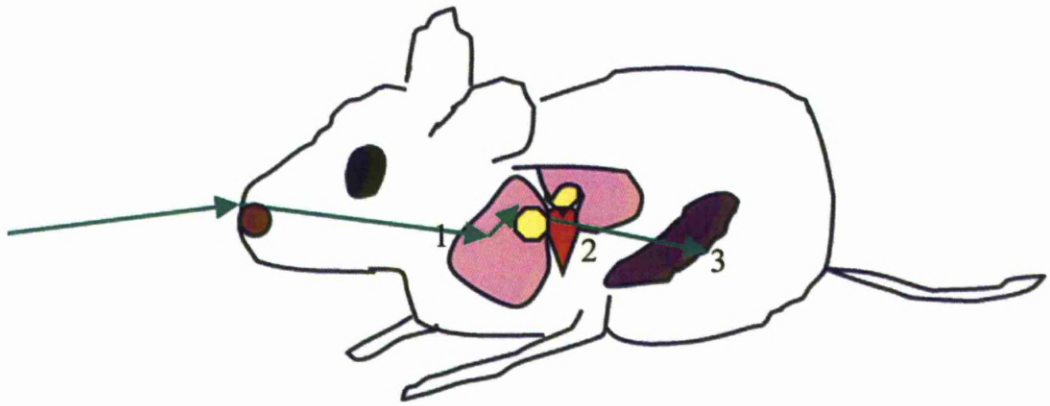

Figure 1.7 Schematic representation of MHV-68 acute replication following intranasal infection.

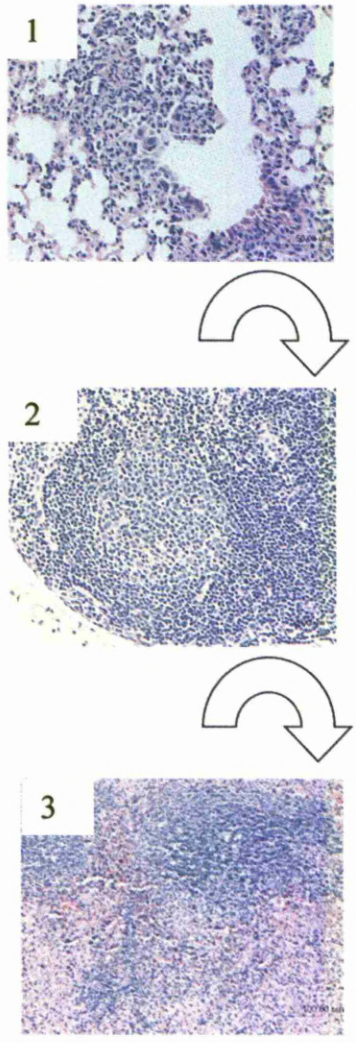

1. Following intranasal infection, high level viral lytic replication occurs in the pulmonary epithelium and mononuclear cells, mainly in macrophages. During this stage of acute replication there is an acute interstitial pneumonia.

2. Through lymphatic drainage, the virus spreads to mediastinal lymph nodes where MHV-68 infects B lymphocytes, macrophages and dendritic cells.

3. Further dissemination of infectious virus occurs to the spleen with infection of lymphocytes, macrophages and dendritic cells. Secondary splenic and peripheral mononucleosis develops and there is a transient splenomegaly and adenopathy.

1.3.2 Inflammatory response to infection

During acute infection, the pulmonary inflammatory infiltrate is initially mainly composed of macrophages. Macrophages are most numerous at day 3 p.i.[164]. After this time there is an increase in the number of $CD8^+$ T cells (cytotoxic) which are highest in number at day 7 p.i.[164, 268, 276]. $CD8^+$ T cell dominance is very closely related to the time when virus titres are highest in the lung (between day 5 and 7 p.i.)[154]. After the initial peak there is a gradual decrease in the presence of $CD8^+$ T cells and expansion of these cells ceases by day 21 p.i. The decrease in $CD8^+$ T cells is thought to be secondary to MHV-68 induced interference in MHC class I antigen presentation. Expression of K3, a MHV-68 early lytic protein, leads to the ubiquination of MHC class I proteins[40-42] and the transporter associated with antigen processing (TAP)[42, 43] in infected cells. As a result of ubiquination, proteins are degraded through a proteosome-dependent mechanism. K3 also inhibits the expression of endogenous p53 in lytically infected cells. The decrease in $CD8^+$ T cells is accompanied by a decrease in production of Bcl-2 and IL-2, similar to what occurs during EBV infection and other viral infections. Bcl-2 is necessary to prevent apoptosis and IL-2 is necessary for rapid expansion of $CD8^+$ T cells when reinfection occurs.

In latent replication only a subset of genes are expressed including latency associated proteins. Latent replication is detected mainly in B cells and to a lesser extent in T cells, pulmonary epithelial cells, macrophages and dendritic cells. The latently infected cells are present in the spleen, lung, bone marrow and peritoneum[270, 287, 288]. There is proliferation of B cells which is mainly $CD4^+$ T cell mediated and leads to mononucleosis[25, 256, 268, 289]. The B cells prime cytotoxic $CD8^+$ T cell to respond to the latency associated proteins[164]. $CD8^+$ T cells moderate latent infection but do not completely clear it[256, 268, 290]. Latently infected mice exhibit antigen-specific CD8+ T cells with enhanced antiviral potential and a more rapid turnover. This has been related to low level sporadic antigenic stimulation during latent infection that does not cause severe deficits in the effector population. Expansion of $CD8^+$ T cells however is maintained after day 21 p.i. in infected animals with the non-persistent MHV-68 ORF 73 mutant virus[291]. This indicates that the switch to latent replication is what triggers $CD8^+$ T cells contraction.

In long term latency (after two months), the virus is found almost exclusively in B cells germinal centres (GC)[270, 275]. B cells in GC can develop into memory B cells which have a long term survival and circulate systemically, ensuring viral long term survival and spread[164].

1.3.3 MHV-68 and proliferation of lymphoreticular tissue

BALB β2 microglobulin deficient ($\beta 2m^{-/-}$) mice developed atypical lymphoid hyperplasia (ALH) 6 to 12 months following intraperitoneal infection with MHV-68[261]. ALH was observed to consist of the abnormal expansion of plasmacytic $CD138^{+}$ cells which preceded B cell lymphomas[261]. In ALH lesions, not all cells showed vtRNA expression indicating infection of all cells is not necessary for lesion development[260, 261]. ALH development was related to v-cyclin, *M11* (encoding v-Bcl-2) and *M1* gene had a positive effect on inducing ALH on the contrary to ORF 74. This cell dominance is also observed in 35% of polymorphic post transplant lymphoproliferative disorder (PTLD) cases in humans[292].

1.3.4 Wood mouse versus laboratory mouse strain infection

Most of the studies into the pathogenesis of MHV-68 have been undertaken using laboratory mice strains derived from *Mus musculus*[293]. However, these studies may not necessarily represent what occurs during infection in the natural host. Notably, there have been few MHV-68 infection studies performed to date in natural hosts, such as the wood mouse (*Apodemus sylvaticus*)[164]. There are distinct differences in the MHV-68 infection profile in the wood mouse and laboratory mice strains derived from *Mus musculus* such as the BALB/c mouse. In the wood mouse, there is less lytic replication but latency is more efficiently established[5]. Also, the infiltrate seen in the lung following infection is macrophage dominated. Furthermore, the lymphocytic infiltration is less intense and there is an increase in B cells and induced bronchial associated lymphoid tissue (iBALT) formation[154]. The detection of vtRNA in B cells indicates latent replication occurs in these cells[154]. iBALT is structurally similar to secondary follicles in lymphoid tissues and is associated with inflammation/infection[294]. iBALT has been shown to be the main site where cells latently infected with MHV-68 reside in the lung of the wood mouse[2,3]. In BALB/c mice, MHV-68 infection is not associated

with iBALT formation and the infiltrate seen in the lung shows a higher predominance of T cells[5].

1.4 The protein of interest – MHV-68 M1 protein

The *M1* gene is positioned between 2023 and 3282 base pairs of the MHV-68 genome[163]. Previous work found that *M1* gene encodes a secreted protein[6]. Little is known regarding the contribution of M1 in MHV-68 pathogenesis.

Genetically, *M1* presents 25% homology (Figure 1.8) with MHV-68 *M3* and *M4* gene, which encodes the abundant secretion of a chemokine binding protein[81, 163, 269, 295]. Evidence suggests that the M1 protein shares functional similarities with the chemokine-binding proteins resulting from the closely related genes, *M3* and *M4*[9]. If M3 expression is inhibited in MHV-68 infection of wood mice, iBALT formation is no longer observed. Furthermore in the absence of M3 instead of a lymphocytic response which is B cell dominated, there is a relative increase in T cells[5, 9]. Quantification of M1, M2, M3 and M4 expression in the lung of infected wood mice at day 7, 10, 12 and 14 p.i found M1 to be the protein with highest expression at 7 days p.i. (Figure 1.9)[9] . This time also coincided with when M1 mRNA expression was highest[9]. At day 7 and day 14 p.i., M1 was transcribed at a higher levels in wood mice than in BALB/c mice, the difference being most at day 7 p.i. [Hughes, DJ, unpublished] (Figure 1.10).

M1 also shares homology with poxvirus serpin (serine protease inhibitors) proteins[163]. However, the *M1* sequence lacks the critical domains/residues for serpin activity.

Intranasal infection of inbred laboratory mice with vtRNAs and *M1* gene knock-out virus, found that *in vitro* replication and *in vivo* latency was still maintained[8, 296]. This showed that M1 is not essential for latency establishment. In C57BL/6J-Rag1^{tm1Mom} infected intraperitoneally with MHV-68 with lacZ insert disrupting M1 ORF found M1 suppressed reactivation. Mice infected with the viral mutants had a fivefold increase in reactivation efficiency[7]. M1 suppression of viral reactivation occurs through activation of Vβ4+ CD8+ T cells. Vβ4$^+$ CD8$^+$ T cells resist functional exhaustion and consequently there is long term secretion of IFN-γ[6]. These cells also secrete TNF-α and IL-2 *in vitro*[297]. The notion that M1 effect on reactivation is mediated through IFN-γ increase is supported by the maintenance of Vβ4+ CD8$^+$ T cell activation but not of M1 suppressive effect on reactivation in the infection of IFNγR$^{-/-}$

mice. Additionally, in the infection of IFNγR$^{-/-}$mice there are more extensive pathological changes including severe inflammation and fibrosis of several organs. Further studies in C57BL/6J using recombinant viruses with a deletion or a stop insertion in the M1 gene found persistent viral replication in the lungs during chronic infection. However this was not observed in all mice studied suggesting that viral replication occurs in a interrupted manner and not continuously[297]. M1 mediated activation of Vβ4+ CD8$^+$ T cells, is not to a feature in MHV-68 infection of BALB/c mice[297]. The different effect of M1 on the activation of Vβ4+ CD8$^+$ T cells is possibly related to the different genetic background of the mouse strains studied and different immune responses inherent to the host including bias in CD4$^+$ T cell polarization. C57BL/6 have been described has having a Th1 dominated response whilst BALB/c mice have a Th2 dominated response[298-301].

During chronic infection of both C57BL/6 and BALB/c mice, impairment of M1 secretion led to an increase in latently infected IgD$^-$ B cells present in the spleen[297]. M1 effect in decreasing the presence of latently infected cells in chronic infection was hypothesized as a protective measure employed by the virus to avoid further pathological changes in the host such as lymphoproliferation.

In MHV-68 infection of IFNR$^{-/-}$ mice in there is extensive fibrosis in the lung at 2 weeks p.i. and in mediastinal lymph nodes and spleen at 3 weeks p.i. The most severe fibrosis is seen at the peak of latent infection in the tissues described. If CD4$^+$ and CD8$^+$cells were extracted prior to infection, there was no onset of the fibrosis[214-216], indicating the role of these cells in the induction of fibrosis. The splenic fibrosis was related to alternative activation of macrophages with no change to classical activation of macrophages[209]. Taken together the IFN R$^{-/-}$ mice studies could suggest that M1 could modulate activation of macrophages and be involved in induction of fibrosis in laboratory mice strains.

1.5 This thesis

The aim of the present work is to determine the effect of M1 expression in MHV-68 infection. For this, *in vitro* and *in vivo* studies were performed using vM1stop virus and its genetically repaired counterpart, vM1rev virus. vM1stop virus is an MHV-68 virus with an in-frame stop codon in the *M1* locus. The stop codon impairs expression of M1 without exerting interference with the remaining genome. The objective was to

ascertain the influence of M1 in MHV-68 infection through comparison of infection in the presence or absence of M1 expression.

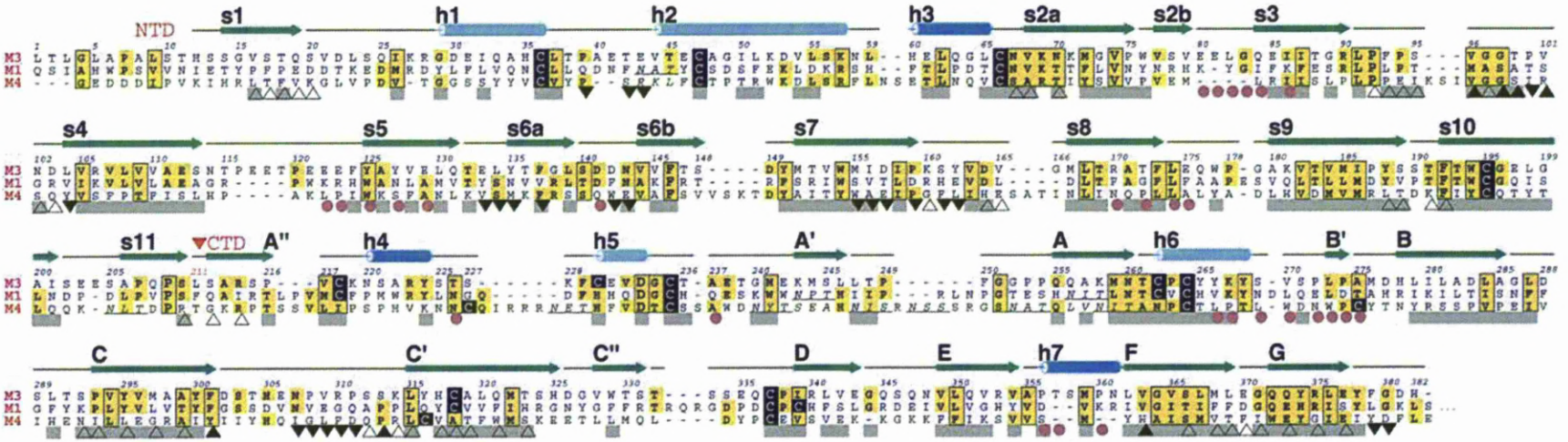

Figure 1.8. M3, M1 and M4 sequence alignment.
Taken from[81].
M1 and M4 sequences (after signal cleavage) aligned with M3 considering burial of core hydrophobic residues, Cys placement, and location of possible N-linked glycosylation sites (underlined) away from core folding elements.
In grey underscore: Dominantly inaccessible residues of M3 binding interface.
Black filled triangles: Residues buried in the M3 dimer interface
Upward pointing open triangles: Residues at the NTD-CTD interface of a single monomer.
Upward pointing filled triangles Residues buried both in the dimer interface and the NTD-CTD interface

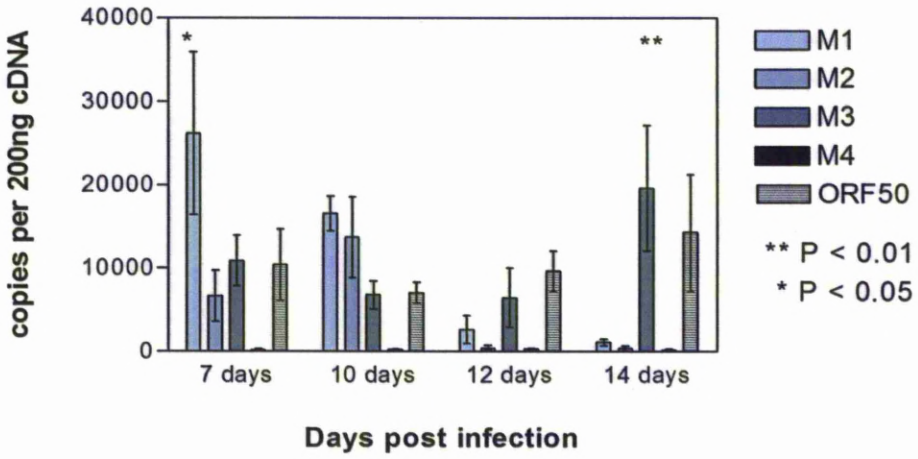

Figure 1.9 Expression of *M1, M2, M3, M4* and *ORF 50* in the woodmouse lung at day 7, 10, 12 and 14 post intranasal infection with MHV-68.
Taken from[9]
Quantification performed by qRT-PCR. ORF50 assessed as a general reference for lytic-cycle gene expression. The copy numbers of individual viral-gene RNAs (as cDNAs) were normalized to those for cellular RPL8. Error bars represent the standard error of the mean from three wood mice per time point. Analysis of expression from the M1-M4 locus of infected wood mice. M1 was the protein with highest expression at 7 days p.i. and this was the timepoint when M1 transcript expression was the highest of all examined timepoints.

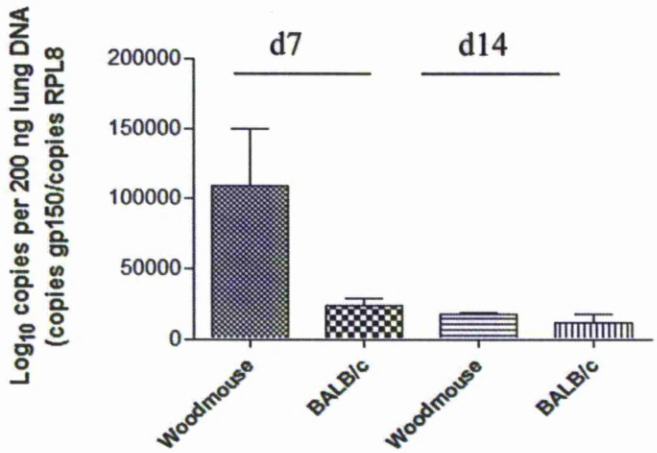

Figure 1.10 *M1* expression in the woodmouse and BALB/c mouse at day 7 and day 14 post intranasal infection with MHV-68.
Quantification was performed by qRT-PCR. The copy numbers of individual viral-gene RNAs (as cDNAs) were normalized to those for cellular RPL8. Error bars represent the standard error of the mean from three wood mice per time point. At day 7 and day 14 p.i., M1 was transcribed at a higher level in wood mice than in BALB/c mice, the difference being most at day 7 p.i.

2. Materials and Methods

2. Materials and methods

2.1 Cell culture

The cell lines used in this study were BHK-21, αβSV1, NIH 3T3 and MH-S. Baby hamster kidney cells (BHK-21) clone 13 is a cell line derived from the kidney cells of one day old hamsters[302]. αβSV1, is a fibroblast transformed cell line derived from IFN-αβR-/-129/Sv[303] mouse embryos (Stewart JP, unpublished). NIH3T3 is a fibroblast cell line derived from the SV40 transformation of Swiss mouse embryo cells[304]. The MH-S alveolar macrophage cell line was obtained from ATCC, UK (CRL-2019). This cell line is an alveolar macrophage cell line derived by SV40 transformation of adherent macrophages from a BALB/c mouse. Alveolar macrophage morphology and phagocytic capacity is maintained. They are adherent, esterase positive and peroxidase negative. Lipopolysaccharide (LPS) treatment stimulates IL-1 production. The cells are capable of suppressing the *in vitro* plaque forming cell (PFC) response in a cell dose-dependent manner [305].

Cells were routinely grown in 75cm^2 and 175cm^2 vented tissue culture flasks (Iwaki) and 25 ml of growth medium. The growth medium varied with cell type (Table 2.1). For passaging, the growth medium was discarded and the monolayer was washed three times with 5 mls of sterile PBS at 37°C. Cells were then incubated at 37°C with 5 mls of 2.5% (v/v) trypsin (Gibco) and 0.02% (w/v) versene (Lonza) solution until they detached from the bottom of the flask, usually after 2 to 5 minutes. Then 5 mls of growth medium was added to the flask and vigorously pipetted to produce an even suspension. The cell suspension was centrifuged at 500 g for 3 min and the pellet was resuspended in 5 mls of growth medium. To assess the concentration of cells, 10 µl of the cell suspension was mixed with 90 µl of 0.04% (w/v) Trypan Blue (Sigma). The mixture was mixed vigorously and the concentration of cells determined by counting the cells present in 10 µl in a haematocytometer. Cells not stained by Trypan Blue were interpreted as having an intact cellular membrane and thus were deemed viable. During routine cellular passage, 1 ml of the resuspended cell pellet was placed into new flasks containing 20 ml of growth medium. The cells were grown at 37°C in an atmosphere of 5% carbon dioxide until they reached subconfluency.

Cell line	BHK-21	αβSV1	NIH3T3	MH-S
Medium [1]	GMEM	DMEM	DMEM	RPMI
Calf serum [2]	10% (v/v) newborn	10% (v/v) foetal	10% (v/v) foetal	10% (v/v) foetal
L-glutamine [3]	2mM	2mM	2mM	2mM
P/S [4]	100 i.u/ml	100 i.u/ml	100 i.u/ml	100 i.u/ml
Tryptose phosphate broth [1]	10% (v/v)	-	-	-
Hepes [1]	-	-	-	10mM
2-mercaptoethanol [5]	-	-	-	0.05 mM
Sodium pyruvate [1]	-	-	-	1mM

Table 2.1 Growth media formulations used for the BHK-21, αβSV1, NIH3T3 and MH-S cell lines.
Abbreviations: GMEM: Glasgow minimal essential medium; DMEM: Dulbecco's Modified Eagles Medium; RPMI: Roswell Park Memorial Institute Medium; P/S: penicillin-streptomycin. [1]: Lonza; [2]: (Biowest); [3]: Invitrogen Life Technologies; [4]: Invitrogen Life Technologies; [5]: Sigma Aldrich; i.u.: international units

2.2 Virological techniques

2.2.1 The viruses

2.2.1.1 vM1stop and vM1rev viruses

The recombinant MHV-68 deficient in the M1 function [M1 knock-out virus (vM1stop)] and the marker rescue virus (vM1rev) were a kind gift from Dr B.M. Dutia (University of Edinburgh). The aim of the construction of the vM1stop virus was to insert a stop codon and diagnostic restriction site close to the start codon of M1 ORF at position 2023.

Two PCR fragments were prepared with stop/HpaI site at the 3' and 5' ends respectively. They were then combined and amplification of DNA was performed in a second PCR to create a mutant PCR fragment (Figure 2.1). The 5' PCR product has a StuI site at the 5'end, while the 3' product has a BsaBI site at the 3'end. The mutant fragments were cloned into MHV-68 HindE clone (106-6261nt) using StuI and BsaBI. The HindE fragment mutant was then subcloned into the pST76K_SR shuttle vector. The shuttle vector was ultimately transformed into DH10B containing MHV-68 BAC and mutants were selected by PCR. Primers used in PCR reactions are shown in Figure

2.2. Virus stocks were produced by transfection of BAC DNA into BHK-21 cells. BAC sequences were excised from the reconstituted virus by passage through mouse NIH3T3 cells expressing cre recombinase[306].

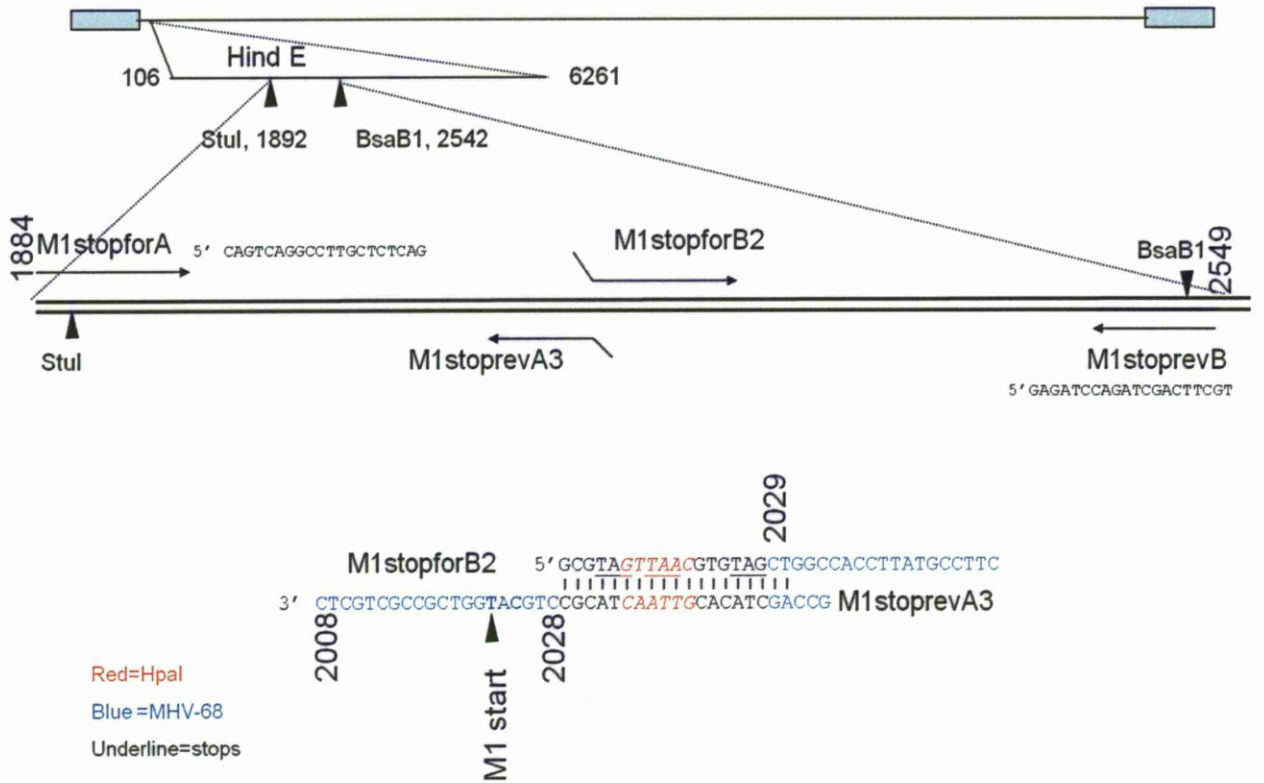

Figure 2.1 vM1rev vM1stop virus constructs

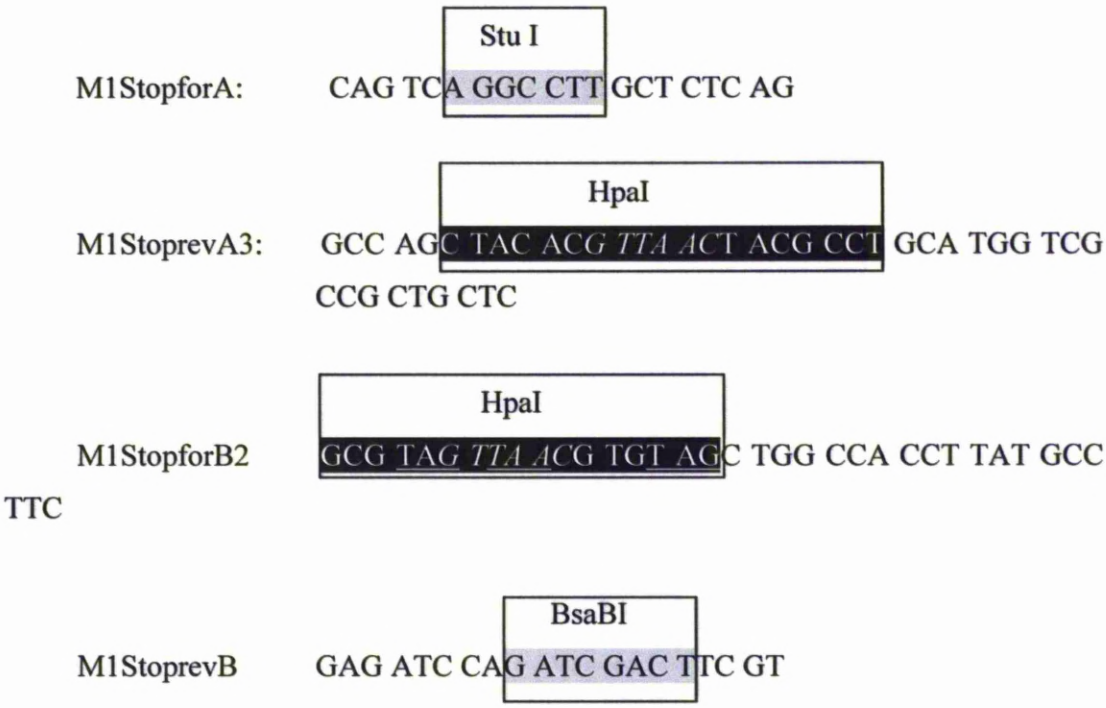

Figure 2.2 Primers used in the construction of the vM1stop virus.
Boxed areas are representative of restriction digest sites

2.2.1.1.1 Verification of deletion in the vM1stop virus stocks

In order to confirm the state of deletion in the various virus prepared stocks, viral DNA was extracted from the virus stocks and PCR was performed using M1 primers. The reaction mix consisted of: 0.5 µM forward and reverse primers (MWG Biotech), 0.25mM dATP, dTTP, dCTP and dGTP (GE Healthcare), 1.5 mM Mg Cl_2, 20 mM Tris-HCl (pH 8.4), 50 mM KCl (Invitrogen Life Technologies) and diH2O to a final volume of 50µl. To the reaction mix, 10µl of the virus stock was added followed by 2µg of Proteinase K (Invitrogen Life Technologies). The mixture was then incubated at 55°C for 20 minutes. To deactivate the Proteinase K, there was a further incubation at 95°C for 10 minutes. To this mixture was added 1 U of Taq DNA Polymerase Platinum and RT-PCR was performed using a previously described protocol (Section 2.2.2). PCR products were then analysed by gel electrophoresis to determine the size of the PCR products.

2.2.1.2 LHΔgfp

LHΔgfp virus was a kind gift from Dr B.M. Dutia (University of Edinburgh). LHΔgfp virus is a MHV-68 virus which was constructed by co-transfection of MHV-68 viral DNA with DNA containing a human cytomegalovirus (HCMV) immediate-early promoter-driven green fluorescent protein cassette (CMV-GFP) into BHK cells[215].

2.2.1.3 MHV-68

MHV-68 working stocks were constituted of sub-master stocks of MHV-68 clone g2.4[25].

2.2.2 Preparation of virus stocks

On the day prior to infection, 10^6 αβSV1 cells per flask were seeded onto 150 cm^2 flasks. The cells were infected with virus at a multiplicity of infection of 0.05 PFU/cell. The inoculum volume was 5 ml per flask. Infected cells were then incubated for 1.5 hours at 37° C. After this period, 25 ml of medium (formula mentioned in section 2.1) was added per flask. Infected cells were observed daily and incubated at 37° C for four to six days, until 100% cytopathic effect (CPE) was seen.

Cells were harvested and a pellet was obtained by centrifugation at 1000 g at 4° C for 20 minutes. The supernatant was removed and all the following steps were performed on ice. The lowest possible volume of PBS was used to resuspend the pellet present in one centrifuge tube and the solution was then transferred to the next centrifuge tube and so forth until all pellets were resuspended. Then the total volume resulting from the pellet resuspension was introduced into a previously cooled douncer. The contents were crushed using the dounce homogeniser (to assure breakage of cell walls and release of intracellular viral particles). The crushed mixture was then centrifuged at 2000 g at 4° C for 20 minutes. The supernatant solution was then removed and kept in a separate centrifuge tube. The remaining pellet was resuspended in the smallest volume possible (one to two ml) of PBS solution. The solution was transferred once again into the douncer and crushing of contents was repeated. Centrifugation of resuspension solution was performed at 2000 g at 4° C for 20 minutes. Finally, the supernatant was removed, mixed with the previously separated supernatant and distributed into cryovials to be stored at -80°C.

2.2.3 Virus stock titration

Titration was performed using 6-welled plates (Iwaki). On the day prior to infection, plates were seeded with 10^6 NIH3T3 cells per plate. Serial 10-fold dilutions of the virus preparation were performed to obtain 10^{-1} to 10^{-12} dilutions in 1 ml of media. Each diluted virus preparation was then introduced into the respective well. Infected cell plates were incubated for one hour at 37°C. After the incubation period, the inoculum was removed and 4 ml of medium was introduced. Infected cell plates were then incubated for four days at 37°C.

After four days, the cells were fixed by introduction of 4% (v/v) formal saline for 30 minutes into each well. After fixation, infected cells were stained with 0.1% (w/v) toluidine blue for 30 min or overnight if solution old or reused. Once dried, cell plates were analyzed under the microscope for viral plaques (Figure 2.3).

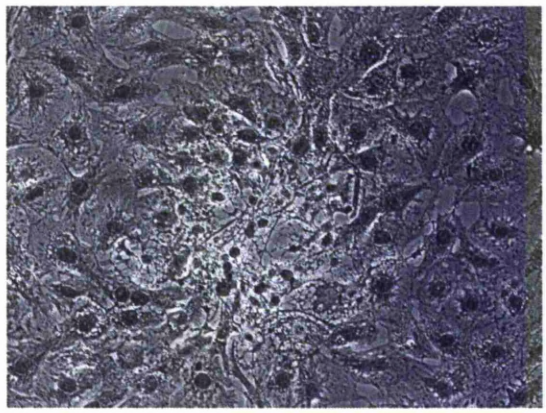

Figure 2.3 Plaque forming unit in NIH3T3 cells infected with MHV-68.
Magnification: 40 x 0.45

2.2.4 Multi-step growth curve

The multi-step growth curve was performed using 24-welled plates (Iwaki). On the day prior to infection, 24 well cell plates were seeded with $1x10^6$ NIH3T3 cells per plate. Cells were infected using a multiplicity of infection (MOI) of 0.01 PFU/cell in 250µl of media per well and incubated for 1 hour at 37 °C. To calculate the MOI, cells were considered to have divided at least once overnight. After this, an inoculum was removed and 1 ml per well of citrate buffer (135 mM NaCl, 10 mM KCl, 40 mM citric acid (pH 3.0))[307] was introduced for one minute to kill any unbound virus. Cells were then washed three times with DMEM medium with 10% (v/v) calf serum (Biowest),

2mM L- glutamine (Invitrogen Life Technologies) and 100 i.u/ml P/S (Invitrogen Life Technologies). Cells were incubated in 1 ml of DMEM at 37 °C. A baseline sample was taken at 0 hours by scraping cells and removing the medium completely and cell/virus mixture. Five more samples were taken at six hour intervals. Then four more samples were taken at 24 hour intervals. Samples were frozen at -80 °C until being titrated. Prior to titration (Section 2.2.3) samples were freeze-thawed three times (to cause cell breakage and release of virus particles) and centrifuged at 2000 g for five minutes.

2.2.5 One-step growth curve

One-step growth curves were performed using 24-welled plates (Iwaki). On the day prior to infection, $2x10^6$ NIH3T3 cells per plate were used when NIH3T3 cells were employed. However, $4x10^6$ NIH3T3 cells per plate were utilised when MH-S cells were used. NIH3T3 cells were infected at an MOI of 5 and MH-S cells were infected at an MOI of 10. The infection protocol was identical as mentioned for the multi-step growth curve (Section 2.2.4) apart from the incubation time and media used when the study was performed in MH-S cells. In MH-S cells, the incubation with the inoculum was for two hours and the media used was RPMI with 10% (v/v) foetal calf serum (Biowest), 2mM L-glutamine (Invitrogen Life Technologies), 100 i.u/ml P /S (Invitrogen Life Technologies), 10mM Hepes (Lonza), 0.05 mM2-mercaptoethanol (Sigma Aldrich) and 1mM sodium pyruvate (Lonza).

The samples corresponding to 0 hours were taken at this time point by scraping cells and removing the medium completely and cell/virus mixture. Six more samples were taken at four hour intervals. Then, two samples were taken at six hour intervals. Finally, three more samples were taken at 12 hour intervals.

Samples were stored at -80C until titration of virus stock was performed following a protocol described in Section 2.2.3.

2.2.6 Preparation of cell pellets for transmission electron microscopy

Infected cell pellets were produced by seeding 75 cm^2 flasks (Iwaki) at an MOI of 5 PFU/cell. After 48 hours, cells were detached by trypsinisation and a pellet was obtained by centrifugation at 800 g for five minutes. The pellet was resuspended in 2.5% (v/v) glutaraldehyde in 0.1 M sodium cacodylate buffer (pH 7.4) and centrifuged

at 800 g for three minutes (reagents: TAAB Laboratories). The resulting pellet was resuspended in the fixative 4% (v/v) paraformaldehyde and 2.5% (v/v/) glutaraldehyde in 0.1M sodium cacodylate buffer) and kept at -4° C until further processing.

Further processing consisted of washing of the pellets with 0.1M sodium cacodylate buffer and fixation in 1 % (v/v) osmium tetroxide for 90 minutes. A second wash using distilled water was performed. The pellets were then stained en bloc with 2% (v/v) uranyl acetate in 0.69% (v/v) maleic acid for 90 minutes, dehydrated in incrementing concentrations of ethanol (50, 70, 90, 100%) (v/v) and finally in 100% (v/v) acetone. Next the pellets were infiltrated in epoxy at incrementing concentrations of resin:acetone (25:75, 50:50, 75:25) (w/v). This was performed for 10 minutes, two times, at each concentration and finally pellets were infiltrated in 100% epoxy resin (3 x 10 minutes) resin in acetone. Pellets were added to embedding capsules and left overnight in fresh resin at 60 °C to polymerise. In ordinary preparations of samples for ultrastructural examination, the next step consisted of the processing of semi-thin sections (0.5 μm). Semi-thin sections were cut using an ultramicrotome (Reichert-Jung Ultracut) with a diamond knife (Diatome Ltd.) and stained with 0.1 % (w/v) toluidine blue to enable examination by light microscopy and selection of areas of interest. However, the infected cell pellets were too small and friable. Following embedding, the next processing step was the production of ultrathin sections (60 nm) for ultrastructural examination. Ultrathin sections were cut using a diamond knife, mounted on copper grids, stained with Reynold's lead citrate. Ultrastructural examination was performed on a H600 transmission electron microscope (Hitachi) and on a FEI EM208S transmission electron microscope (Philips).

2.2.7 Extraction of genomic DNA from virus stocks

100 μl of virus preparation was added to 100 μl of PBS. To enable digestion, 20 μl of proteinase K was added along with 200 μl of lysis buffer (DNeasy Blood & Tissue Kit, Qiagen). The solution was then mixed by agitation on a vortex for 15 seconds and centrifuged at 20,000 g for 15 seconds, before being incubated in a water bath at 56°C for 10 minutes. To stop the digestion, 230 μl of molecular grade ethanol (Bhd) was added, the solution was mixed by agitation on a vortex for 15 seconds and centrifuged at 10,000 g for 10 seconds. The final mixture was then placed in a spin column and centrifuged at 8000 g for one minute. Wash buffer AW1 (500μl) was added to the

column that was respun at 8000 g for one minute. Buffer AW2 (500µl) was also added to the column and was respun at 11,000 g for three minutes. The spin column was then cleared by an extra spin at 14,000 g for one minute. The DNA was eluted in 60µl of Buffer AE, which was added to the column, left at room temperature for ten minutes and then centrifuged at 6000 g for one minute. The flowthrough was stored at -20°C until further use.

2.2.8 Optimisation of MH-S cell line infection

On the day prior to infection, cells were seeded 12 hours prior to infection in 24 well plates, at increasing cellular densities ranging from 10^6 to 4 x 10^6 cells per well. LHΔgfp virus was diluted in 200 µl of inoculum as to have a MOI of 1, 5 or 10 PFU/cell and incubated for a period of one, two or three hours. Plates were then washed with PBS or not washed with PBS and RPMI media was added to have 1 ml of media overlaying cells. Fluorescence was measured to ascertain the percentage of cells infected. NIH3T3 and MH-S cell infection experiments were performed in parallel since NIH3T3 cells are more permissive to MHV-68 *in vitro* infection and so were a positive control of infection.

2.3 *In vivo* studies

2.3.1 Infection of mice

All wood mice used in these studies were from a laboratory-bred colony maintained at the Leahurst campus, School of Veterinary Science, University of Liverpool[308, 309] under semi-barrier conditions. The colony was created by J. Clarke in 1995 and mice were descendents from captive-bred colonies from the Department of Zoology, University of Oxford. Introduction of animals from the wild was done intermittently. Mice were tested (see appendix 1 - Figure 5.1) for the major infections of laboratory rodents (Harlan United Kingdom Technical Services, Loughborough, United Kingdom) and tested negative for these infections. MHV-68 infection has not been detected in this colony by either serology or PCR analysis[19]. BALB/c mice were purchased from Bantin and Kingman (Hull, United Kingdom).

Animals were anesthetized with isoflurane and infected intranasally with the virus solution (40 µl) which contained 4x 10^5 PFU diluted in sterile phosphate-buffered saline

(PBS). For each time point studied, three animals were infected. The timepoints studied were day 3, 7, 14 and 28 p.i.. Animals were culled according to local and national schedule I requirements and all procedures were carried out in compliance with the Animal Scientific Procedures Act (1986).

2.3.2 Collection of tissue samples

Wood mice were humanely euthanized by cervical dislocation after sedation and anaesthesia with isofluorane. Spleen and lungs with trachea, thymus, mediastinal and bronchial lymph nodes and brain were collected. Half of the spleen and the left lung lobe were introduced separately into cryovials (Nunc), immersed in liquid nitrogen and then stored at -80°C. A longitudinal third of the right middle and accessory lung lobes and approximately a third of the distal 6th of the right distal lung lobe were immersed in Optimal Cutting Temperature (OCT) embedding medium (Raymond A Lamb Laboratory supplies) within an aluminium foil tube that was then frozen in isopentane cooled in a bath of liquid nitrogen. (see Figure 2.4 for location of lobes). A longitudinal third of the right middle and accessory lung lobes, approximately a third of the distal 6th of the right distal lung lobe and part of the mediastinal and bronchial lymph nodes were collected and immersed in 4% (v/v) PFA + 2.5% (v/v) glutamine in 0.1M sodium cacodylate buffer for examination by transmission electron microscopy. The remaining lung, thymus, meadiastinal and bronchial lymph nodes, spleen and brain were immediately immersed in 4% (v/v) paraformaldehyde. In a separate pot and after opening of the skull and removal of the skin, the remaining animal tissues were also immersed in 4% (v/v) paraformaldehyde.

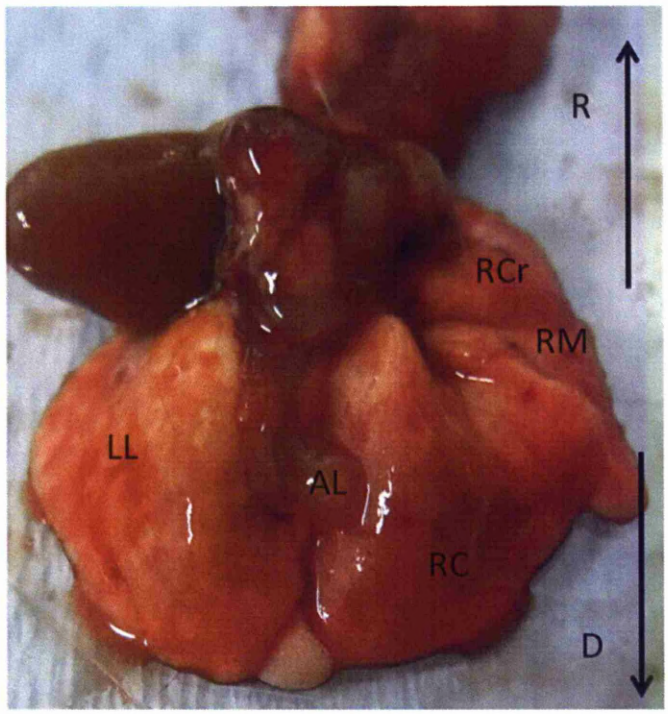

Figure 2.4 Wood mouse lung.
Abbreviations: R: rostral; D: distal; LL: left lung lobe; RC: right caudal lung lobe; RM: right middle lung lobe; AL: Accessory lung lobe; RCr: right cranial lung lobe

2.3.3 Preparation of tissues for histological examination

Lung, thymus, mediastinal, bronchial lymph nodes, spleen and brain were collected from study animals and fixed overnight in 4% (w/v) buffered paraformaldehyde (pH 7.4). On the day following sampling, tissues were routinely embedded in paraffin wax. Sections (3-5 μm) were prepared and placed on glass slides. In the case of the nasal cavity, on the day following sampling the unskinned nasal cavity was cut sequentially using a diamond saw into sections (3-5 μm) and left in 10% (w/v) EDTA solution (pH7.4), for one week prior to embedding in paraffin.

For histopathological examination purposes, the tissues were laid on plain glass slides (ColourSlides, Solmedia Laboratory Supplies). Paraffin embedded sections used for immunohistology examination and *in situ* hybridisation were laid on adhesive-coated glass slides (Polysine TM, VWR International). Sections were dewaxed by immersion in xylene for 10 minutes. Rehydration of samples was then performed by incubation for three minutes, twice in isopropanol and once in 96% (v/v) ethanol. Dewaxed sections were stained with haematoxylin-eosin (HE).

2.3.4 Cryosectioning

Tissue embedded in OCT was sectioned into 4-8 μm sections using a Leica CM1900UV cryostat with the cryochamber at -30°C. The cut sections were mounted on adhesive coated slides (Polysine TM, VWR International). Sections were allowed to dry on the slides at room temperature for 10 minutes. Ice cold acetone was applied to the sections and they were allowed to dry at 4°C. Tissues were then stored at -80°C until further processed.

2.3.5 Immunohistology

Immunohistology was performed by the Histology Laboratory, Veterinary Laboratory Services, School of Veterinary Science, University of Liverpool.

Detection of CD4 and CD8 antigens was performed on frozen tissue sections fixed in acetone. Detection of the remaining antigens was performed on tissue sections embedded in paraffin and fixed in 4 % (v/v) paraformaldehyde. The detection method of choice was the peroxidase antiperoxidase method (PAP) technique [310].

2.3.5.1 Immunohistology of acetone fixed sections

Acetone fixed sections were thawed for two hours at room temperature. For the purpose of endogenous peroxidase inactivation, sections were incubated in methanol with 0.5 % (v/v) H_2O_2 at room temperature (Perhydrol 30 %, Fisher Scientific), for 15 minutes. Sections were then washed in Tris-Buffered Saline (TBS) for 5 minutes and placed in coverplates in Sequenza racks (Thermo Shandon). See Section 2.3.5.2 for details of further processing.

2.3.5.2 Immunohistology of paraffin embedded sections

Paraffin embedded sections were dewaxed by immersion in xylene for 10 minutes. Tissue sections were rehydrated by sequentially immersing the sections twice in 100 % (v/v) ethanol for three minutes and then once in 96 % (v/v) ethanol for three minutes. For the purpose of endogenous peroxidase inactivation, sections were incubated in methanol with 0.5 % (v/v) diH_2O_2 at room temperature (Perhydrol 30 %, Fisher Scientific), for 30 minutes. The sections were washed twice in TBS. What follows is the description of the protocol for MHV-68 detection. However, there were some variations to this method depending on the used antibodies (see Table 2.3). Pre-

treatment was performed by incubation in 10mM citrate buffer (0.9 % (v/v) 0.1 M citric acid, 1 % (v/v) 0.1M sodium acetate (pH 6.0) for 25 to 30 minutes at 97 °C.

For the remainder of the experiment, slides were placed in coverplates in Sequenza racks (Thermo Shandon). Tissues were washed with TBS (pH 7.4). In order to block non-specific binding by the anti-serum, tissues were incubated with 50 % (v/v) swine serum in TBS for 10 minutes at room temperature. This was followed by incubation with primary antibody diluted in 20 % (v/v) swine serum in TBS for 15 to 18 hours at 4 °C (see Table 2.3). The tissues were then washed with TBS and incubated with 1:100 dilution of swine antirabbit IgG in 20 % (v/v) swine serum (Stratech Scientific Ltd., Vector Laboratories, Peterborough) in TBS for 30 minutes at room temperature. A second wash was done using TBS alone. The tissues were then incubated with 1:100 PAP-rabbit (Stratech Scientific Ltd.) in TBS at room temperature for 30 minutes. Slides were then washed in TBS and removed from the coverplates. Finally, tissues were incubated with 3,3′-diaminobenzidine tetrahydrochloride (DAB, Sigma-Aldrich Co. Ltd.) and 0.01 % (v/v) diH_2O_2 in 0.1 M imidazole buffer (0.1 M imidazole, 0.1 M HCl (pH 7.1)) at room temperature for 10 minutes and washed three times with TBS and once with distilled water.

In order to increase the contrast between tissue sections and to aid visual examination, counterstaining with Papanicolaou's special haematoxylin was performed. In all experiments, a positive and a negative control were included as to assess specificity and sensitivity of the reactions and validate the experiment.

2.3.6 Preparation of tissues for transmission electron microscopy

See section 2.2.7 for details of processing.

Antigen	Pre-treatment	Blocking	Primary antibody	Secondary antibody	Detection method
MuHV-4 *	Citrate buffer pH 6.0	50 % (v/v) swine serum in TBS	PAb rabbit anti-MHV-68 at 1:2000	Swine anti-rabbit IgG 1:100 [1]	PAP; Rabbit 1:100 [1]
Lysozyme (macrophages, and DCs)	Protease	50 % (v/v) swine serum in TBS	PAb rabbit anti-human lysozyme 1:800[1]	Swine anti-rabbit 1:100 [1]	PAP; Rabbit 1:100 [1]
CD45R (B cells)	Citrate buffer pH 6.0	Undiluted horse serum	MAb rat anti-mouse (B220-Ly5) 1:1000 [3]	Biotinylated rabbit anti-rat IgG 1:100 [2]	ABC [2]
CD3* (T cells)	Protease	50 % (v/v) swine serum in TBS	PAb human anti-CD3 Pre-diluted [1]	Swine anti-rabbit IgG 1:100 [1]	PAP; Rabbit 1:100 [1]
TNF- α (Cytokine)	None	Undiluted rabbit serum	PAb goat anti-mouse-TNF-α [4]	Rabbit anti-goat IgG 1:100 [2]	ABC [2]
CD4 (helper T cells)	None	Undiluted horse serum	MAb rat anti-mouse CD4 [3] diluted in 10% rabbit serum & 2.5% mouse serum)	Rabbit anti-rat IgG 1:100 [2]	ABC [2]
CD8 (cytotoxic T cells)	None	Undiluted horse serum	MAb rat anti-mouse CD4 [3] diluted in 10% rabbit serum & 2.5% mouse serum	Rabbit anti-rat IgG 1:100 [2]	ABC [2]
SP-C (typeII pneumocytes)	None	20% (v/v) swine serum in TBST	PoAb rabbit anti SP-C [4] 1:50	Swine anti-rabbit [1] 1:100	PAP Rabbit [5] 1:250
IFN-γ	Citrate buffer pH 6.0	Goat Serum	PAb rabbit Polyclonal [4] 1:100	Goat anti Rabbit 1:100 [2]	ABC [2]

Table 2.2 Specific treatments used in immunohistology.
MAb:Monoclonal antibody; PAb: Polyclonal antibody; [1]: Dako; [2]: Vector Laboratories; [3]: Southern Biotech; [4]: Santa Cruz Biotech; [5]: Covance

2.4 Molecular biology techniques

2.4.1 Extraction of genomic DNA from tissues

Lung and splenic tissue (25 mg) from infected mice, was cut into small fragments and placed in a 2 ml centrifuge tube with 180 µl of ATL buffer (DNAeasy Qiagen kit, Qiagen). Proteinase K (20µl) was then added to the mixture and was mixed by agitation on a vortex mixer. The sample was then incubated overnight in a water bath at 56 °C to enable full digestion. The next day, the mixture was centrifuged in a fast spin cycle at 20,000 g and then 200 µl of AL buffer (Qiagen) was added. The solution was mixed by pulse-vortexing for 15 seconds and incubated for 10 minutes in a water bath at 70 °C. Next, 200µl of molecular grade ethanol (Bhd) was added and mixed by pulse vortexing, followed by fast spin centrifugation at 20,000 g. The mixture was then placed in a spin column and centrifuged at 6000 g for one minute. Buffer AW1 (500µl) (Qiagen) was added to the column that was centrifuged at 6000 g for 1 minute. Buffer AW2 (500µl) (Qiagen) was then added to the column that was respun at 6000 g for one minute. Finally, 200µl of buffer AE (Qiagen) was added and the tube was left at room temperature for ten minutes before being centrifuged at 6000 g for one minute. The flowthrough was stored at -20°C until further use.

2.4.2 Reverse transcriptase PCR (RT- PCR)

All RT-PCR and quantitative PCR (qPCR) reaction mixtures were prepared in a "PCR clean room" in a Captair Bio hood® (Erlab) with ultraviolet light. All used plastics and equipment were treated by UV light radiation for a minimum of 10 minutes prior to the experiment being performed to remove any residual nucleic acids.

DNA concentration was measured using a Nanodrop (Thermo scientific) spectrophotometer and 200 ng was diluted in 8 µl of distilled water (diH_2O). In all experiments a test sample was included where instead of DNA, the equivalent volume of water was used in order to assess if there was contamination of reaction mix or water.

The RT-PCR reaction was performed in a Thermo Hybaid MBS thermo cycler (Thermo Electron Corporation). Reactions were performed in 0.2 ml thin walled tubes (Bioplastics). The reaction mix was composed of: 0.5 µM forward and reverse primers, 0.25mM dATP, dTTP, dCTP and dGTP (GE Healthcare), 1.5 mM Mg Cl2, 20 mM Tris-HCl (pH 8.4), 50 mM KCl, 1 U of Platinum Taq DNA Polymerase (Invitrogen Life Technologies), 20 µg/ml of acetylated BSA (Promega), 0.15% (v/v) Triton X-100 and diH2O to make up the final volume to 12 µl.

The cycling parameters used were 94 °C for 90 seconds; followed by the annealing step for 20 seconds, which was dependent on the primer set chosen (Table 2.3); and 72 °C for 2 minutes. Cycles were repeated 35 times. There was a final extension period at 72 °C for 7 minutes and samples were maintained at 4°C.

2.4.3 Quantitative polymerase chain reaction (qPCR)

Amplification of DNA for qPCR was performed in an Opticon Monitor 2 (bio-rad) real-time PCR machine. The qPCR reaction mix was composed of: 0.5 µM forward and reverse primers, 0.25mM dATP, dTTP, dCTP and dGTP (GE Healthcare), 1.5 mM Mg Cl2, 20 mM Tris-HCl (pH 8.4), 50 mM KCl and 1 U of Platinum Taq DNA Polymerase (Invitrogen Life Technologies), 20 µg/ml of Acetylated BSA (Promega), 0.15% (v/v) Triton X-100, 0.5x Sybr Green (Lamb Bioscience) and diH2O to a final volume of 12 µl. DNA concentration of samples to be tested was determined as described in Section 2.4.1. In all experiments a test sample was included where instead of DNA, the equivalent volume of water was used in order to assess if there was contamination of reaction mix or water.

The cycling parameters used were: a hot start at 94 °C for 10 minutes followed by either 35 or 40 cycles of amplification. The cycling parameters used were dependent on the experiment type. Where the target DNA was found to be higher, as in viral genomic DNA experiments, 35 cycles of amplification were performed. Where the target DNA was found to be lower, as in the quantification of cytokine expression, 40 cycles of amplification were performed.

The amplification cycles consisted of a DNA denaturation step at 94 °C for 10 seconds followed by an annealing step. The annealing temperature chosen was dependent on the primer sets used (Table 2.3). The annealing temperature was maintained for 20 seconds and followed by an extension period at 72 °C for 15 seconds. A step at 75 °C for 1 second was included to melt off possible primer-dimers, before the plate was read. At the end a melting curve analysis was performed between 65 °C and 95 °C with 0.2 °C increments every one second.

Where necessary, primer optimization was performed using the thermal gradient feature in the PCR machine to evaluate which was the optimal annealing temperature. The protocol used was decided based on the lowest cycle threshold (Ct) value obtained in the quantification curve, without evidence of primer-dimer formation in the tested sample. The latter was confirmed by checking the size of the PCR product by agar gel

electrophoresis. This was especially important because the used primers for cytokine expression studies were designed against laboratory mouse strain sequence data. Even though in the wood mouse, the species studied, a high degree of similarity is assumed, it was necessary to confirm this. Primer specificity was confirmed by gel electrophoresis of qPCR products

Primer set	Sequence	Annealing temperature	Product size
L8[9] (MWG Biotech)	F: 5'- CAGTGAATATCGGCAATGTTTTG-3' R: 5'- TTCACTCGAGTCTTCTTGGTCTC-3'	60 °C	163 bp
L8 int[9]* (Sigma Aldrich)	F: 5'- ACAGAGCCGTTGTTGGTGTTGT-3' R: 5'- CAGTTCCTCTTTGCCTTGTACT-3'	60 °C	100 bp
gp150[9] (MWG Biotech)	F: 5'CTACTTCTTCATCGGACGCT-3' R: 5'CGGGATCTGTCGGACTGT-3'	60 °C	159 bp
ORF 73	F: 5'-ATGGCTGCTGGTTTGTTGAAGC -3' R: 5'- CCACATCCCCACCGACTAC -3	60 °C	88 bp
M1* (MWG Biotech)	F: 5'-TTGTAAGGGTACTCTCATCACC -3' R: 5'- TAGAGGCGCAGCTGTAGATG --3'	60 °C	1726 bp
M1 (MWG Biotech)	F: 5'-GACTGCCCTTGTCACTTTTC-3' F: 5'-CCAGGTAAGAGATCCTGTGT-3'	60 °C	127 bp
TNF-α (Sigma Aldrich)	F: 5'-CAC CAC CAT CAA GGA CTC AA3' R: 5'-GAC AGA GGC AAC CTG ACC AC--3'	60 °C	100 bp
IFN-γ[311] (Sigma Aldrich)	F: 5'- TAGCTCTGAGACAATGAACGCTAC -3' R: 5'- GTGATTCAATGACGCTTATGTTGT -3'	62 °C	302 bp
IL-10[312] (Sigma Aldrich)	F: 5'- TTTAAGGGTTACTTGGGTTGC-3' R: 5'- TCAAATGCTCCTTGATTTCTG-3'	60 °C	120bp
MIP1-α[313] (Sigma Aldrich)	F: 5'-GCCCTTGCTGTTCTTCTCTGT-3' R:5'-GGCAATCAGTTCCAGGTCAGT--3'	60 °C	258 bp
MIP1-β[314] (Sigma Aldrich)	F: 5'-CCTGACCAAAAGAGGCAGAc-3' R : 5'-GAGGAGGCCTCTCCTGAAGT--3'	60 °C	134 bp
Arginase I[146] (Sigma Aldrich)	F: 5' -TTGCGAGACGTAGACCCTGG-3' R: 5'- CAAAGCTCAGGTGAATCGGC-3'	60 °C	160 bp
iNOS[146] (Sigma Aldrich)	F: 5 ' -GCCACCAACAATGGCAACA--3' R: 5 ' -CGTACCGGATGAGCTGTGAATT-3 '	60 °C	103 bp
TGF-β[312] (Sigma Aldrich)	F: 5'- TCAGCTCCACAGAGAAGAACTG -3 R: 5'- AAGTTGGCATGGTAGCCCTTG -3'	60 °C	106 bp
Rantes[315] (Sigma Aldrich)	F: 5'-AAGATCTCTGCAGCTGCCCTC-3' R: 5'-TTGAACCCACTTCTTCTGTGG--3'	65 °C	243 bp

Table 2.3 List of used primers in PCR reactions

Footnotes: * refers to primers only used in RT-PCR reactions; **refers to sequence of ribosomal protein mRNA, but these primers do not contain the intron sequences to enable specificity towards cDNA yielded from RNA and not genomic DNA.

2.4.3.1 Establishment of qPCR standard for assessment of viral load

To assess viral load, PCR-amplification of vgp150, a viral glycoprotein, was performed. To normalize the input DNA between different samples, amplification of RPL8, a ribosomal protein, was performed within the same experiment.

To quantify the DNA amplified, serial dilutions (from 10^8 to 10^3 copy numbers) of known plasmid concentrations containing the genes of interest were performed. The plasmid concentration was assessed by the measurement of the absorbance using a nanodrop and the known molecular weight of the plasmid plus gene insert using the equation on Figure 2.5

Molecular weight (Da)=(bp of plasmid + insert)(330 Da x 2 nucleotide per bp)

$$\text{Molecular weight of 1 Copy number} = \frac{\text{Molecular weight in Daltons}}{\text{Avogrado's number}}$$

$$\text{Avogrado's number} = 6.02214199 \times 10^{23}$$

$$\text{Concentration of plasmid (copies/µl)} = \frac{\text{Absorbance (g/µl)}}{\text{molecular weight of 1 copy number}}$$

Figure 2.5 Equation used to calculate the plasmid concentration
Avogadro's number represents the number of protons present in one mole and 330 Da is the weight in Daltons of a single nucleotide.

2.4.3.2 Analysis of qPCR results

Analysis of the qPCR results was based on the fluorescence measured at each cycle. In the case of the samples of known concentrations, these measurements enabled the construction of standard curves.

In order to assess whether the standard curves were acceptable, a straight line was drawn crossing the curves Ct values (threshold line) at a point where the magnitude of the signal is higher than the background and increases exponentially (Figure 2.6 A).

Using the Ct value and the base 10 logarithm of the initial copy numbers, a straight line was automatically plotted, which is the standard graph plot (Figure 2.6 B). In order to further verify the correct positioning of the Ct line, the y and the r^2 values

yielded from this plot were used. Y represents the line equation: y = mx+b where m is the slope and b the y-intercept and it should be close to -0.3 when perfect doubling has occurred. On the other hand, r^2 (square of correlation coefficient), indicates the proximity of the data points to the regression line and it should be close to 1, optimally greater than 0.990.

Melting curve analysis (Figure 2.7) was also performed on all reactions, including test reactions, and examined for abnormal peaks indicative of primer-dimer complex formation. Also, melting temperatures were examined and were accepted only if they were in the region of 86° for RPL8 and 82° for gp150 primed reactions.

The efficiency of qPCR reactions was also monitored. Efficiencies were accepted when equal or greater than 70%, the optimal being 100%. DNA quantification of test samples was based on a comparison of their Ct values and those of the standard curves.

To ensure that the copy number retrieved for the target gene referred to the same DNA loaded into the reaction, the housekeeping gene values were used as calibrators of input DNA. The correction value was determined by dividing by the lowest copy number of the reference gene. All the values obtained for the gene of interest were then divided by the corresponding correction value.

When standard curves were not available analysis of qPCR results was performed using the Pfaffl equation [316] represented in the Figure 2.8.

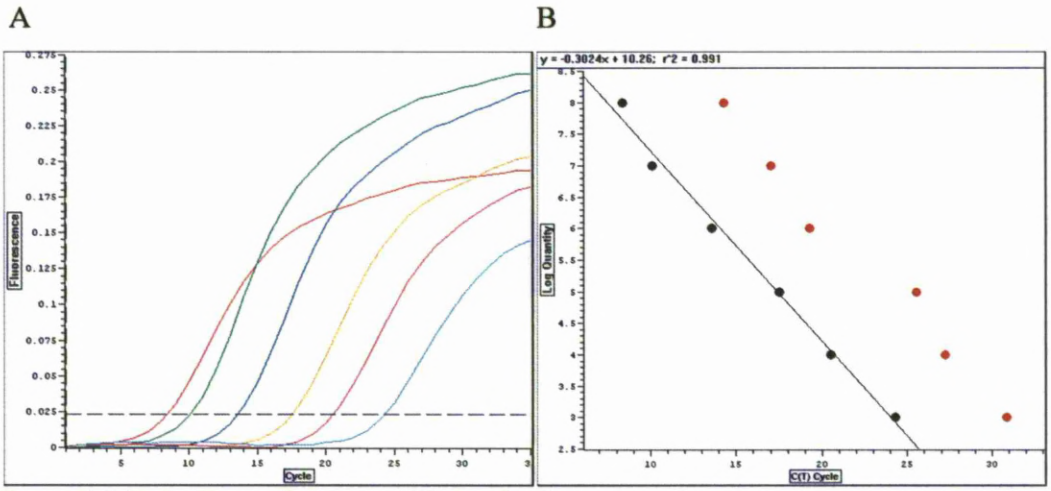

Figure 2.6 Left: Example of a gp150 standard curves.
A: Fluorescence curves of plasmids at different concentrations. The dilutions of plasmid used were sequential tenfold dilutions from 10^3(red line in A) until 10^8 (light blue line in A) ; Threshold represented by dashed line; B: Standard curve line equation with r^2 value on top. Y axis represents fluorescence measured and X axis represents cycle numbers

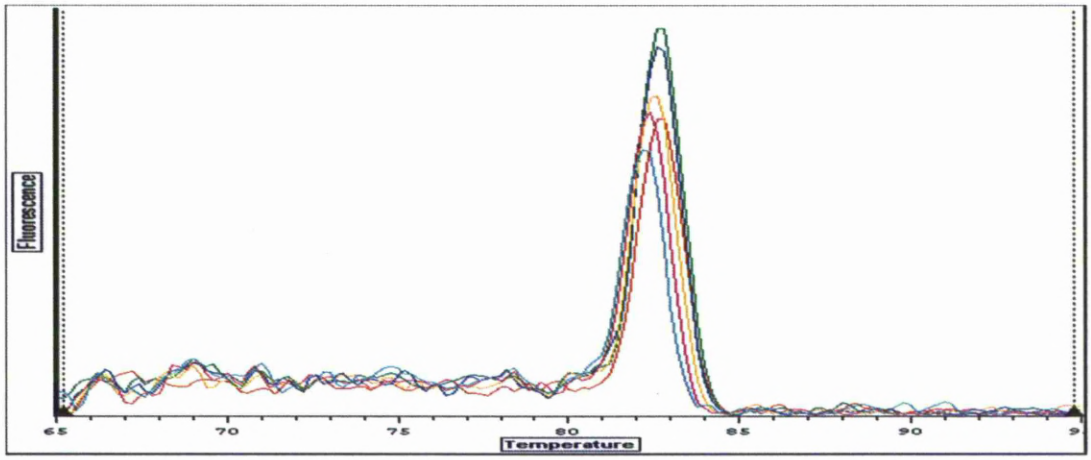

Figure 2.7 Melting curve of the standards represented in Figure 2.6. Y axis represents fluorescence measured and X axis represents temperature in °C.

$$Ratio = \frac{(E\ target\ gene)^{\Delta\ CP\ (control-sample)}}{(E\ reference\ gene)^{\Delta\ CP\ (control-sample)}}$$

Figure 2.8 Pfafl equation.
Footnotes: (E) refers to mean of reaction efficiencies in samples examined

2.4.4 Agarose gel electrophoresis

Agarose gels were prepared by adding 0.8 g of molecular biology grade agarose (Invitrogen Life Technologies) to 100 mls of TAE buffer (40 mM Tris base, 20 mM Glacial Acetic acid, 1 mM EDTA) and microwaving at medium power for 10 minutes. This was cooled to 55 °C in a water bath and 0.01x ethidium bromide added before pouring into an electrophoresis system gel tank. The gel was allowed to set at room temperature. TAE buffer was added to the tank until it covered the gel by a few mm. Each amplification product (10μl) was mixed with 1 μl of loading dye (50% (v/v) glycerol, 100 mM Tris-HCl, 10 mM EDTA, 0.02% (w/v) Orange G dye). A 1Kb Plus® DNA ladder (Invitrogen Life Technologies) was also loaded to enable the determination of PCR product size. The gel was run at approximately 5 - 7 V/cm. The run was stopped after migration of at least 5 cm had occurred. The gel was then visualized on a UV transilluminator (BioRad) at a wavelength of 302 nm. Images were recorded using GeneSnap software (Syngene). Specificity of the product was also determined by evaluating band yields per product lane.

2.4.4.1 Agarose gel electrophoresis of RNA

When gel electrophoresis was performed on RNA samples, denaturation of RNA was performed by incubating it at 65°C for 5 minutes. Also, 1.8ml of 37% (v/v) formaldehyde (to degrade secondary structures) was added per 100ml of 1% (w/v) agarose gel. The running buffer used was 1 x MOPS (3-(N-morpholino) propanesulfonic acid) buffer as it has a neutral pH and RNA is more susceptible to alkali cleavage than DNA. 200 ηg RNA was mixed with 5x RNA loading buffer and loaded into the respective electrophoresis gel lane. Amplification product was mixed with loading dye (50% v/v glycerol, 100 mM Tris-HCl, 10 mM EDTA, 0.02% (w/v) Orange G dye) and loaded onto a 0.8 % (w/v) agarose gel with 0.1 μg/ml of ethidium bromide (Sigma). A Kb Plus® DNA ladder (Invitrogen) was also loaded within the same experiment. Electrophoresis was performed on a horizontal tank containing MOPs. Gel electrophoresis ran at approximately 5-7 V/cm and was stopped after migration of at least 5 cm had occurred. The gel was then visualized on a UV transilluminator (Figure 2.9). RNA integrity was assessed by the clear demarcation of the 28S and 18S ribosomal RNA (rRNA) bands. Optimally the first should be twice as strong as the second, as 18S is more labile, if this is not the case or these are smeared, it

is representative of RNA degradation. The molecular size of the reaction products were estimated by comparison with the ladder. Specificity of product was also determined by evaluating band yields per product lane.

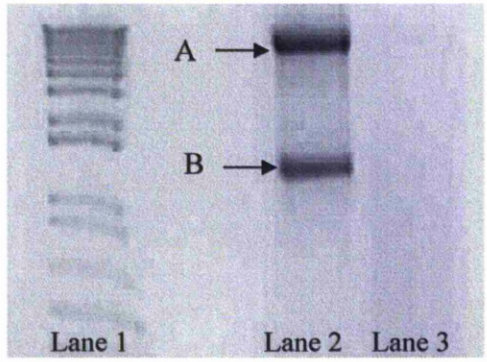

Figure 2.9 Agarose gel electrophoresis showing intact and degraded RNA.
Lane 1 was loaded with Kb Plus® DNA ladder. Lanes 2 and 3 were loaded with 2 µg of total RNA. Lane 2 shows intact RNA which exhibits two well demarcated bands, corresponding to the 18S rRNA (A) and 28S rRNA (B). Lane 3 shows degraded RNA, which appears as a lower molecular weight smear.

2.4.5 Synthesis of DIG-labelled probes for RNA *in situ* hybridisation

Template DNA (plasmid with inserted sequence of interest) was incubated at 37°C for two hours with endonucleases with activity upstream and downstream from the sequence of interest (see Table 2.4). Notably, the incubation temperature for SmaI digest was 25 °C and not 37 °C as the other enzymes.

The sequence of interest consisted of the entire M1 or M3 ORF amplified from MHV-68 DNA and cloned into pCRII (Invitrogen)[9] or transcripts to the MHV-68 vtRNA genes 1-4 within plasmid pEH1.4[269].

Digests were performed in a total volume of 100 µl, using 10 µl of DNA, 10 µl of the appropriate enzyme (10U), 10 µl of the recommended enzyme buffer and 70 µl of diH_2O.

Gene	Vector	Enzyme for sense probe	Enzyme for anti- sense probe
MHV-68 vtRNA 1.4	pBluescript	EcoRI (Biolabs)	HindIII (Roche)
sPLUNC	pBluescript	SmaI* (Biolabs)	EcoRV (Biolabs)
M1	pcr II TOPO	EcoRV (Biolabs)	BamH1 (Biolabs)
M3	pcr II TOPO	EcoRV (Biolabs)	BamH1 (Biolabs)

Table 2.4 Restriction digest enzymes used to cut template DNAs used in the synthesis of vtRNA, sPLUNC, M1 and M3 RNA probes.
Footnotes:* incubation temperature for SmaI digest was 25 °C and not 37 °C as the other enzymes.

To test if the correct sequence was obtained, agarose gel electrophoresis was performed. The linear templates were then transcribed into a DIG-labelled RNA probe using the DIG RNA labelling kit (Roche). To remove the DNA template, RNase-free DNase I (Roche) was added to the solution and incubated for 15 minutes at 37°C. This was followed by a phenol-chloroform extraction. In order to produce short riboprobes, alkaline hydrolysis was initiated. 5 µl of 0.4M sodium bicarbonate (Sigma) was added and incubated at 60°C for the time value (T) obtained using the equation in Figure 2.10. The reaction was stopped by neutralization with 5µl of 3M ammonium acetate (Sigma) and followed by ethanol precipitation.

$$T = \frac{Li - Lf}{K \times Li \times Lf}$$

Figure 2.10 Formula used for calculation of incubation time for hydrolysis
K is 0.11 Kb/min; Li: initial length of the fragment (Kb); Lf desired final length (Kb).

Probes were produced and labelled RNA probes, including a positive control (Roche) were tested by dot-blot using Hybond H+ (Amersham Bioscience) membrane. Serial dilutions of the riboprobes were applied to the membrane and then fixed through the use of UV Stratalinker (Stratagene). The membrane was incubated twice for five minutes in Buffer 1 (0.1 M maleic acid, 0.15 M NaCl) and once for 30 minutes in

Buffer 2 (Buffer 1 with 0.1% (v/v) casein blocking agent). The membrane was then incubated for an hour with a 1:5000 dilution of the antibody (alkaline phosphatase conjugated anti-DIG fab fragments (Roche) in Buffer 2). Next, the membrane was incubated for five minutes in Buffer 1 with 0.3% (v/v) Tween 20 and for five minutes in Buffer 3 (0.1M Tris-HCl, 0.1M NaCl, 50mM $MgCl_2$). Finally, the membrane was left in the dark in colour solution (45 µl of NBT (Sigma), 35µl of BCIP (Sigma), 10 ml of Buffer 3) until a positive reaction (colour change).

2.4.5.1 RNA *In situ* hybridisation (RNA-ISH)

RNA *In situ* hybridisation was performed following a protocol previously described[317].

2.4.5.1.1 Paraffin embedding of tissue samples

See section 2.5.3.

2.4.5.1.2 Proteolysis and post-fixation

Deparaffinization and re-hydration of samples was performed by sequential incubation of slides for 5 min in xylene (twice), 98% (v/v) alcohol (twice), 70% (v/v) alcohol and distilled water with 0.1% (v/v) DEPC (diethyl pyrocarbonate). An extra incubation in water with DEPC was performed for one minute followed by a wash in PBS for 5 minutes. Slides were incubated twice for 20 minutes in 0.2M HCl. This step was followed by incubation at 50 °C in 2x saline-sodium citrate buffer (SSC) and 5mM EDTA. Proteolysis was performed using 5µl of proteinase K diluted in a 60 ml solution of distilled water containing 0.1% (v/v) DEPC, 1ml of 1M Tris and 1ml of 0.1M $CaCl_2$. Slides were incubated in this solution for 15 minutes. Fixation of the slides was performed by incubation for 5 minutes in 0.2% (v/v) glycine-PBS solution followed by incubation for 4 minutes in 4% (v/v) paraformaldehyde and finally one minute incubation in 1x PBS and 5mM $MgCl_2$.

2.4.5.1.3 Acetylation

Acetylation was performed by incubation of slides for 10 minutes in 0.25% (v/v) acetic anhydride and 0.1M triethanolamine solution. This was followed by two washes for one minute and one wash for 15 minutes with PBS.

2.4.5.1.4 Pre-hybridisation and hybridization of riboprobes

Prehybridisation was performed by incubation of slides at 52 °C for at least 1 hour in a solution composed of 49.5 ml of prehybridisation buffer, 0.5 ml of 10 mg/ml ssDNA and 1ml of RNA. The prehybridisation buffer was prepared as a master stock containing: 450 ml of 20x SSC, 675ml of 100% deionized formamide, 150 ml of 50x Denharts solution and 210 ml of distilled water with 0.1% (v/v) DEPC-treated diH_2O.

Hybridisation was performed by overnight incubation in a moist chamber at 37 °C. The hybridization mixture volume was calculated so as to ensure the availability of 30 to 40µl of mix per tissue section. The buffer was prepared as a master stock with: 16 ml of 100% formamide, 8 ml of 20x hybridization salts, 3.2ml of 50x Denharts solution, 400µl 20U/ml heparine solution and 320µl of 10% (v/v) Triton X-100. Before application on to the samples, the buffer was prewarmed to 52 °C and 18µl of 250µg/ml of RNA, 20µl of 10mg/ml ssDNA, 0.5 to 1µl of RNA probe was added per 698µl of buffer. Samples were then covered with the hydrophobe surface of gel bond and the extremities of the bond fixed to the slide through the use of fixo-gum gel (Marabu).

2.4.5.1.5 Detection of hybridized riboprobes

Slides were washed by sequential incubation twice in 6xSSC, 45% (v/v) formamide at 42 °C for 15 min then twice in 2xSSC for 5 min and finally twice in 0.2xSSC for 15 min. Next, a one minute wash with Buffer 1 (100mM Tris and 100mM NaCl) was performed. This was followed by equilibration of the samples for 30 minutes in a solution of 1.2 ml of neutral sheep serum and 1.8 ml of 10% (v/v) Triton X-100 in 60ml of Buffer 1. Dilution of the antibody was performed by adding 15µl of anti-digoxinenin antibody, 31µl of neutral sheep serum and 94 µl of 10% (v/v) Triton X-100 to 3 ml of buffer 1. Incubation with antibody was then performed for two hours in a moist chamber. After incubation, slides were washed twice for 15 minutes in Buffer 1 and once for two minutes in Buffer 3 (100mM Tris, 100mM NaCl, 50mM Mg Cl_2).

Finally, samples were stained overnight by incubation in the dark (length of time dependent on speed of staining reaction) with 60 ml of Buffer 3 containing 150µl of NBT, 120µl of X-phosphate and 30 mg of levamisole. The staining reaction was stopped by washing the slides for 10 minutes in Buffer 4 (10mM Tris and 1mM EDTA) followed by a five minute wash in distilled water. Counter staining of samples was performed by incubation for 10 seconds with Papanicolau's haematoxylin solution. To remove all stain residues, slides were left in running water for five minutes. A coverslip was then placed on samples after application of one drop of warmed glycer-gel.

In the case of the M1 riboprobe, M1 RNA-ISH was also performed on one tissue section from a vM1stop-infected animal to assess if the synthesised riboprobe was specific for the M1 sequence. vM1stop virus has been designed to inhibit M1 expression. As expected, the experiment using M1 riboprobe in vM1stop-infected animals yielded no reaction. In all experiments both anti-sense (complimentary sequence) and sense (homologue sequence) riboprobes were used in order to control for nonspecific reactions and so assess sensitivity and specificity of reactions.

2.4.6 Transformation of plasmid

Plasmid (5µl) was added to a vial of competent Escherichia coli bacteria (XL1 Blue Stratagene), the mixture was mixed and then placed on ice for 30 minutes. The solution was heat-shocked at 42 °C for 60 seconds and then incubated on ice for five minutes. Next, the mixture was added to 800 µl of Luria-Bertani (LB) medium (1 % (w/v) tryptone, 0.5 % (w/v) yeast extract, 1 % (w/v) NaCl) with 50 µl/ml ampicillin and placed on a orbital shaker at 200 rpm, for 45 minutes. A 100 µl sample was spread on the surface of a 1% (w/v) LB with 50 µl/ml ampicillin agar plate (Sigma-Aldrich). The rest of this LB culture was centrifuged at 2000 g for five minutes and the pellet was resuspended in 100 µl LB medium and spread onto another LB with 50 µl/ml ampicillin agar plate. LB agar plates were incubated at 37 °C overnight. The next day, individual colonies were cultured using 10 ml LB medium containing 50 µg/ml ampicillin and incubated at 37 °C in an orbital shaker at 200 rpm overnight.

2.4.7 Plasmid purification

For plasmid purification, the QIAGEN Plasmid Maxi Kit (Qiagen) was used. The 10 ml LB medium starter culture (containing plasmid transformed bacterial culture) was added to 400 ml LB medium containing 50 µg/ml ampicillin in a two litre Erlenmeyer

flask and incubated at 37 °C in an orbital shaker at 200 rpm overnight. The next day, the culture was centrifuged at 6000 g for 10 minutes at 4 °C. The pellet was resuspended in 10 ml buffer P1 (50 mM Tris-Cl [pH 8.0], 10 mM EDTA, 100μg/ml RNase A). Lysis of bacteria was induced by addition of 10 ml of buffer P2 (200 mM NaOH, 1 % [w/v] SDS and incubating it for five minutes at room temperature. Then 10 ml of neutralisation buffer; buffer P3 (3 M potassium acetate [pH 5.5]) was added and the mixture was incubated on ice for 20 minutes. This was followed by centrifugation at 20,000 g for 30 minutes at 4 °C. The supernatant containing the DNA was collected and centrifuged once more at 20,000 *g* for 15 minutes at 4 °C The supernatant was then added to an equilibrated QIAGEN-tip 500 (10 ml buffer QBT (750 mM NaCl,50 mM MOPS (pH 7.0), 15 % (v/v) isopropanol, 0.15 % (v/v) Triton X-100) and was filtered by gravity flow. The tip was washed twice with 30 ml of buffer QC (1 M NaCl, 50 mM MOPS (pH 7.0), 15 % (v/v) isopropanol). DNA was then eluted using 15 ml buffer QF (1.25 M NaCl, 50 mM Tris-Cl (pH 8.5), 15 % (v/v) isopropanol). Isopropanol (10.5 ml Sigma) was added to the eluate and the mixture centrifuged at 15,000 g for 30 min at 4 °C and the supernatant was removed. The pellet was washed with 5 mls of 70 % (v/v) ethanol and centrifuged again at 15,000 g for 10 minutes. After removal of supernatant, the pellet was air dried and the DNA dissolved in 500 μl TE buffer (pH 8.0). The yield of DNA was calculated using the Nanodrop (Thermo Scientific).

3. Results

3.1 Analysis of M1 expression in a natural host and on a artificial host

M1 RNA *in situ* hybridization (RNA-ISH) was performed to determine and compare the extent and sites of M1 transcription. M1 is the protein of interest in this study. Viruses are highly adapted to their host[150] and gammaherpesviruses are thought to have developed in parallel with their host[18]. In the wild, MHV-68, a gammaherpesvirus has been found to infect the wood mouse (*Apodemus sylvaticus*)[5, 19, 293] but not the mouse (*Mus Musculus*)[293, 318]. Laboratory mouse strains such as BALB/c mice are derived from *Mus Musculus*. The hypothesis tested was that the transcription of M1 would be different in a natural and in an artificial host.

Lung, the main site of acute infection; and the spleen, the main site of latent infection, were examined for M1 expression. The times chosen, were representative of acute infection (day 3, 5, 7, 10 p.i) and latent infection (day 14, 28 and 40 p.i).

3.1.1 Day 3

Wood mice

At day 3 p.i. in the lung of wood mice, expression of M1 was detected in occasional airway epithelial cells, interstitial macrophages and alveolar epithelial cells (type I pneumocytes) (Figure 3.1). In the spleen, expression of M1 occurred in a few lymphocytes scattered in follicles and disseminated in the red pulp. In the red pulp, M1 transcripts were also observed in disseminated macrophages and megakaryocytes (Figure 3.1).

BALB/c mice

At day 3 p.i. M1 expression was also monitored in the lung and spleen of BALB/c mice. In the lung of BALB/c mice, M1 mRNA was detected in scattered both alveolar epithelial cells (type I pneumocytes) and scattered interstitial macrophages. Furthermore, expression was also noted in the lungs in slender cells lining vessels (endothelial cells) and intravascular lymphocytes attached to endothelial surface (rolling) or in the pulmonary interstitium adjacent to vessels (Figure 3.2). In the spleen, M1 mRNA was detected in lymphocytes and macrophages within follicles and in the red pulp in close proximity to follicles (Figure 3.2).

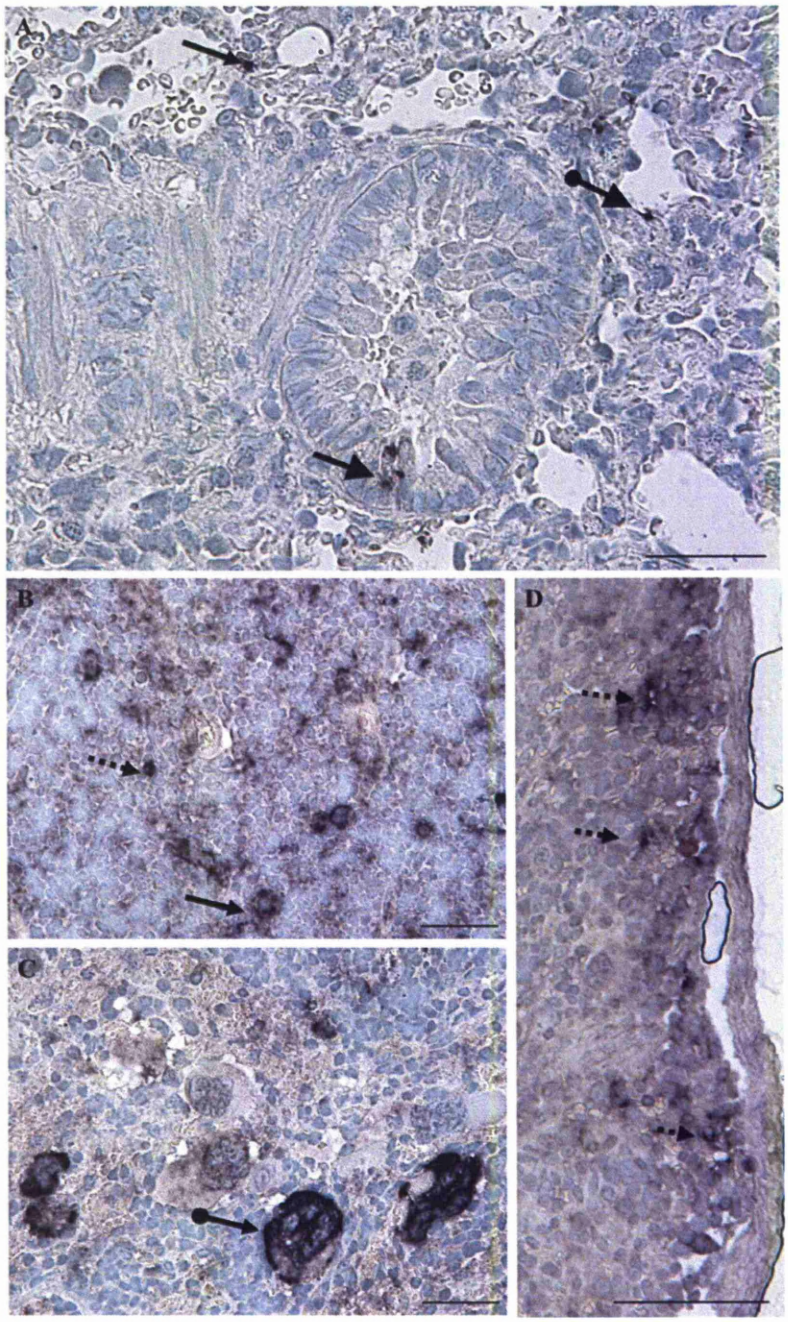

Figure 3.1 Wood mouse, day 3 p.i. Lung and spleen. M1mRNA expression.
A. Lung M1mRNA expression in airway epithelial cells (full arrow head with square tip), in macrophages (full arrow) and type I pneumocytes (full arrow head with round tip); B-D. Spleen M1 mRNA expression in lymphocytes (dashed arrows) in the red pulp (B, C) and in follicles (D). In the splenic red pulp (B, C), expression is also seen in macrophages (full arrow) and megakaryocytes (full arrow head with square tip). RNA-ISH, NBT/BCIP, Papanicolaou's haematoxylin counterstain. Bars: A,B,C= 25μm; D= 100μm

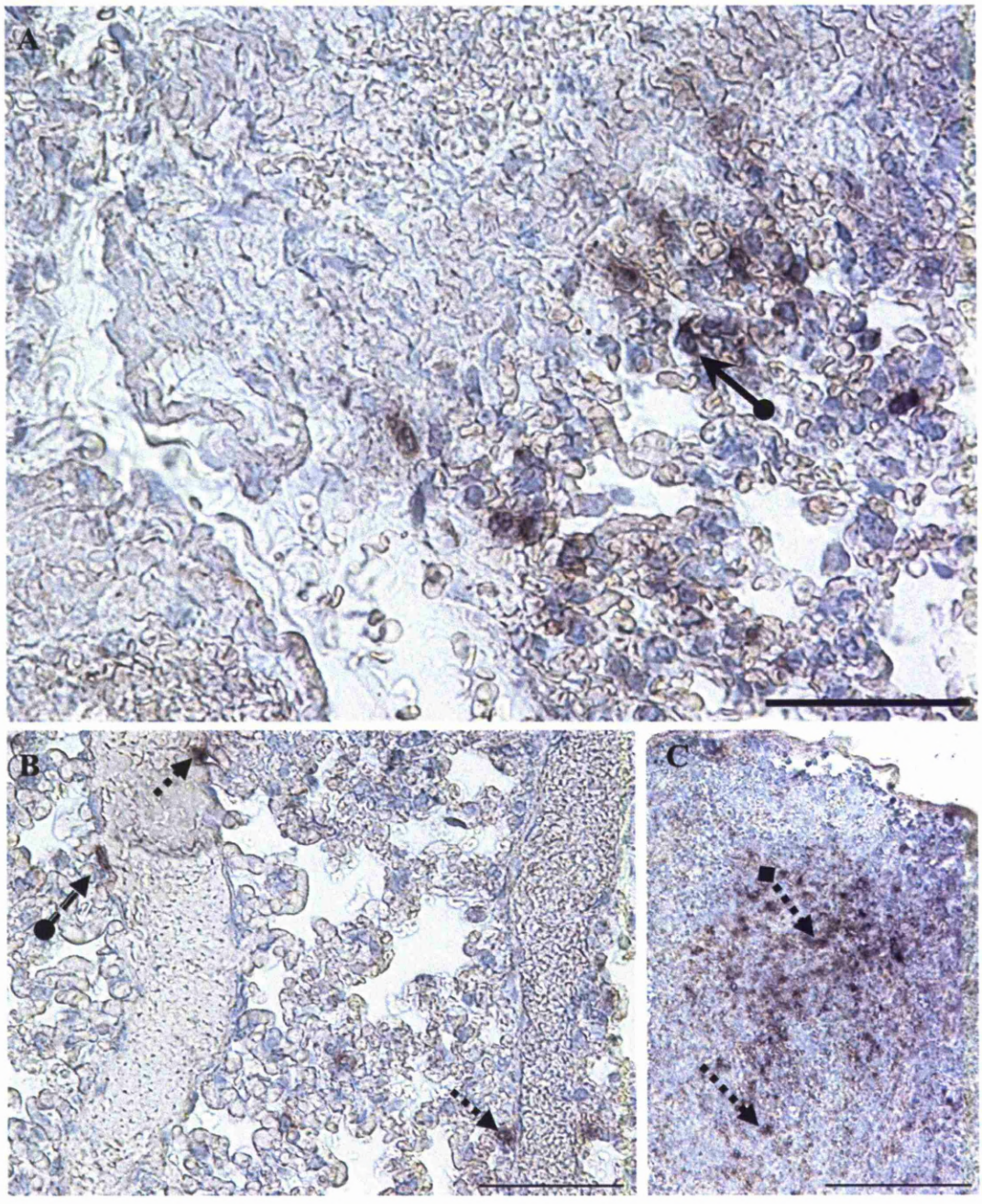

Figure 3.2 BALB/c mouse, day 3 p.i. M1mRNA expression.
A,B. Lung M1mRNA expression in the lungs in scattered interstitial macrophages (full arrow), lymphocytes (dashed arrows), type I pneumocytes (full arrow head with round tip) endothelial cells (dashed arrow with round tip); C. Spleen M1 mRNA expression in lymphocytes in the red pulp (dashed arrow) and in follicles (dashed arrow with square tip). RNA-ISH, NBT/BCIP, Papanicolaou's haematoxylin counterstain. Bars= 50μm.

3.1.2 Day 5

Wood mice

At day 5 p.i. in the lung of wood mice, M1 transcripts were detected in airway epithelial cells (bronchiolar, bronchial and tracheal), intravascular rolling lymphocytes (migrating), alveolar epithelial cells (type I and type II pneumocytes) interstitial macrophages and lymphocytes. Notably, the overall number of cells in the lungs that expressed the M1 transcript was greatly increased by day 5 compared to the day 3 timepoint (Figure 3.3 A-C). Furthermore, in the spleen (Figure 3.3 D), M1 expression was observed in numerous lymphocytes in germinal centres, in the periphery of follicles and to lesser extent in the red pulp. In the red pulp, M1 expression was also detected in disseminated macrophages and megakaryocytes. This pattern of expression in the red pulp was similar to what was observed on day 3 p.i.

BALB/c mice

At day 5 p.i. in the lung of BALB/c mice, expression of M1 was inconspicuous. In the spleen, a few lymphocytes within splenic follicles were found to exhibit M1 mRNA (Figure 3.4).

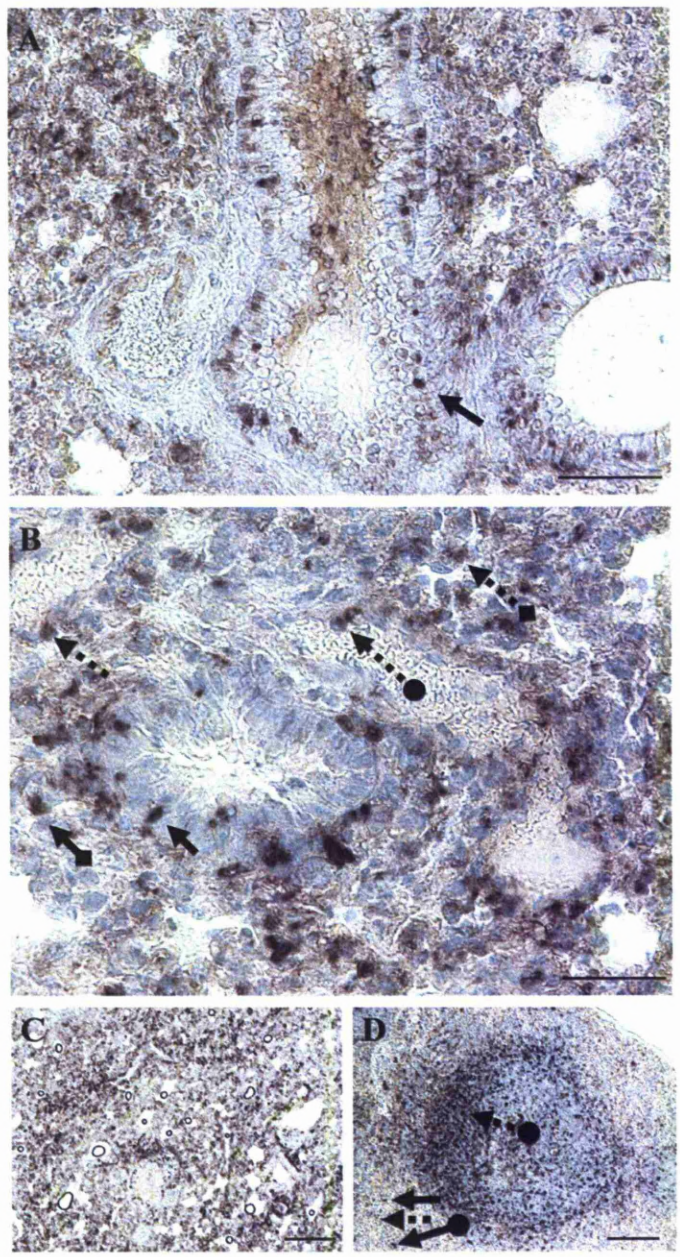

Figure 3.3 Wood mouse, day 5 p.i. Lung M1mRNA expression.
A-C: Lung, M1mRNA expression in airway epithelial cells (full arrow), round intravascular lymphocytes (dashed arrow with round tip), pneumocytes (dashed arrow with square tip), interstitial macrophages (full arrow with square tip) and interstitial lymphocytes (dashed arrow). C: Spleen, M1 mRNA expression in lymphocytes in germinal centres (dashed arrow with round tip), in the periphery of follicles and red pulp (dashed arrow). In the red pulp M1 expression was also seen in disseminated macrophages (full arrow) and megakaryocytes (full arrow with round tip). RNA-ISH, NBT/BCIP, Papanicolaou's haematoxylin counterstain. Bars: A= 50μm; B=25 μm; C= 250μm; D=100μm

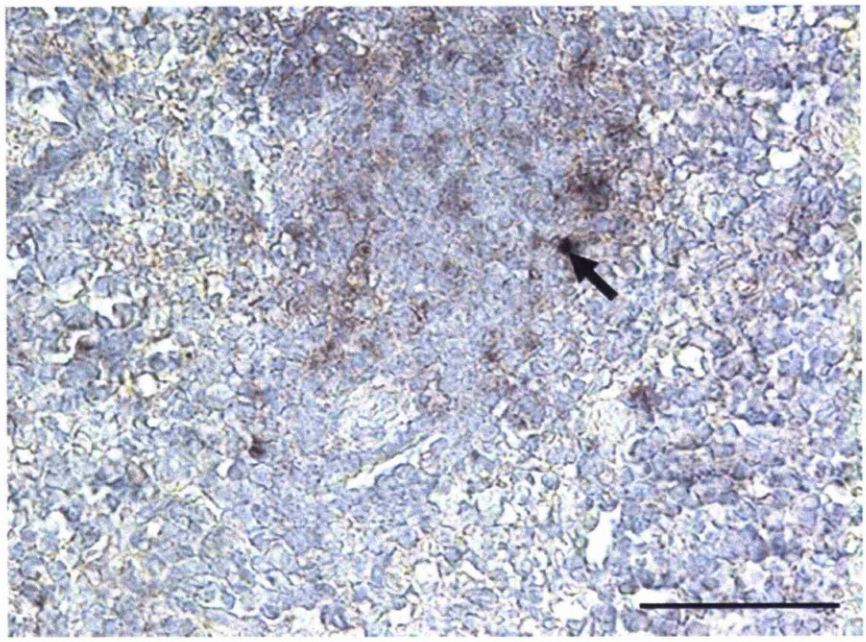

Figure 3.4 BALB/c mouse, day 5 p.i. Spleen M1mRNA expression.
M1mRNA expression in few lymphocytes (arrow) within splenic follicles. RNA-ISH, NBT/BCIP, Papanicolaou's haematoxylin counterstain. Scale bar= 25μm.

3.1.3 Day 7

Wood mice

At day 7 p.i. in the lungs of wood mice, M1 expression was seen in airway (bronchiolar, bronchial and tracheal - Figure 3.5 A) and alveolar epithelial cells (type I and type II pneumocytes) (Figure 3.5 C, D). M1 expression was highest in type II pneumocytes which were often binucleated. In the lungs, M1 expression was also observed in lymphocytes in the iBALT, pulmonary interstitium and rolling within vessels. Macrophages in the pulmonary interstitium and lining, or desquamated into the alveoli, also contained M1 transcripts (Figure 3.5 C). Satellite cells surrounding neuronal bodies in parabronchiolar ganglia expressed M1 transcript (Figure 3.6). Parabronchiolar ganglia were not present in all sections and this is likely related to their small size. As a result, the expression of M1 transcripts in these cells at earlier timepoints could not be ruled out.

In the spleen at day 7 p.i. there was little difference in the pattern of M1 transcript expression compared to day 5 p.i. Numerous lymphocytes in the germinal centres, in the periphery of follicles and to a lesser extent in the red pulp were noted as exhibiting M1 mRNA. M1 transcript expression was also noted in macrophages and megakaryocytes present in the splenic red pulp.

BALB/c mice

In the lung of BALB/c mice at day 7 p.i. M1 mRNA expression was restricted to scattered type I pneumocytes (Figure 3.7 A). In the spleen of infected BALB/c mice, M1 mRNA was detected in numerous lymphocytes within follicles (Figure 3.7, Panel B) and very rarely in the red pulp.

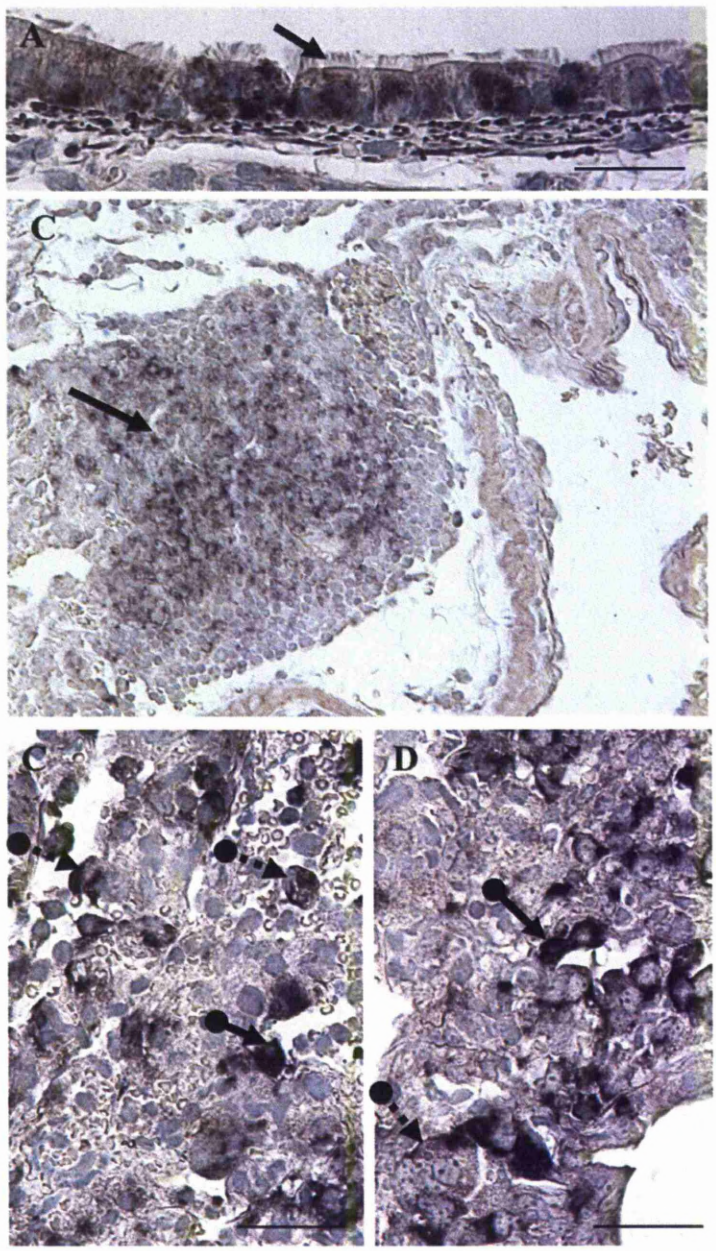

Figure 3.5 Wood mouse, day 7 p.i. Trachea and lung , M1mRNA expression.
A. Trachea, M1 mRNA expression in numerous ciliated (arrow) tracheal epithelial cells. B-D, Lung M1mRNA expression in lymphocytes in iBALT (full arrow in B), alveolar desquamated macrophages (dashed arrows with round tip in C), type II pneumocytes, (full arrow with round tip in C and D), including multinucleated pneumocytes (dashed arrow head with round tip in D), RNA-ISH, NBT/BCIP, Papanicolaou's haematoxylin counterstain. Bars: A, C, D= 25μm; B= 50μm; E=50 μm

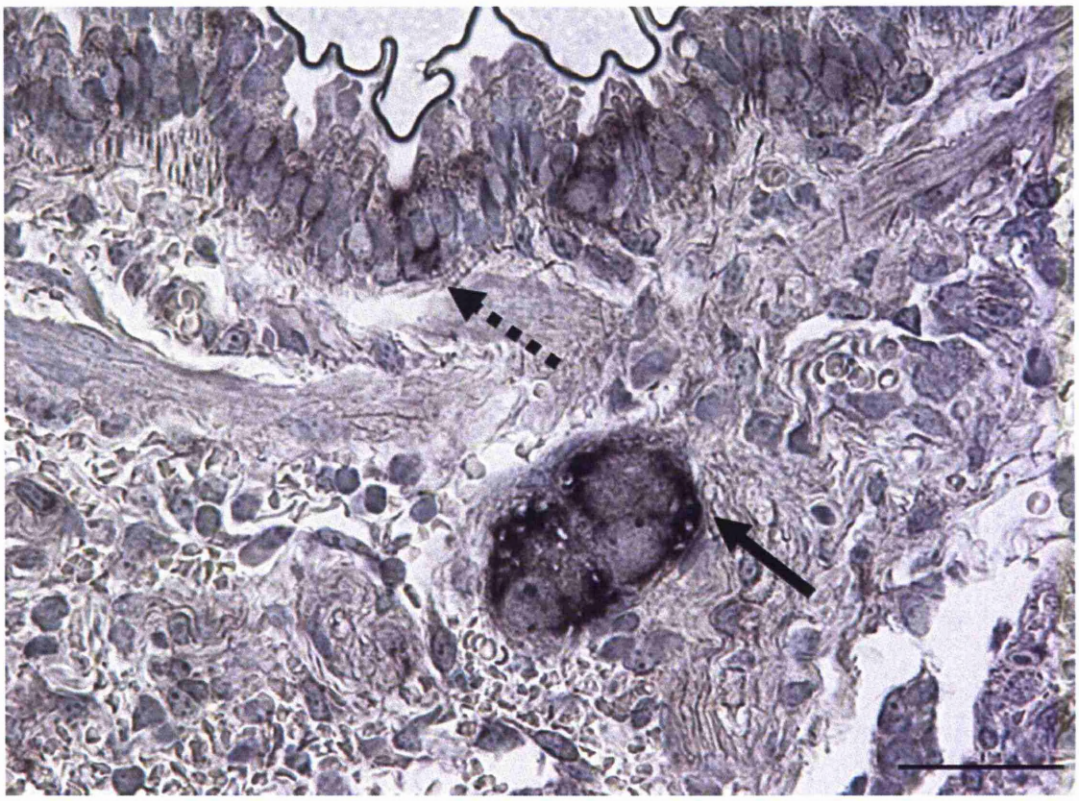

Figure 3.6 Wood mouse, day 7 p.i. Bronchus and adjacent ganglia, M1mRNA expression. M1 mRNA expression in ciliated bronchial epithelial cells (dashed arrow), and satellite cells surrounding neuronal bodies (full arrow) in parabronchiolar ganglia. RNA-ISH, NBT/BCIP, Papanicolaou's haematoxylin counterstain. Bar= 25μm

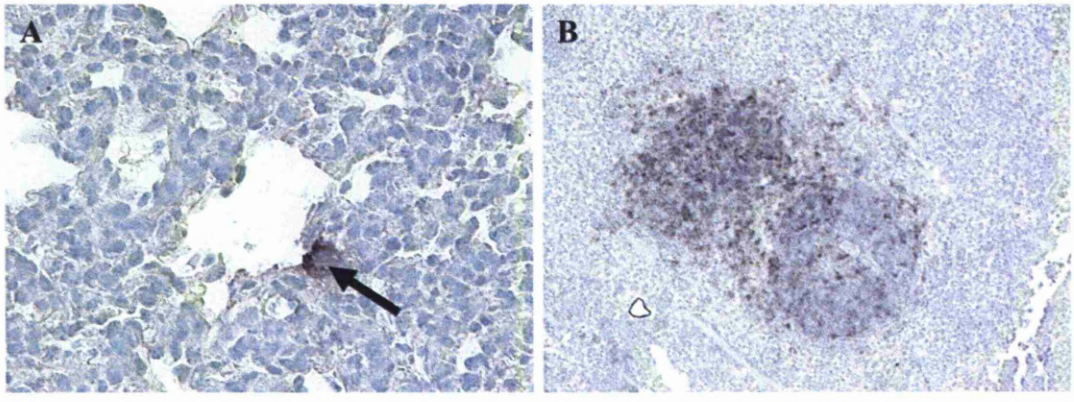

Figure 3.7 BALB/c mouse, day 7 p.i. Lung and spleen, M1 mRNA expression.
A. Lung, M1 mRNA expression in type I pneumocytes (arrow). B. Spleen, M1 mRNA expression numerous lymphocytes within follicles and very rarely in the red pulp. RNA-ISH, NBT/BCIP, Papanicolaou's haematoxylin counterstain. Bars: A= 25 μm; B= 100 μm

3.1.4 Day 10

Wood mice

In the lung of wood mice, expression of M1 mRNA was observed in the same type of cells on day 10 p.i. as described on day 7 p.i. These were airway (tracheal, bronchial and bronchiolar) epithelial cells, type I and type II pneumocytes. Expression in type II pneumocytes was more frequent than in type I pneumocytes. Within the lung, M1 transcript expression was also detected in lymphocytes in the iBALT, pulmonary interstitium and intravascularly but adjacent to the endothelium (rolling/migrating). Macrophages in pulmonary interstitium and lining/desquamated into the alveoli also exhibited M1 transcripts.

In the spleen, there was also little difference in the pattern of M1 expression at day 10 p.i. from that described at day 5 and day 7 p.i. Numerous lymphocytes in the germinal centres, in the periphery of follicles and to a lesser extent in the red pulp were observed to contain M1 mRNA. Macrophages and megakaryocytes present in the splenic red pulp were also seen to exhibit M1 transcript expression.

BALB/c mice

By day 10 p.i. in the lung of the BALB/c mouse, M1 mRNA expression was inconspicuous. Similarly to the findings on day 7 p.i. M1 mRNA expression was present in lymphocytes in splenic follicles and very rarely in the red pulp.

3.1.5 Day 14

Wood mice

By day 14 p.i. M1 mRNA expression in the lung of wood mice was detected mostly in airway (tracheal, bronchial and bronchiolar) epithelial cells, occasional type I and type II pneumocytes, lymphocytes within the iBALT and pulmonary interstitium. There was a marked decrease in the number of cells that expressed M1 transcripts in comparison to previous timepoints (Figure 3.8 A). The pattern of M1 expression in satellite cells surrounding neuronal bodies in parabronchiolar ganglia was similar to what was observed at day 7 p.i in that these on day 14 p.i. also expressed M1 mRNA. To a lesser extent than

that which was seen at day 10 p.i., at day 14 p.i., macrophages in pulmonary interstitium and lining/desquamated into the alveoli, also exhibited, M1 transcripts.

Within the spleen, numerous lymphocytes in the germinal centres and in the periphery of follicles, to a lesser extent in the red pulp, exhibited M1 mRNA. Macrophages and megakaryocytes present in the splenic red pulp expressed M1. At this time, cells in the splenic red pulp, mostly macrophages and lymphocytes, exhibiting M1 expression were more numerous than those seen in previous timepoints (Figure 3.8 B).

BALB/c mice

By day 14 p.i, in the lung of the BALB/c mouse, M1 mRNA expression was restricted to occasional lymphocytes in close proximity to bronchioles and/or vessels (Figure 3.9 A).

In the spleen, M1 expression was detected in lymphocytes within follicles (Figure 3.9 B). The pattern of M1 transcript expression was similar to what was observed at earlier timepoints.

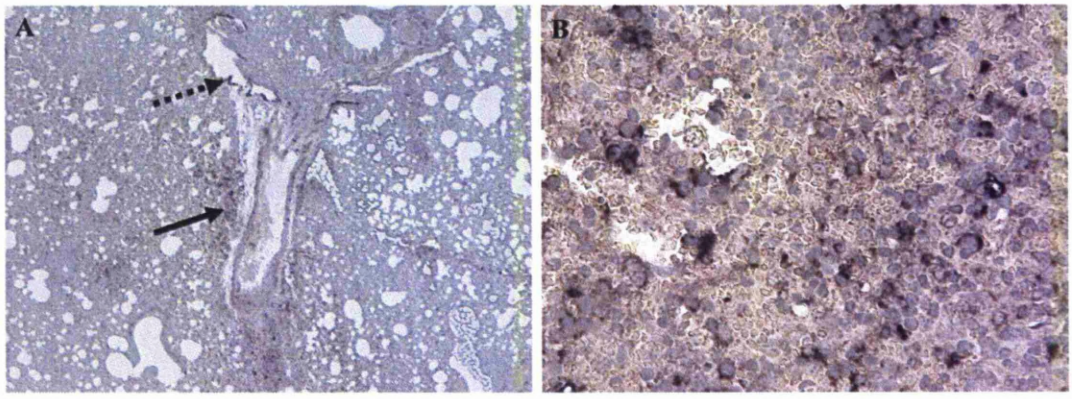

Figure 3.8 Wood mouse, day 14 p.i. Lung and spleen, M1mRNA expression.
A. Lung, M1 mRNA expression mostly in airway (dashed arrow) and lymphocytes within the iBALT. (full arrow).B, Splenic red pulp, overall frequency of cells, mostly macrophages, exhibiting M1 expression increased when compared to previous timepoints. RNA-ISH, NBT/BCIP, Papanicolaou's haematoxylin counterstain. Bars: A= 250 μm; B= 25 μm

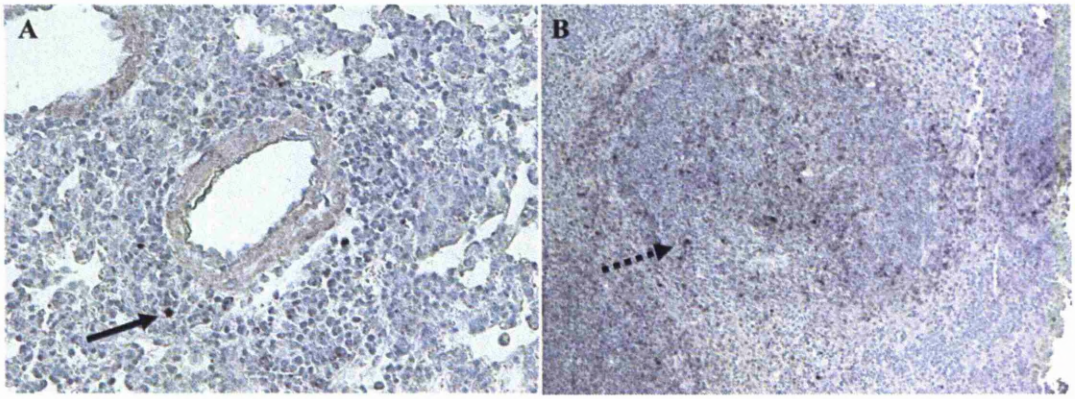

Figure 3.9 BALB/c mouse, day 14 p.i. Lung and spleen, M1mRNA expression.
A. Lung, M1 mRNA expression restricted to occasional lymphocytes in close proximity to vessel (full arrow); B. Spleen, M1 expression within follicles (dashed arrow). RNA-ISH, NBT/BCIP, Papanicolaou's haematoxylin counterstain. Bars: A= 25 μm; B= 100 μm

3.1.6 Day 28

3.1.6.1 Wood mice

At day 28 p.i similarly to day 14 p.i, in the lung of the wood mouse, M1 mRNA expression was observed mostly in airway (tracheal and bronchial) epithelial cells, occasional type I and type II pneumocytes, lymphocytes within the iBALT and pulmonary interstitium (Figure 3.10 A,B). Likewise, as described for day 14 p.i. occasional macrophages in pulmonary interstitium and lining, or desquamated into the alveoli, also exhibited, M1 transcripts.

In the spleen, M1 expression was seen in lymphocytes within follicles. Numerous lymphocytes in the germinal centres and in the periphery of follicles, to a lesser extent in the red pulp were seen to exhibit M1 mRNA. Macrophages and megakaryocytes present in the splenic red pulp were also seen to exhibit M1 expression. Similarly to day 14 p.i. the overall frequency of cells that exhibited M1 expression in the splenic red pulp, macrophages, lymphocytes and megakaryocytes, were increased when compared to day 3 and day 7 p.i (Figure 3.10 C).

3.1.6.2 BALB/c mice

BALB/c mice culled at day 28 were not included in this experiment.

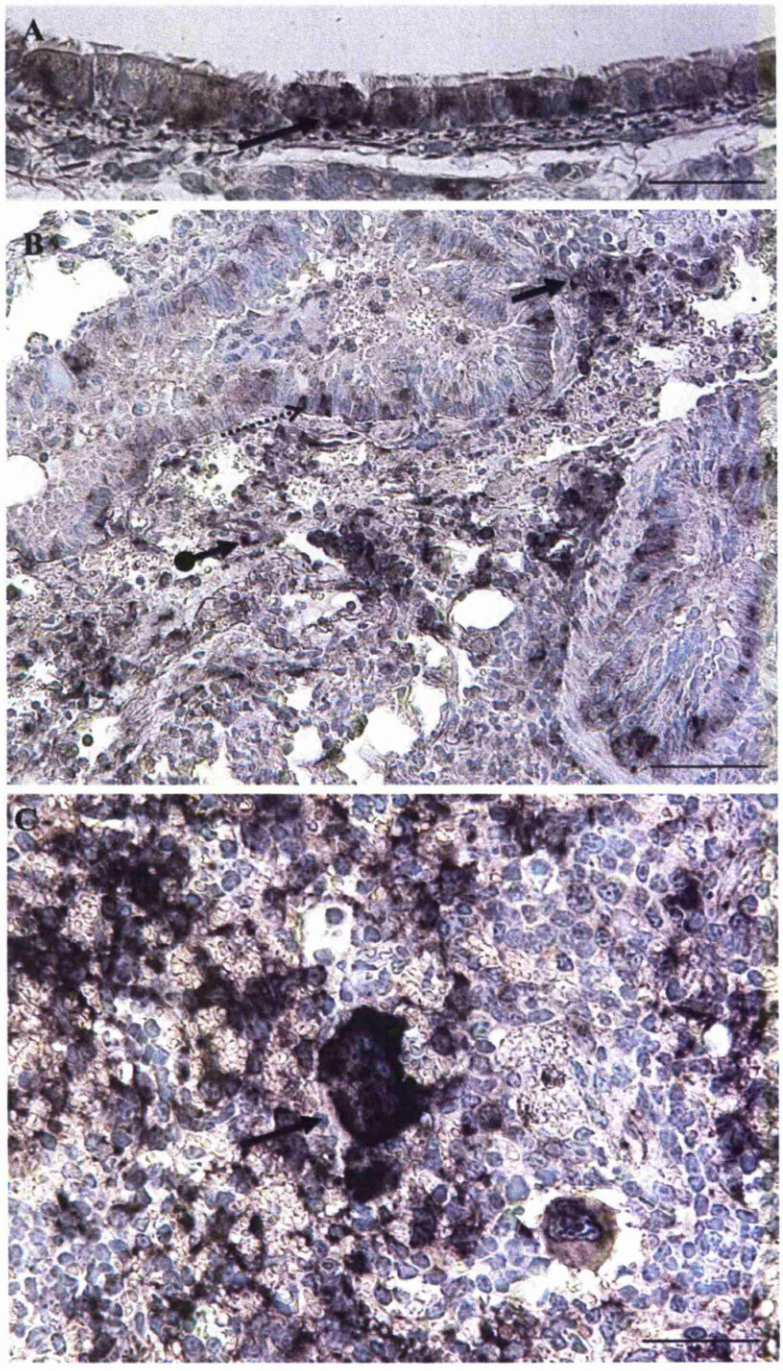

Figure 3.10 Wood mouse, day 28 p.i. Trachea, lung and spleen, M1mRNA expression.
A. Trachea, M1mRNA expression in ciliated tracheal epithelial cells (arrow) B. Lung, M1 mRNA expression mostly in airway (dashed arrow), alveolar epithelial cells (arrow with round tip) and lymphocytes within the iBALT. (full arrow). C, Splenic red pulp, overall frequency of cells, similarly to day 14 p.i. exhibiting increased expression when compared to day 3 and day 7 p.i. Arrow highlighting megakaryocytes showing presence of M1 transcript. M1 RNA ISH, NBT/BCIP, Papanicolaou's haematoxylin counterstain. Bars: A,C= 25 μm; B= 50 μm

3.1.7 Day 40

3.1.7.1 Wood mouse

At day 40 p.i, in the lung of the wood mouse, M1 mRNA expression was seen in very occasional lymphocytes present within iBALT (Figure 3.11 A) and within interstitium. M1 expression was lower at this time point than observed at earlier timepoints in infected lungs.

In the spleen, M1 expression was detected in lymphocytes within follicles and to a lesser extent in red pulp (Figure 3.11 B).

3.1.7.2 BALB/c mouse

At day 40 p.i, in the lung of the BALB/c mouse, M1 mRNA expression was seen in in close proximity to bronchioles and/or vessels. This pattern of expression was consistent with the pattern of expression exhibited at previous timepoints.

In the spleen M1 mRNA expression was inconspicuous.

3.1.8 Summary of M1 transcript expression analysis in the wood mouse and BALB/c mouse over a 40 day timecourse by RNA-ISH.

The findings of M1 transcript expression analysis by RNA-ISH in the lung and spleen of the wood mouse and BALB/c mouse are summarized in Table 3.1 and

Table 3.2.

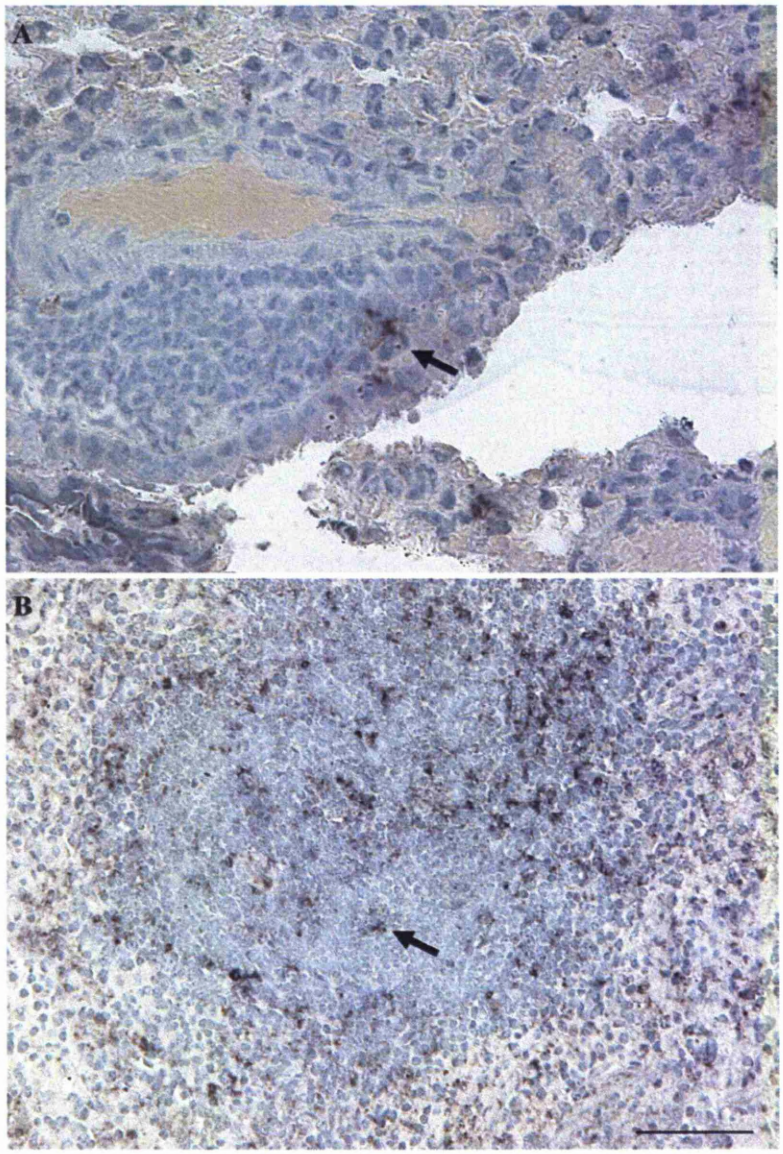

Figure 3.11 Wood mouse, day 40 p.i. Lung and spleen, M1mRNA expression.
A. M1 mRNA expression in occasional lymphocytes within the iBALT. (arrow).B, Spleen, M1 expression within follicles (arrow). In the red pulp, overall frequency of cells, exhibits decreased M1 expression when compared to day 14 and day 28 p.i. RNA-ISH, NBT/BCIP, Papanicolaou's haematoxylin counterstain. Bars= 25 μm

Days p.i.	Lung of wood mouse	Lung of BALB/c mouse
3	Airway epithelial cells (+) Type I pneumocytes (+) Macrophages, interstitial (+)	Endothelial cells (+) Type I pneumocytes (+) Macrophages, interstitial (+) Lymphocytes rolling (+) perivascular (+)
5	Airway epithelial cells (++) Type I pneumocytes (++) Type II pneumocytes (++) Macrophages, interstitially (++) Lymphocytes rolling/perivascular (+)	Inconspicuous
7	Airway epithelial cells (++) Type I pneumocytes (++) Type II pneumocytes (++) Macrophages: interstitially (++) & desquamated (++) Lymphocytes: rolling/perivascular (+)iBALT (+) & interstitial (+)	Type I pneumocytes (occasional)
10	Airway epithelial cells (++) Type I pneumocytes (+) Type II pneumocytes (++) Macrophages: interstitially (++) & desquamated (++) Lymphocytes: rolling/perivascular (+), iBALT (+)& interstitial (+)	Inconspicuous
14	Airway epithelial cells (+) Type I pneumocytes (+) Type II pneumocytes (+) Macrophages: interstitially (+) & desquamated (+) Lymphocytes: rolling/perivascular (++), iBALT (++) & interstitial (+)	Lymphocytes peribronchiolar/perivascular (+)
28	Airway epithelial cells (+) Type I pneumocytes (+) Type II pneumocytes (+) Macrophages: interstitially (+) & desquamated (+) Lymphocytes: rolling/perivascular (++); iBALT (++) & interstitial (+)	Not included in the experiment
40	Lymphocytes in iBALT (+)	Lymphocytes peribronchiolar/perivascular (+)

Table 3.1 Summary of the pattern of M1 transcript expression in the lung of wood mice and BALB/c mice over a 40 day timecourse following MHV-68 infection.
Semiquantitative parameters used to represent number of cells exhibiting M1 transcript expression: + (scattered cells); ++ (moderate number of cells); +++ (numerous cells)

Days p.i.	Spleen of Wood mouse	Spleen of BALB/c mouse
3	Lymphocytes in follicles (+) and red pulp (+) Macrophages in red pulp(+) Megakaryocytes in red pulp(+)	Lymphocytes in follicles (+) and red pulp(+) Macrophages in follicles (+) and red pulp (+)
5	Lymphocytes in follicles (+++) and red pulp (++) Macrophages in red pulp (++) Megakaryocytes in red pulp(+)	Lymphocytes in follicles (+) and red pulp(+)
7	Lymphocytes in follicles (++) and red pulp (++) Macrophages in red pulp (++) Megakaryocytes in red pulp(+)	Lymphocytes in follicles (++) and red pulp (rarely)
10	Lymphocytes in follicles (++) and red pulp (++) Macrophages in red pulp (++) Megakaryocytes in red pulp(+)	Lymphocytes in follicles (+) and red pulp (rarely)
14	Lymphocytes in follicles (++) and red pulp (++) Macrophages in red pulp (+++) Megakaryocytes in red pulp(+++)	Lymphocytes in follicles (+) and red pulp (rarely)
28	Lymphocytes in follicles (++) and red pulp (++) Macrophages in red pulp (+++) Megakaryocytes in red pulp(+++)	Not included in the experiment
40	Lymphocytes: follicles (+) and red pulp (rare)	Inconspicuous

Table 3.2 Summary of M1 transcript expression analysis in the spleen of wood mice and BALB/c mice over a 40 day timecourse after MHV-68 infection.
Semiquantitative parameters used to represent number of cells exhibiting M1 transcript expression: + (scattered cells); ++ (moderate numbers of cells); +++ (numerous cells).

3.2 *In vivo studies* on the effect of M1 expression on MHV-68 infection in a natural host

In order to determine the effect of M1 expression in MHV-68 infection of a natural host, the wood mouse, *in vivo* experiments were performed using vM1stop virus and its genetically repaired counterpart, vM1rev virus. vM1stop virus is an MHV-68 virus with an in-frame stop codon in the *M1* locus which impairs expression of the M1. The hypothesis tested was that the presence or absence of M1 transcription would lead to different MHV-68 induced pathogenesis and/or virus replication. The lung, the main site of acute MHV-68 infection, and the spleen, the main site of latent MHV-68 infection, were examined for morphological changes, viral gene transcripts, viral load, presence of viral antigen and cytokine expression. The chosen timepoints following infection were representative of acute infection (day 3 p.i. and 7 p.i.) and latent infection (day 14 p.i. and 28 p.i.).

3.2.1 Airways and lung

3.2.1.1 Mock infected wood mice. Histological, immunohistological and ultrastructural examination

Wood mice instilled intranasally using PBS (mock infected) served as negative controls to determine any potential effects of the infection protocol. Accordingly, the examination of this group of mice served to identify normal structure and baseline leukocyte numbers. The morphology of the lower airways and lung are similar to that of laboratory mice strains. The lower airways are represented by bronchi and bronchioles (Figure 3.12) lined by pseudostratified and columnar ciliated epithelium and Clara cells with microvilli on their apical surface. The alveoli are lined by two specialised epithelial cells: pneumocytes type I and pneumocytes type II. Pneumocytes are connected to each other by the *zona adherens*. Occasionally, the alveolar lining/space contains macrophages that have migrated from the interstitium into the alveolar space, these communicate with other cells through filopodia. Macrophages can also be discerned by the presence of lysosomes. The interstitium is mostly composed of connective tissue with a low number of leukocytes, mainly T and B cells, fewer macrophages embedded in an intensely vascular meshwork (Figure 3.13).

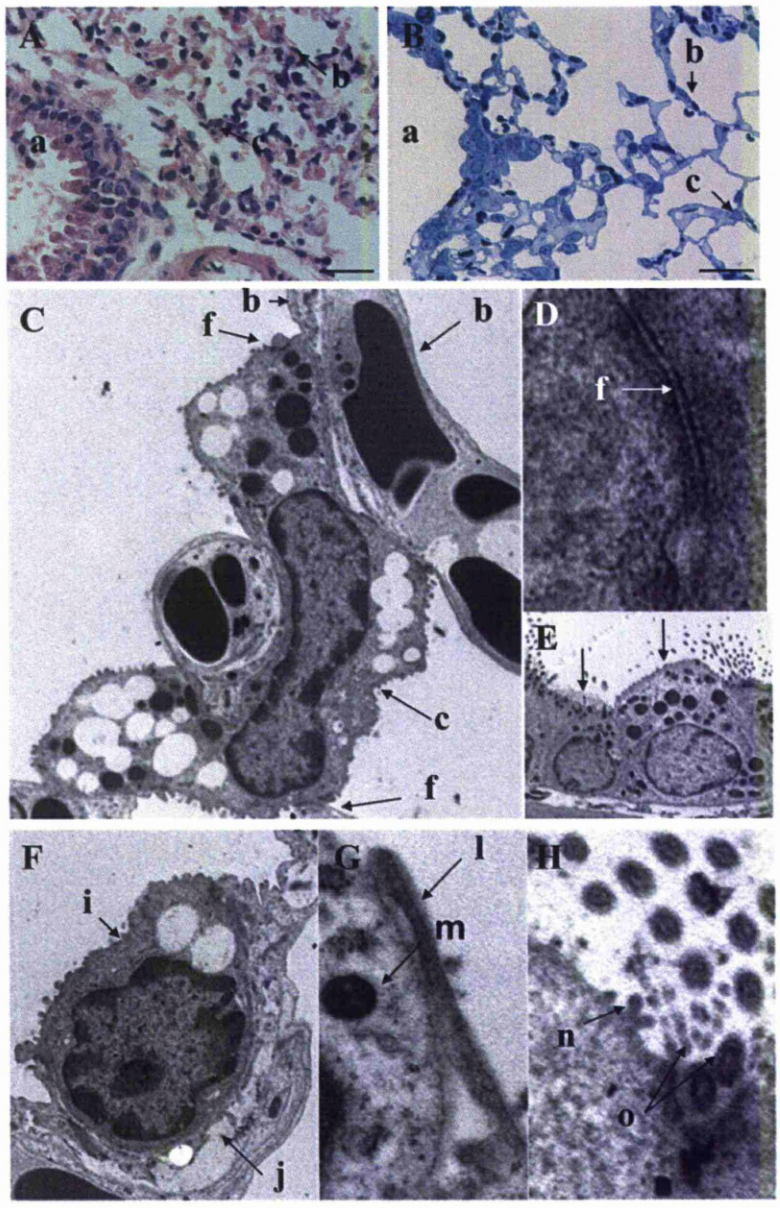

Figure 3.12 Wood mouse, mock infected. Lung, histology and ultrastructure.
Lower airways: bronchi and bronchioles (a) lined by columnar cells with cilia on apical surface (o) and Clara cells with microvilli on apical surface (n). Alveoli lined by type I pneumocytes (b) and type II pneumocytes (c), connected by *zona adherens* (f). Occasionally, the alveolar lining/space exhibited macrophages that migrated from the interstitium (j, gap in alveolar epithelium with macrophage (i) migrating from the interstitium), Macrophages exhibited lysosomes (m) and contacted with other cells through filopodia (l). A: Haematoxilin & eosin (H&E) stained section; B: Toluidine blue (TB) semithin section; C-H: Electron microscopy (EM); Scale bars A,B= 100 μm

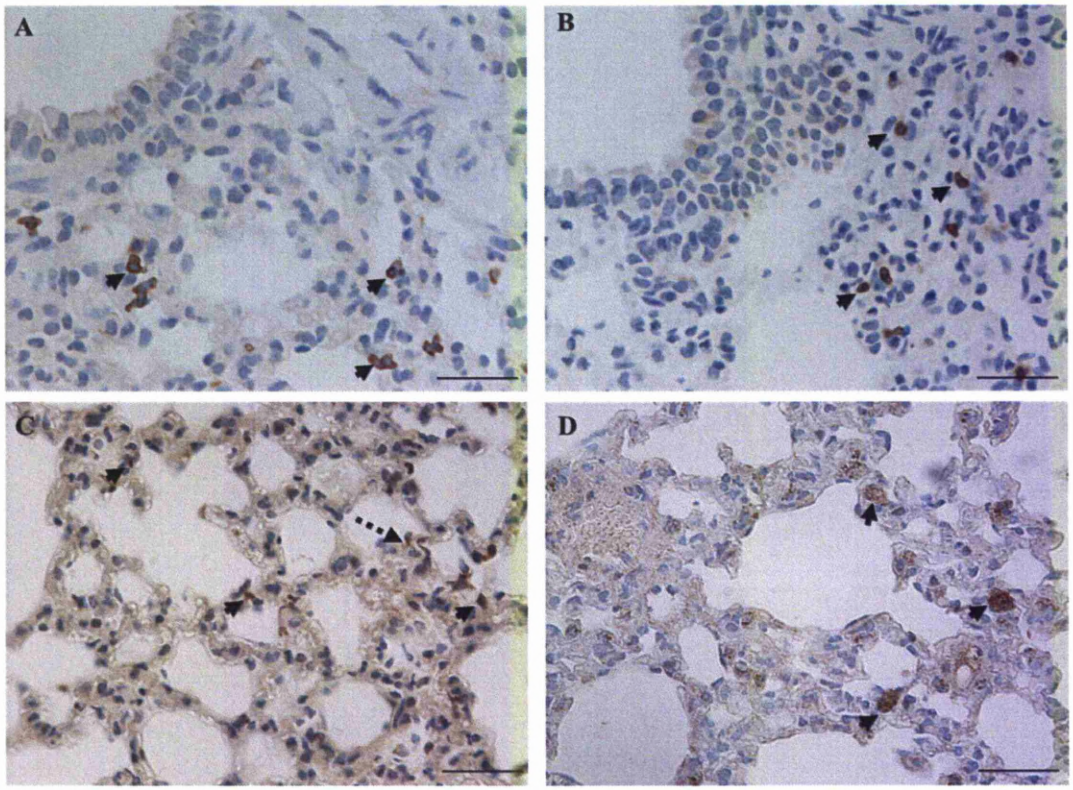

Figure 3.13 Wood mouse, mock infected, lung. Immunohistology for T cells (CD3-positive), B cells (CD45R-positive) macrophages (lysozyme-positive) and type II pneumocytes (SP-C-positive).

The interstitium was composed of connective tissue with scarce leukocytes, mainly B cells (arrow in A); T cells (arrowheads in B) and fewer macrophages (arrowheads in C), embedded in a vascular meshwork. Macrophages were also seen lining the alveoli (dashed arrows in C). Type II pneumocytes (arrowheads in D; alveolar macrophages) were observed most frequently in the angles of alveoli and occupied a small proportion of the alveolar lining surface. PAP method (CD3, SP-C, lysozyme); ABC method (CD45R), Papanicolaou's heamatoxylin counterstain. Bars = 25μm

3.2.1.2 Inflammatory response in wood mice following vM1stop and vM1rev infection

3.2.1.2.1 The lower airways

The morphological changes seen in the lower airways following infection with vM1rev and vM1stop were similar. At day 3 p.i., the lower airways (bronchi and bronchioles) showed a mild to moderate increase in cellularity, leading to protrusion of the epithelium into the lumina. Cells lining the airways were mostly columnar and ciliated. Also they showed mild to moderate anisocytosis and mild anisokaryosis (mild respiratory epithelium hyperplasia) (Figure 3.14). Furthermore, these cells also showed various degenerative changes such as extensive mitochondrial swelling, hyperchromatic and shrunken nuclei (Figure 3.15).

At day 7 p.i., the epithelial hyperplasia was more intense than at day 3 p.i. and bronchiolar lumina often contained apoptotic/necrotic cells. Occasionally bronchioles exhibited vacuolated macrophages and/or multinucleated cells amongst the cellular debris in the lumina.

At day 14 p.i. and day 28 p.i., the bronchial/bronchiolar epithelium appeared unaltered apart from a few desquamated and apoptotic cells.

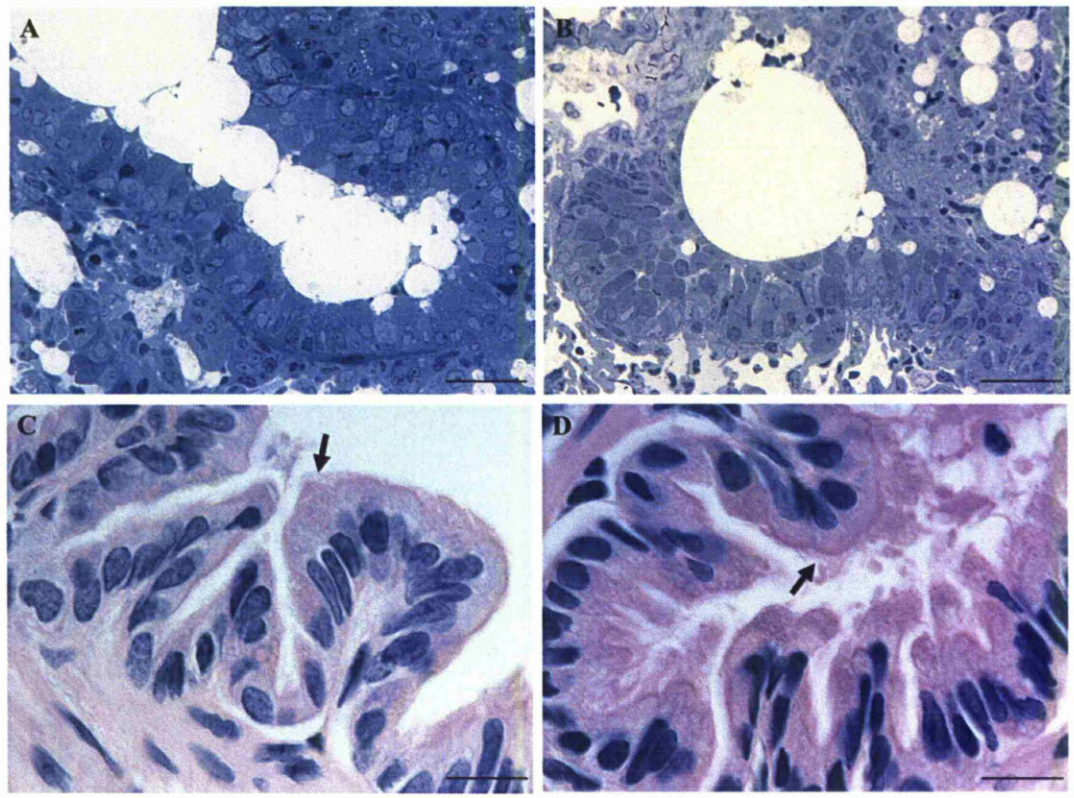

Figure 3.14 Wood mouse, vM1stop and vM1rev infected, day 3 p.i. Histology of bronchiolar epithelium.
Bronchiolar epithelial cells were observed protruding into the alveolar lumen and showed mild to moderate anisocytosis and mild anisokaryosis. These cells were mostly ciliated (arrows in C and D). A, B: TB stained semithin sections; C, D: H&E stained sections. Bars: A,B= 25μm; C, D=10 μm

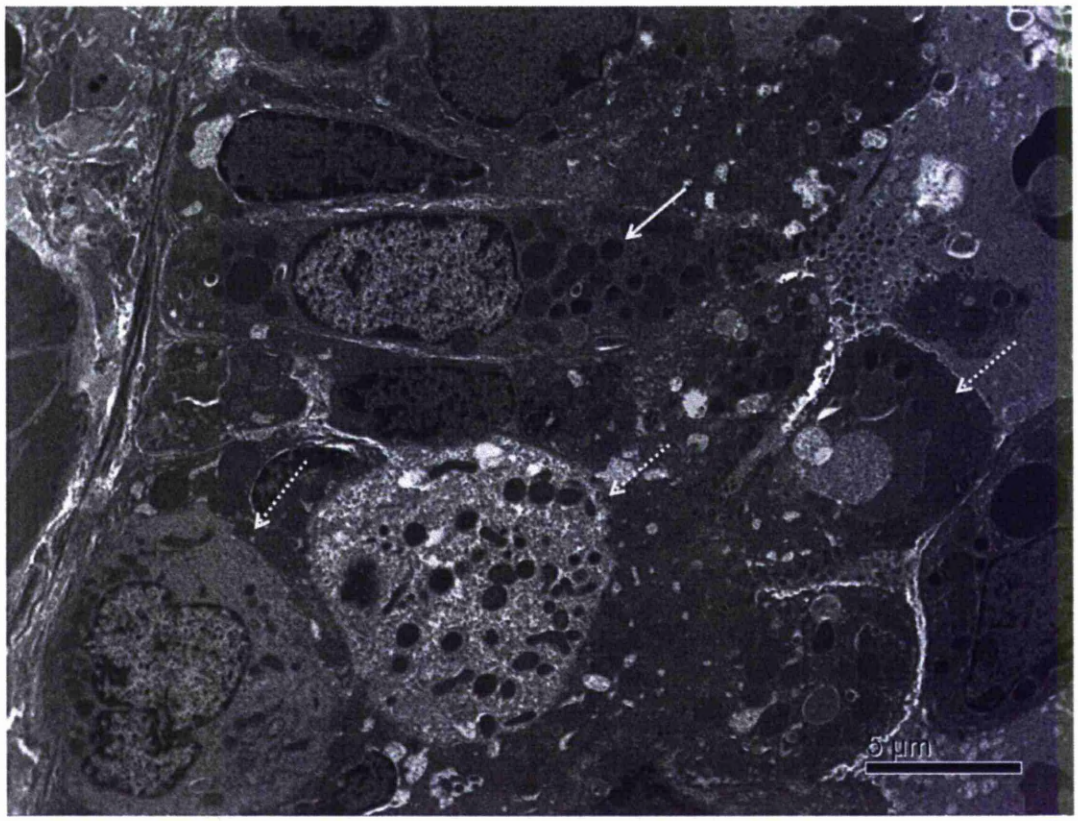

Figure 3.15 Wood mouse, vM1rev infected, day 3 p.i Ultrastructure of bronchiolar epithelium.
The bronchiolar epithelium was hyperplastic and was comprised of scattered degenerate cells but did not contain identifiable viral particles. Bronchiolar epithelial cells showed extensive mitochondrial swelling (full arrow) and/or extensive degenerative changes (dashed arrows) were noted. EM

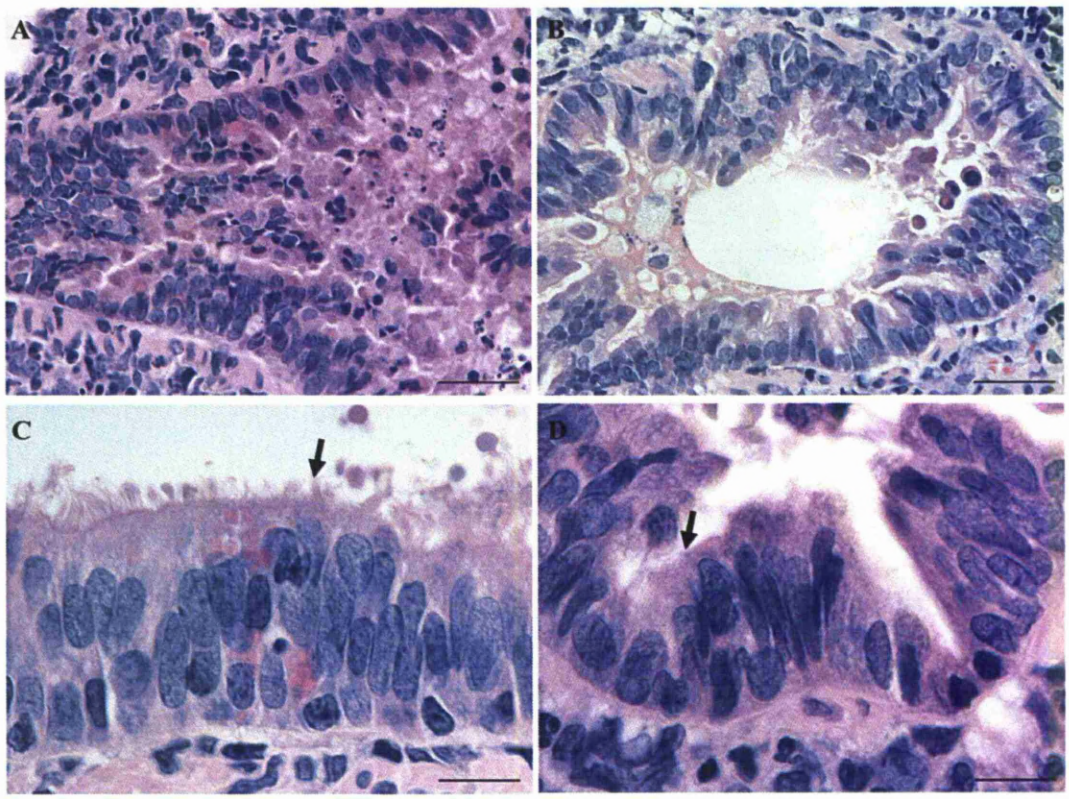

Figure 3.16 Wood mouse, vM1stop and vM1rev infected, day 7 p.i Histology of bronchiolar epithelium.
A,B: Overview of bronchioles; C,D: Close up of bronchiolar epithelial cells. Bronchiolar lumina with numerous apoptotic/necrotic cells (A, B). Ciliated epithelial cells (arrows) were observed protruding into the alveolar lumen and showed moderate anisocytosis and anisokaryosis. H&E stained sections. Bars= A,B= 25μm; C,D=10 μm

3.2.1.2.2 The lung

3.2.1.2.2.1 Day 3

Infection with vM1stop and vM1rev led to an increase in the overall cellularity in the lung. At day 3 in the vM1rev infected wood mouse, the increase in cellularity was multifocal and mild (Figure 3.17A) and was mostly due to a mild increase in macrophages infiltrating the interstitium and/or lining alveoli and mild type II pneumocyte hyperplasia (Figure 3.18B). However in the vM1stop infected mice there was a multifocal moderate to severe increase in cellularity. These made air spaces inconspicuous where the changes were most severe (Figure 3.17B). In the vM1stop infected mice the increase in cellularity occurred in the alveolar lining due to mild to moderate type II pneumocyte hyperplasia (Figure 3.18 and Figure 3.19) and the presence of foamy macrophages, associated with type I pneumocyte necrosis. Type II pneumocytes were occasionally binucleated. In the interstitium there was mild to moderate interstitial infiltration by lymphocytes and macrophages (Figure 3.18 and Figure 3.19). In vM1stop infected mice there was also a more frequent and pronounced formation of induced bronchial associated lymphoid tissue (iBALT) which was minimal in vM1rev infected mice (Figure 3.17).

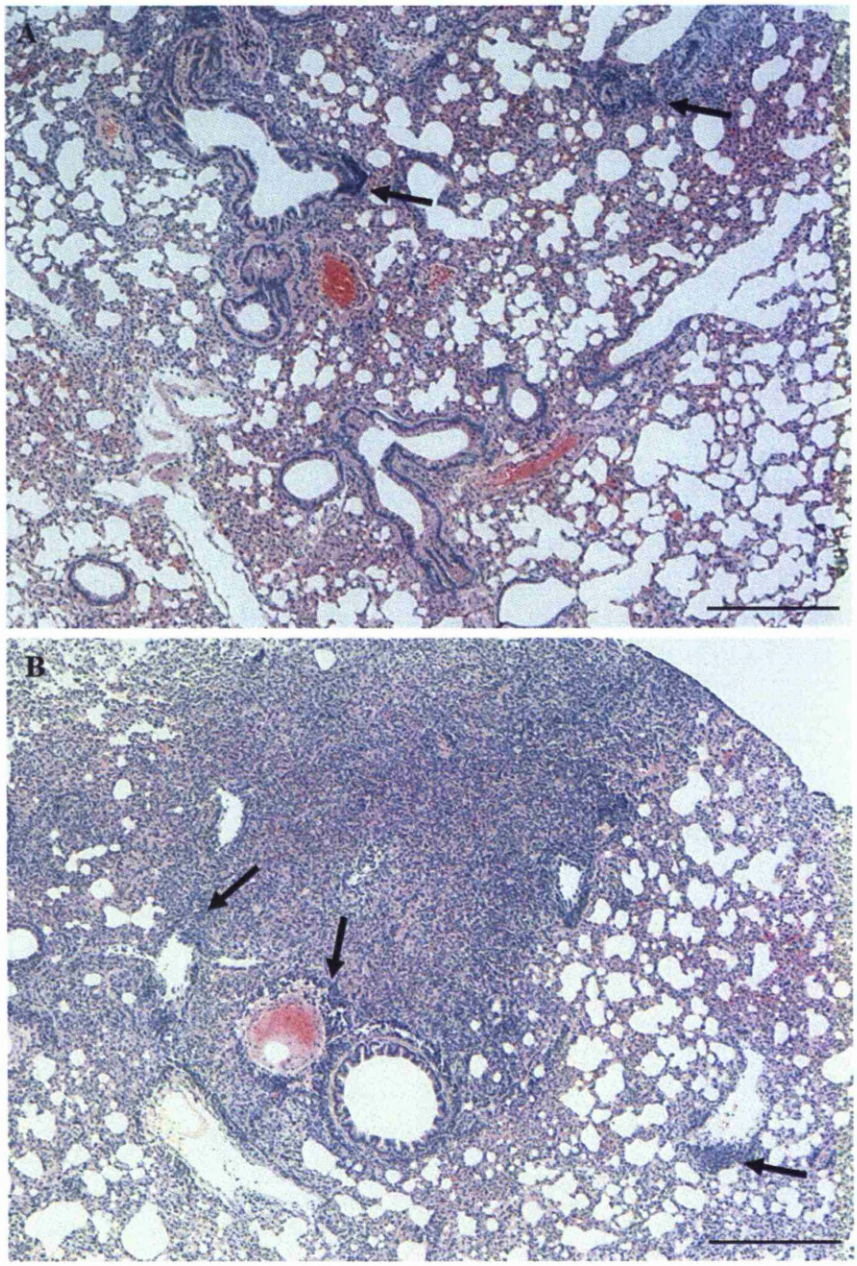

Figure 3.17 Wood mouse. vM1rev and vM1stop infected, day 3 p.i. Histology of lung.
A: vM1rev infected wood mouse; B: vM1stop infected wood mouse. An increased cellularity in the lung following infection was observed. In the vM1rev infected wood mouse the increase in cellularity was mild and multifocal. In the vM1stop infected wood mouse, this increase was more intense with infection leading to multifocal to a focally extensive, moderate to severe increase in cellularity. Furthermore in vM1stop infected woodmice, iBALT (arrows) formation was more frequent and pronounced. H&E stained sections. Bars= 250 μm

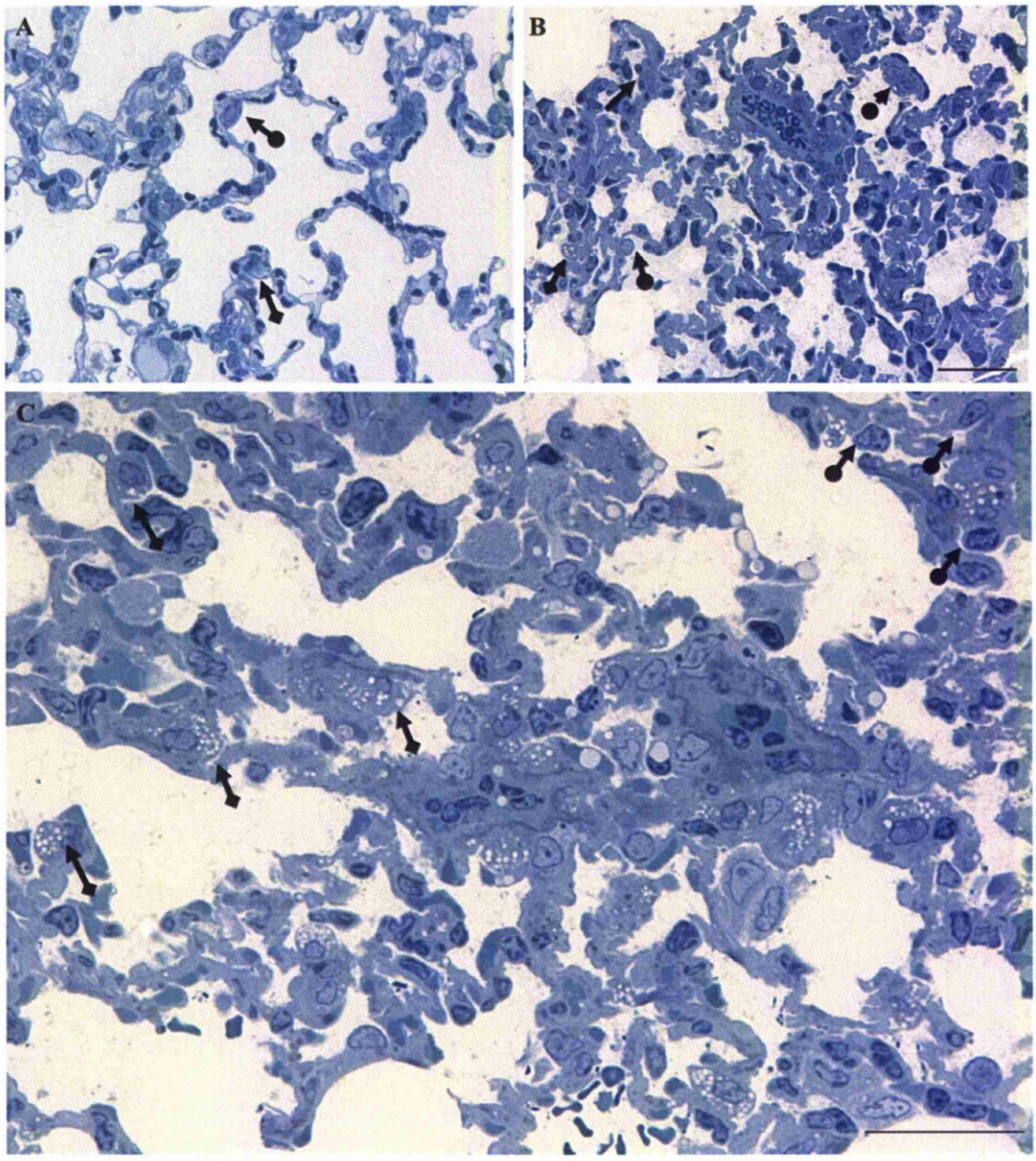

Figure 3.18 Wood mouse. Mock, vM1rev and vM1stop infected, day 3 p.i. Histology of lung.

A. Mock infected; B: vM1rev infected; C. vM1stop infected, in an area where increased cellularity was not severe to enable clearer observation of the cell types involved. Both infections led to an increase in macrophages (arrow with square tip) infiltrating the interstitium and/or lining alveoli. These macrophages were often highly vacuolated (activated). There was also type II pneumocyte hyperplasia, (arrow with round tip). Type II pneumocytes showed moderate anisocytosis and anisokaryosis and were occasionally binucleated (dashed arrow with TB stained semithin sections. Bars= 25 μm

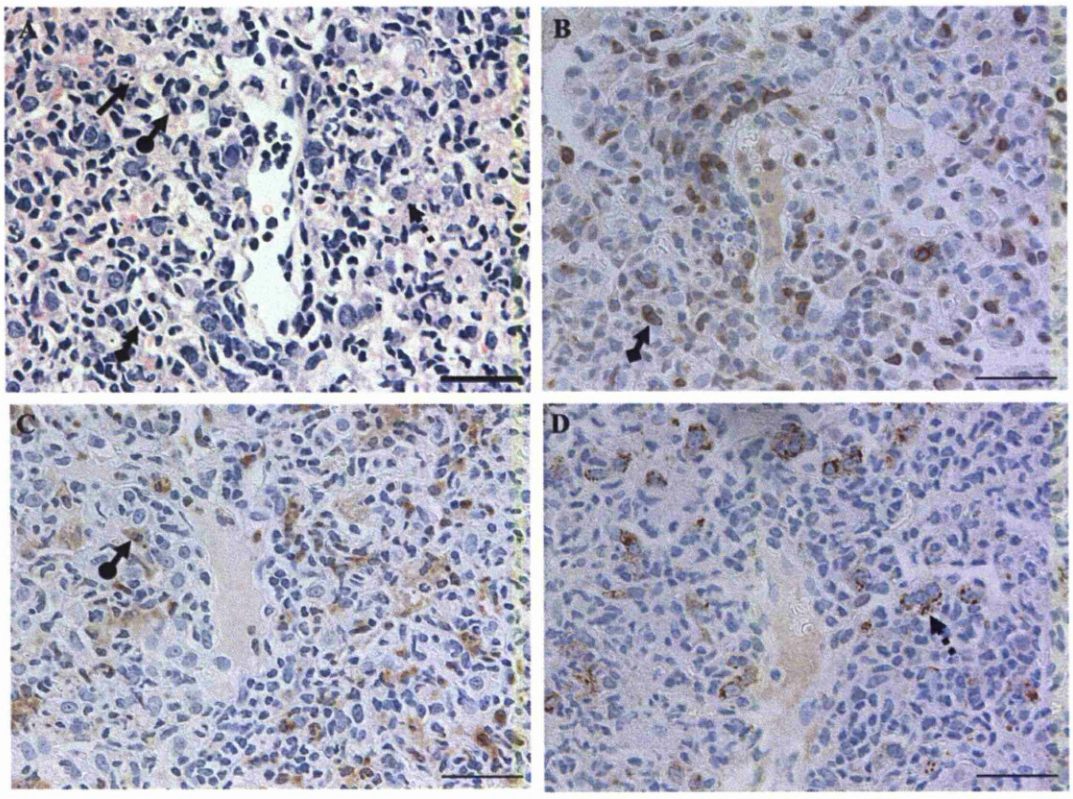

Figure 3.19 Wood mouse, vM1stop infected, day 3 p.i. Histology and immunohistology of area with severely increased cellularity.
A: H&E stained; Immunohistology using T cell (B), macrophage (C) pneumocyte type II (D), markers. The immunohistology confirmed that the foci of increased cellularity were due to disseminated T cells (arrow with square tip), macrophages (arrow with round tip) and type II pneumocytes (dashed arrows). A-D: Corresponding areas in the lung section. Necrotic debris (full arrow) was also seen amongst inflammatory infiltrate. PAP method Papanicolaou's haematoxylin counterstain. Bars= 25μm

The ultrastructural examination of vM1stop infected wood mice lung at day 3 p.i, revealed that type I pneumocytes showed more extensive cytoplasmic oedema and basement membrane reduplication, a degenerative change preceding cell death (Figure 3.21). Also when vM1stop infected animals were compared to mock-infected animals, it was observed that lamellar bodies were more numerous per cell and larger in size in type II pneumocytes (Figure 3.21, Figure 3.22). This indicated that type II pneumocytes were actively producing more surfactant. Another feature unique to the vM1stop infected wood mice was that cells frequently exhibited intracytoplasmic lipid droplets (Figure 3.21). The droplets were often numerous and occasionally compressed the nucleus effacing cellular architecture and thus preventing accurate cell type identification. The majority of cells appeared to be alveolar and/or interstitial macrophages. This feature was also observed in the macrophages infected *in vitro* with the vM1stop virus (see Section 3.3.2). The lipid vacuoles were also present extracellularly (likely cells that had degenerated and lost their membranes).

In vM1rev infected wood mice the ultrastructural examination of lung at day 3 p.i revealed the presence of glycogen lakes in the interstitium (Figure 3.22 A). which was not observed in vM1stop infected animals. The presence of binucleated type II pneumocytes was not associated with the presence of viral particles (Figure 3.22 B). This finding indicates the binucleation to represent a type II pneumocyte hyperplasia stage as part of regeneration process in the lung rather than being a change induced by viral infection.

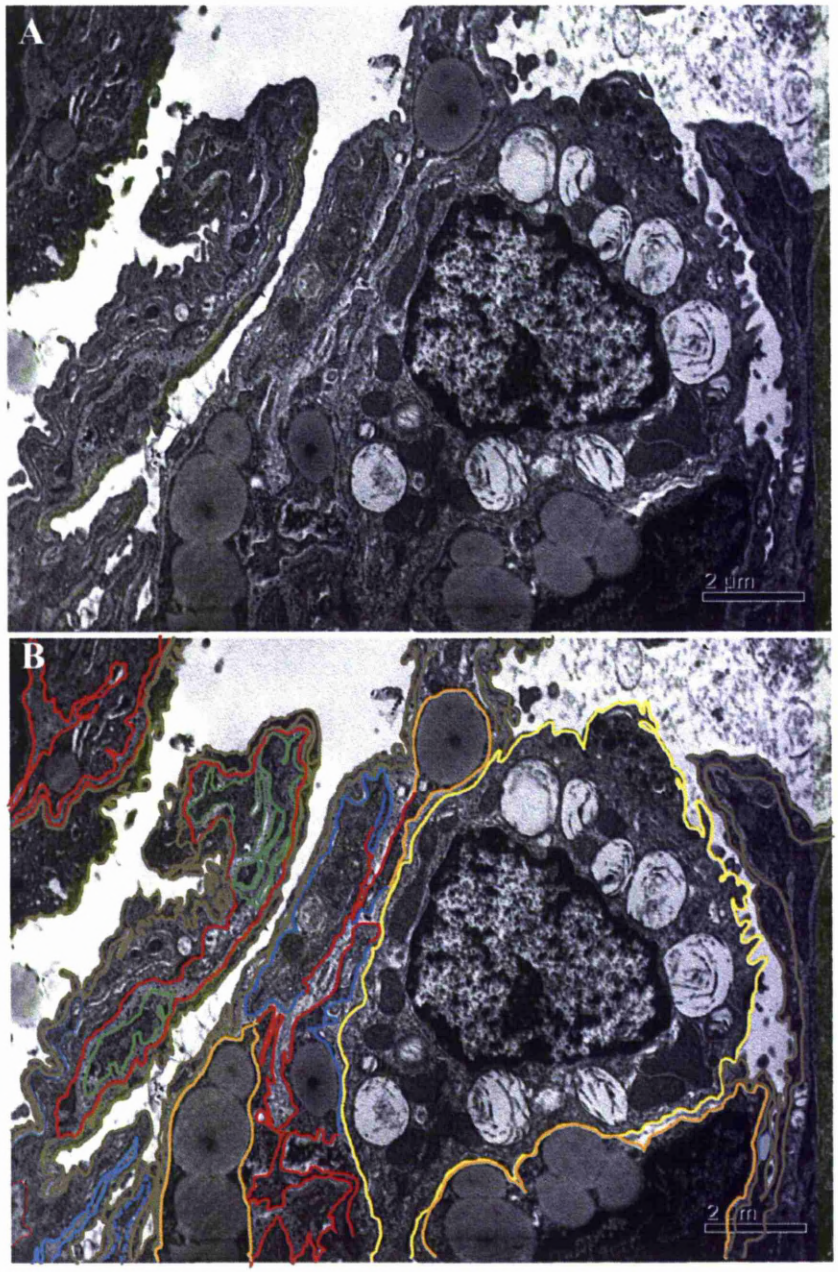

Figure 3.20 Wood mouse, vM1stop infected, day 3 p.i. Ultrastructure.
A,B represent same figure but in B, cells have been outlined using the colour coding (orange: macrophage; yellow: pneumocyte type II; brown: pneumocyte type I; blue: intertitium, red: endothelium; green: intravascular cell. Overview of alveolar wall showing a hyperplastic type II pneumocyte. These contained abundant lamellar bodies and an extremely rugged apical cytoplasmic membrane. Within the interstitium there were macrophages with abundant lipid in the cytoplasm.

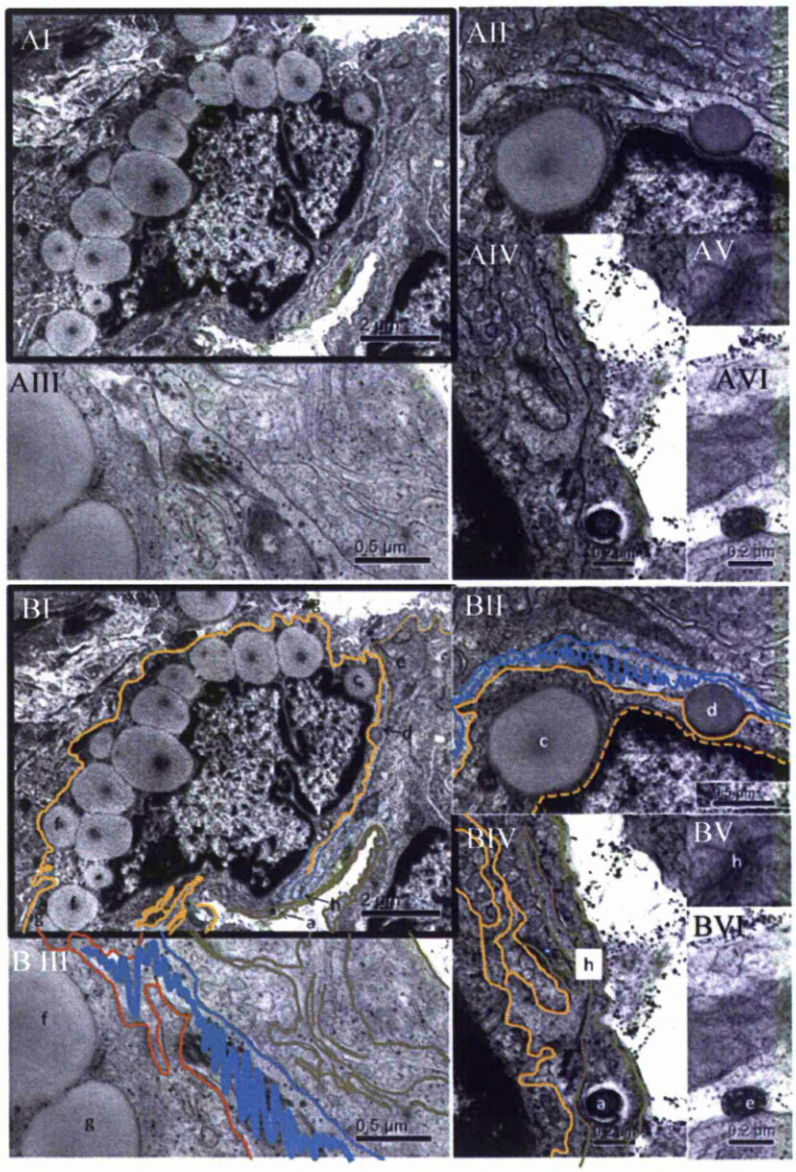

Figure 3.21 Wood mouse, vM1stop infected, day 3 p.i. Ultrastructure.
A,B represent the same figure but in B, the cells have been outlined using the colour coding (orange: macrophage; brown: pneumocyte type I; blue: intertitium. There is also cross referencing of equivalent areas between images using unicase letters. Close up of the interstitial macrophage surrounded by type I pneumocytes; I: Lipid vacuoles occupy most of the cytoplasm and compress nucleus; II: lipid in cytoplasm (c) and within the interstitium (d); III: Extensive basement membrane reduplication, a degenerative change preceding cell death in a type I pneumocyte cytoplasm underlying macrophage; IV: Close up of type I pneumocyte with circular structure resembling size and shape of a viral particle ~155ηm that appears to be being enveloped; V: Close up of *zona adherens* between neighbouring type I pneumocytes; VI: Roughly circular structure within alveolar space and attached to cytoplasmic membrane of type I pneumocyte which has the approximate shape to a viral particle ~130x200 ηm;

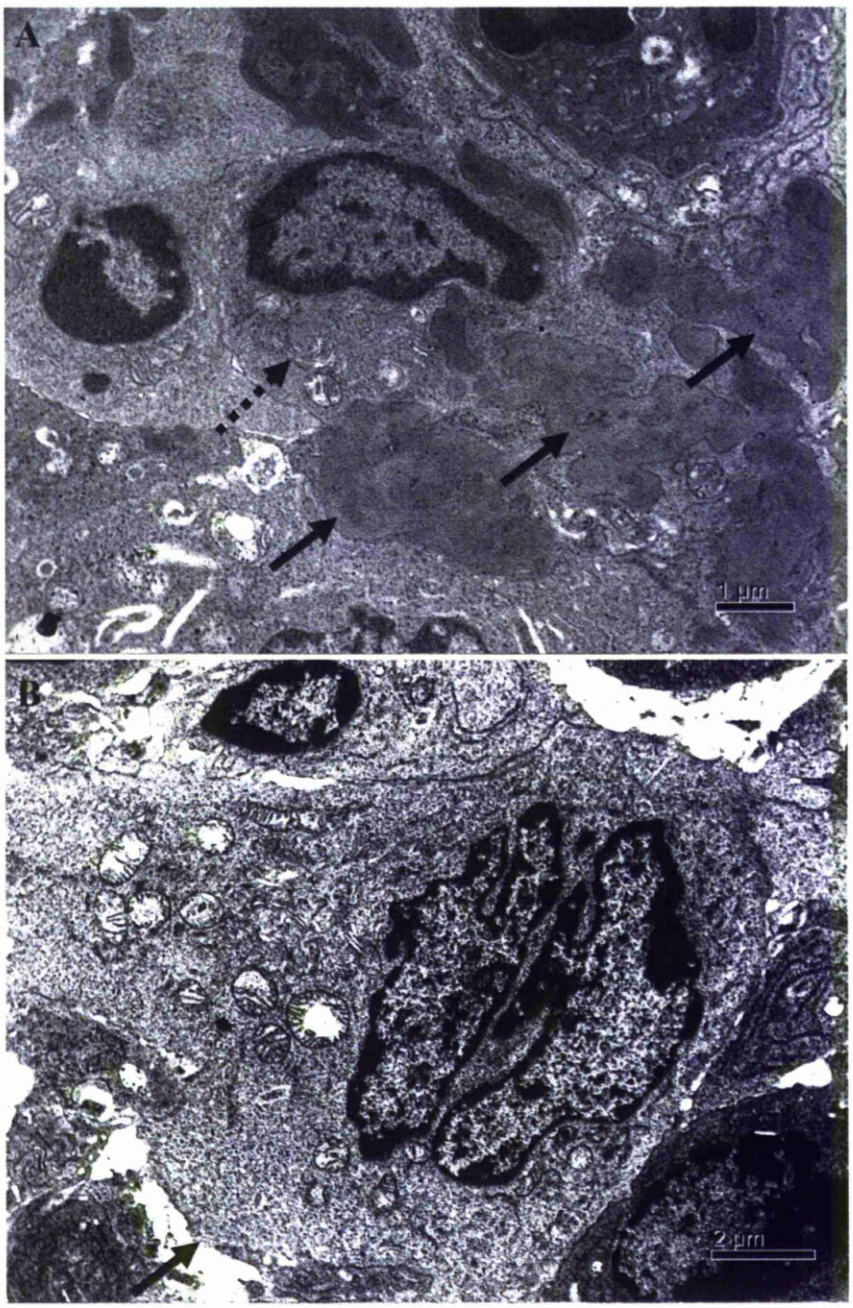

Figure 3.22 Wood mouse, vM1rev infected, day 3 p.i. Ultrastructure.
A: Type II pneumocytes in vMIrev infected mice were observed to have fewer lamellar bodies (dashed arrow) than in vM1stop infected mice (Figure 3.21). Large glycogen lakes (arrows) were also noted in the interstititium.; B: Binucleated type II pneumocyte (arrow) without evidence of active viral replication. EM

3.2.1.2.2.2 Day 7

By day 7 p.i., there was further increased cellularity when compared to day 3 p.i in both vM1rev and vM1stop infected mice. In vM1rev infected mice, the increased cellularity exhibited a more diffuse pattern. However, in the vM1stop infected mice there was a multifocal pattern (Figure 3.23 C, D). This distribution was also obvious at the macroscopic level (Figure 3.23 A, B). In the vM1stop infected animals, despite the multifocal pattern, the changes observed were more intense and included necrotic foci with fibrinous centres (Figure 3.24), a more intense type II pneumocyte hyperplasia (Figure 3.24) and macrophage infiltration. Type II pneumocytes often showed mitotic figures and were occasionally binucleated. In the vM1stop infected animals there was also more frequent, occasionally larger, better demarcated iBALT (Figure 3.23, Figure 3.24) and rare syncytia formation (Figure 3.24). Within the alveolar space, in either infection desquamated macrophages were frequently observed.

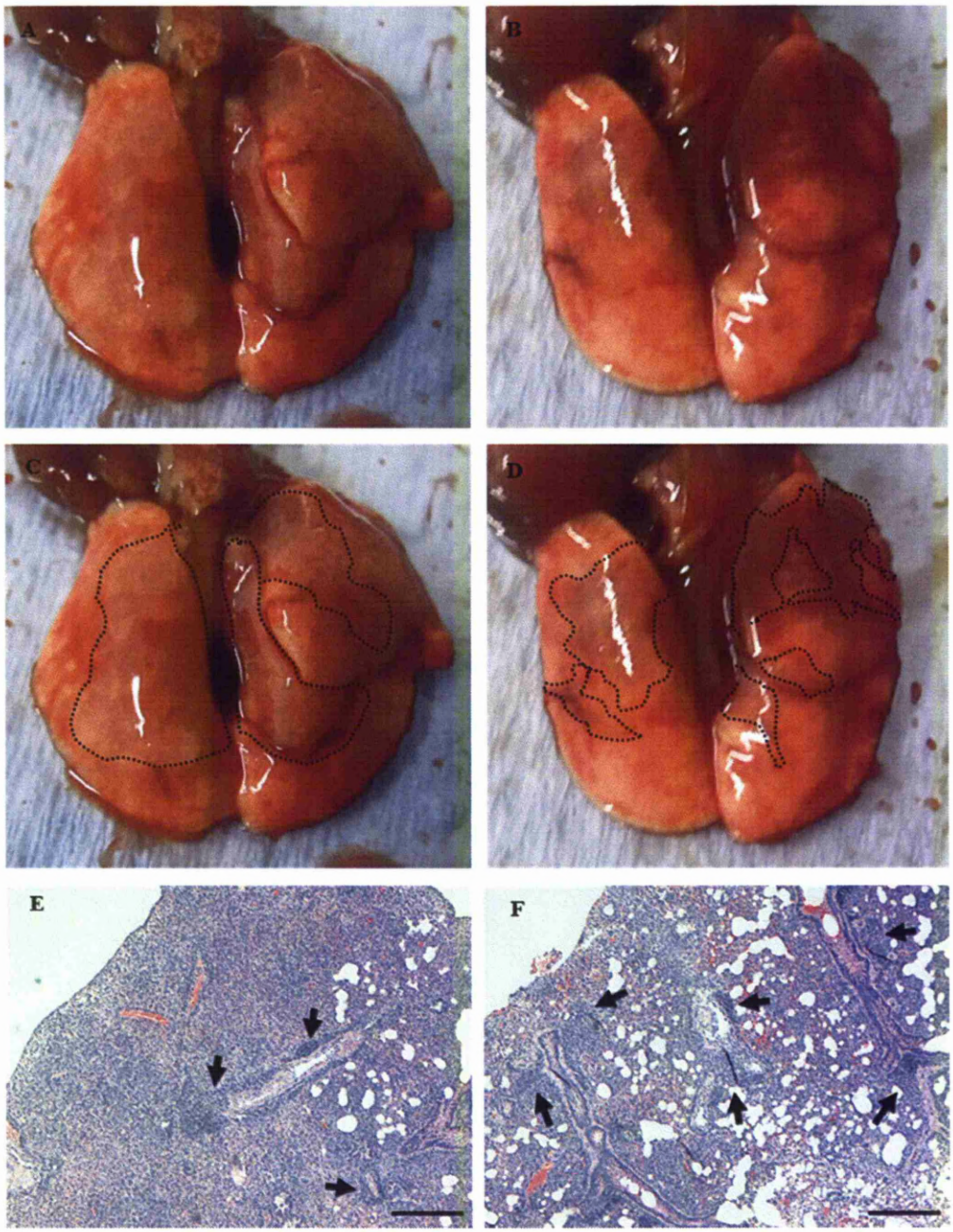

Figure 3.23 Wood mouse, vM1stop and vM1rev infected, day 7 p.i. Macroscopic appearance and histology of lung.
A-D: macroscopic appearance; C, D represent same images as A,B respectively but dashed lines have been drawn to highlight consolidation areas; E, F:, HE stained sections Bars= 250μm; A, C, E: vM1rev, focally extensive areas of consolidation (A) correlated with focally extensive areas of increased cellularity(C); B, D, F: vM1stop, multifocal pattern consolidation (B) correlated with multifocal areas of increased cellularity (D). Arrows in E, F highlight iBALT.

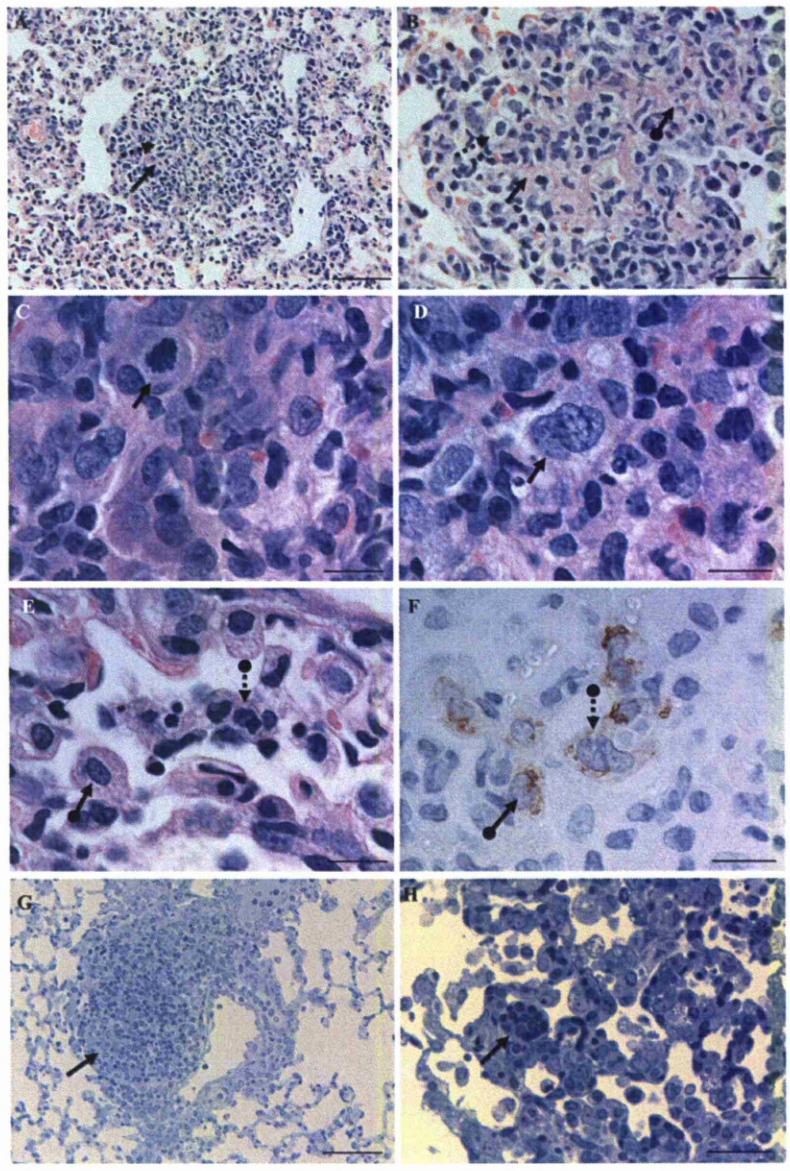

Figure 3.24 Wood mouse, vM1stop infected, day 7 p.i. Lung. Histology and immunohistology.

A,B: Foci of necrotic debris (arrow with round tip) and fibrin deposition (full arrow), surrounded mainly by macrophages (dashed arrow); C,D:. Close up of area of severely increased cellularity. Cells showed severe anisocytosis and anisokaryosis, frequent mitotic figures (arrow in A) and were occasionally binucleated (arrow in B); E,F: Close up of an alveoli with moderate type II pneumocyte (arrows) hyperplasia; D: Immunohistology confirmed cells showing severe anisocytosis and anisokaryosis and binucleated cells (dashed arrow) to be type II pneumocytes (full arrow); E: iBALT surrounding an artery; F: syncytial cell (arrow) within alveolar lining. A, B, C, D, E: H&E stained sections. F: Immunohistology using marker for type II pneumocyte (PAP method, Papanicolaou's haematoxylin counterstain); G,H: Semithin TB stained sections; Bars= A= 20μm; B, C,D, F,G= 25 μm; H=100 μm

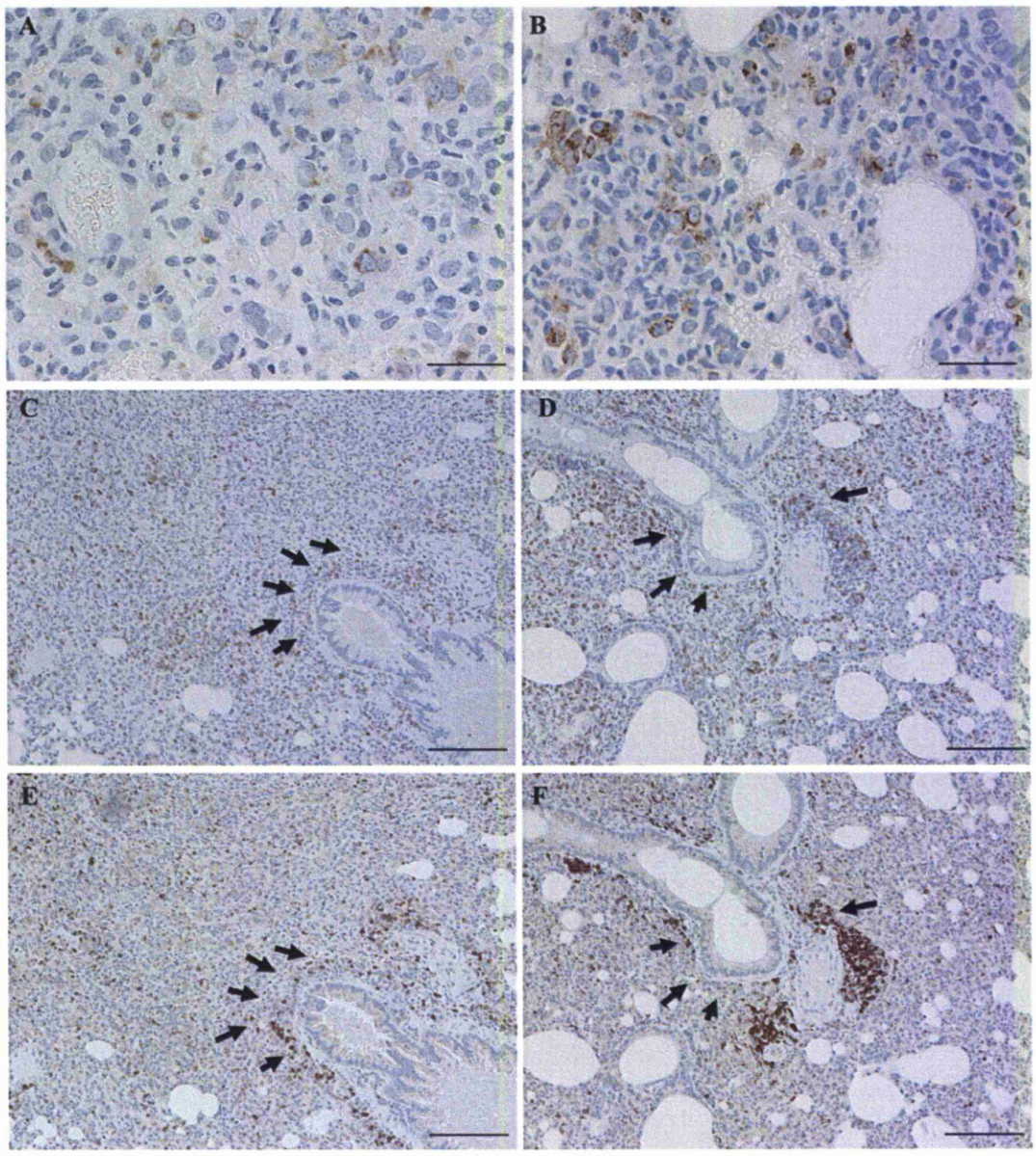

Figure 3.25 Wood mouse, vM1stop and vM1rev infected, day 7 p.i. Lung. Immunohistology using marker for type II pneumocytes, B and T cells.
A,C, E: vM1rev; B,D,F: vM1stop infected wood mice. A,B: Immunohistology using marker for Type II pneumocytes; C,E and D,F: corresponding areas in the lung sections. C,D: Immunohistology using marker for T cells; E, F: Immunohistology using marker for B cells. B cells in iBALT (arrows) form larger and better demarcated clusters (follicles) in vM1stop infected animals. In either infections, iBALT is composed mostly by B cells. PAP method (T cell marker); ABC method (B cell marker), Papanicolaou's haematoxylin counterstain Papanicolaou's haematoxylin counterstain. Bars= A,B= 25 μm; C-F= 100 μm

3.2.1.2.2.3 Day 14

In comparison to previous timepoints, at day 14 p.i. the overall cellularity was markedly reduced but there was very little difference between animals infected with either virus (Figure 3.26). As in the mock infected mice, the alveoli were mainly lined by type I pneumocytes and type II pneumocytes were rarer (Figure 3.27). The septae were mildly to moderately and diffusely expanded due to infiltration of the interstitium mainly by macrophages and to a lesser extent B cells and T cells; the macrophage infiltration being more intense in this location than at previous timepoints (Figure 3.27). In the vM1rev infected animals, when compared to day 7 p.i, the iBALT seen surrounding bronchi/bronchioles and medium size vessels was more frequent and better demarcated (Figure 3.26). In both infections, the iBALT was still composed mainly of B cells, but at this time point also contained a high number of T cells (Figure 3.28).

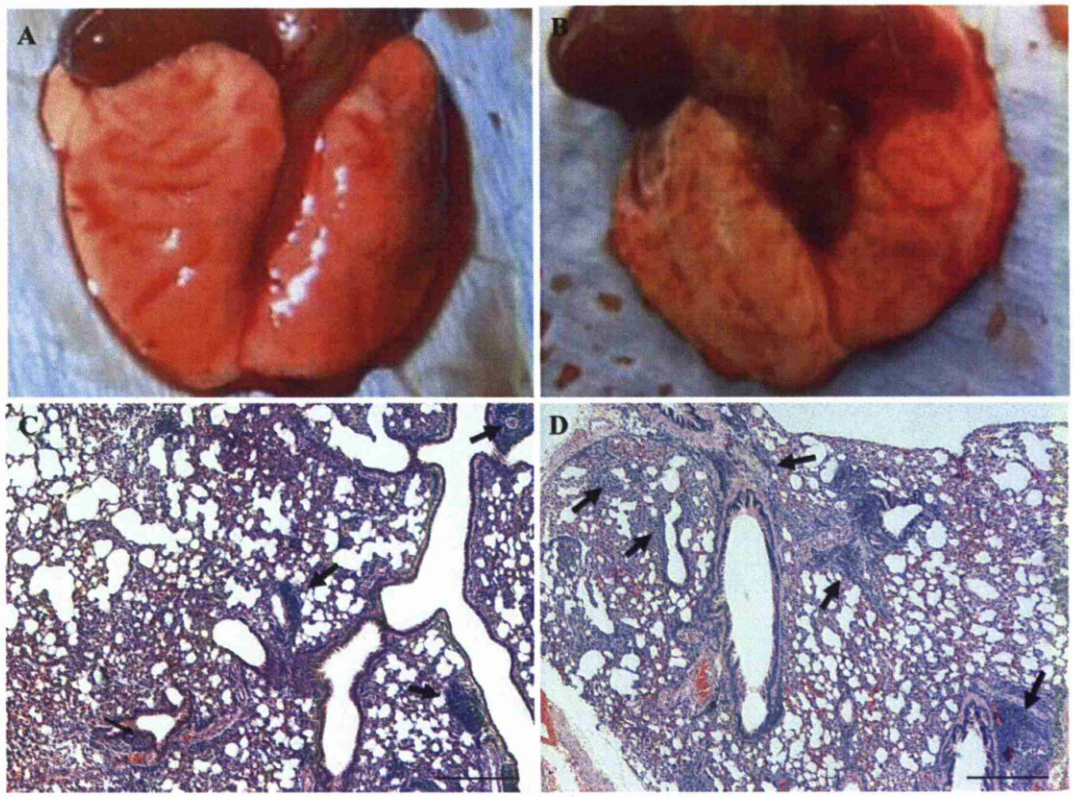

Figure 3.26 Wood mouse, vM1stop and vM1rev infected, day 14 p.i. Lung macroscopic appearance and histology of lung.
A, B: macroscopic appearance; C-E:, HE stained sections. A, C: lung of vM1rev infected wood mouse; B, D: lung of vM1stop infected wood mouse. There was little difference between infections. Macroscopically, lungs appear unaltered. Compared to previous timepoints the overall cellularity was markedly reduced. In the vM1rev infected wood mouse, when compared to day 7 p.i., the iBALT (arrows in B,C) was more frequent and better demarcated and more pronounced. Bars= C,D=250µm;

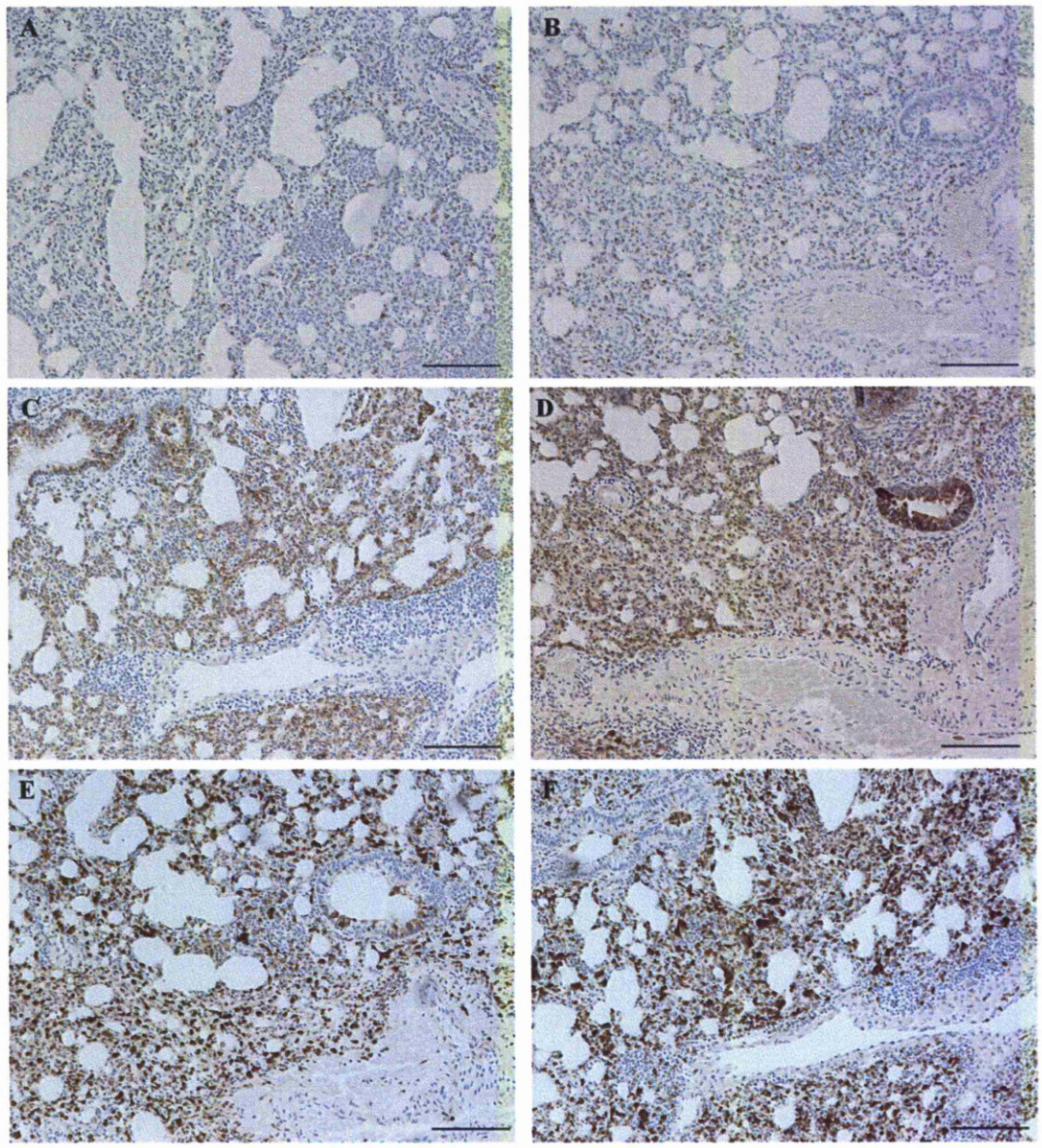

Figure 4.27 Wood mouse, vM1stop and vM1rev infected, day 14 p.i. Immunohistology using marker for type II pneumocytes, epithelial cells, macrophages.
A, C, E: corresponding areas in the lung of vM1rev; B, D, F: corresponding areas in the lung of vM1stop infected. Immuhistology using markers for type II pneumocytes (A,B), epithelial cells (C, D). macrophages (E,F). Slender cells lining alveoli, not positive when using type II pneumocyte marker, interpreted as type I pneumocytes. There is little difference between the infections. However, when compared to day 7 p.i, at day 14 p.i., in both infections, in the alveolar lining, type II pneumocytes were much decreased in numbers whilst type I pneumocytes were much increased and were the majority of cells present. Furthermore, when compared to day 7 p.i, the interstitium, at day 14 p.i. showed increased infiltration by macrophages. PAP method Papanicolaou's haematoxylin counterstain. Bars=100 μm

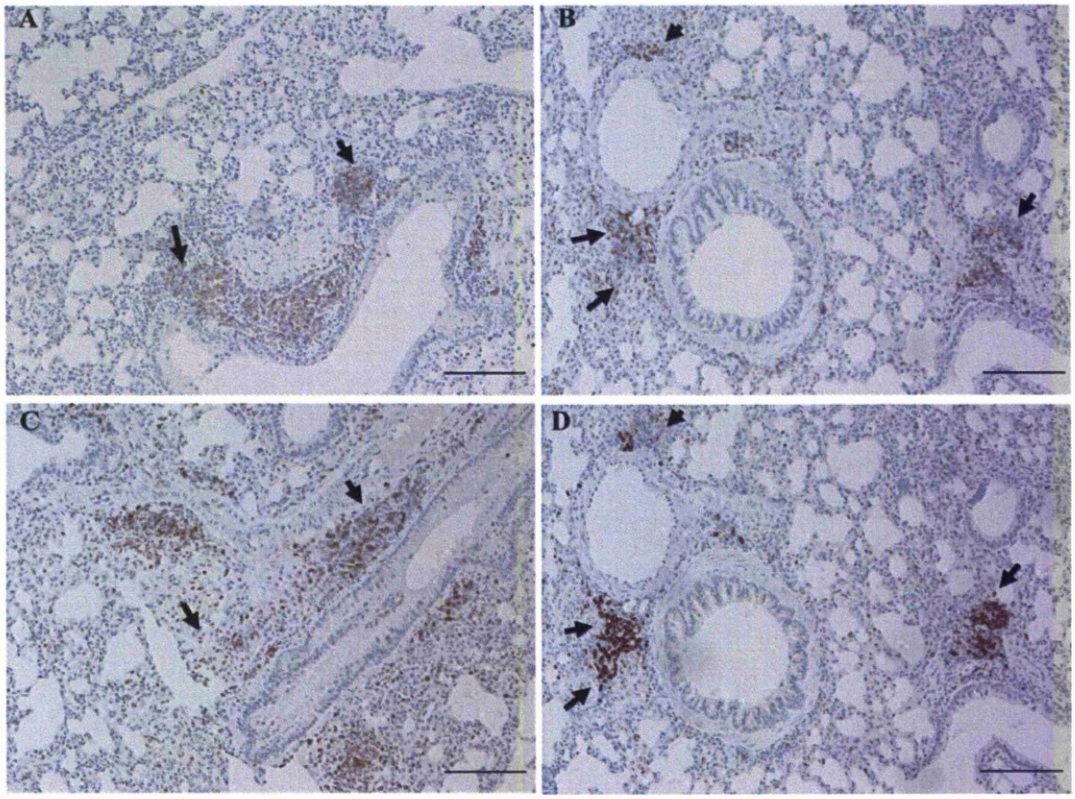

Figure 3.28 Wood mouse, vM1stop and vM1rev infected, day 14 p.i. Lung immunohistology using marker for T and B cells.

A, C: corresponding areas in the lung of vM1rev; B, D: corresponding areas in the lung of vM1stop infected. Immuhistology using markers for T cells (A,B) and B cells (C,D). Arrows highlight iBALT surrounding arteries and bronchioles. There is little difference between infections. However when compared to day 7 p.i, at day 14 p.i. the proportion of T cells in the iBALT, in relation to B cells was increased. PAP method Papanicolaou's haematoxylin counterstain B cell marker: ABC method Papanicolaou's haematoxylin counterstain. Bars= 100μm

3.2.1.2.2.4 Day 28

At day 28 p.i, histologically there was very little difference between the overall cellularity in the lungs of animals infected with either virus (Figure 3.29). At day 28 p.i., the most significant difference between the vM1stop and vM1rev infection was the presence of more frequent and pronounced iBALT surrounding bronchi/bronchioles and medium sized vessels in the vM1stop infected mice. iBALT was mostly composed of B cells, but also contained numerous T cells as seen in day 14 p.i (Figure 3.29). When compared to mock infected wood mice, in the vM1rev infected mice in the interstitium, there was still a mild infiltration by macrophages (Figure 3.30). The presence of type II pneumocytes in the alveolar lining, in either infection was similar to that seen in mock infected wood mice.

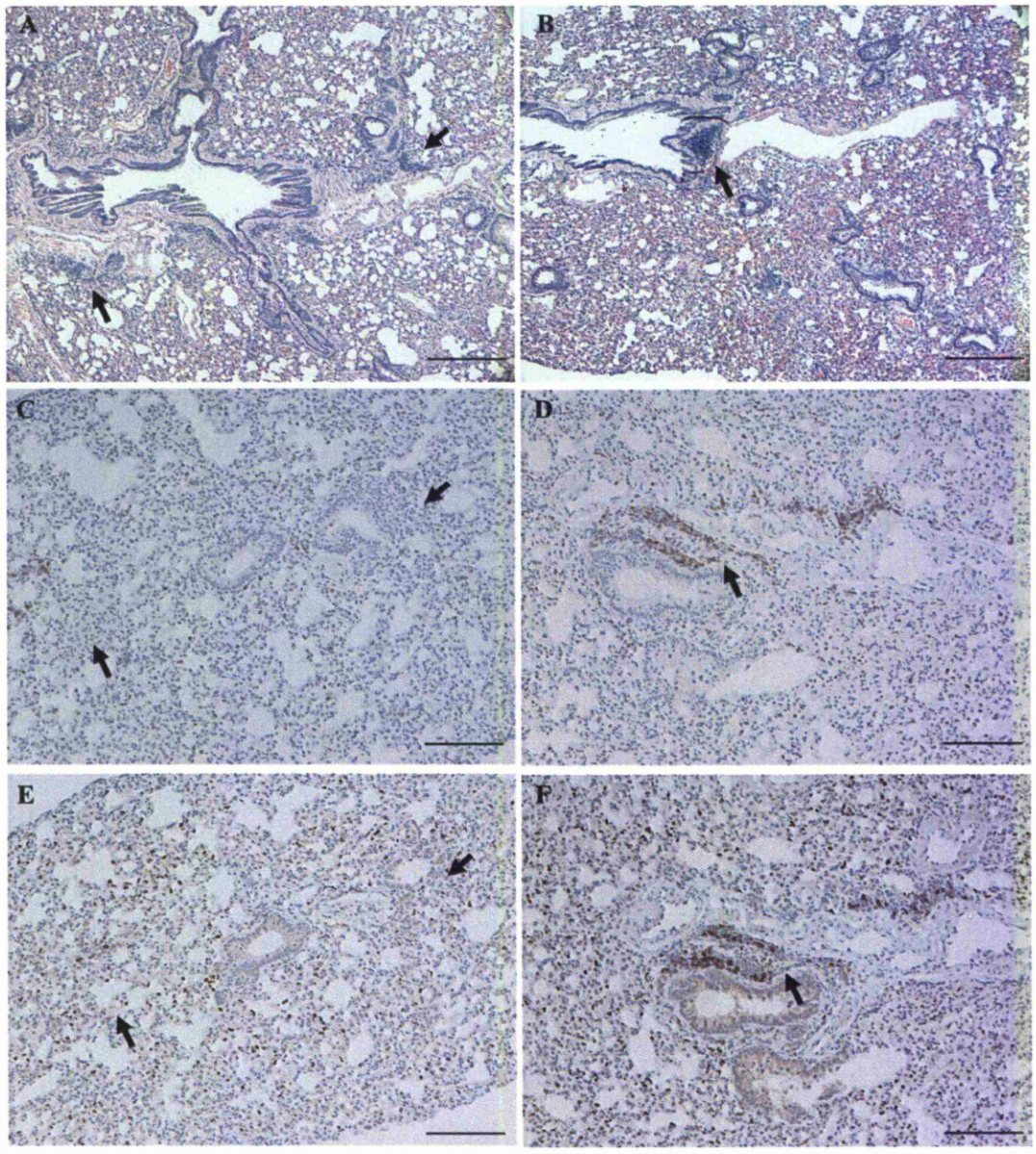

Figure 3.29 Wood mouse, vM1stop and vM1rev infected, day 28 p.i. Lung. Histology and immunohistology using marker for T and B cells.
A,C,E: corresponding areas in the lung of vM1rev infected animal; B,D,F: corresponding areas in the lung of vM1stop infected animal. A,B: HE stained sections; C,D: Immunohistology using marker for T cells; E,F: Immunohistology using marker for B cells. On histology there is little difference between infections but immunohistology confirmed iBALT (arrows) being more pronounced in the vM1stop infection. A, B: HE stained sections. PAP method (T cell marker); ABC method (B cell marker) Papanicolaou's haematoxylin counterstain. Bars= 100μm

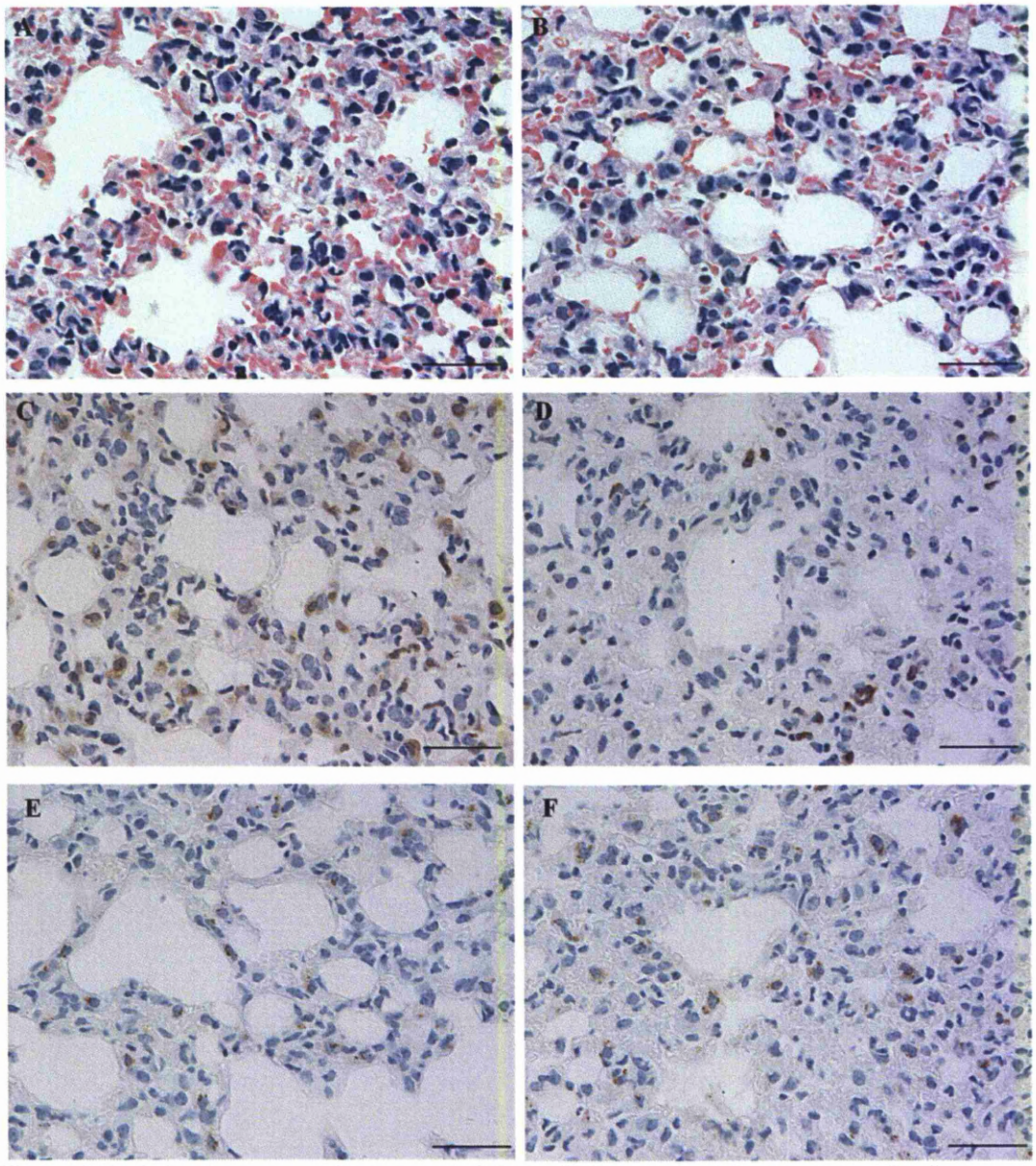

Figure 3.30 Wood mouse, vM1stop and vM1rev infected, day 28 p.i. Lung. Histology and immunohistology using marker for macrophages and type II pneumocytes.
A, C: corresponding areas in the lungs of vM1rev infected animal; B, D: corresponding areas in the lungs of vM1stop infected animal. A, B: HE stained sections; C, D: Immunohistology using marker for macrophages; E, F: Immunohistology using marker Type II pneumocytes. On histology there is little difference between infections but immunohistology confirmed mild interstitial infiltration by macrophages in the vM1rev infected wood mice. Type II pneumocytes presence in alveolar lining, in either infections however was similar to that seen in mock infected wood mice. A, B: HE stained sections. C-F: PAP method Papanicolaou's haematoxylin counterstain. Bars= 25 μm

3.2.1.3 Viral load in the nasal cavity and lung following vM1stop and vM1rev infection

Viral load was measured in order to assess MHV-68 replication. The tissues examined were, nasal cavity, the route of infection in this experiment and the lung the main site of MHV-68 acute infection. The hypothesis tested was that in the natural host, the presence or absence of M1 transcription would lead to changes in MHV-68 replication.

The viral load in the nasal cavity was assessed at day 3 and day 7 p.i., times representative of acute infection. The viral load was highest in vM1stop and vM1rev infection at day 3 p.i and decreased by day 7 p.i (Figure 3.31). However, the statistical analysis using an unpaired t test did not reveal a significant difference ($P>0.05$), this is likely due to high biological variability per infection.

In the lung, viral load was determined at day 3 and 7 p.i (times representative of acute infection) and day 14 and 28 p.i. (times representative of latent infection). Similarly to that seen in the nasal cavity, viral load was highest at day 3 p.i and decreased thereafter. Differences in viral load between viral infections were statistically significant at day 14 and 28 p.i (Figure 3.31). At day 14 p.i vM1stop infected animals showed more than a tenfold less of viral load when compared to vM1rev infected animals. At day 28 p.i. in vM1stop infected animals, the viral load observed at day 14 p.i remained approximately the same. On the other hand, at day 28 p.i in vM1rev infected mice, there was a greater decrease in viral load of approximately a hundredfold when compared to the values on day 14 p.i. Within the vM1rev infection there was a significant decrease in the viral load between day 7 and day 14 p.i. and between day 14 and day 28 p.i.

A

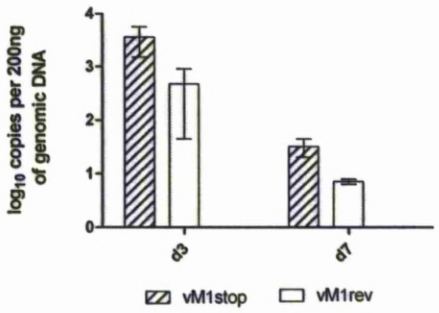

B

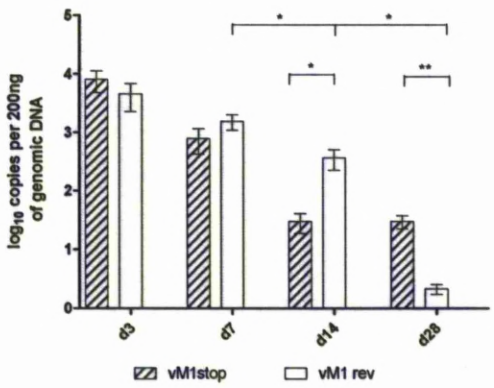

Figure 3.31 Wood mouse, vM1stop and vM1rev infected. Viral load in nasal cavity and lung tissue.

A and B are representations of viral load determined by 2 separate real time PCR experiments, using genomic DNA extracted from nasal cavity tissue (A) and lung (B) of wood mice infected with vM1rev and vM1stop virus. n=3 per virus per time point. Error bars represent SEM and significant differences were determined by an unpaired t test (*$p<0.05$, **$p<0.01$). In the nasal cavity, there were no significant statistical differences detected at day 3 and 7 p.i. In the lung the time when viral load was highest in either infections was at 3 d.p.i and it decreased thereafter. Differences in viral load between viruses were statistically significant at day 14 and 28 p.i. vM1stop infected animals showed more than a tenfold less of viral load at day 14 p.i when compared to vM1rev infected animals. The viral load observed at day 14 p.i remained approximately the same at day 28 p.i. in vM1stop infected animals. On the contrary, in vM1rev infected mice, at day 28 p.i there was a great decrease in viral load of approximately a hundredfold when compared to the values on day 14 p.i.

3.2.1.4 Presence of viral antigen in the nasal cavity and lung

Immunohistology was performed using anti-MHV-68 antibody. The antibody used is a rabbit polyclonal anti-MHV-68 serum raised against infected RK-13 cells and with specificity for structural proteins and thus is an indicator of lytic infection.

In the nasal cavity, no viral antigen was detected at any time. In the lungs, at day 3 p.i., in both infections, lytic infection was shown in mainly type I pneumocytes and to a much lesser extent type II pneumocytes. At day 7, in both infections, the overall presence of viral antigen was reduced. However lytic infection was still shown in type I and type II pneumocytes as seen in day 3 p.i. and was also seen in macrophages (Figure 3.32). In both infections the increased cellularity did not correlate with the amount of antigen detected and on the contrary the majority of cells seen in the areas of increased cellularity, did not exhibit the presence of viral antigen. Viral antigen was more frequently seen in areas where pathological changes were less severe.

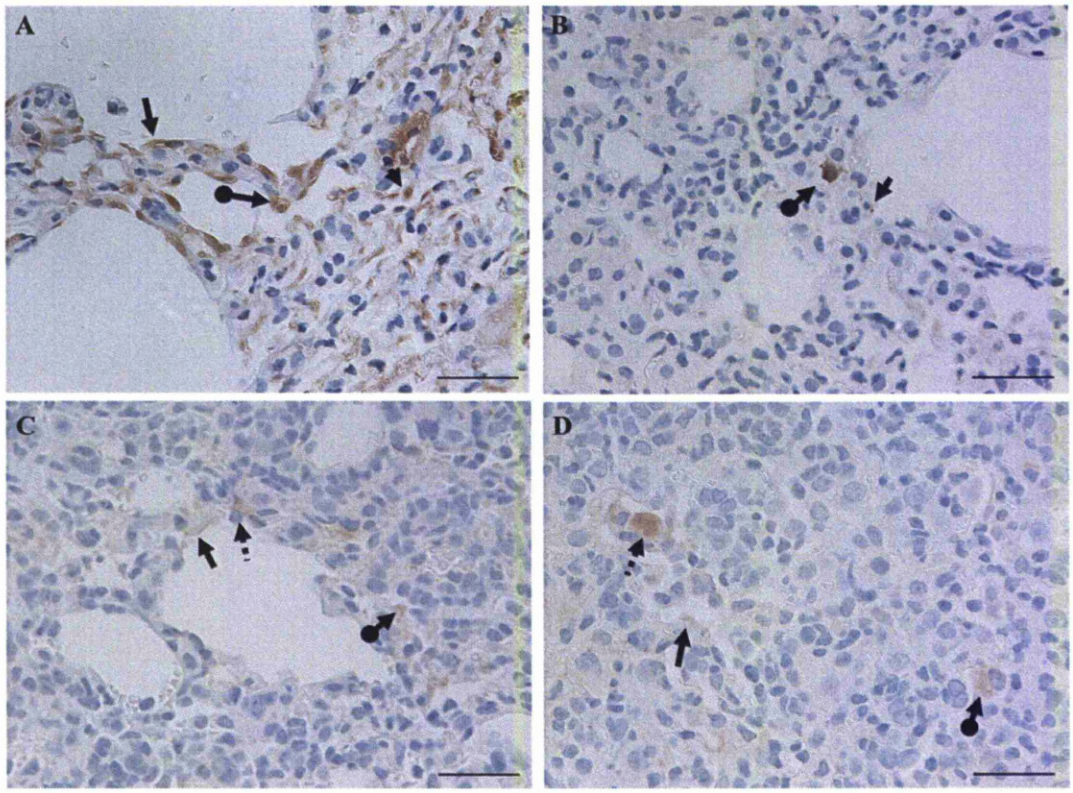

Figure 3.32 Wood mouse, vM1stop and vM1rev infected, day 3 and 7 p.i. Lung. Immunohistology for demonstration of viral antigen.
A, C: vM1rev infected animals; B, D vM1stop infected animals. A,B: day 3 p.i.; C,D: day 7 p.i.; Cells bearing antigen include pneumocytes type I (full arrows); pneumocytes type II (arrow with round tip) ; macrophages (dashed arrow). At day 3 p.i, in both infections, lytic infection was shown in mainly type I pneumocytes and to a much lesser extent type II pneumocytes. In the vM1stop infected animals the majority of cells seen in the areas of increased cellularity (B), did not exhibit the presence of viral antigen. At day 7, in both infections, the presence of viral antigen was reduced. However lytic infection was shown in macrophages, type I and type II pneumocytes (Figure 3.32). In both infections the majority of cells seen in the areas of increased cellularity, did not exhibit the presence of viral antigen. PAP method Papanicolaou's haematoxylin counterstain Bars= 25μm

3.2.1.5 Viral gene expression in latently infected cells in the lung

RNA-*in situ* hybridisation was performed using a vtRNA riboprobe on sections from the nasal cavity and lung. vtRNA refers to vtRNA-like sequence elements located at the extreme 5 `end of the genome, which are known to be expressed both in lytic and latent replication. If vtRNA transcript is detected and not associated with viral antigen, it is assumed that it represents latent infection. Tissues examined were from wood mice culled at day 3, 7, 14 and 28 p.i. with either vM1rev or vM1stop MHV-68. In the nasal cavity, no vtRNA transcripts were detected at any time.

At day 3 p.i, in the lung of wood mice infected with either vM1rev and vM1stop virus, vtRNA was detected in lymphocytes within the iBALT, intravascularly and occasionally in the interstitium. However, this was less intense and less frequent in the vM1stop infected animals (Figure 3.33).

At day 7 p.i. vtRNA transcripts were detected equally in both infections in lymphocytes within the iBALT, intravascularly and occasionally in the interstitium (Figure 3.33). Furthermore, at day 7, in the lung of vM1stop infected animals vtRNA was also detected in type II pneumocytes in the alveolar lining and in macrophages in the interstitium and desquamated into the alveolar space (Figure 3.35).

The samples examined from day 14 and day 28 p.i. showed tRNA transcripts in lymphocytes in the iBALT.

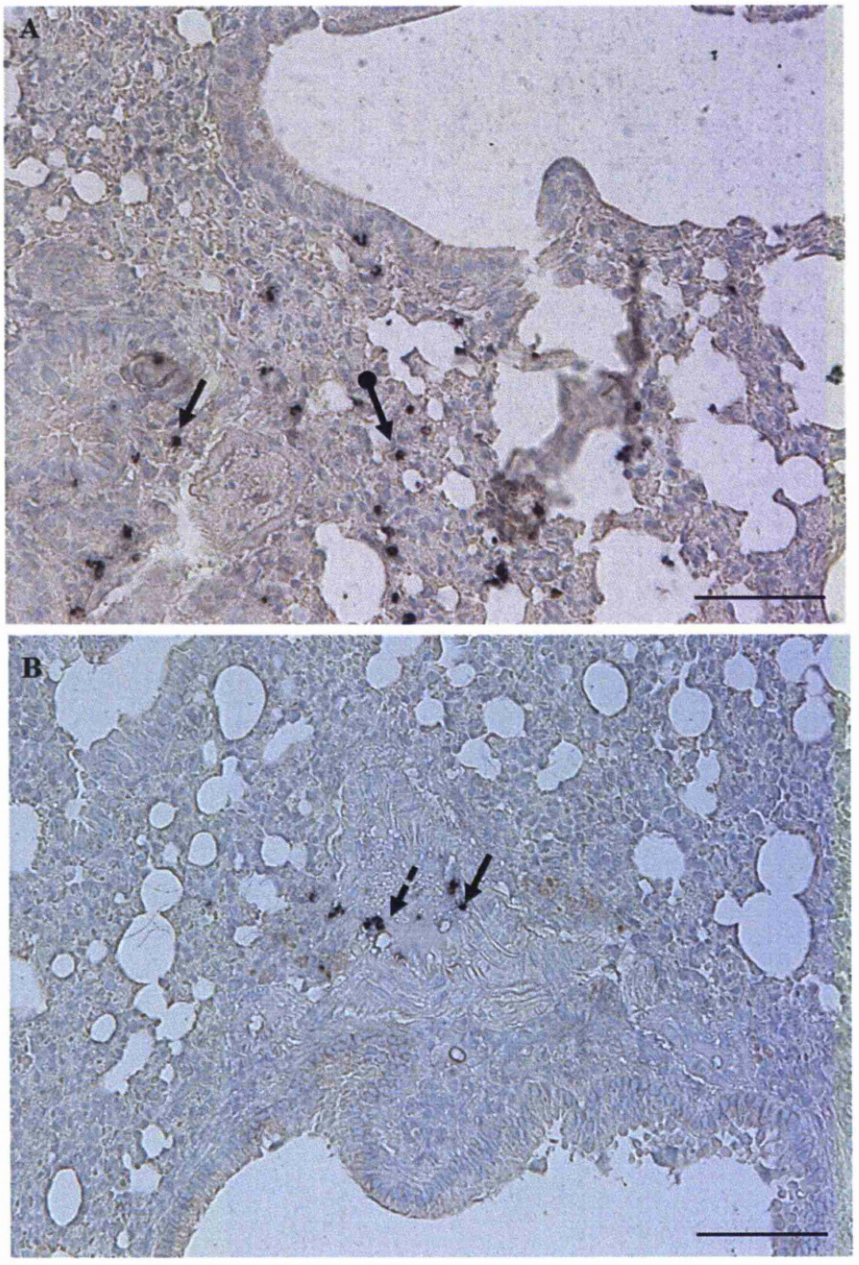

Figure 3.33 Wood mouse, vM1stop and vM1rev infected, day 3 p.i. Lung. RNA-ISH using vtRNA riboprobe.
A,C: vM1rev infected wood mice; B: vM1stop infected wood mice. Transcription of vtRNA detected in lymphocytes in peribronchiolar/perivascular areas (arrow), intravascularly (dashed arrow) and occasionally within the alveolar wall (arrow with round tip). This is most frequently seen in the vM1rev infected animals. RNA-ISH, NBT/BCIP, Papanicolaou's haematoxylin counterstain. Scale bars 50 μm

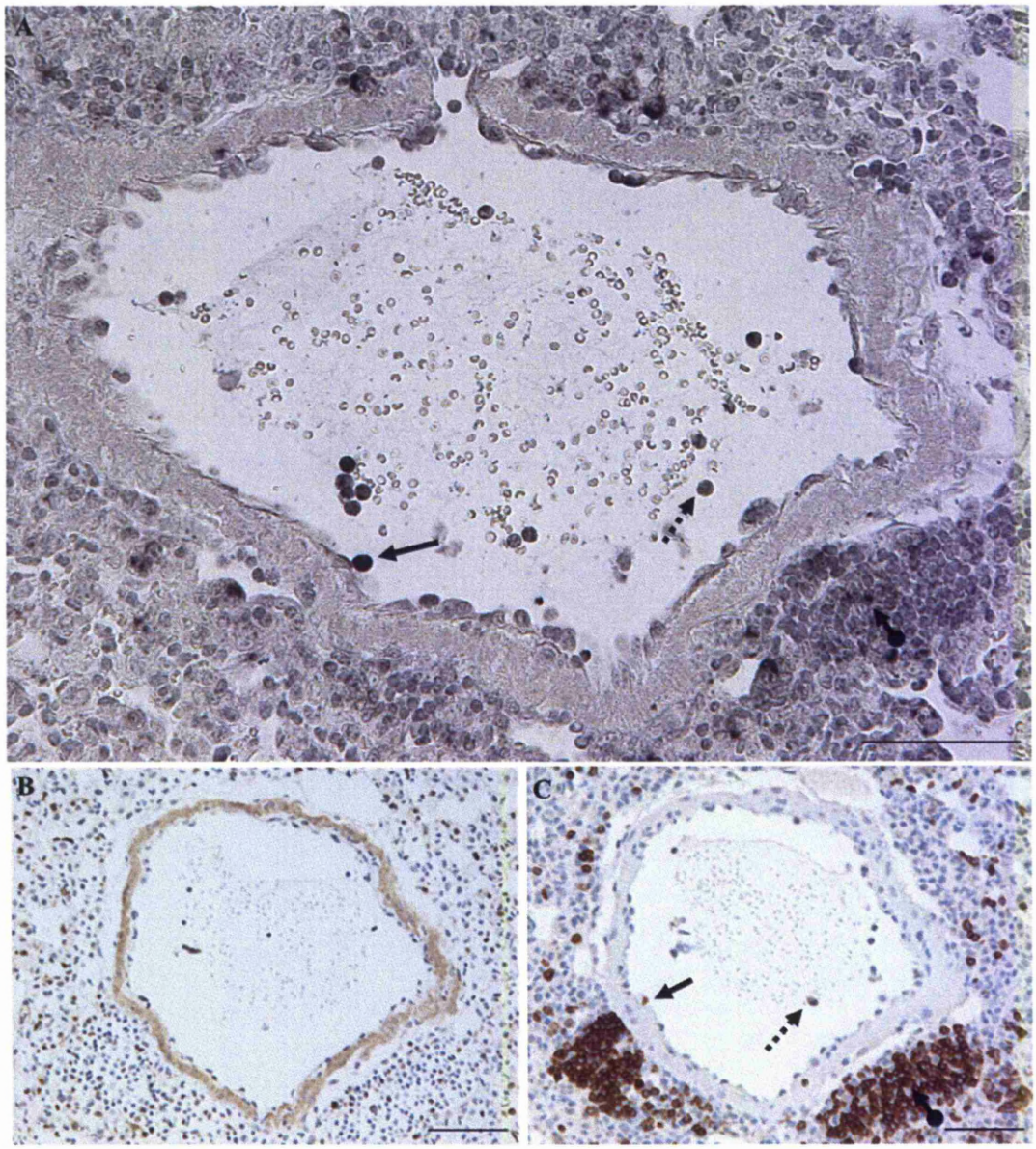

Figure 3.34 Wood mouse vM1rev infected, day 7 p.i. Lung. RNA-ISH using vtRNA riboprobe and immunohistology using marker for T and B cells.
A,B,C: Represent sequential sections of same area. A: RNA-ISH using vtRNA riboprobe. vtRNA transcripts in lymphocytes clustered within the iBALT (arrows with round tip), single lymphocytes intravascular (dashed arrow) and lymphocytes adjacent to endothelial surface, rolling (full arrow); B: Immunohistology using marker for T. The cells observed to show vtRNA transcripts are not T cells; C: Immunohistology using marker for B cells. Cells observed to exhibit vtRNA transcripts are B cells: lymphocytes clustered within the iBALT (arrow with round tip), single lymphocytes intravascular (dashed arrow) and lymphocytes adjacent to endothelial surface, rolling (full arrow). RNA-ISH, NBT/BCIP, Papanicolaou's haematoxylin counterstain. PAP method (T cell marker); ABC method (B cell marker), Papanicolaou's haematoxylin counterstain; Bars=25 μm

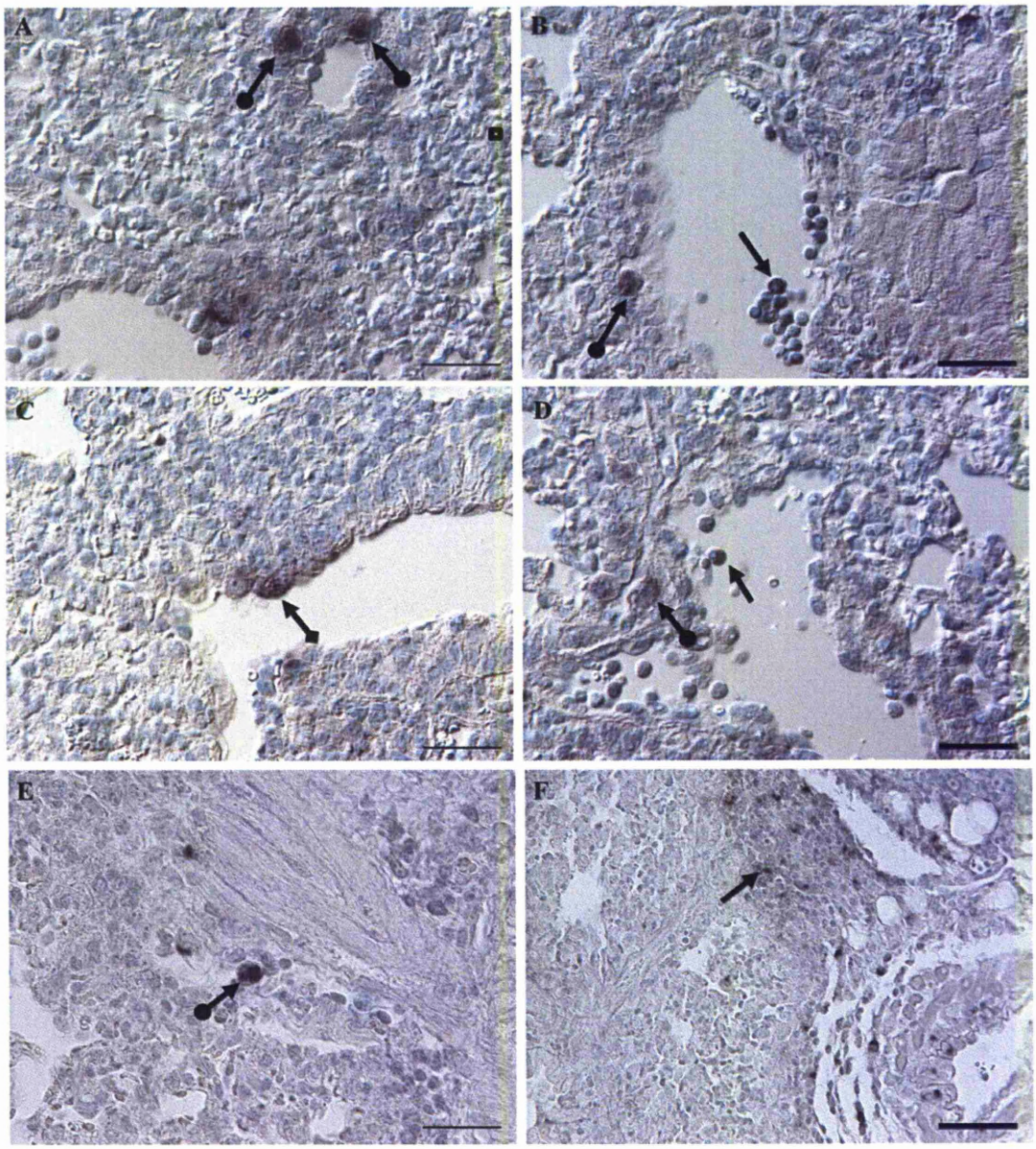

Figure 3.35 Wood mouse, vM1stop infected, day 7 p.i. Lung RNA-ISH using vtRNA riboprobe.

vtRNA positive lymphocytes (full arrows) within the iBALT, intravascular and in adjacent alveoli. In the interstitium (A,B,D) and desquamated into alveoli (E) vtRNA positive cells (arrows with round tip) larger than lymphocytes consistent with macrophages are seen. Also occasional cells lining alveoli, consistent with type II pneumocytes were positive for vtRNA(arrow with square tip in C). RNA ISH, NBT/BCIP, Papanicolaou's haematoxylin counterstain. Bars: A,B,C= 25 μm; D=50 μm

3.2.1.6 Ultrastructural study of viral replication in the lung

Electron microscopy was used to examine viral replication *in situ*. Active viral replication was only seen in vM1rev infected animals at day 3 p.i. The cells where replication was observed showed extensive degenerative changes when replication was highly active (Figure 3.36 - Figure 3.38). These cells were identified to be type II pneumocytes due to the presence of lamellar bodies and/or the intercellular junctions, *zona adherens*. The nuclei of these cells were swollen and exhibited peripheralization of the chromatin leading to a thick electron dense area adjacent to the inner nuclear membrane. The remaining nucleus exhibited lake like areas where the chromatin was mildly denser and where the "viral factories" were seen (Figure 3.37). "Viral factories" consisted of areas where empty and packed capsids measuring 73-76 ηm were most numerous and often clustered. The space between the inner and outer leaflet of the nuclear membrane was irregularly expanded and the profile of the latter showed wide "corrugations". In the cytoplasm the viral particles were within membrane bound tubules consistent with a swollen Golgi apparatus and were bigger than those seen in the nucleus. There were two types of viral particle, those with several circular demarcations and those which were completely electron dense with no identifiable structure. The inner circular demarcation was of the same size as the ones seen in the nucleus thus likely represents the capsid, the middle demarcation ~115-126ηm in diameter likely represents the primary envelope and the outer demarcation, ~ 168-172ηm likely represents the secondary envelope. The cytoplasmic viral particles were occasionally surrounded or adjacent to abundant electron dense material, possibly tegument related. The cytoplasmic organelles including Golgi and mitochondria were frequently expanded with the mitochondrial cristae profile being effaced.

3.2.1.7 Summary of morphological and immunohistological findings in the lung.

The findings in the lung of wood mice infected with vM1stop and vM1rev are summarized in Table 3.3.

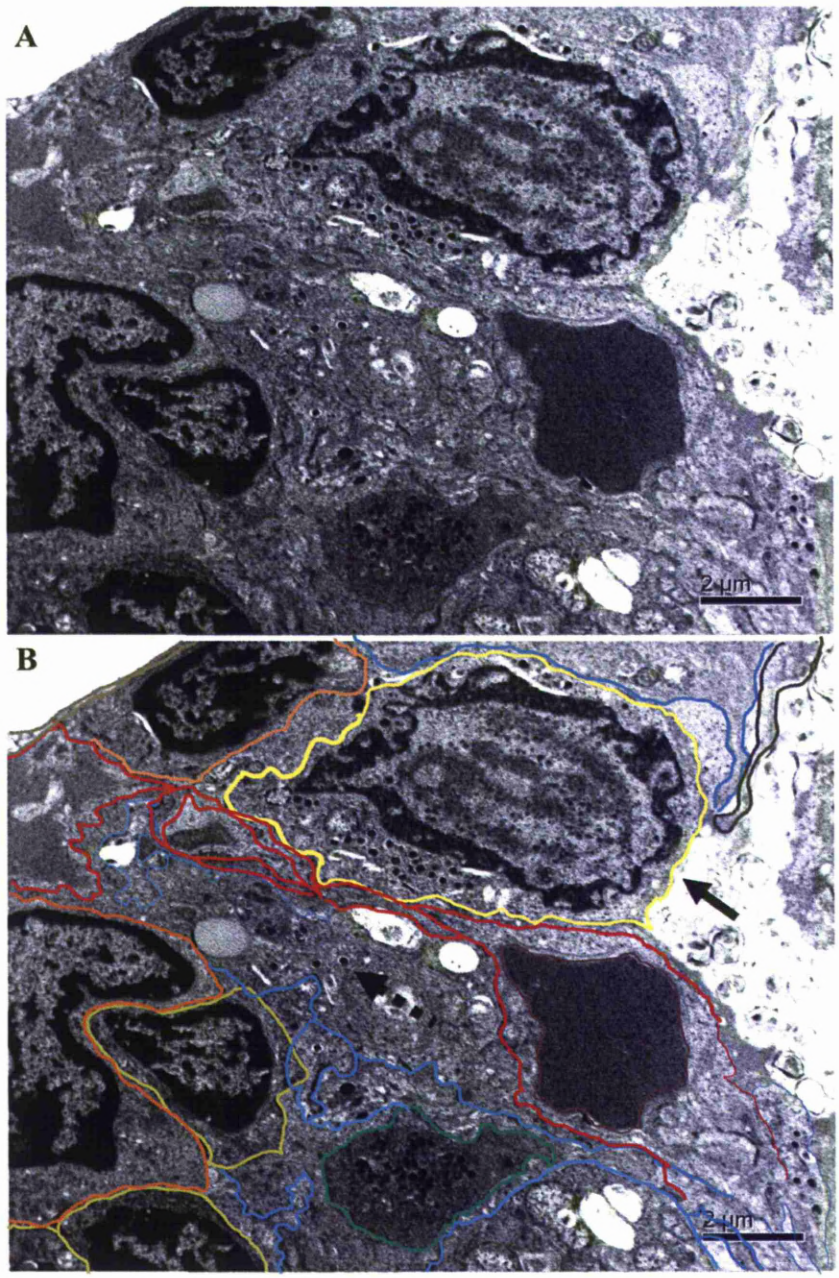

Figure 3.36 Wood mouse, vM1rev infected, day 3 p.i. Lung Ultrastructure.
A,B - Overview of the alveolar architecture. B represents the same image as A but with the cells outlined using the following colour code: macrophage (orange), pneumocyte type II (yellow), pnemocyte type I (brown, in the top right corner of the picture); endothelium (red); intravascular cell (green) and interstitium (blue). In the alveolar lining, there is a type II pneumocyte showing active viral replication (full arrow in B). The interstitium is severely expanded due to necrotic debris and cellular infiltration. Within the interstitium there are cellular processes with numerous fully formed viral particles (dashed arrow in B).

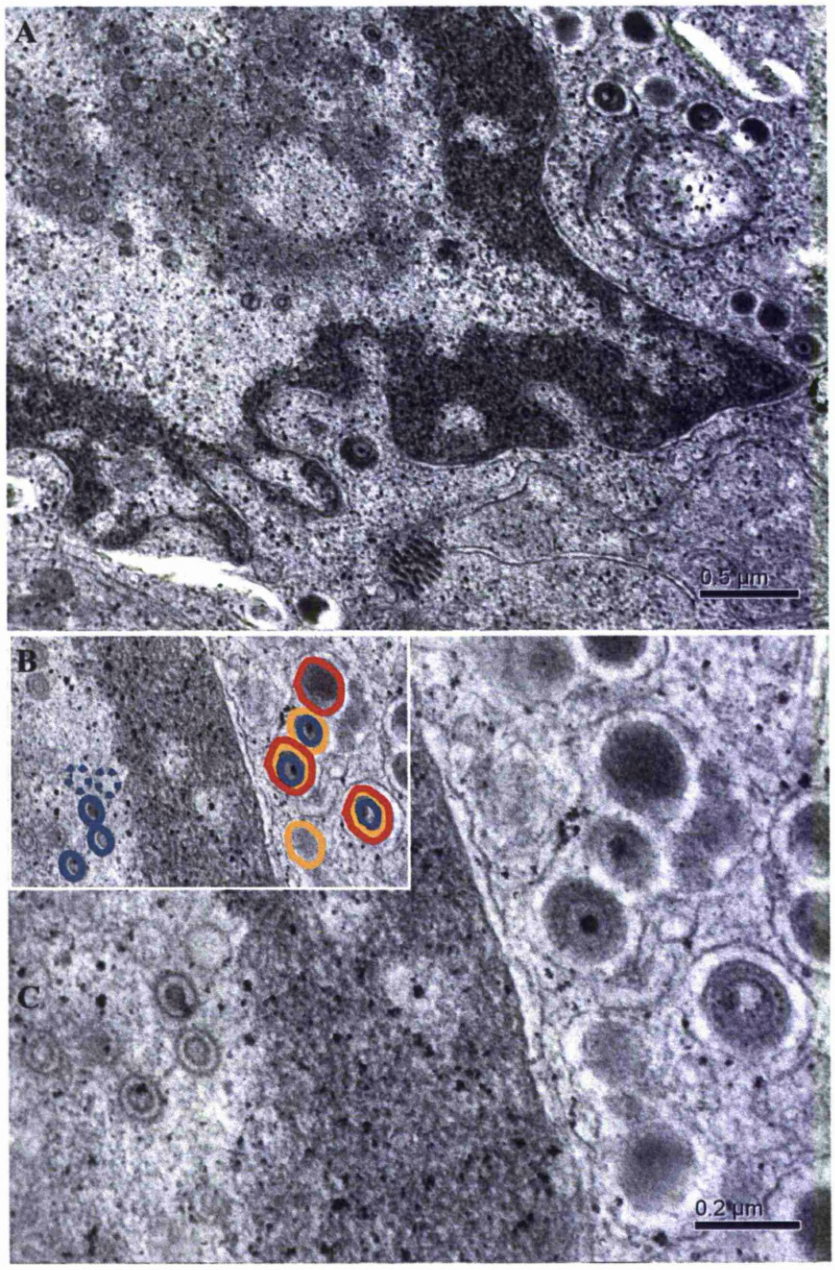

Figure 3.37 Wood mouse, vM1rev infected, day 3 p.i. Lung Ultrastructure of viral particles.

A,B: Close up of the type II pneumocyte highlighted with full arrow in Figure 3.36 B, showing the viral particles at the different locations. Intranuclear distribution of chromatin and effacement of cytoplasmic organelles; B,C: represent the same image but in B circular demarcations of the viral particles outlined using the following colour code as to facilitate the discerning of the different structures. Dashed blue: empty capsid; Blue: packed capsid; Yellow: primary envelope; Red: secondary envelope;

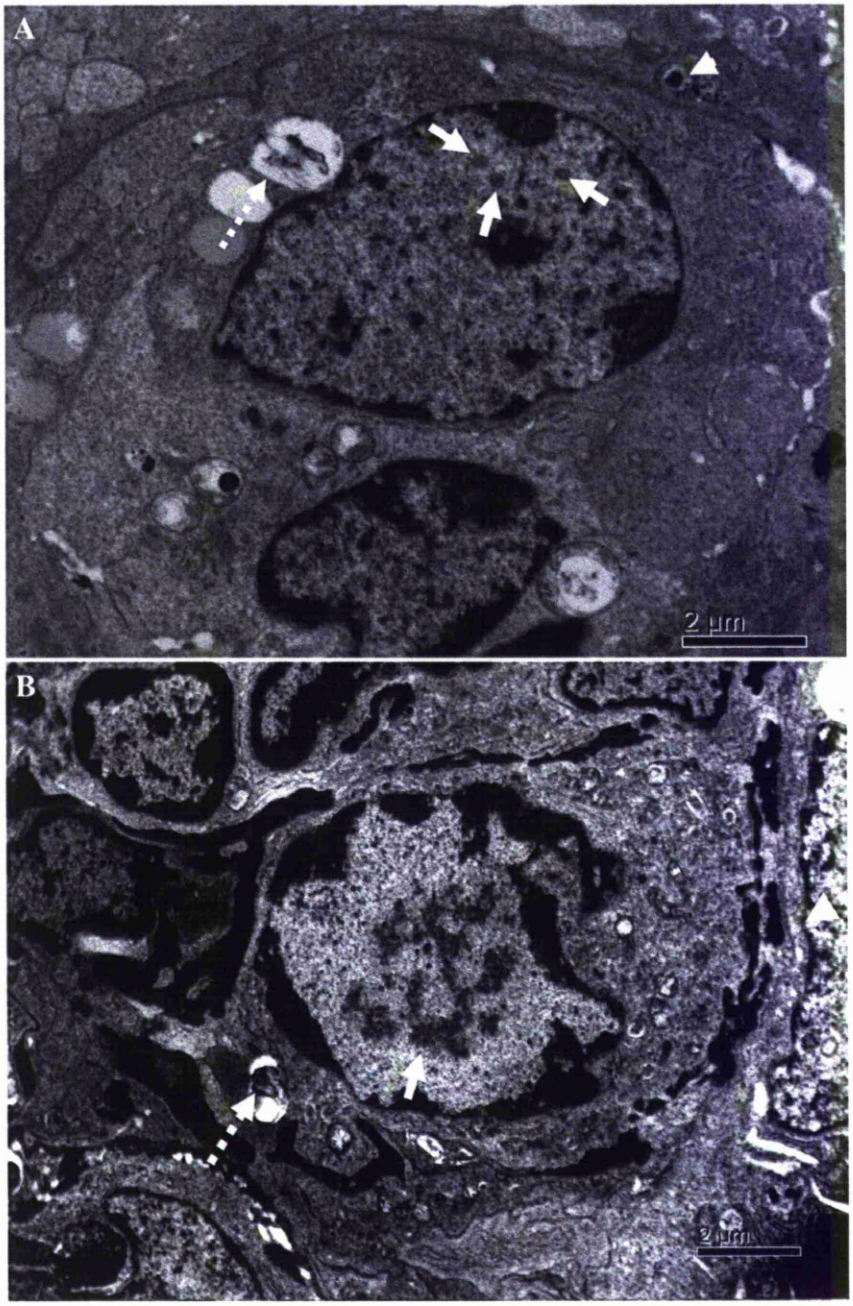

Figure 3.38 Wood mouse vM1rev infected, day 3 p.i. Lung. Ultrastucture.
A: Type II pneumocyte with intranuclear structures consistent with fully formed viral particles (~170 ηm – arrows) but showing no evidence of active viral replication. There is a virion in the adjacent extracellular space (arrowhead). B: Area of increased interstitial cellularity composed mostly of hyperplastic and active type II pneumocytes, macrophages and not identifiable degenerating cells. There is a cell in the centre showing active viral replication (white arrow). In the cytoplasm of the central cell there are numerous lamellar bodies indicating this to be a type II pneumocyte (dashed white arrow). A,B: lamellar bodies highlighted by dashed arrows.

Days p.i.	Lung of vM1stop Infected wood mouse	Lung of vM1rev infected wood mouse
3	MF > cellularity (++/+++) >Type II pneumocytes (+/++) Macrophages often containing lipid: interstitial (+/++); alveolar (+/++) Lymphocytes, interstitial (+/++) More frequent iBALT (+) vAg: type I & type II pneumocytes vtRNA: lymphocytes - iBALT, intravascular and interstitial (+) Viral load peak	MF increase in cellularity (+) > Type II pneumocytes (+) Viral factories: type II pneumocytes: Macrophages: interstitial (+); alveolar (+) Lymphocytes, interstitial (+) Minimal iBALT (+) vAg: type I & type II pneumocytes vtRNA: lymphocytes - iBALT, intravascular and interstitial (+/++) Viral load peak
7	MF increase in cellularity (++/+++) Type II pneumocytes hyperplasia(++/+++) Type I pneumocyte necrosis (+/++) MF fibrino-necrotic foci Macrophages: interstitial (++); alveolar (++/+) Lymphocytes, interstitial (+/++) More frequent iBALT (+) vAg: type I and type II pneumocytes and macrophages – more frequent in less altered areas vtRNA: lymphocytes - iBALT, intravascular and interstitial; type II pneumocytes; macrophages	D increase in cellularity (++/+++) Type II pneumocytes hyperplasia(++/+) Type I pneumocyte necrosis (+/++) Macrophages: interstitial (+/++); alveolar (+/+++) Lymphocytes, interstitial (+/++) iBALT (+) vAg: type I and type II pneumocytes and macrophages – more frequent in less altered areas vtRNA: lymphocytes - iBALT, intravascular and interstitial
14	MF increase in cellularity (+) Type II pneumocytes hyperplasia(+) Macrophages: interstitial (++/+++); alveolar (+) Lymphocytes, interstitial (+/++) iBALT (++) vtRNA: lymphocytes - iBALT < viral load than d7 p.i. & vM1rev at day 14 p.i.	MF increase in cellularity (+) Type II pneumocytes hyperplasia(+) Macrophages: interstitial (++/+++); alveolar (+) Lymphocytes, interstitial (+/++) iBALT (++) vtRNA: lymphocytes – iBALT < viral load compared to day 7 p.i.
28	iBALT (++) vtRNA: lymphocytes – iBALT Viral load similar to day 14 p.i.	iBALT (+) vtRNA: lymphocytes – iBALT < viral load compared to day 14 p.i.

Table 3.3 Summary of main findings in the lung of wood mice over a 28 day timecourse following vM1stop or vM1rev infection.

Semiquantitative parameters used to represent number of cells: + (scattered cells); ++ (moderate number of cells); +++ (numerous cells); MF: multifocal; D: diffuse; vAg: viral antigen; <: significant decrease;
>: significant increase;

3.2.1.8 Cytokine expression in the lung and airways following infection of the woodmouse with vM1stop and vM1re v

Considering the increase in macrophages in the absence of M1 expression, studies were performed to determine the mechanism of their activation and their secretion profile. CCSP expression was semiquantified using RNA-ISH. Secretion of TNF-α was assessed by immunohistology. Further cytokines were semiquantified using qPCR: IL-10, TNF-α, IFN-γ, MIP1-α, MIP-1β, RANTES, TGF-β, HGF and IL-10p35. qPCR was also used to determine the relative expression of the enzymes Arginase 1 and iNOS.

3.2.1.8.1 Mock infected wood mice.

Wood mice instilled intranasally using PBS (mock infected) served to identify the baseline for the semiquantitative analysis of cytokine/enzyme expression and secretion.

CCSP expression in mock infected wood mice was seen to be restricted to Clara cells lining bronchioles (Figure 3.39). TNF-α secretion was seen sparsely in few scattered cells including occasional bronchiolar epithelial cells and macrophages within the pulmonary interstitium, mainly in close proximity to bronchioles (Figure 3.40). qPCR analysis was performed using the Pfaffl equation. In this analysis the baseline (the value of 1) corresponds to the values obtained in mock infected wood mice.

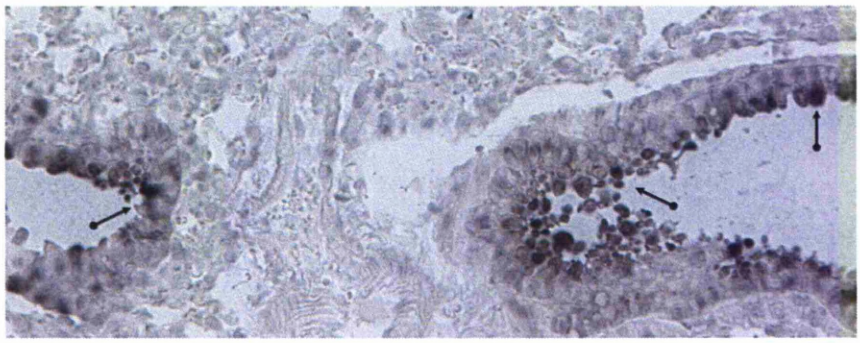

Figure 3.39 Wood mouse, mock infected. Lung. CCSP mRNA expression.
CCSP expression by Clara cells (arrows with round tip) lining the lower bronchi and bronchiolar epithelium in all animals. RNA-ISH, NBT/BCIP, Papanicolaou's haematoxylin counterstain. Bar = 25 μm

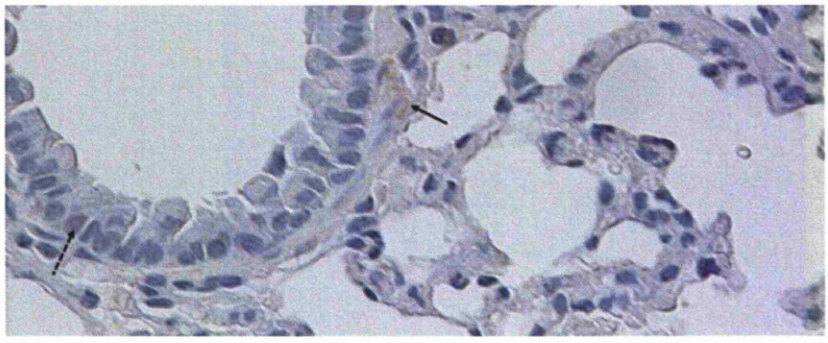

Figure 3.40 Wood mouse, mock infected. Lung. Immunohistology for demonstration of TNF-α.
TNF-α secretion is seen sparsely in few scattered cells including bronchial epithelial cells (dashed arrow) and macrophages in close proximity to bronchioles (arrow). ABC method Papanicolaou's haematoxylin counterstain. Bars A = 25 μm

3.2.1.8.2 CCSP *in situ* expression in the lower airways of infected wood mice

Expression of CCSP in the lower airways and lung was assessed by RNA-ISH using a CCSP riboprobe. This experiment was performed on sections of lung from vM1stop and vM1rev infected animals. The times chosen were day 3 and day 7 p.i, representative of acute infection.

At day 3 p.i. in comparison to the mock infected wood mouse, in the vM1stop infected mouse, there was a severe decrease in the expression of CCSP in cells (Clara cells) lining the lower bronchi and bronchiolar epithelium (Figure 3.41).

At day 7 the expression of CCSP in cells (Clara cells) lining the lower bronchi and bronchiolar epithelium was decreased in both types of infection. When comparing both types of infection, the decrease was greater in the vM1stop infected wood mice (Figure 3.41).

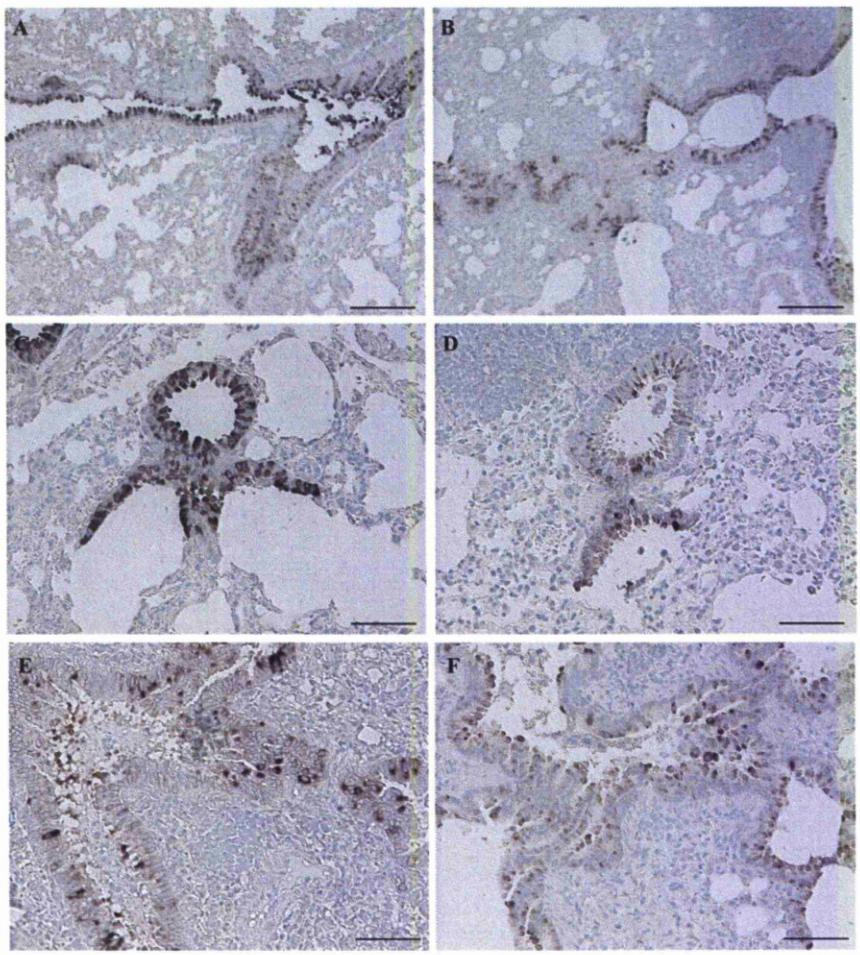

Figure 3.41 Wood mouse, mock, vM1rev and vM1stop infected, day 3 and 7 p.i. Lung CCSP mRNA expression.

A,C,E: vM1rev infected; B, D, F: vM1stop infected animals; CCSP expression by cells (Clara cells) lining the lower bronchi and bronchiolar epithelium in all animals. At day 3 p.i (A-D), in the vM1stop infected mouse, there was a severe decrease in the expression of CCSP in. At day 7 (E, F) the expression of CCSP was decreased in both types of infection, the decrease being greater in the vM1stop infected wood mice. RNA-ISH, NBT/BCIP, Papanicolaou's haematoxylin counterstain. Bars: A, B= 100 μm; C, D = 25 μm E,F= 50 μm

3.2.1.8.3 TNF-α secretion in the lower airways and lung of infected wood mice

Secretion of TNF-α was assessed by immunohistology in vM1stop and vM1rev infected wood mice at day 3, 7, 14 and 28 p.i.

At day 3 (Figure 3.42) and to a greater extent at day 7 p.i. (Figure 3.43), in both vM1stop and vM1rev infection, TNF-α was seen in the cytoplasm of tracheal, bronchial and bronchiolar respiratory epithelial cells, macrophages within interstitium and type II pneumocytes. Secretion was also detected in numerous cells in close proximity to the bronchioles, including within the iBALT (Figure 3.42). However the proportion of positive cells was higher in the lung from vM1stop infected wood mice, in particular in the multifocal areas of increased cellularity (Figure 3.42).

At day 14 p.i. (Figure 3.44) in both infections, TNF-α presence was no longer detected in tracheal and bronchial respiratory epithelial cells but was still seen in bronchiolar respiratory epithelial cells, macrophages within interstitium and type II pneumocytes. Secretion was also detected in numerous cells in close proximity to the bronchioles, including within the iBALT. Secretion was severely decreased when compared to previous times and there were few differences between vM1stop and vM1rev infection.

At day 28 TNF-α presence was similar to that which was observed in mock infected wood mice.

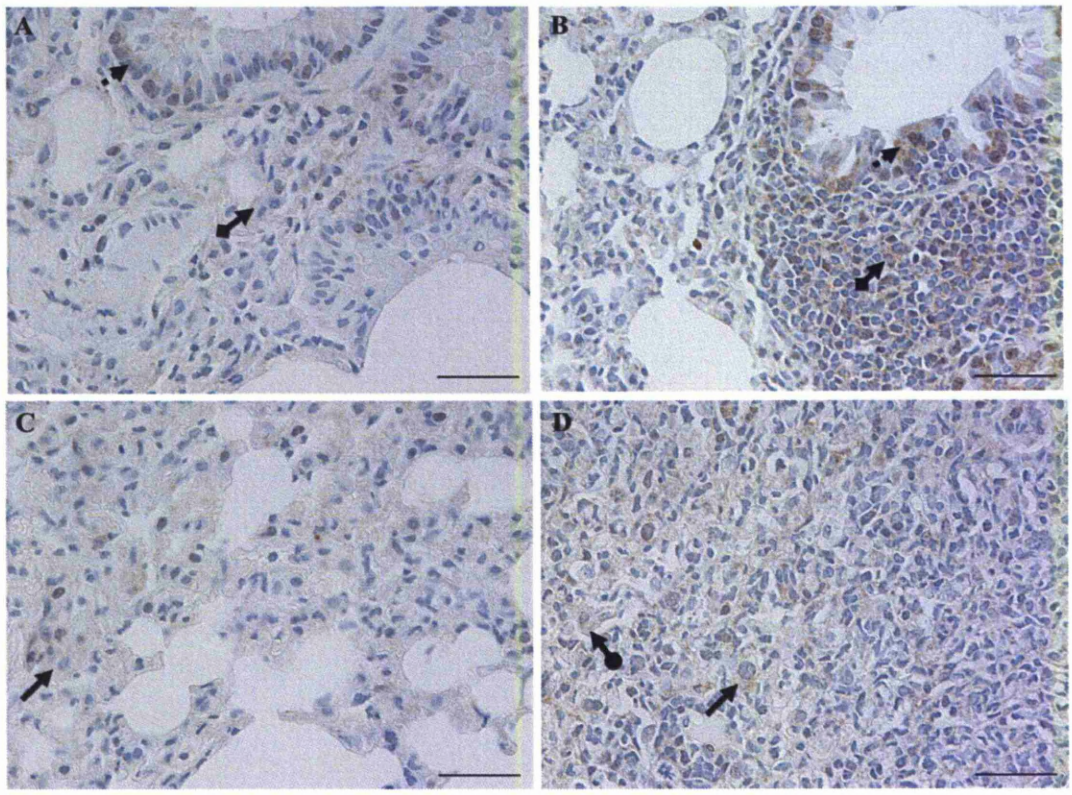

Figure 3.42 Wood mouse. Mock, vM1rev and vM1stop infected, day 3 p.i. Lung. Immunohistology for demonstration of TNF-α.
A, B: vM1rev; C, D: vM1stop infected; vM1rev and vM1stop infected animals show increased secretion of TNF-α in comparison to mock infected mice. TNF-α in the cytoplasm bronchiolar epithelial cells (dashed arrows), macrophages within interstitium (full arrow) and type II pneumocytes (arrow with round tip). Secretion was also detected in numerous cells in parenchyma in close proximity to bronchioles (arrow with square tip), including within the iBALT. The proportion of positive cells was higher in the lung from vM1stop infected wood mice, in particular in the multifocal areas of increased cellularity (D). ABC method Papanicolaou's haematoxylin counterstain. Bars A-D = 25 μm

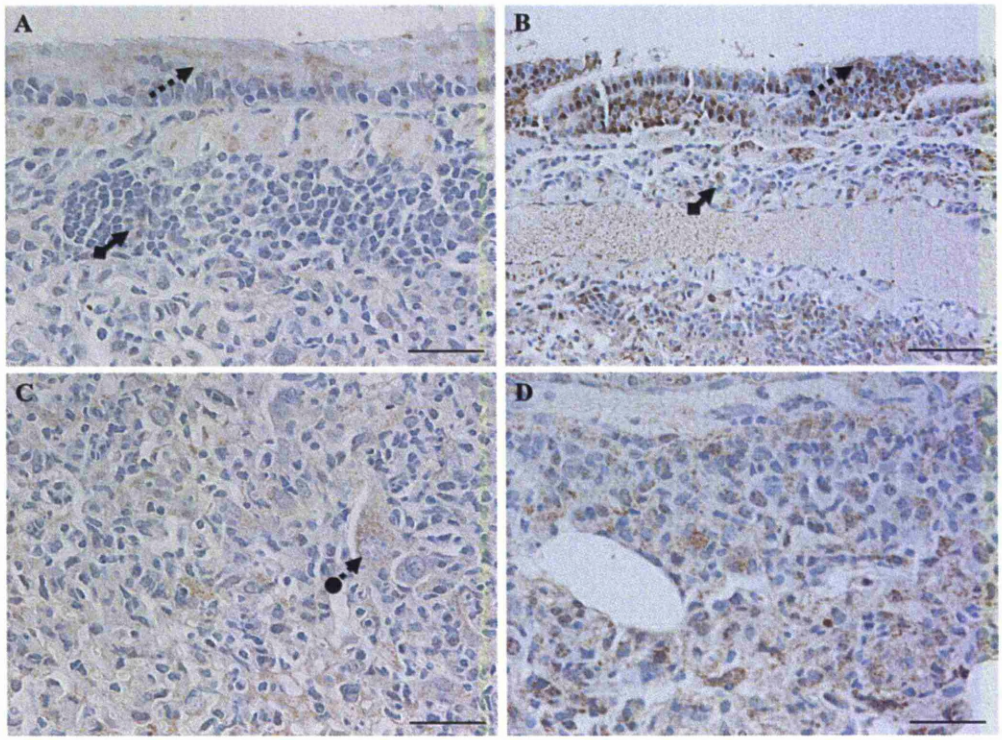

Figure 3.43 Wood mouse, vM1rev and vM1stop infected, day 7 p.i. Lung. Immunohistology for demonstration of TNF-α.
A,C: vM1rev infected; B-D: vM1stop infected; TNF-α in the cytoplasm tracheal epithelial cells (dashed arrows), macrophages within interstitium and type II pneumocytes ((dashed arrow with round tip - binucleated). Secretion was also detected in cells in close proximity to bronchioles (arrow with square tip). The proportion of positive cells and the intensity of signal was higher in the lung from vM1stop infected wood mice. ABC method Papanicolaou's haematoxylin counterstain. Bar = 25 μm

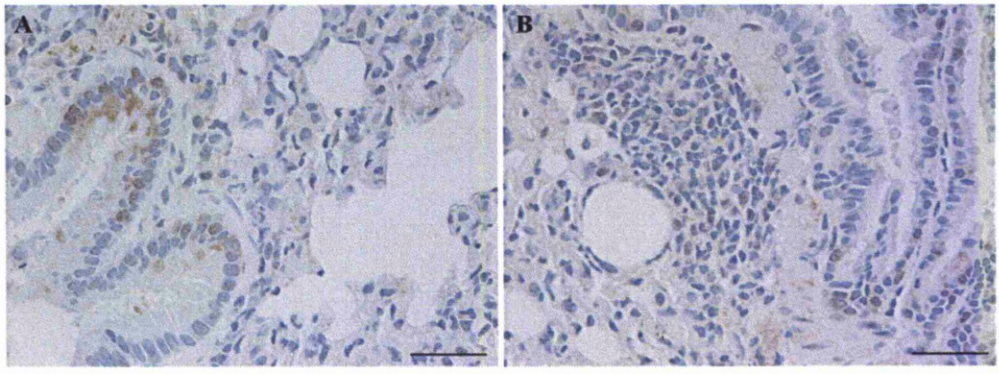

Figure 3.44 Wood mouse, vM1rev and vM1stop infected, day 14 p.i. Lung. Immunohistology for demonstration of TNF-α.
A: vM1rev infected; B: vM1stop infected; TNF-α is severely reduced compared to previous times and there is little difference between types of infection. ABC method Papanicolaou's haematoxylin counterstain. Bar = 25 μm

3.2.1.8.4 Expression of enzymes and cytokines involved in macrophage activation

Cytokine expression was evaluated by real time PCR performed on cDNA synthesised using RNA extracted from lung tissue of wood mice infected with vM1stop and vM1rev and culled at day 7 p.i. The gene expression ratio was determined using the Pfaffl equation [316] with values of test samples being normalized against the Ct values obtained from mock infected wood mice. Cytokines assessed were IL-10, TNF-α, IFN-γ, MIP1-α, MIP-1β, RANTES, TGF-β, HGF, IL12p40 and IL-10p35.

Also analysed was the expression of the enzymes NOS2 and Arginase I in order to determine the main pathway leading to macrophage activation.

As Figure 3.45 shows in wood mice infected with vM1rev, there is almost a tenfold increase in IL-10 and NOS2 expression. To a lesser extent there is an increase in MIP1-β, TNF-α and TGF-β and a decrease in HGF expression. When compared to the vM1stop infection it can be seen that there is the same trend in the expression of most cytokines. However, in the vM1stop infection, there is almost a tenfold further increase in expression of IL-10 and TNF-α. Other differences in expression seen in vM1stop infection were an increase in MIP1α expression, a decrease in MIP1-β and arginase I expression, and no change in HGF expression.

3.2.1.8.5 Summary of findings in the *in vivo* studies of relative cytokine expression/secretion

The findings of CCSP transcript expression analysis by RNA-ISH, TNF-α secretion analysis by immunohistology and relative expression of IL-10, TNF-α, IFN-γ, MIP1-α, MIP-1β, RANTES, TGF-β, HGF, IL12p40 and IL-10p35 analysis by qPCR, are summarized in Table 3.4.

A

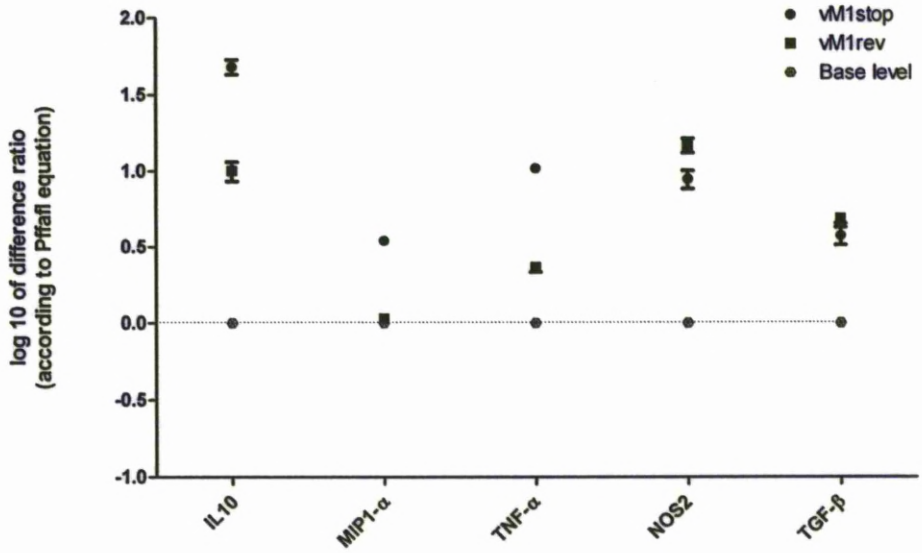

B

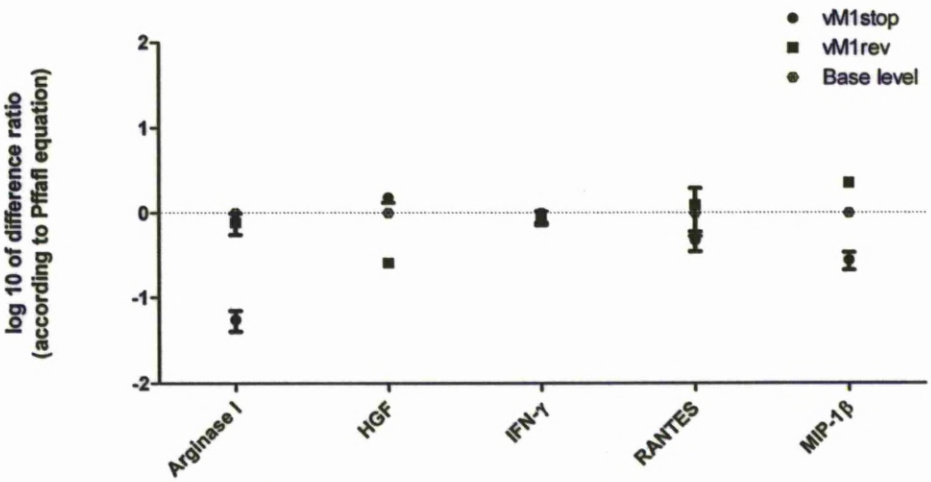

Figure 3.45 Cytokine/enzyme expression in vM1stop and vM1rev infected woodmice in comparison to expression in mock infected wood mice, at day 7 p.i.
Values obtained through qPCR performed on cDNA synthetized from RNA extracted from the lung tissue of infected wood mice. n=3 per time point, per infection. Error bars represent the standard error of the mean. Base level (dashed line) represents values obtained from mock infected mice. A: In both types of infection there is an increase in IL-10, TNF-α, NOS- and TGF-β The increase is however highest in the vM1stop infected animals which also showed an increase in MIP-1α expression. The latter was not observed in vM1rev infected animals. B: In wood mice infected with vM1rev, there is little change in the expression of arginase I and in IFN-γ. IFN-γ shows also little change in the vM1stop infected animals. Contrary to the findings in vM1rev infected animals, in vM1stop infected woodmice, Arginase I and to less extent HGF and MIP1-β showed a decrease in expression. vM1rev infected animals showed a mild increase in MIP1-β expression. RANTES expression showed too much variability within types of infection in order to allow a conclusive interpretation.

Lung	vM1stop	vM1rev
3	Immunohistology: < CCSP by Clara cells >>TNF-α by respiratory epithelial cells (trachea, bronchi & bronchioles), macrophages and type II pneumocytes (++)	Immunohistology: No Δ in CCSP by Clara cells >TNF-α by respiratory epithelial cells (trachea, bronchi & bronchioles), macrophages and type II pneumocytes (+)
7	<< CCSP by Clara cells >TNF-α by:respiratory epithelial cells(trachea, bronchi & bronchioles), macrophages and type II macrophages (+++) qPCR (approximate fold change): 75x > IL-10 10x > MIP-1α 10x: > TNF-α 5x < MIP1-β No Δ in IFN-γ 10x > iNOS 10x < Arginase I 5x > TGF-β Little Δ HGF	< CCSP by Clara cells >>TNF-α by respiratory epithelial cells (trachea, bronchi & bronchioles), macrophages and type II macrophages (++) qPCR(approximate fold change): 10x > IL-10 No Δ in MIP-1α 2.5x: > TNF-α 2.5x > MIP1-β No Δ in IFN-γ 10x > iNOS Little Δ Arginase I 5x > TGF-β 10x < HGF
14	Immunohistology: >TNF-α by respiratory epithelial cells(bronchioles), macrophages (inc. in iBALT) and type II pneumocytes (+)	Immunohistology: >TNF-α by respiratory epithelial cells(bronchioles), macrophages (inc. in iBALT) and type II pneumocytes (+)
28	Immunohistology: TNF-α secretion returned to baseline levels	Immunohistology: TNF-α secretion returned to baseline levels

Table 3.4 summarising findings in the study of relative cytokine expression/secretion in the lung of vM1stop and vM1rev infected wood mice in comparison to mock infected wood mice.

Semiquantitative parameters used to represent number of cells: showing expression + (scattered cells); ++ (moderate numbers); +++ (numerous cells)

Scale for change >: significant increase; <:significant decrease; Δ: change in expression

3.2.2 Spleen

3.2.2.1 Mock Infected wood mouse. Histological, immunohistological examination

Mock infected wood mice served as negative controls in order to determine any potential effects of the infection protocol. Accordingly, the examination of this group of mice served to identify normal structure and baseline leukocyte numbers. The morphology of the spleen in wood mice is very similar to that of laboratory mice. In mock infected animals, the white pulp is composed of primary follicles and small T cell zones (Figure 3.46). The red pulp is filled with a wide variety of leucocytes and haematopoietic cells including numerous megakaryocytes.

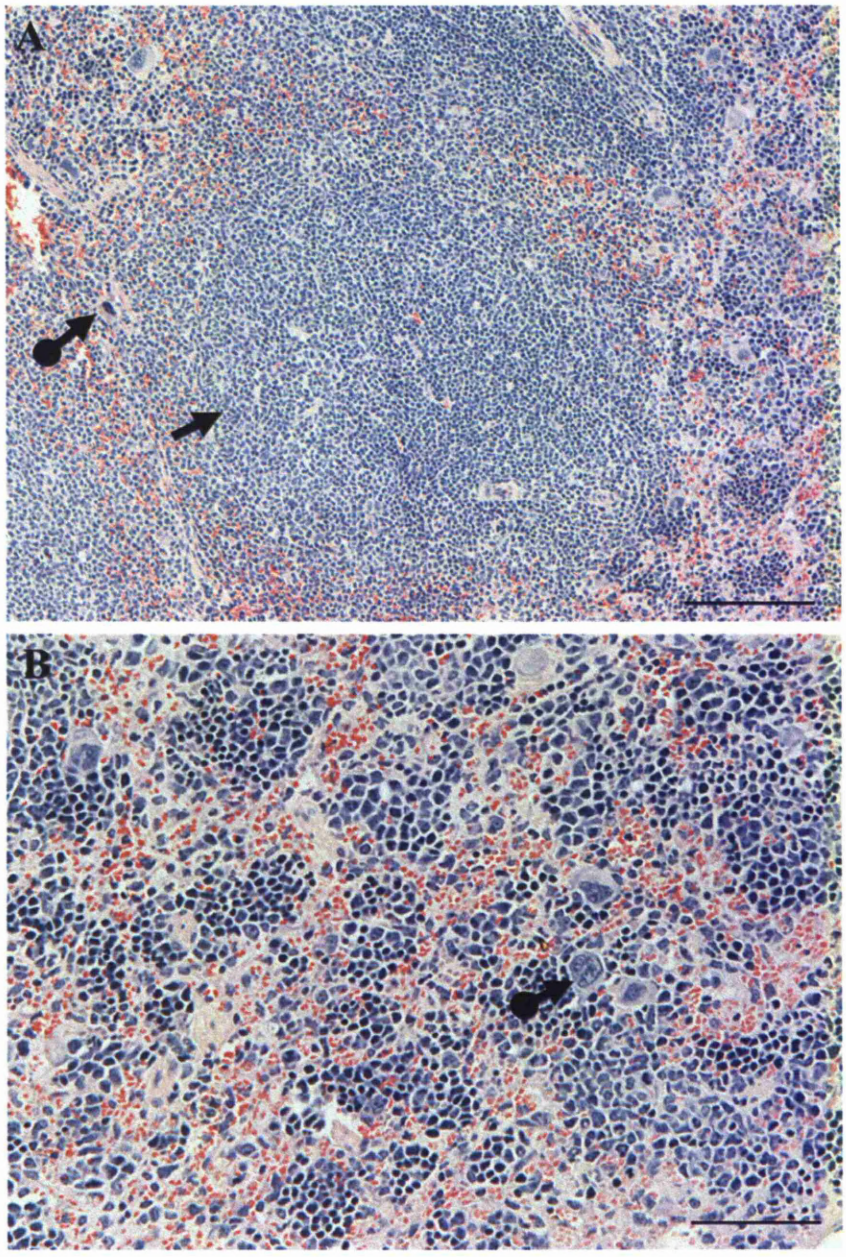

Figure 3.46 Wood mouse, mock infected. Spleen, white pulp.
A: Close up of lymphoid follicle (arrow). B: Close up of red pulp. In the red pulp megakaryocytes are highlighted using arrows with round tip in A and B. HE stained section. Bars: A = 50µm; B= 25µm

3.2.2.2 Changes in the wood mouse spleen in vM1stop and vM1rev infection

There were very little differences between the white pulp of mock and mice virally infected mice with either virus at day 3 p.i. At day 7 p.i., in both infections, follicles had a paracentral cluster of lymphocytes, without evidence of plasma cell formation (beginning of secondary follicle formation) (Figure 3.47). From day 14 p.i., in both infections, secondary follicles showed numerous plasma cells, apoptotic figures, were well demarcated and large sized. In the red pulp, in vM1stop infected wood mice, megakaryocytes exhibited intracytoplasmic vacuolation (Figure 3.48), most severe at day 3 p.i. but also present on day 7 p.i. (Figure 3.47). At day 14 and day 28 p.i., spleens of virally infected mice were grossly enlarged (Figure 3.49).

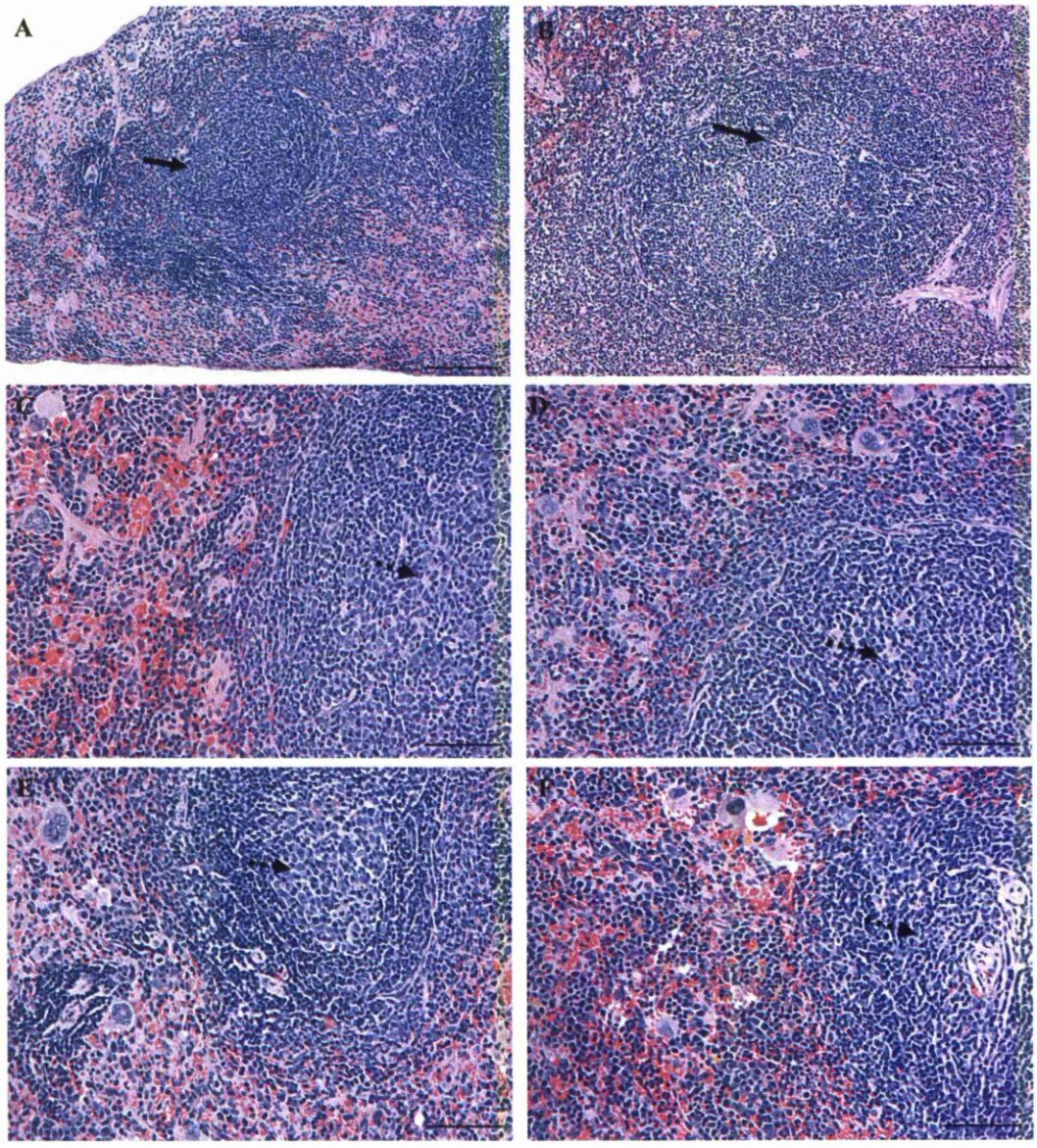

Figure 3.47 Wood mouse, mock, vM1stop and vM1rev infected, day 3, 7, 14 and 28 p.i. Spleen, white pulp.
A, C, E: vM1rev; B, D, F: vM1stop infected wood mice. A, B: day 7 p.i.; C, D: day 14 p.i.; E, F: day 28 p.i. At day 7 p.i. follicles appear to have paracentral clusters of lymphocytes (arrow), without evidence of plasma cell formation (beginning of secondary follicle formation). Secondary follicles (dashed arrows) show numerous plasma cells and apoptotic figures and are well demarcated and large sized from day 14 p.i. There were very little differences in respects to the white pulp between virally infected mice throughout the infection time course. HE stained sections. Bars: A, B= 50μm; D-F:100 μm

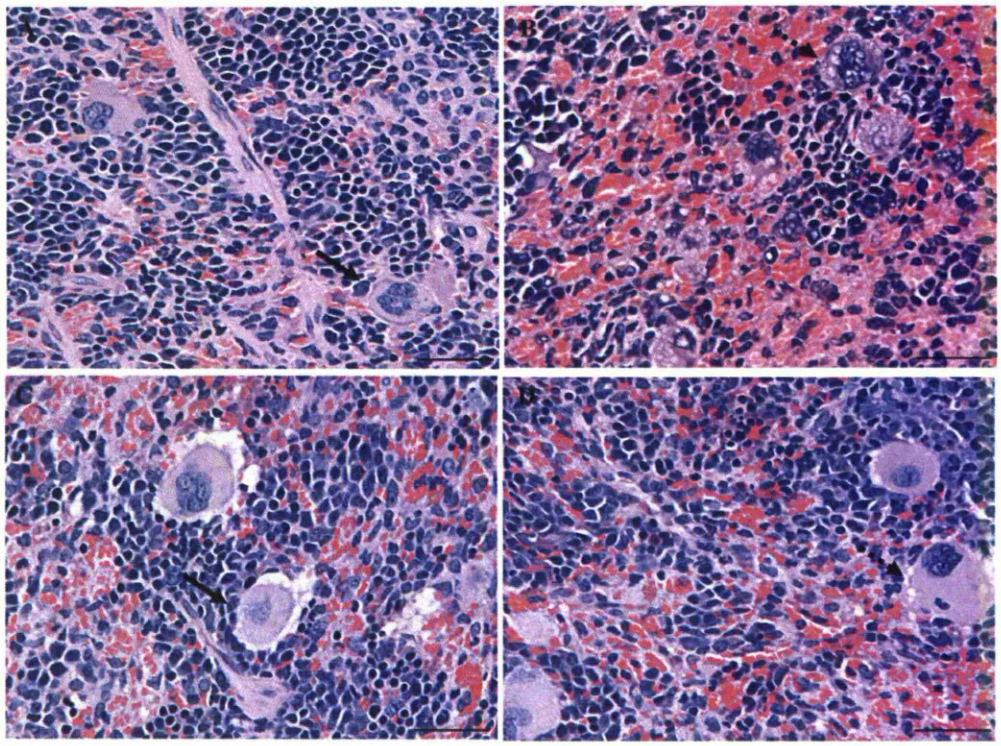

Figure 3.48 Wood mouse, mock, vM1stop and vM1rev infected, day 3 and 7 p.i. Spleen, red pulp.
A, C: vM1rev; B, D: vM1stop infected wood mice; A,B: day 3 p.i; C,D: day 7 p.i.. At day 3 p.i., in both infections, the red pulp showed a very high number of megakaryoctes (arrows) similarly to mock infected wood mice. In vM1stop infected wood mice, these frequently exhibited intracytoplasmic vacuolation (dashed arrow). At day 7 p.i., in both infections, the red pulp showed a very high number of megakaryoctes (arrows). In vM1stop infected wood mice, these frequently exhibited intracytoplasmic vacuolation but this change was milder than what was seen at day 3 p.i. (dashed arrow). HE stained sections. Bars= 25 μm

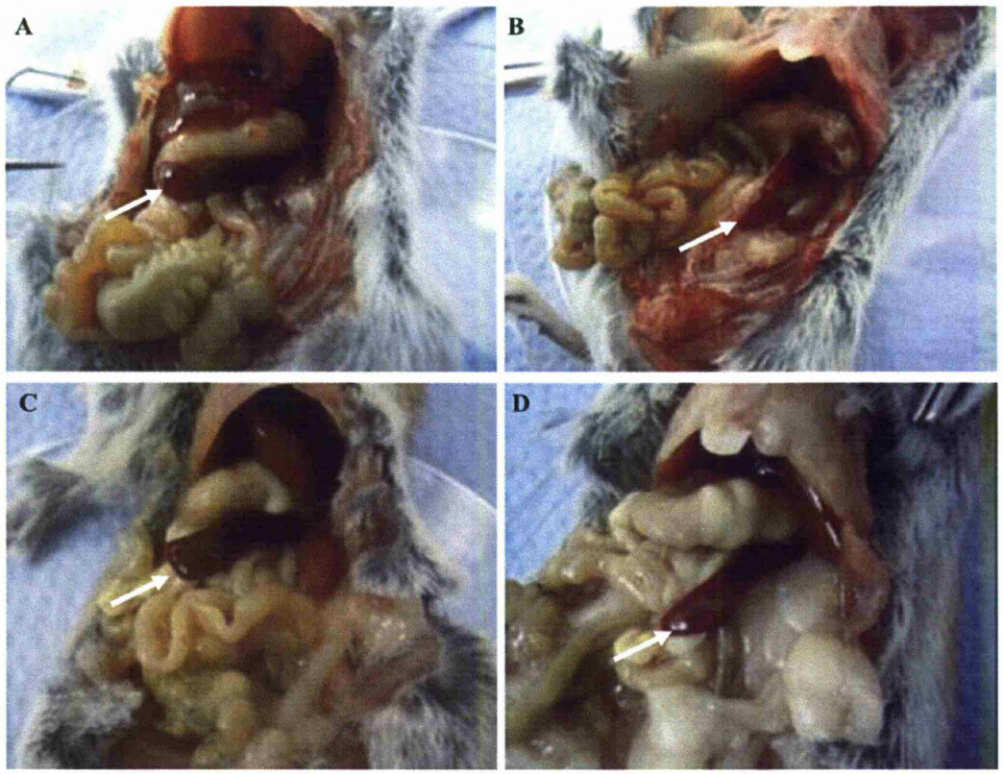

Figure 3.49 Wood mouse, vM1stop and vM1rev infected, day 7 and 14 p.i. Macroscopic view of abdominal cavity.
Abdominal cavity at day 7 (A,B) and 14 (C,D) p.i. Arrow pointing towards spleen. A, C: vM1rev infected wood mice; B, D: vM1stop infected wood mice. Spleens are enlarged on day 14 p.i. in both infections in comparison to day 7 p.i.

3.2.2.3 Viral load in the spleen

The viral load was assessed in the spleen of vM1rev and vM1stop infected wood mice at day 3, 7, 14 and 28 p.i. It was highest in both types of infection at day 14 p.i. However, statistical analysis using an unpaired t test, revealed there was no significant difference ($P>0.05$), this is likely due to the high biological variability in the results obtained per infection.

3.2.2.4 Presence of viral antigen in the spleen

Immunohistology was performed using anti-MHV-68 antibody with specificity for structural proteins and thus is an indicator of lytic infection. In the spleen, viral antigen was only detected in vM1stop infected animals at day 7 p.i. in lymphocytes within the splenic red pulp (Figure 3.51).

3.2.2.5 Viral gene expression in latently infected cells in the spleen

RNA-*in situ* hybridisation was performed using a vtRNA riboprobe. vtRNAs are expressed both in lytic and latent replication. If vtRNA transcript is detected and not associated with viral antigen, it is assumed that it represents latent infection. At day 3 p.i., vtRNA-transcripts were detected in multinucleated cells in the red pulp of both infections (Figure 3.52). At day 7 (Figure 3.53), 14 and 28 p.i., vtRNA transcripts were detected in both infections in follicular lymphocytes and in megakaryocytes.

3.2.2.6 Summary of findings in the spleen.

The findings in the spleen of wood mice infected with vM1stop and vM1rev are summarized in Table 3.5.

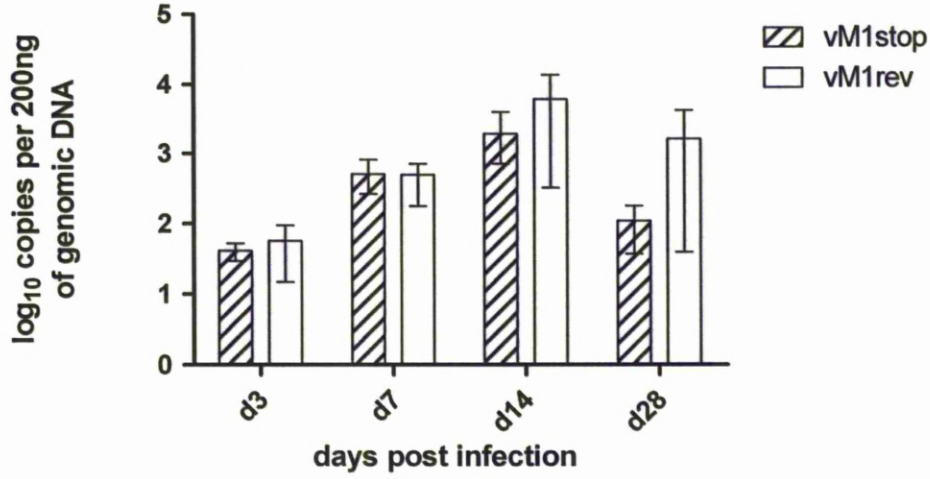

Figure 3.50 Wood mouse, vM1stop and vM1rev infected, day 3, 7, 14 and 28 p.i. Viral load in splenic tissue.
Representation of viral load determined by 2 separate real time PCR experiments, using genomic DNA extracted from the spleen of infected wood mice. n=3 per virus per time point. Error bars represent SEM. Viral load was highest in both types of infection at day 14 p.i. Significant statistical differences were not detected when analysis was performed by an unpaired student t test.

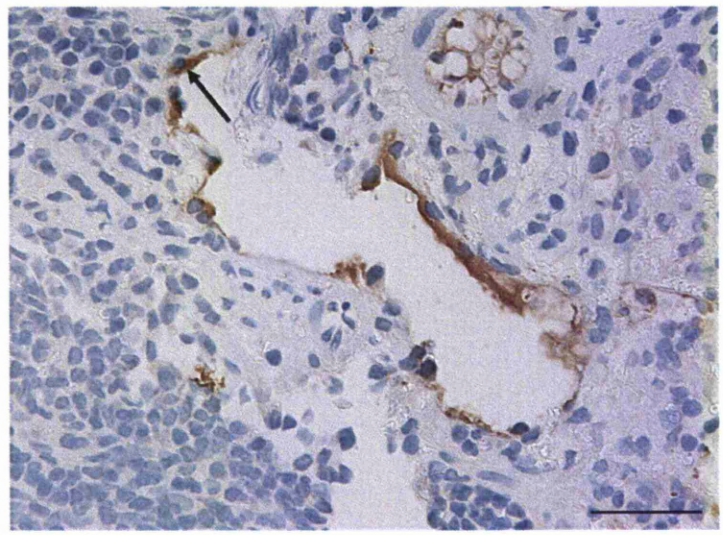

Figure 3.51 Wood mouse, vM1stop infected, day 7 p.i. Spleen. Immunohistology for demonstration of viral antigen.
Lymphocytes (arrow) in the red pulp were seen bearing antigen. PAP method Papanicolaou's haematoxylin counterstain Bar= 25μm

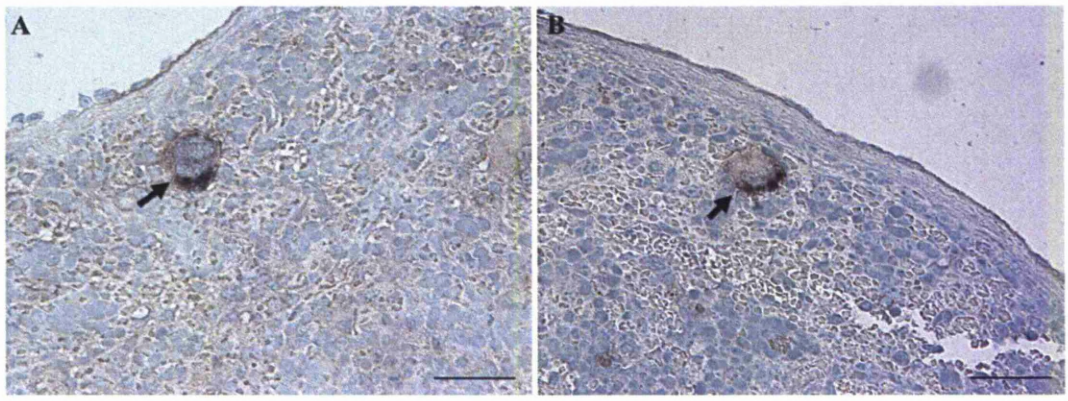

Figure 3.52 Wood mouse, vM1stop and vM1rev infected, day 3 p.i. Spleen RNA-ISH using vtRNA riboprobe.
A: vM1rev infected; B: vM1stop infected. Transcription of vtRNA is detected megakaryocytes in red pulp. RNA-ISH, NBT/BCIP, Papanicolaou's haematoxylin counterstain. Bars=25 μm

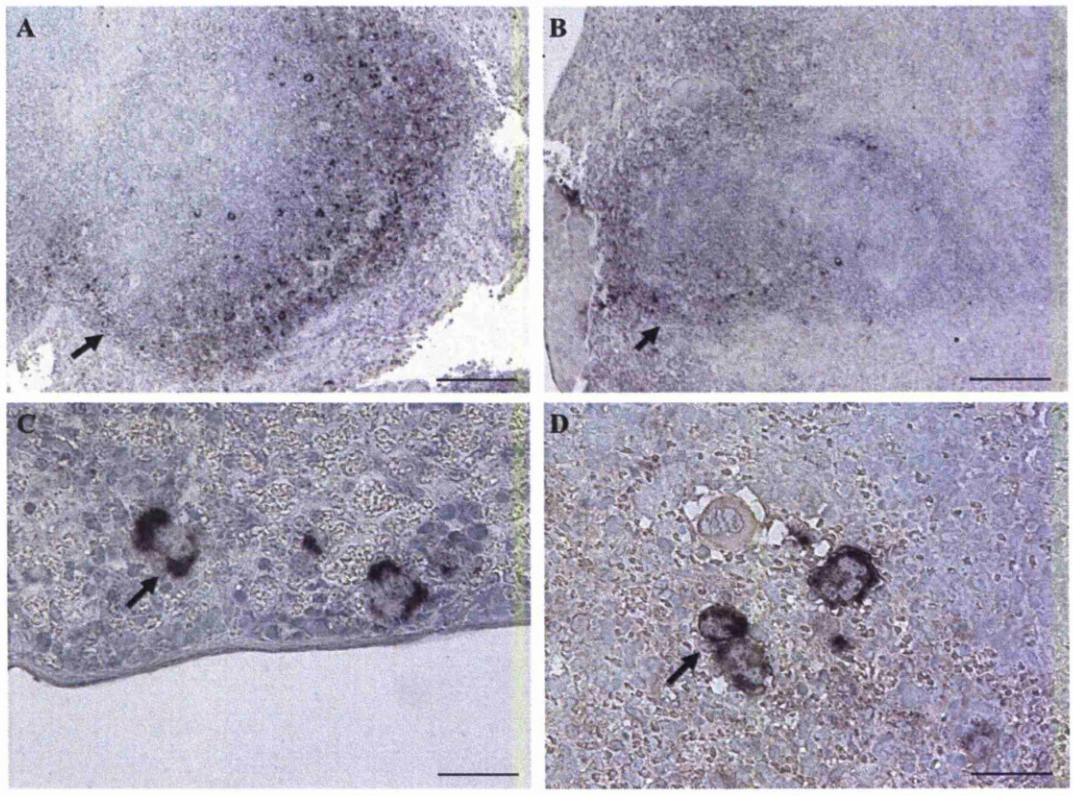

Figure 3.53 Wood mouse, vM1stop infected, day 7 p.i. Lung vtRNA *in situ* hybridisation.
A: vM1rev infected; B: vM1stop infected. Transcription of vtRNA is seen in lymphocytes at the periphery of follicles (arrows in A and B) and megakaryocytes in red pulp (arrows in C and D). RNA-ISH, NBT/BCIP, Papanicolaou's haematoxylin counterstain. Bars A,B= 50 μm; C,D= 25 μm

Days p.i.	Spleen of vM1stop Infected wood mouse	Spleen of vM1rev infected wood mouse
3	Megakaryocytes (++) vacuolated (++) Mitosis in red pulp (+/++) vtRNA: megakaryocytes	Megakaryocytes (++) Mitosis in red pulp (+/++) vtRNA: megakaryocytes
7	Megakaryocytes (++) vacuolated (+) Mitosis in red pulp (+) vtRNA: megakaryocytes; follicular lymphocytes	Megakaryocytes (++) vacuolated (+) Mitosis in red pulp (+) vtRNA: megakaryocytes; follicular lymphocytes vAg: red pulp lymphocytes
14	Splenomegaly Secondary follicle formation Peak in viral load Megakaryocytes (++) Mitosis in red pulp (+) vtRNA: megakaryocytes; follicular lymphocytes	Splenomegaly Secondary follicle formation Peak in viral load Megakaryocytes (++) Mitosis in red pulp (+) vtRNA: megakaryocytes; follicular lymphocytes
28	Secondary follicle formation Megakaryocytes (+) Mitosis in red pulp (+) vtRNA: megakaryocytes; follicular lymphocytes	Secondary follicle formation Megakaryocytes (+) Mitosis in red pulp (+) vtRNA: megakaryocytes; follicular lymphocytes

Table 3.5 Summary of main findings in the spleen of wood mice over a 28 day timecourse following vM1stop or vM1rev infection.
Semiquantitative parameters used to represent number of cells: + (scattered cells); ++ (moderate number of cells); +++ (numerous cells);
vAg: viral antigen.

3.3 *In vitro* studies

The aim of this part of the study was to determine the effect of M1 expression in MHV-68 infection of cell cultures. For this, *in vitro* studies were performed using LHΔMHV-68, vM1stop virus and its genetically repaired counterpart, vM1rev virus. LHΔMHV-68 is a GFP labelled MHV-68 virus which expresses an immediate-early promoter-driven green fluorescent protein. In LHΔMHV-68 infection, fluorescence in infected cells was used as an indicator of lytic infection. vM1stop virus is an MHV-68 virus with an in-frame stop codon in the *M1* locus. The stop codon impairs expression of M1 without exerting interference with the remaining genome. The vM1rev virus has been genetically repaired so represents in this studies MHV-68 wild type virus. By comparing infections with vM1stop and vM1rev virus, the effect of M1 was assessed. Two cell lines were used in the *in vitro* studies of MHV-68 infection: NIH3T3 (murine fibroblasts) and MH-S (murine alveolar macrophages) cells.

The hypothesis tested with these experiments was that in cell cultures, the presence or absence of M1 transcription would lead to different pathogenesis induced by MHV-68 infection and/or interfere with MHV-68 replication. Furthermore when these cells were macrophages this effect would be further enhanced.

3.3.1 NIH3T3

3.3.1.1 LHΔMHV-68 infection

NIH3T3 cells infected with LHΔMHV-68 were examined for morphological changes and fluorescence. Observations were made at 0, 24, 48, 72 h.p.i.

Mock infected NIH3T3 cells were observed in parallel to virally infected cells, in order to have a control. Prior to 48 h.p.i. there was little difference between viral and mock infected cells in respects to cell numbers and morphology. At 48 and 72 h.p.i. (Figure 3.54, in mock infected cells, the total number of cells kept increasing, contrary to virally infected cells (described later). Degenerative changes were only seen in a few scattered cells, probably as a result of over confluence and lack of media renewal.

In virally infected cells, fluorescence was detected as early as 3 h.p.i. (after incubation and removal of inoculum - Figure 3.55 A, B) in scattered cells. At 24 h.p.i. (Figure 3.55 C, D) all cells were observed to exhibit fluorescence indicating that all were

infected and the virus was undergoing lytic replicating. Despite all cells being infected only scattered cells showed obvious degenerative changes such as a rounded cell morphology and cytoplasmic vacuolation. At 48 h.p.i.(Figure 3.55 E, F), cells still exhibited fluorescence throughout but this was accompanied by severely altered cellular morphology. All cells were rounded and intracellular components were inconspicuous. The number of cells was also reduced and there was abundant cellular debris in solution. This is consistent with extensive apoptosis. These observations were enhanced at 72 h.p.i. (Figure 3.55 G, H) with further reduction of identifiable cells and increase in the cellular debris.

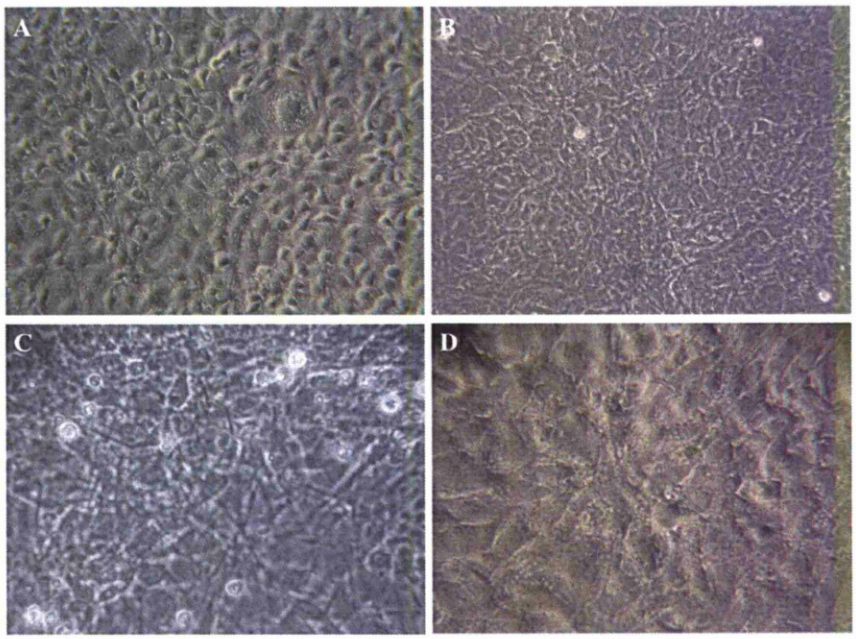

Figure 3.54 NIH3T3 cells. Mock infected at 3, 24, 48 and 72 h.p.i.
Mock infected NIH3T3 cells at 48 h (A) and 72 h p.i (B) continued dividing and only scattered cells showed degenerative changes.

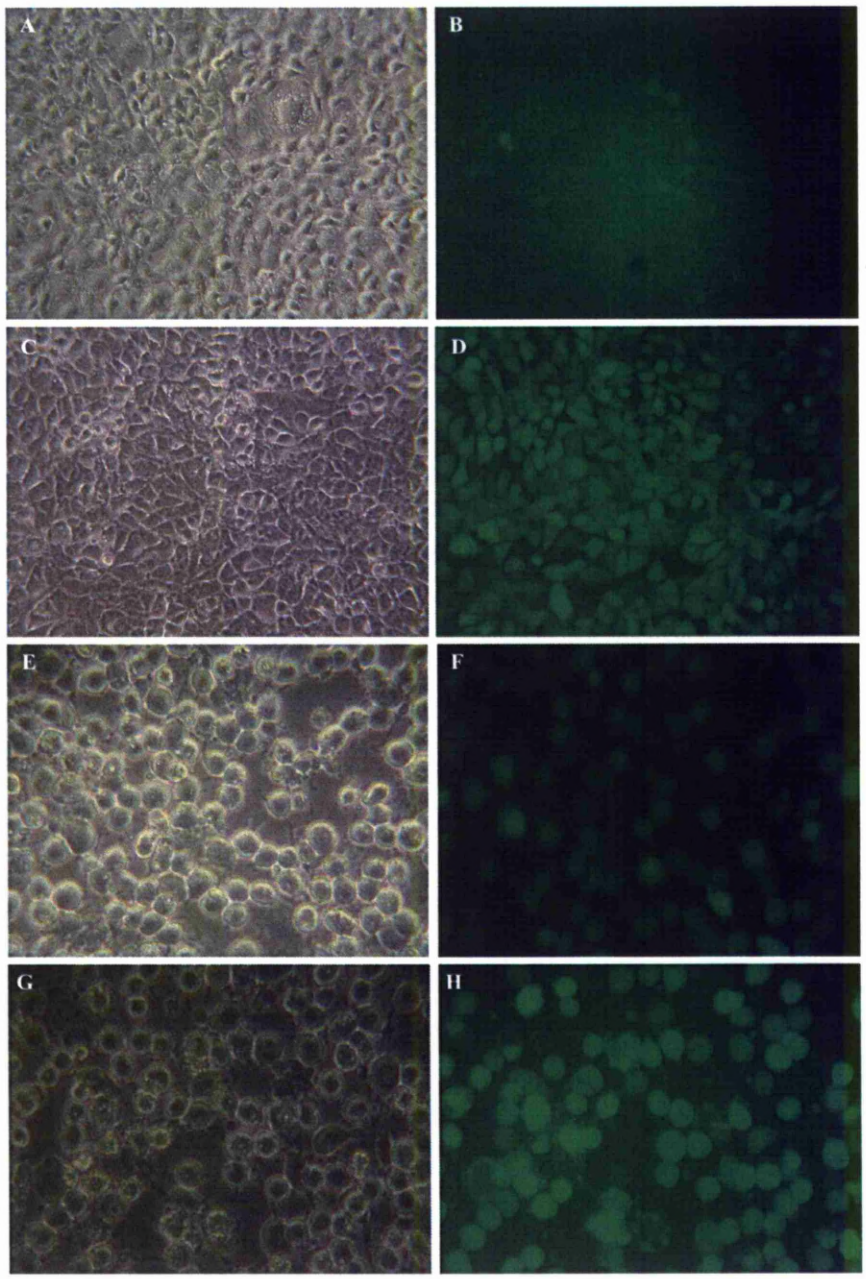

Figure 3.55 NIH3T3 cells. LHΔMHV-68 infected at 3, 24, 48 and 72 h.p.i.
At 3 h.p.i. (A,B), scattered virally infected cells showed fluorescence. At 24 h.p.i. (C, D) all virally infected cells showed fluorescence but few showed degenerative changes. At 48 h.p.i. (E, F), all virally infected cells exhibited fluorescence and extensive degenerative changes. The number of cells was reduced. These observations were enhanced at 72 h.p.i. (G, H).

3.3.1.2 Infection of NIH3T3 cells with vM1rev and vM1stop MHV-68 viruses

3.3.1.2.1 M1 expression

NIH3T3 cells were infected with vM1rev virus at an MOI (multiplicity of infection) of 5. At 24 h.p.i. cells were fixed and a pellet was created. M1 mRNA-ISH was performed in order to see the extent of M1 expression *in vitro* in this cell type. Immunohistology was performed using a marker for the viral glycoprotein to determine which cells exhibited fully formed viral particles, an indicator of lytic replication. M1 expression was only seen in scattered cells (Figure 3.56) despite the fact that all of these cells were lytically infected. This indicates that M1 expression during the *in vitro* infection of NIH3T3 cells is minimal despite cells being permissive to infection.

3.3.1.2.2 Viral plaque morphology

NIH3T3 cells were infected with vM1rev and vM1stop MHV-68 viruses and examined under light microscopy for viral plaque morphology. Comparatively, infected cells showed no obvious difference in respects to the viral plaque morphology "comet like tails" (Figure 3.57).

3.3.1.2.3 One step and multi step growth curve

NIH3T3 cells were infected with vM1stop and vM1rev MHV-68 viruses using an MOI of 0.05 (multi-step growth curve) and 5 (one step growth curve). The cells were harvested at different timepoints and were collected together with the overlying media. The collected material was then assessed for viral titre using a plaque assay. Statistical analysis of one step (Figure 3.58 A) and multi step (Figure 3.58 B) growth curves yielded similar results. The statistical analysis performed using two way ANOVA and Bonferroni post test showed there was no significant difference between the different types of infections. The only source of variation that led to a significant difference in viral titres ($P<0.0001$) was the post infection time. The statistical analysis comparing the different timepoints confirmed the significant differences between timepoints mostly between early timepoints and the later ones.

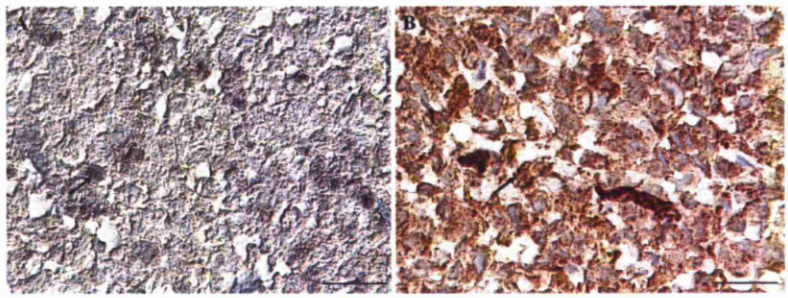

Figure 3.56 NIH3T3 cells vM1rev infected. M1mRNA expression and immunohistology for demonstration of viral antigen.
A: M1 mRNA is seen in scattered cells (arrow). B: Immunohistology for demonstration of viral antigen. Abundant viral antigen is seen throughout in all cells, confirming 100% of the cells exhibiting viral lytic replication. Arrows seen in A and B represent the same cell in sequential sections. A: RNA-ISH, NBT/BCIP, Papanicolaou's haematoxylin counterstain. B: PAP method Papanicolaou's haematoxylin counterstain .Bars = 25 μm

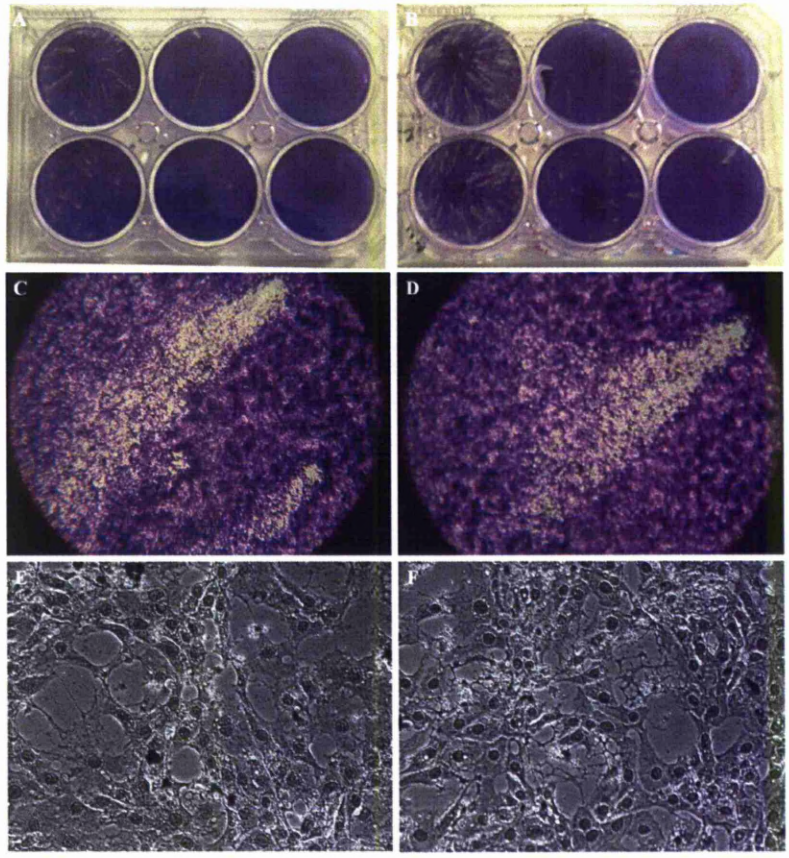

Figure 3.57 NIH3T3 cells. vM1rev and vM1stop infected. viral plaques.
A, C, E: vM1rev infected; B, D, F: vM1stop infected. A, B: overview of 6-well plates; C, D: viral plaques at 4x 0.45; E, F: viral plaques at 40 x 0.45. Toluidine blue stained. There is little difference in viral plaque morphology.

A

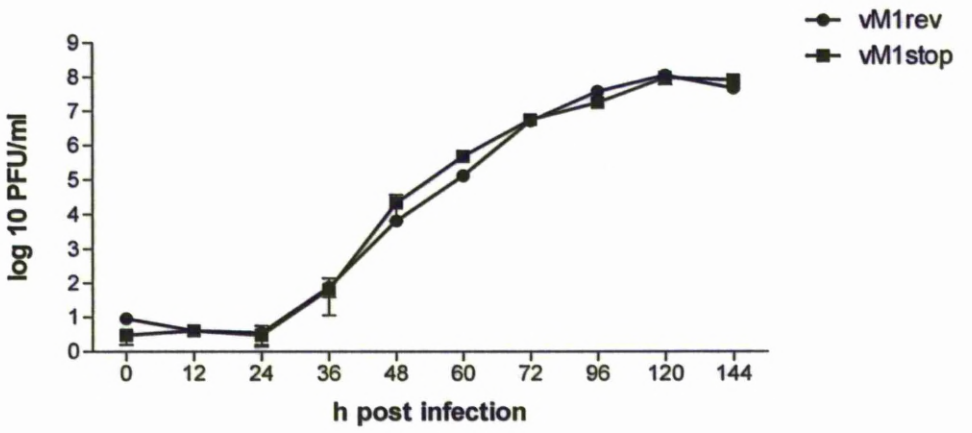

B

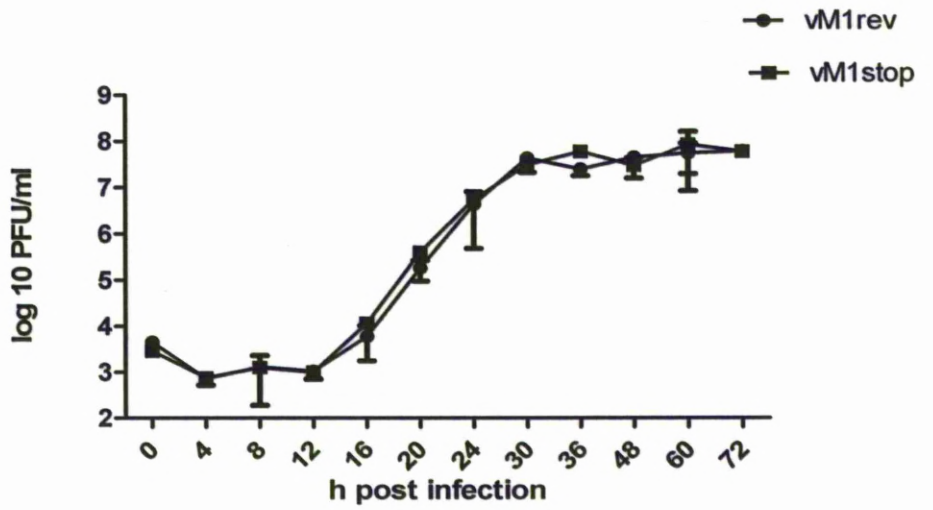

Figure 3.58 NIH3T3 cells. One step and multi step growth curve of vM1stop and vM1rev infection.

A Multistep growth curve. B: One step growth curve. Representation of viral titres determined from collected cells and media in NIH3T3 cells infected with vM1rev and vM1stop virus at an MOI of 0.05. n=2 per virus per time point. Error bars represent SEM and significant differences were determined using two way ANOVA and Bonferroni post test (*$p<0.05$, **$p<0.01$ ***$p<0.0001$). There was no significant difference between the types of infections.

3.3.1.2.4 Ultrastructural study of NIH3T3 infected with vM1rev and vM1stop

Cells showing active replication had a severely enlarged electrolucent nucleus and a large highly vacuolated cytoplasm. This led to an overall increase of cellular size in comparison with cells where active replication was not observed. The different stages of viral particles found are represented in Figure 3.59. In cells where active replication was observed, in the nucleus, multifocal areas of chromatin condensation (nucleolus) were observed and generally these contained numerous empty and packed capsids (~70-75 ηm in diameter) at the periphery. These capsids were also seen disseminated in the nuclei (Figure 3.60 - Figure 3.62). In addition, in the nucleus, numerous vesicles, lined by a single or a double layer and containing viral particles that were larger than the ones seen in the nucleoplasm were frequently seen. These vesicles were seen in areas where the inner and/or outer nuclear membranes were irregular and likely represent deep invaginations of the nuclear membrane into the nucleoplasma. In multifocal areas between the inner and outer nuclear membrane and in the invaginations of the nuclear membrane there were viral particles larger than the packed capsids (~ 130-135 ηm in diameter) suggesting that primary envelopment had occurred. In the dilated Golgi apparatus, viral particles were often surrounded or adjacent to abundant electrodense material-tegument.

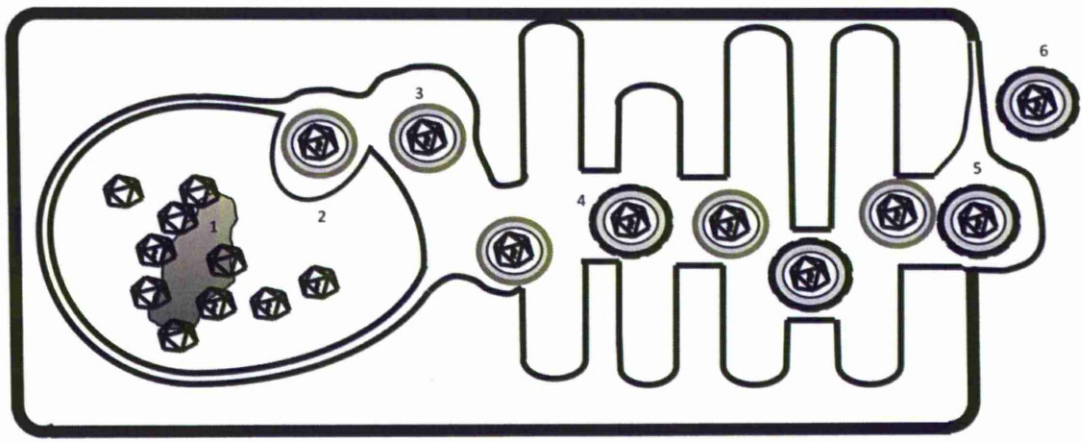

Figure 3.59 Schematic representation of viral egress based on findings from ultrastructural examination.
1) Empty and packed capsid in the nucleus most frequently surrounding nucleoli. 2) Filled capsid (capsid and genome) after fusing with the inner nuclear membrane (primary envelopment) 3) Primarily enveloped virus as it migrates between inner and outer leaflet of nuclear membrane and smooth endoplasmatic reticulum. 4) Enveloped and tegumented viral particles migrating through Golgi apparatus. 5) Enveloped and tegumented viral particles in Golgi apparatus vesicle which continues with the space between the inner and outer leaflet of the cytoplasmic membrane 6) Tegumented viral particles in the extracellular space.

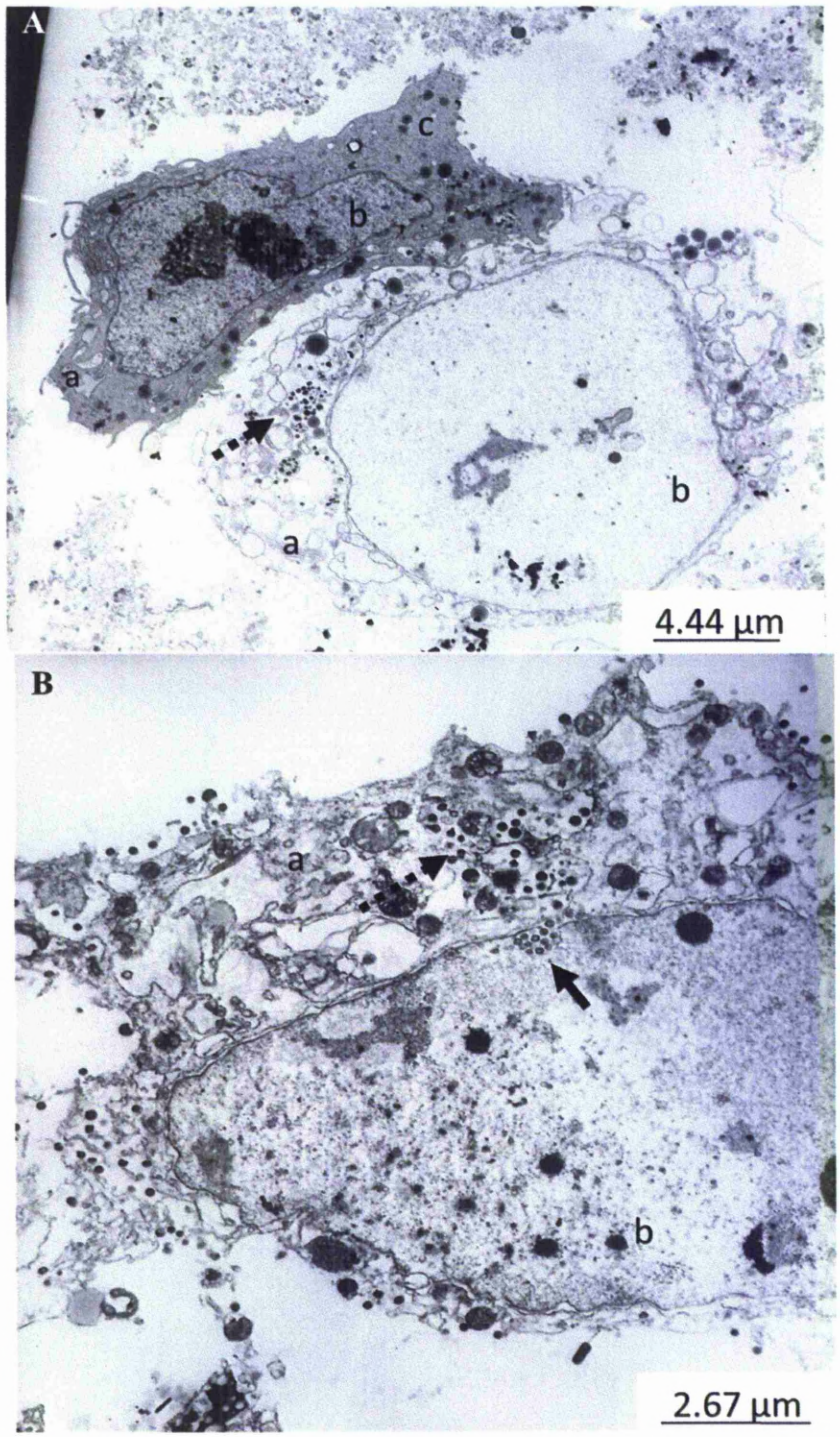

Figure 3.60 NIH3Te. vM1rev and vM1stop infected. Ultrastructure.
A: vM1rev infected; B: vM1stop infected; a: cytoplasm; b: nucleus; c: cell without evidence of active viral replication. Full arrow: nuclear viral particles; Dashed arrow: cytoplasmic viral particles eggressing. Cells showing active replication exhibited severely enlarged electrolucent nucleus and large highly vacuolated cytoplasm. There is little difference between infections.

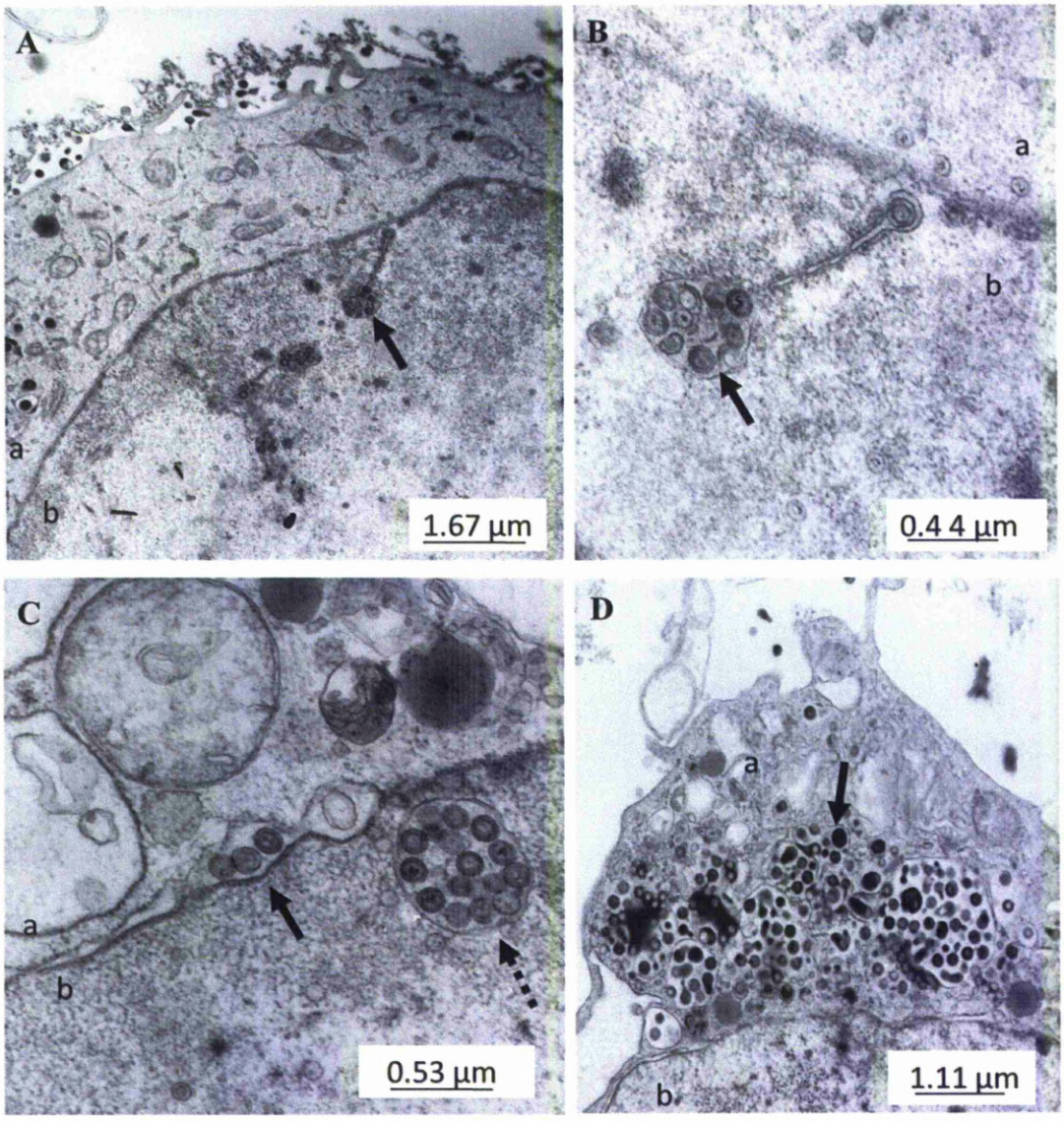

Figure 3.61 NIH3T3 cells. vM1rev infected. Ultrastructure.
a: Cytoplasm; b: Nucleus; In the cell nucleus, numerous vesicles (arrow in A and B) lined by a single or a double layer and containing viral particles larger than the ones seen in the nucleoplasm were seen. In multifocal areas between the inner and outer nuclear membrane (arrow in C) and in the invaginations of the nuclear membrane (dashed arrow in C) there were viral particles larger (~ 130-135 ηm in diameter) than the packed capsids present in the nucleoplasm suggesting that primary envelopment had occurred. In the dilated Golgi apparatus, viral particles were often surrounded or adjacent to abundant electrodense material (arrow in D -tegument).

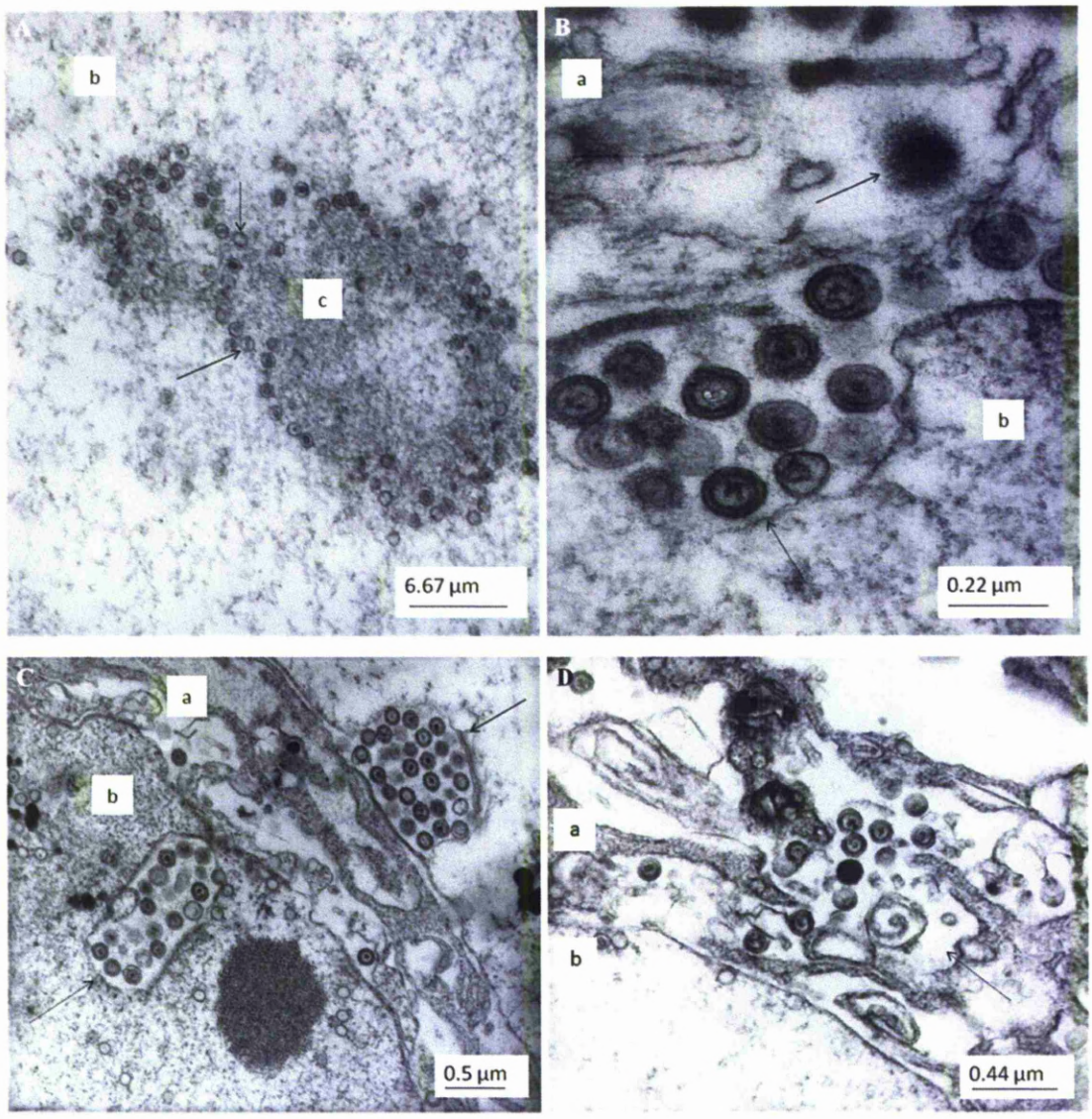

Figure 3.62 NIH3T3 cells. vM1stop infected. Ultrastructure.
a: Cytoplasm; b: Nucleus; c: Nucleolus; Areas of chromatin condensation (nucleolus) with numerous empty (dashed arrow in A) and packed capsids (~70-75 ηm in diameter – arrow in A) at the periphery. Invaginations of nuclear membrane into nucleoplasm (dashed arrow in B and C) and of the cytoplasmic membrane into to extracellular space (arrow in C), contained viral particles (~ 130-135 ηm in diameter) equally sized and with similar morphology. These particles were larger than the ones seen in the nucleoplasm suggesting that these were enveloped. In the dilated Golgi apparatus (dashed arrow in D), viral particles were often surrounded or adjacent to abundant electrodense material (arrow in B and D - tegument?).

3.3.2 MH-S (alveolar macrophages)

3.3.2.1 LHΔMHV-68 infection

The cell line MH-S is a murine alveolar macrophage cell line. The particular interest in this cell line arose following a finding in the *in vivo* studies which indicated that infection of alveolar macrophages was increased in vM1stop infection compared to the vM1rev infection. MH-S cells were infected with LHΔMHV-68 in order to assess if these cells became infected by MHV-68 virus and if so the rate of infection. To assess infection, cells were examined for morphological changes and fluorescence. Observations were made at 0, 24, 48, 72 h.p.i.

Normal cellular morphology consists of mostly round and to lesser extent spindloid or triangular shaped cellular outline (Figure 3.64). Preliminary experiments led to the observation that these cells were not infected as easily as NIH3T3 cells and so for the full experiment, a higher MOI of 10 was used and the incubation of the infectious inoculum was increased to 2 h.

Mock infected MH-S cells were observed in parallel with virally infected cells in, in order to have a control. There was little difference between viral and mock infected cells with respect to cell growth or morphology in the early timepoints observed. At 48 h.p.i. mock infected cells showed mild degenerative changes that were enhanced at 72 h.p.i. These changes were interpreted as secondary and due to lack of media renewal (Figure 3.63).

At 0 h.p.i., no fluorescence was observed (Figure 3.64). At 24 h.p.i. the percentage of cells exhibiting fluorescence varied within the plate between 15 to 25%. The cell morphology at this time was not altered. At 48 h.p.i., the fluorescence decreased greatly throughout and was variable within the plate, the percentage of cells exhibiting fluorescence being in the range of 3 to 18%. The cell morphology at this time was severely altered and the well demarcated rounded cellular profile was no longer apparent and instead it was irregular and cells exhibited a granular appearance, this is consistent with degenerative changes, most likely apoptosis. The number of cells was also reduced and there was abundant cellular debris in solution. The most confluent areas of cellularity were mostly seen at the periphery of the wells. These changes were enhanced at 72 h p.i and were accompanied by little fluorescence.

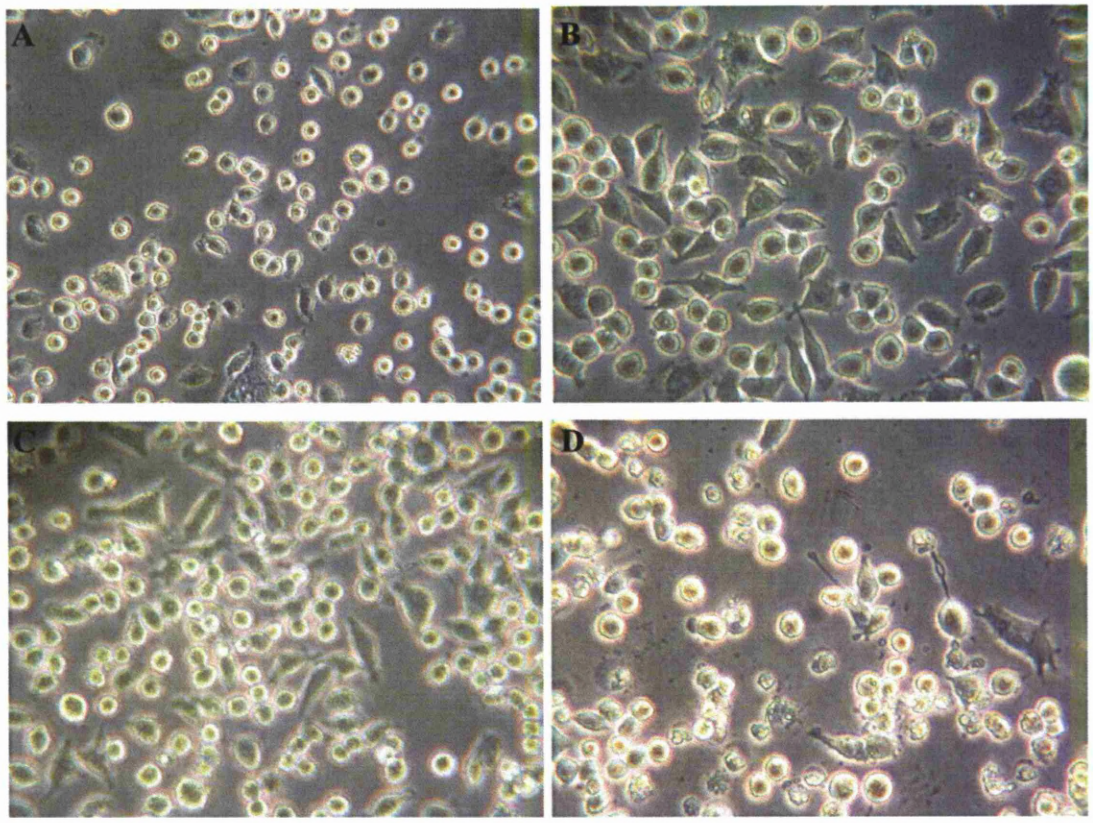

Figure 3.63 MH-S cells. Mock infected at 3, 24, 48 and 72 h.p.i.
Mock infected at 3 (A), 24 (B), 48 (C) and 72 (D) h.p.i. At 48 h.p.i. mock infected cells starded showing mild degenerative changes that were enhanced at 72 h.p.i. At 72 h.p.i plates were not as cell rich as at 48 h.p.i. likely as a result of cell death as cellular debris was also present. The degenerative changes observed were interpreted as secondary and due to lack of media renewal.

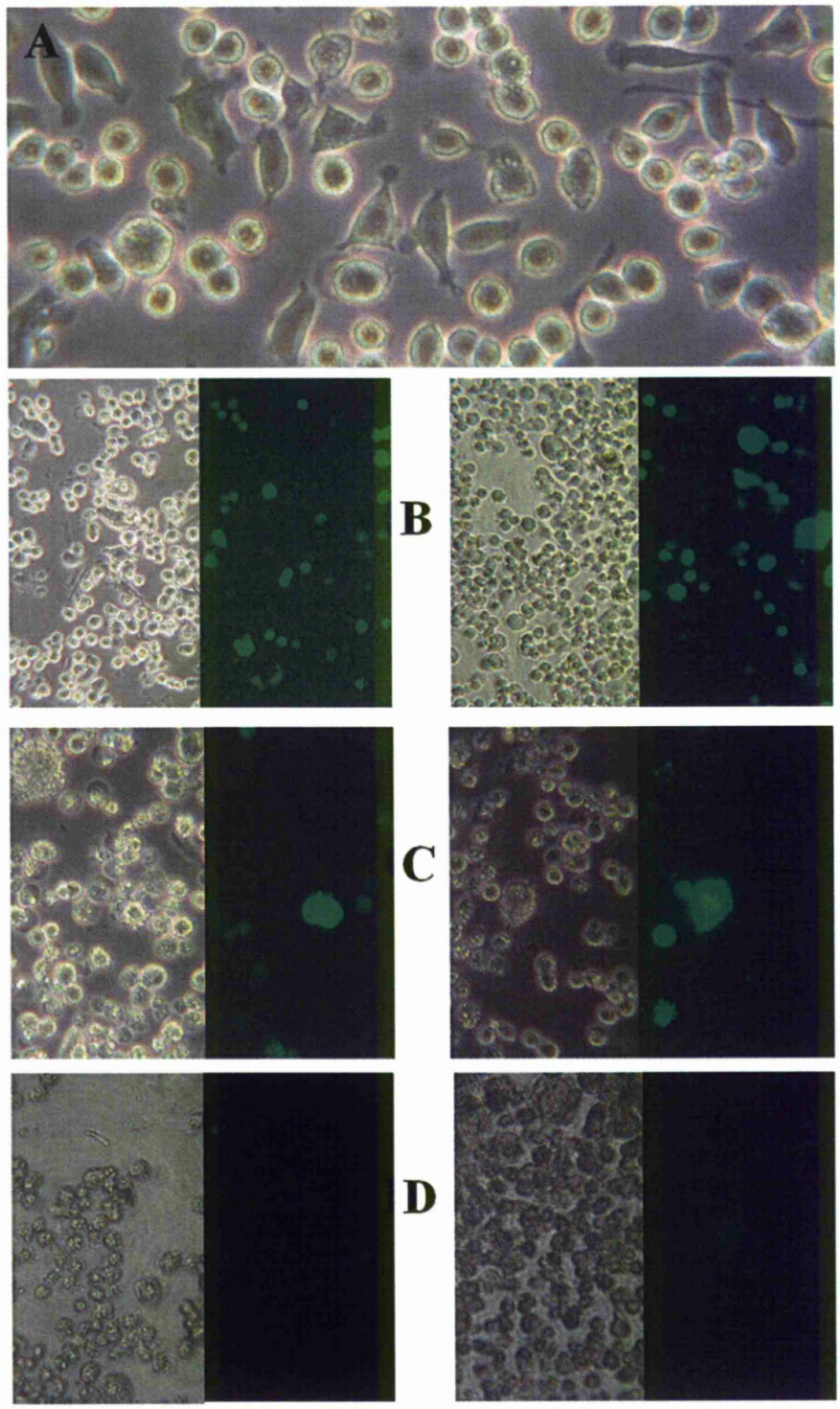

Figure 3.64 MH-S cells. LHΔMHV-68 infected at 3, 24, 48 and 72 h.p.i.
At 0 h.p.i. (A), no fluorescence was present and cell morphology was mostly unaltered. At 24 h.p.i.(B) the fluorescence varied within the plate (15-25%) and cell morphology was unaltered. At 48 h.p.i. (C) the fluorescence decreased greatly throughout and varied within the plate (3-18%). The cell morphology at this time was severely altered and cellular profile was irregular and cells exhibited a granular appearance (apoptosis). The number of cells was also reduced and there was abundant cellular debris in solution. These changes were enhanced at 72 h.p.i. (D) and were accompanied by little fluorescence.

3.3.2.2 One step growth curve

MH-S cells infected with vM1stop and vM1rev MHV-68 viruses using an MOI of 10. The cells were scraped at different timepoints (0, 24, 48, 72, 96 h. p.i.) and were collected together with the overlying media. The collected material was then assessed for viral titre using a plaque assay. With these results a viral growth curve was drawn (Figure 3.65). Statistical analysis of the one step growth curves yielded similar results. The statistical analysis performed using two way ANOVA and Bonferroni post test showed that there was no significant difference when the two infections were compared.

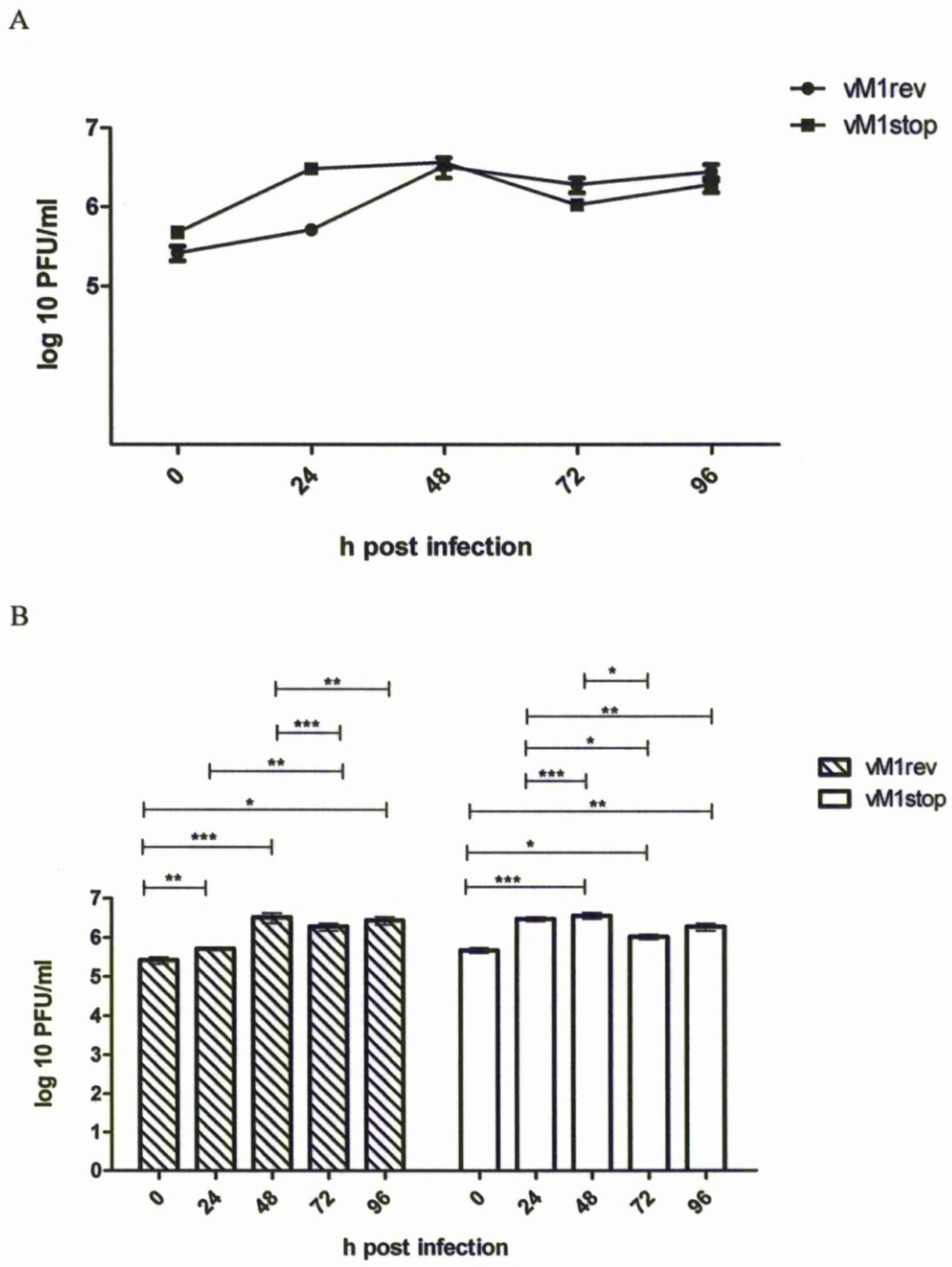

Figure 3.65 One step growth curve of MH-S cells infected with either vM1stop or vM1rev.

A and B represent the same viral titre results. Viral titres were determined from the collected MH-S cells and media infected with either vM1rev or vM1stop virus at an MOI of 10. n=2 per virus per time point. Error bars represent SEM. Significant differences were determined using two-way ANOVA and Bonferroni post test (*$p < 0.05$, **$p < 0.01$ ***$p < 0.0001$).

3.3.2.3 Ultrastructural study of MH-S infected cells

Ultrastructural examination was also performed on MH-S cells infected with either vM1stop or vM1rev virus at an MOI of 10 at 24 and 72 h.p.i. It was noted that the number of viral particles was much lower in both vM1stop and vMM1rev infection of MH-S cells, than those observed in NIH3T3 cells (Section 3.2.1.3). At 24 h.p.i., scattered cells infected with vM1rev virus showed viral particles clustered in large vacuoles within the cytoplasm (Figure 3.66). In these vacuoles, the size of the viral particles was highly variable (~28 ηm - 85ηm in diameter). These finding were similar to those described in S11 cells, which are cells derived from B lymphocytes from mice with persistent MHV-68 infection[319]. Cells that were exposed to vM1rev virus also exhibited a mild increase in cytoplasmic vacuolation and dilation of mitochondria, which showed a less demarcated profile of their cristae. These findings were independent of the observation of viral particles within cells. At 24 h.p.i., no viral particles were seen in cells infected with vM1stop virus. At 72 h.p.i., there was little difference between MH-S cells infected with either vM1rev or vM1stop (Figure 3.67, Figure 3.68). At this timepoint, the cellular architecture had altered notably in both types of infection. Extensive vacuolation, effacement of organelles, discontinuity of both cytoplasmic and, less frequently, nuclear membranes was observed. At 72 h.p.i.iral particles were much more numerous in both infection types and were morphologically similar to viral particles seen at 24 h.p.i. in the vM1rev infected cells. These viral particles were also seen within the nucleus but were often contained within a double lined space, suggesting that these were invaginations of the nuclear membrane. In vM1stop infected cells, binucleated cells were also present and cells with evident lytic replication showed frequent lipid droplets in the cytoplasm.

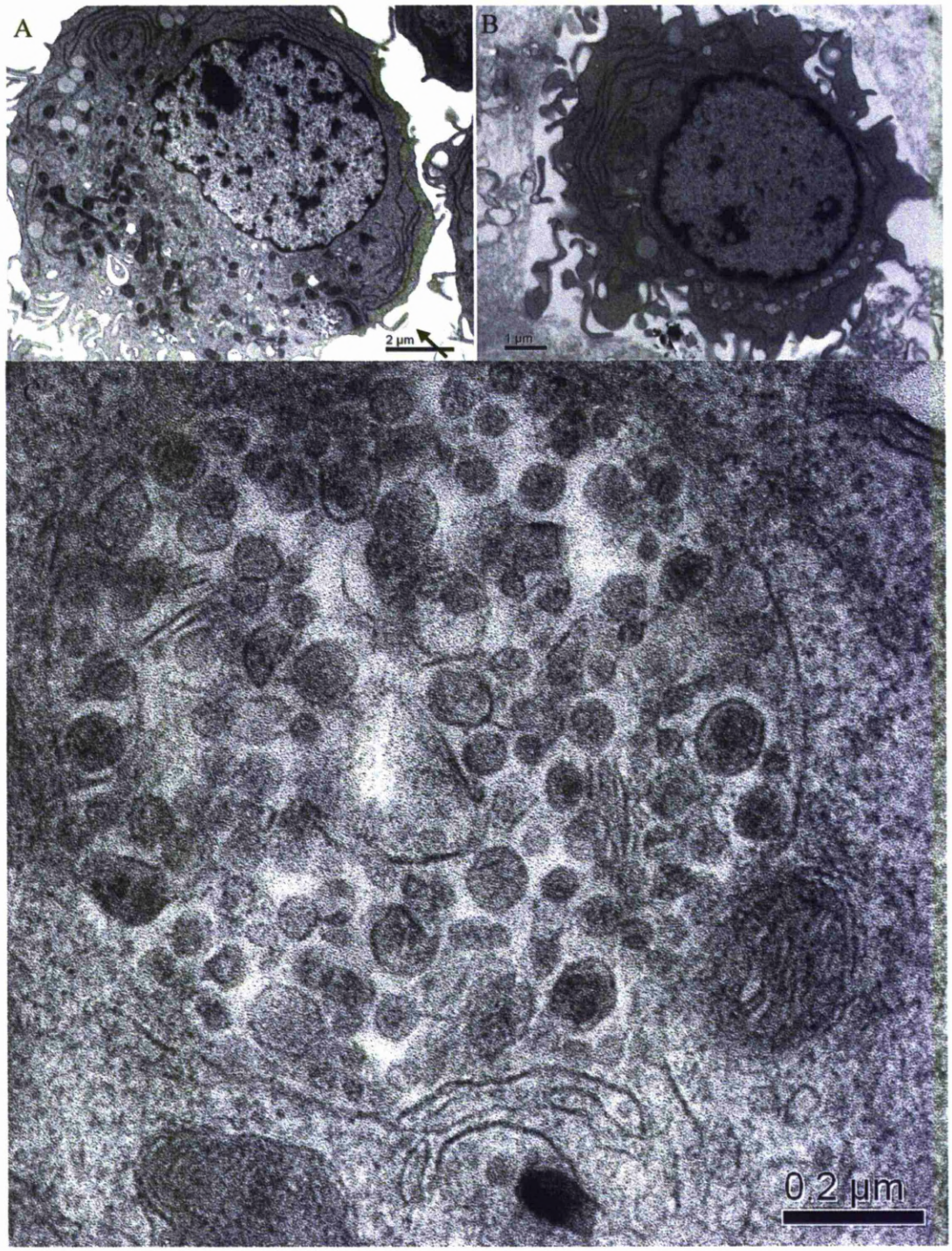

Figure 3.66 MHS cells infected with either vM1rev or vM1stop infected at 24 h.p.i. Ultrastructure.
A: vM1rev infected cell with the cytoplasmic vacuole containing viral particles (arrow); B: vM1stop infected cell; C: cytoplasmic vacuole of vM1rev infected cell containing viral particles.

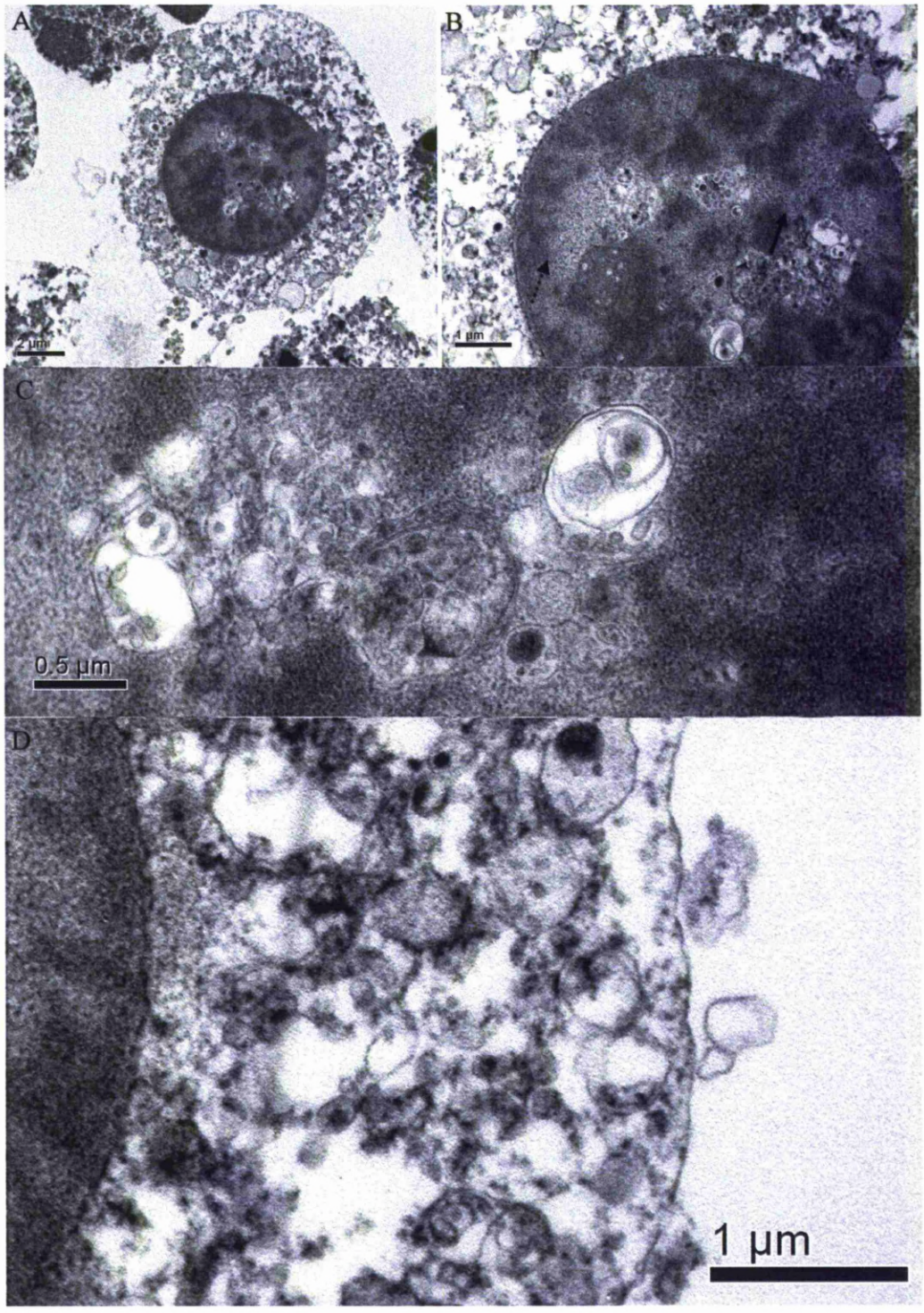

Figure 3.67 MH-S cells infected with vM1rev at 72 h.p.i.
A: Overview of cell; B: Vacuoles with viral particles within the nucleus (full arrow) and cytoplasm (dashed arrow); C: nuclear vacuoles containing viral particles; D: cytoplasmic vacuole containing viral particles.

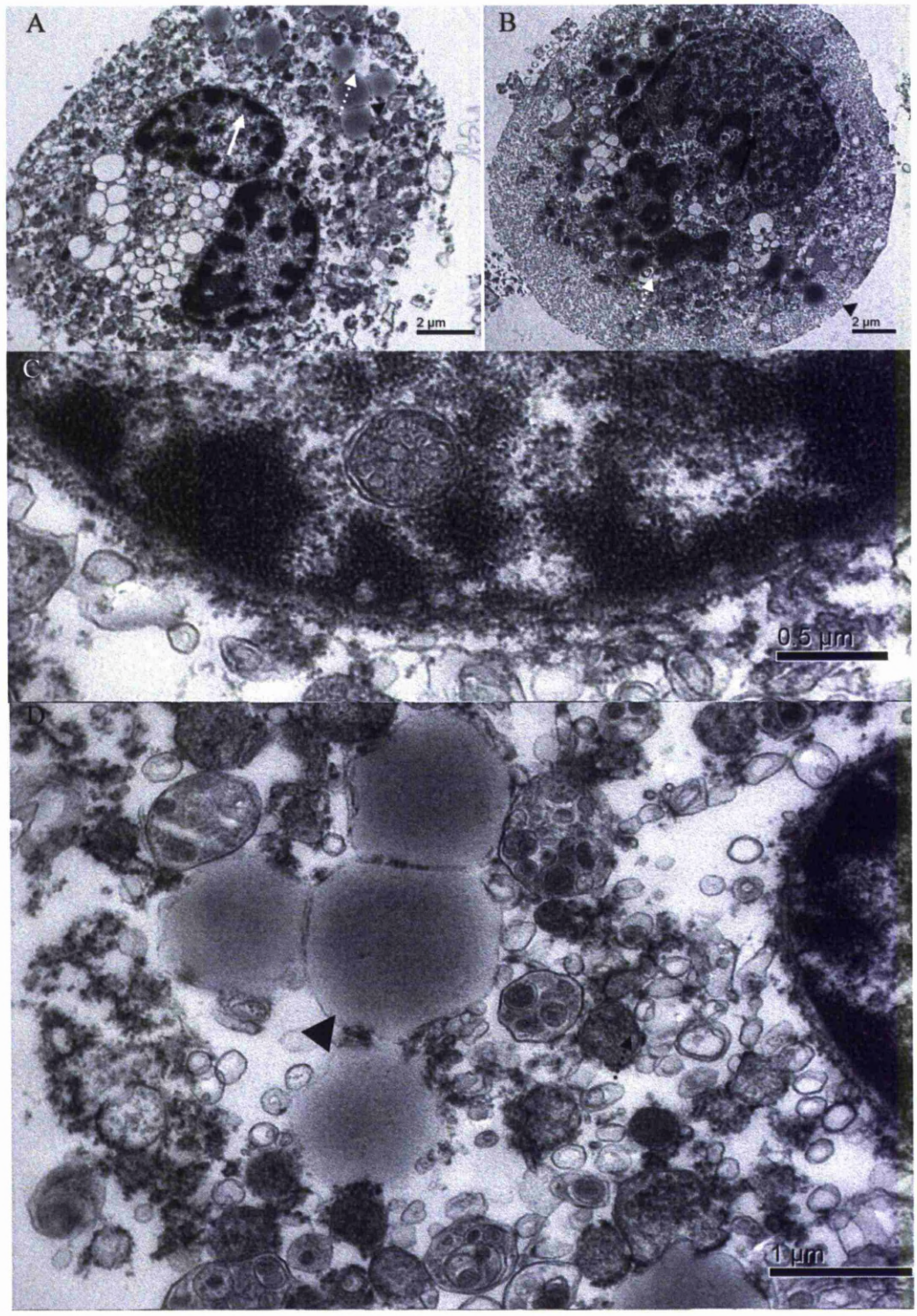

Figure 3.68 MH-S cells infected with vM1stop at 72 h.p.i. Ultrastructure.
A: Overview of a binucleated cell; B: Overview of a mononucleated cell; C, D: nuclear (C) and cytoplasmic (D) vacuoles with viral particles. Vacuoles were observed with viral particles within the nucleus (full arrow) and the cytoplasm (dashed arrow). Lipid droplets were also frequently seen (arrowhead).

3.3.2.4 Viral gene expression in MH-S cells infected with vM1stop and vM1rev

Viral gene transcript expression was monitored in MH-S cells infected with either vM1stop or vM1rev virus over a 72 hour time period. Two genes were selected: *gp150*, a gene expressed during lytic replication, and *ORF73*, a gene expressed during latent replication. Expression of *M1* transcripts were also monitored in cells infected with vM1rev virus. The gene expression ratio was determined using the pfaffl equation. Values obtained from test samples were normalized against the Ct values obtained from vM1rev infected cells at 0 h.p.i.

In vM1rev infected cells, *M1* transcript expression was highest during the first 24 h.p.i. (Figure 3.69). This increase in *M1* transcript expression was accompanied by an increase in *gp150* transcript expression, a significant increase in the viral titre and a decrease in *ORF 73* transcript expression. These findings were consistent with enhanced lytic replication during the first 24 hours of viral infection. Between 24 and 48 h.p.i. there was a decrease in *M1, gp150* and *ORF73* transcript expression. Furthemore, a plateau in the viral titre was noted. These findings were consistent with the absence of viral replication from 24 to 48 h.p.i. From 48 h to 72 h p.i, M1 transcript expression was unaltered. However, *ORF 73* transcript expression increased and there was a significant decrease in the viral titre. These findings were consistent with latent replication from 48 to 72 h.p.i.

In vM1stop infected cells, there was a decrease in the *gp150* transcript expression and an increase in *ORF 73* transcript expression during the first 24 hours of viral infection (Figure 3.70). No expression of *M1* transcript was detected. This was accompanied by an insignificant change in the viral titre. These observations were consistent with enhanced latent replication during the first 24 h p.i. Between 24 and 48 h p.i., there was an equivalent decrease in gp150 and ORF 73 transcript expression. This was accompanied by a significant change in the viral titre. This gene expression profile suggested that viral replication paused during this period. However, the increase in viral titres was not consistent with this conclusion. From 48 to 72 h.p.i., the *gp150* transcript remained unaltered and there was an increase in ORF 73 transcript expression. Again, *M1* transcript expression was not detected. This was accompanied by a significant decrease in the viral titre. These findings were consistent with latent viral replication from 48 to 72 h.p.i.

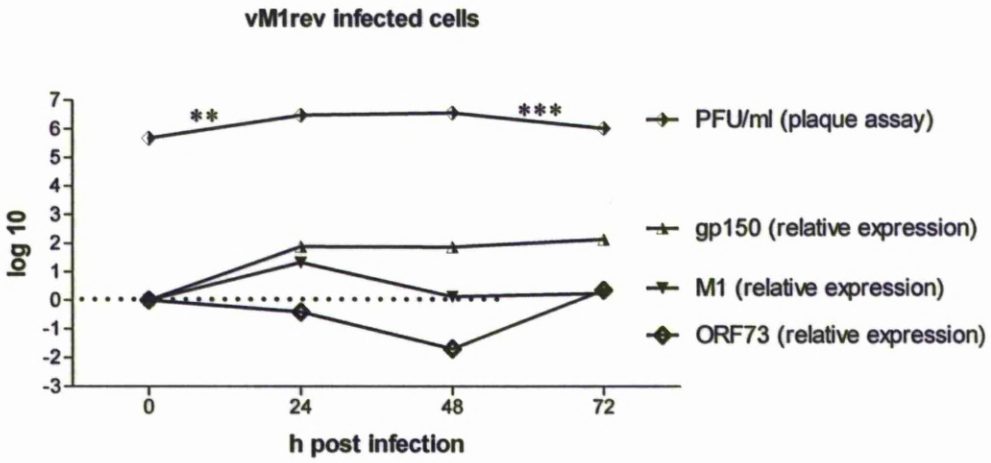

Figure 3.69 MH-S cells. vM1rev infected. Relative viral gene expression and viral titres in infected cells.
Viral gene expression values obtained through qPCR performed on cDNA synthetised from RNA extracted from infected cells. n=1 per virus per timepoint.. Base level (dashed line) represents values obtained from vM1rev infected cells. Significant differences in viral titres from sequential times after infection were determined using two way ANOVA and Bonferroni post test (*$p<0.05$, **$p<0.01$ ***$p<0.0001$) as mentioned in section 3.3.2.2. In vM1rev infected cells, M1 expression was highest in the first 24 h.p.i.This rise accompanied the increase in the expression of gp150, a significant increase in the viral titre (Figure 3.65), and decrease in expression of ORF 73. Between 24 and 48 h.p.i. there was a decrease in M1 expression accompanied by a decrease in the expression of the other viral genes tested, gp150 and ORF73 and a plateau in the viral titre. From 48 h to 72 h p.i, M1 expression was unaltered, this being accompanied by an increase in the expression of ORF 73 and significant decrease in the viral titre.

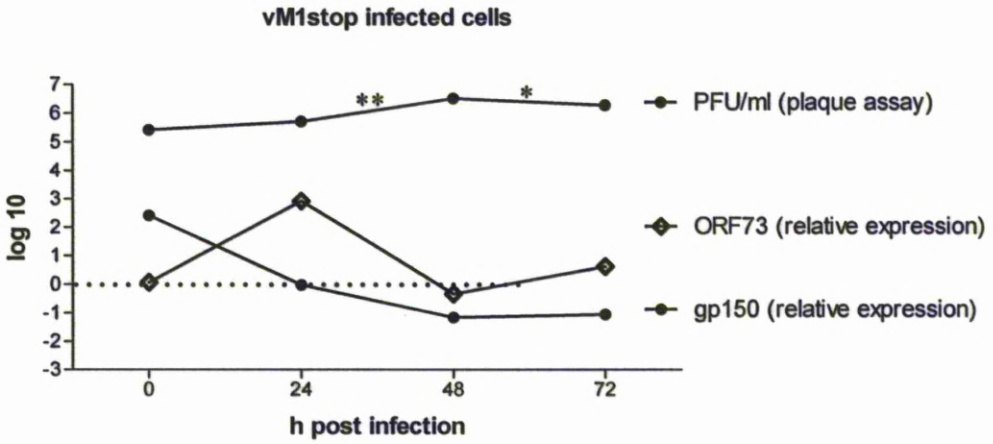

Figure 3.70 MH-S cells. vM1stop infected. Relative viral gene expression and viral titres in infected cells.

Viral gene expression values obtained through qPCR performed on cDNA synthetised from RNA extracted from infected cells. n=1 per virus per timepoint.. Base level (dashed line) represents values obtained from vM1rev infected cells. Significant differences in viral titres from sequential times after infection were determined using two way ANOVA and Bonferroni post test (*$p<0.05$, **$p<0.01$ ***$p<0.0001$) as mentioned in section 3.3.2.2. In vM1stop infected cells, in the first 24 h.p.i. there was a decrease in the expression of gp150 and an increase in expression of ORF 73. This was accompanied by an insignificant change in the viral titre. Between 24 and 48 h.p.i. there was a equivalent decrease in the expression of gp150 and ORF 73. This was accompanied by a significant increase in the viral titre. From 48 h to 72 h.p.i., the expression of gp150 mostly remained unaltered and there was an increase in expression of ORF 73. This was accompanied by a significant decrease in the viral titre.

3.3.2.5 Cytokine expression in MH-S cells infected with vM1stop and vM1rev

Expression of cytokines was determined in MH-S cells infected either with vM1stop or vM1rev virus and mock infected. The cytokines selected for study were TNF-α., RANTES and GM-CSF. The timepoints examined were 0, 24, 28 and 72 h.p.i.

TNF-α transcript expression followed a similar trend in cells infected with either vM1rev or vM1stop (Figure 3.71). At 0 h.p.i. in both vM1stop and vM1rev infected cells, TNF-α transcript expression was increased compared to mock-infected cells being highest in vM1rev infected cells. After 24 h.p.i. in both vM1rev and vM1stop infected cells, TNF-α expression decreased gradually. To assess is the experiment protocol altered the expression of TNF-α independently of viral infection, the expression of this cytokine was also monitored and compared at the different timepoints in the mock infected cells. For this values obtained from the different timepoints in the mock infected cells were normalized with those obtained at 0 h.p.i. in mock infected cells. Mock-infected cells exhibited a decrease of TNF-α expression, suggesting that the protocol used in the maintenance of the cell culture had an effect upon TNF-α transcript expression.

In addition, RANTES transcript expression was also monitored. In vM1rev infected cells, expression of this transcript was observed to be highest at 0 h.p.i. but decreased thereafter (Figure 3.72). However, in vM1stop infected cells RANTES transcript expression was lower than vM1rev infected cells at 0 h.p.i. and increased until 24 h.p.i. Once again, to assess the effect of the experimental protocol on the expression of RANTES by these cells, the expression between the different timepoints was also compared within the mock infected cells by using as control the values obtained from mock infected cells at 0 h.p.i. There was no correlation between the changes in mock and viral infected cells, suggesting that the values obtained were not the effect of culturing.

When RANTES and ORF73 transcript expression patterns were plotted, it was noted that during the first 48 h.p.i. both followed the same trend for either vM1stop infection (Figure 3.73 A) or vM1rev infection (Figure 3.73 B).

3.3.3 Summary of *in vitro* studies findings

The findings from the *in vitro* studies using NIH3T3 and MH-S cells infected with vM1stop and vM1rev are summarized in Table 3.6.

A

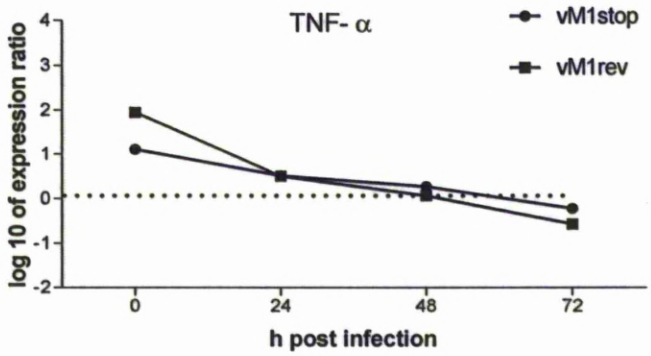

B

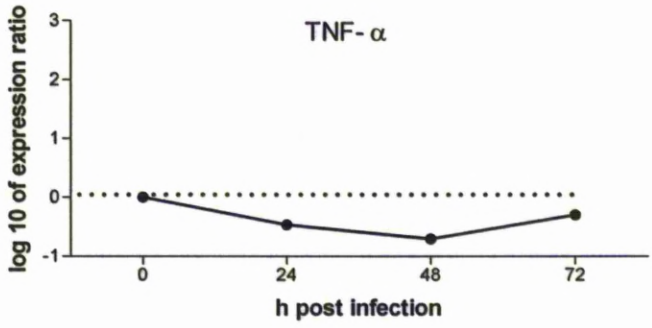

Figure 3.71 MH-S cells. Mock, vM1rev and vM1stop infected. TNF-α expression. Representation of difference ratios in cytokine expression. Values obtained through qPCR performed on cDNA synthetized from RNA extracted from infected cells. n=1 per virus per timepoint. A: TNF-α expression in vM1rev and vM1stop infected MH-S cells. Values were normalized against the values obtained at each time point from mock infected cells. B: TNF-α expression in mock infected MH-S cells. Values were normalized against those obtained at 0 h.p.i. There was little difference in the expression of TNF-α when comparing the different viral infections. However, at 0 h.p.i. the expression of TNF- α was seen to be higher in virally infected cells when compared to mock infected cells with the difference being heightened in the vM1rev infected cells. Beyond 24 h.p.i. TNF-α expression decreased gradually in both virally and mock infected cells. These findings suggest that the decrease of TNF-α expression is an effect which is independent of the viral infection and likely related to the maintenance of the cell culture during the infection experiment.

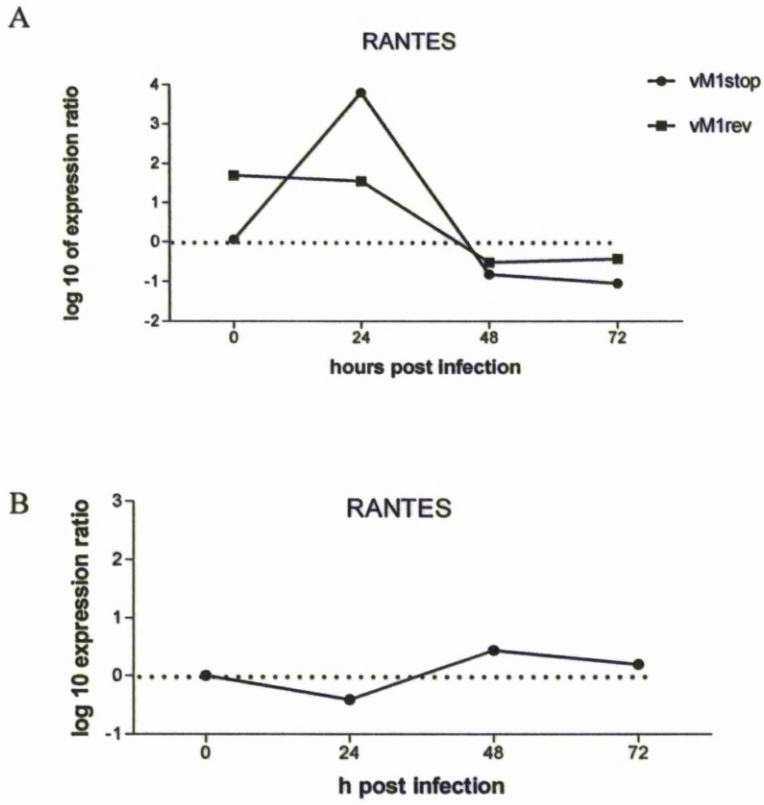

Figure 3.72 MH-S cells. Mock, vM1rev and vM1stop infected. RANTES expression. Representation of difference ratios in cytokine expression. Values obtained through qPCR performed on cDNA synthetized from RNA extracted from infected cells. n=1 per virus per timepoint. A: RANTES expression in vM1rev and vM1stop infected MH-S cells. n=1 per virus per timepoint.Values were norm alized against the values obtained at each time point from mock infected cells. B: RANTES expression in mock infected MH-S cells. Values were normalized against those obtained at 0 h.p.i. RANTES expression was observed to be highest initially at 0 h.p.i. in vM1rev infected cells but then decreased thereafter. In the vM1stop infected cells, the opposite occurred at the initial timepoints, with expression being lower at 0 h to then peak at 24 h.p.i. There was no correlation between the changes in mock and virally infected cells, suggesting that the trend obtained in virally infected cells were not the related to the maintenance of the cell culture during the infection experiment.

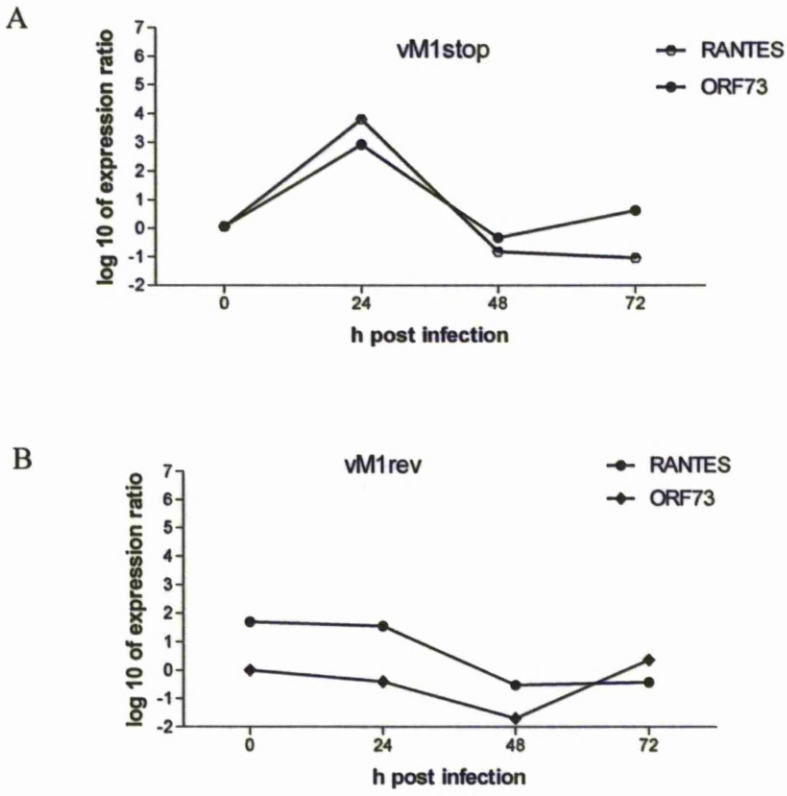

Figure 3.73 MH-S cells. vM1rev and vM1stop infected. ORF73 and RANTES expression.

A; vM1stop infected cells; B: vM1rev infected cells. Representation of difference ratios in RANTES and ORF73 viral gene expression. Values obtained through qPCR performed on cDNA synthesised from RNA extracted from infected cells as mentioned in Sections 3.3.2.2 and 3.3.2.4. n=1 per virus per timepoint. A: Expression in vM1stop infected MH-S cells. B: Expression in vM1rev infected MH-S cells. In the first 48 h.p.i. these follow the same trend, in both types of viral infections.

	NIH3T3 cells	MH-S cells
LHΔMHV-68	24h: 100% fluorescence 48h: 100% fluorescence ++ morphological Δ 72h: 100% fluorescence ++ apoptosis	24h: 15-25% fluorescence 48h: 3-18% fluorescence ++ morphological Δ 72h: little fluorescence ++ apoptosis
OS Growth curves	Plateau in titres at 30 h	Plateau in titres at 24 h*
Ultrastructure	Extensive lytic replication	Fewer viral particles and no evidence of viral factories

* No measurements made at 30 hours

MH-S	vM1stop	vM1rev
Ultrastructure	Viral particles from 72 h > lipid	Viral particles from 24 h
Viral gene expression	24 h: <gp150 > ORF 73 no Δ viral tire 48 h: <gp150 < ORF 73 < viral tire 72 h: >ORF 73 < viral tire	24 h: >gp150 ~ no Δ ORF73 >viral tire >M1 48 h: <gp150 < ORF 73 no Δ viral tire <M1 72 h: >ORF 73 < viral tire
Cytokine expression	RANTES:> first 24 h < after 24 h TNFα: < following infection	RANTES:no Δ first 24 h < after 24 h TNFα: < following infection

Table 3.6 Table summarising findings in NIH3T3 cells and MH-S cells infected with vM1stop, vM1rev and LHΔMHV-68.
+, ++, +++: scale regarding number of cells: showing expression + (scattered cells); ++ (moderate numbers); +++ (numerous cells)
>, <, ~, and Δ relates to relative change. >: increased; <: decreased; Δ: change; ~: approximately

4. Discussion

Most MHV-68 studies are performed in laboratory mouse strains (*Mus musculus*). However, in the wild, MHV-68 does not infect *Mus musculus*[293, 318]. Sequencing and serological studies have identified the wood mouse (*Apodemus sylvaticus*) as one of the natural hosts for MHV-68 infection[5, 19, 293]. The use of laboratory mouse strains, as opposed to a natural host, is useful but may not necessarily mirror what happens during the course of a natural infection. The need to study infection using a natural host is further justified by the fact that gammaherpesviruses are thought to have developed in parallel with their host[18]. These viruses are highly adapted to their host and often exert only mild pathogenicity except in the very young, foetuses, immunosupressed or accidental hosts[150].

The aim of the present study was to ascertain the influence of the expression of *M1* on MHV-68 infection in the natural host, the wood mouse. There are distinct differences in the infection profile between the wood and BALB/c mouse. In the wood mouse there is less lytic replication but latency is more efficiently established[5]. In the wood mouse, the infiltrate seen in the lung following infection, is macrophage dominated and there is a less intense lymphocytic infiltration mostly composed of B cells[5]. Unique to the wood mouse, bronchial associated lymphoid tissue (iBALT) is induced during MHV-68 infection[5]. The iBALT is structurally similar to secondary follicles in lymphoid tissues and is associated with inflammation/infection[294] and has been shown to be the main site where cells latently infected with MHV-68 persist in the lung of an infected wood mouse[9, 154]. In the BALB/c mice, MHV-68 infection is not associated with iBALT formation and the infiltrate seen in the lung shows a higher predominance of T cells[5].

M1 shares homology with the sequences encoding for poxvirus serpin (serine protease inhibitors) proteins[163]. However, the *M1* sequence lacks the critical domains/residues for serpin activity. Previous studies in laboratory mouse strains have indicated M1 as a suppressor of reactivation from latency[6]. This M1 activity is IFN-γ dependent and is seen together with activation of $V\beta4^{+}CD8^{+}$ T cells which resist functional exhaustion[6-8]. In the wood mouse, MHV-68 infection does not lead to significant changes in IFN-γ expression (Figure 3.31). This suggests the previously described role of M1 is not applicable to the wood mouse infection. *M1* has been found to encode for a secreted protein[6] and sequence homology suggests that the M1 protein shares functional similarities with the chemokine-binding proteins resulting from the closely related genes, M3 and M4[9]. If M3 expression is inhibited in the MHV-68

infection of wood mice, iBALT formation is no longer observed. Furthermore in the absence of M3 instead of a lymphocytic response which is B cell dominated, there is a relative increase in T cells[5, 9] similar to what is seen in the infection of BALB/c mice. As mentioned previously, in MHV-68 infection, B cells are the main cell type where latent replication occurs[28, 82]. Therefore it is of benefit to the virus to increase the availability of B cells which is achieved partly by preventing T cell activation[9]. Quantification of M1, M2, M3 and M4 expression in the lung of infected wood mice at 7, 10, 12 and 14 d.p.i found M1 to be the protein with highest expression at day 7 p.i.[9]. This time also coincided with when M1 was expressed the most[9].

4.1 M1 expression in the lung of the wood mouse and BALB/c mouse

M1 expression was assessed by RNA-ISH in sections of lung from MHV-68 infected BALB/c and wood mice. The aim of this study was to determine in which cells M1 expression occurs. Comparing the species determined whether there are similarities in the M1 expression pattern between an artificial and natural host. M1 expression was detected in type I pneumocytes in both BALB/c and wood mice, at day 3, 7, 10 p.i. and also at day 14 p.i. in the wood mouse. M1 transcripts were also detected in interstitial and intravascular (migrating) lymphocytes of both mice at all the timepoints examined. The extent of M1 expression from day 14 p.i. was much reduced in the wood mouse, in agreement with previously published qPCR data[9]. In the BALB/c mouse, M1 expression was lower than in the woodmouse. M1 expression was not as frequent and decreased from day 3 p.i. onwards.

Additionally, in the BALB/c mouse M1 transcripts were detected in endothelial cells at day 3 p.i. In the BALB/c mouse, phlebitis is a feature of MHV-68 infection[5, 28]. M1 expression in endothelial cells of BALB/c mice could indicate a possible role of M1 in the development of the phlebitis in the laboratory mouse strain.

In the wood mouse, lymphocytes exhibiting M1 expression were also seen within iBALT from day 7 p.i. Interestingly, in the wood mouse at day 5, 7, 10, 14 and 28 p.i tracheal and bronchial epithelial cells showed M1 expression. This is the first time a MHV-68 gene product has been described in this location. Intranasal infection is thought to be the main route of infection for MHV-68[28]. Following intranasal infection of laboratory mouse strains or wood mice there is development of pneumonia[5, 28]. It is likely that the airway has a role in MHV-68 infection since it is interspaced between the

nose (site of infection) and the lung (main site of acute viral replication). The expression of M1 in airway epithelial cells together with the fact that no other MHV-68 genes to date have been described in such a location, suggest that M1 expression could play a role in airway-mediated viral entry into the lung. Airway epithelial cells provide a physical barrier and regulate the host immune response[55] by secreting anti-viral substances such as cytokines[51]. Cytokine expression in airway epithelial cells is mostly localized in the basolateral pole of the cells. The purpose of the secretion in this location is thought to be modulation of inflammatory cell migration into areas adjacent to the airways[55]. Respiratory viruses including Influenza A virus often target the basolateral membrane of airway epithelial cells and interfere with the cytokine expression at this site[51, 55, 320]. With Influenza A virus infection there is induction of MIP1-α and TNF-α secretion at the basolateral pole of airway epithelial cells[55]. In this study at the early timepoints, day 3 and 7 p.i., of vM1stop and vM1rev infection, there was mild respiratory epithelium hyperplasia which is a sign of regeneration. Regeneration and the presence of apoptotic cells in the bronchiolar lumina are an indication that viral infection only induced mild degenerative changes to airway epithelial cells. Taking these results together, one could extrapolate that the effect induced by the heightened M1 expression in these cells is not mainly cytopathic but instead leads to interference with the respiratory epithelial cell metabolism/function. Amongst the differences observed when comparing vM1stop to vM1rev infection was the extent of TNF-α expression. In vM1stop infection, there was almost a tenfold increase in TNF-α expression. This enhanced secretion was localized to various cells including the upper and lower airway epithelial cells (Figure 3.43). Likewise, qPCR studies at day 7 p.i. also found that in vM1stop infected animals, there was an increase in the expression of MIP1-α in approximately the same magnitude as TNF-α. However, the localization of MIP1-α expression was not determined. CCSP expression by airway Clara cells was decreased in the vM1stop infection with the difference being greater at day 3 p.i. (Figure 3.41). CCSP effects include a decrease in TNF-α in airway fluid and a decrease in TLR4 expression by alveolar macrophages leading to decreased chemotaxis of macrophages [321]. TNF-α has also been described as an inhibitor of the CCSP promoter and thus of CCSP expression[322]. Furthermore, a decrease in CCSP expression has been associated with increased MIP1-α in various viral infections including in MHV-68 M3 stop infection (mutated in the M3 locus)[323-325]. MIP1-α and TNF-α, secreted by airway

epithelial cells, have been reported to exert a positive role on macrophage recruitment[326, 327]. Another feature of vM1stop infection was an increase in macrophage infiltration and activation which was most significant in the early timepoints following infection. Also, at day 14 p.i. in the vM1stop infection, there was a decrease in viral load. The evidence from this study suggests that the presence of M1 protein could be involved in the attenuation of TNF-α and MIP1-α expression by airway epithelial cells following MHV-68 infection. This could be a result of or lead to an increase in the CCSP expression, a potent anti-inflammatory cytokine secreted by Clara cells. Ultimately this would induce a decrease in macrophage migration to the site of infection and a decrease in phagocytosis of virally infected cells. The decreased lytic replication at day 14 p.i. in vM1stop infected mice may be secondary to a more efficient phagocytosis of infected cells earlier in infection, as the findings at day 3 and day 7 p.i. suggest.

Furthermore, M1 transcripts were observed in parabronchial ganglia specifically in the satellite cells surrounding the neuronal bodies in the woodmouse at day 7 and 14 p.i. This is the first time that a MHV-68 gene product has been described in this location. All neuronal tissues examined, including the brain, did not exhibit evidence of neuronal pathogenesis. VZV viral proteins have been described in satellite cells within the dorsal root ganglia (DRG) and these cells are suggested to be a means of entry into the neuronal system[328]. In the wood mouse, pathological changes to neuronal system cells are not a feature of infection. However, meningitis has been described following intranasal infection of BALB/c mice that have a deletion of type-I interferon receptor gene[230] or newborn BALB/c mice[231]. Furthermore, MHV-68 is able to persist in the central nervous system (CNS) during the infection of the laboratory mouse strain[232]. This indicates that in BALB/c mice MHV-68 shows neurotropism despite it not being the primary infected tissue following innoculation. Taking this into consideration and coupled to the finding of M1 expression in satellite cells of the parabronchial ganglia, neurotropism by MHV-68 in the wood mouse cannot be ruled out. M1 expression in satellite cells of parabronchial ganglia might represent a site of neuronal entry despite the lack of evidence for neuronal pathogenesis in this species. Further studies have to be carried out to fully clarify this, particularly because the parabronchial ganglia was not a targeted in this study and was not present in all sections examined.

When M1 expression was evaluated in *in vitro* in NIH3T3 cells, M1 transcripts were rarely detected despite all the cells being lytically infected. This indicates that M1 expression is enhanced in the animal model.

In summary, M1 expression was found to be higher in the natural host in comparison to the artificial host, with respects to intensity, frequency and cell types involved. Furthermore M1 expression was seen to be minimal in laboratory mouse strain derived cells that are highly permissive to infection. These findings indicate that the role of M1 is of more importance in the natural host than in the artificial one.

4.2 M1 effect on viral replication and virally induced pathogenesis in the lung of the wood mouse

In order to determine the effect of M1 expression in MHV-68 infection of the natural host, *in vitro* and *in vivo* studies were performed in the wood mouse using vM1stop virus and its genetically repaired counterpart, vM1rev virus. The vM1stop virus is a MHV-68 virus with an in-frame stop codon in the *M1* locus. The stop codon impairs expression of M1 without interfering with the expression of the remaining genome. The objective was to ascertain the influence of M1 in MHV-68 infection through comparison of pathogenesis in the presence or absence of M1 expression.

The time at which viral load was highest was at day 3 p.i. Viral antigen was detected in both infections in type I pneumocytes, type II pneumocytes and macrophages. Ultrastructural examination of the lung in vM1rev infected animals, showed viral particles in scattered type II pneumocytes. The stages included nuclear "viral factories" and budding particles. Host infected cells showed degenerative changes proportional to the extent of viral replication. This is the first time that the different stages of MHV-68 viral particles have been described *in situ* in the lung by electron microscopy. Latent replication in both infections, was observed in lymphocytes in iBALT, alveolar interstitium and intravascularly. In the vM1stop infected animals latent replication was also detected in type II pneumocytes and in macrophages. Histological examination of the lung showed that there was an overall increase in cellularity in both infections that was more severe in the vM1stop infected animals. This was mostly due to higher macrophage infiltration and more severe type II pneumocyte hyperplasia in the vM1stop infection. Another feature seen in the vM1stop infection was the presence of lipid droplets in the cytoplasm of macrophages within alveoli and interstitially and in

the extracellularly in the pulmonary interstitium. The latter, likely represents macrophages that had degenerated and thus showed no obvious cellular outline. These lipid droplets were also seen *in vitro* in infected alveolar macrophages at 72 h.p.i. The presence of lipid in the single cell cultures of macrophages, rules out the lipid being related to altered surfactant production by the hyperplastic type II pneumocytes. In H1N1 IA30 (1918 pandemic derived) studies, a relationship between viral induced changes to lipid metabolism and cellular death early in infection (day 5 p.i) was established[329]. It is known that lipids play fundamental roles in Influenza infection including virus entry, assembly and budding and host cell repair[329]. The lipid droplets found in the current study are thought to represent enhanced degenerative changes.

At day 7 p.i., viral antigen presence was detected in both infections in type I pneumocytes, type II pneumocytes and macrophages. The viral load was decreased compared to day 3 p.i but this decrease was not statistically significant. The number of cells exhibiting latent replication increased at day 7 p.i. in comparison to day 3 p.i. in both infections. Similarly to what was observed at day 3 p.i., latent replication at day 7 p.i. was seen in both infections in lymphocytes in iBALT, alveolar interstitium and intravascularly. Furthermore, at day 7 p.i., in the vM1stop infection latent replication was also detected in type II pneumocytes and macrophages. These cells were seen either lining alveoli or desquamated in the alveolar space (Figure 3.35). Latent replication in these cells may be related in part to their increased presence in the vM1stop infection which showed a more severe type II pneumocyte hyperplasia and macrophage infiltration. Viral tropism for type II pneumocytes has been associated with increased pathogenesis in H5N1 influenza virus infection due to an infection induced increase in cellular metabolism[62]. Further morphological changes consisted of type I pneumocyte necrosis in both infections and iBALT formation. The iBALT formation was most frequent in the vM1stop infection which also exhibited multifocal foci of necrotic cells with fibrinous centres. The morphological changes occurred in a multifocal pattern in the vM1stop infection whilst in the vM1rev infection they occurred in a diffuse pattern. This pattern in the vM1stop infection suggests that the area where more extensive viral induced pathogenesis occurs, is at the periphery of the airways. The increased severity of changes in the vM1stop infection was not associated with a higher viral load, suggesting that pathological changes are not directly related to viral replication but possibly induced by host cell products (such as cytokines). In the vM1stop infection at day 7 p.i. there was almost a tenfold increase in TNF-α expression. This enhanced

secretion was localized to airway epithelial cells, macrophages and type II pneumocytes. TNF-α is a known inducer of apoptosis but in viral infections such as RSV such an effect has been reported to be abrogated[330]. RSV infected cells are resistant to TNF-α induced apoptosis and fuse to form syncitia with cellular death occuring eventually due to necrosis[330]. In the present study syncitial cells were occasionally seen. When immunohistology was performed using a marker for caspase 3, there were very few cells showing its presence. These findings together with the cell morphology, indicate that in the current study cell degeneration occurs by induction of necrosis rather than apoptosis despite an increase in TNF-α expression. This indicates that in MHV-68 infection, as in RSV infection, cells are resistant to TNF-α induced apoptosis. In this study there was also an increase in TGF-β expression in both vM1rev and vM1stop infected wood mice (Figure 3.45). MHV-68 infection studies using laboratory mouse strains have found that infection led to increased TGF-β expression by alveolar fibroblasts, alveolar macrophages and latently-infected pneumocytes[122]. This increase in TGF-β expression was associated with increased resistance to apoptosis[123]. Thus even though TGF-β increase results from MHV-68 infection it is not a direct result of the M1 expression, it is most likely related to the resistance against TNF-α induced apoptosis observed in the vM1stop infected wood mice.

Other TNF-α effects include the enhancement of tight junction permeability in alveolar epithelial cells[112]. Tight junctions are important for the maintenance of epithelium integrity, communication and transport between neighbouring epithelial cells[51]. In Influenza A virus infection of *ex vivo* human endothelial cells, TNF-α has been associated with increased cellular permeability[331]. *ZO1*, a tight junction, is maintained by ATP[331]. TNF-α is known to increase mitochondrial O_2 species production and decrease ATP production consequently leading to *ZO1*-actin dissociation[331]. The TNF-α increase in the absence of M1, may play an important role in the enhancement of the endothelial and epithelial permeability and consequently in the leakage of fibrin explaining its presence in the vM1stop infection.

At day 14 p.i. the differences in viral load between vM1stop and vM1rev infections were statistically significant. In vM1stop infected animals there was more than a tenfold decrease in viral load at day 14 p.i when compared to the vM1rev infected animals. At the earlier timepoints, day 3 and 7 p.i. in vM1stop infection, there were increased pathological changes when compared to vM1rev infection. Decreased

lytic replication at day 14 p.i. in vM1stop infected mice may be due to a more efficient phagocytosis of infected cells earlier in infection. In both vM1stop and vM1rev infection latent replication at this timepoint was restricted to lymphocytes present in the iBALT. There was no noticeable difference in the pathological changes induced in the lung following vM1stop or vM1rev infection. In comparison to previous timepoints, there was a marked decrease in the overall cellularity in the lung. As in the mock infected mice, the alveoli were mainly lined by type I pneumocytes and type II pneumocytes were rarer. The interstitial infiltration by macrophages was however more intense than at previous timepoints. In both vM1stop and vM1rev infection, the iBALT was still composed mainly of B cells, but at this time point also contained a high number of T cells. These findings suggest a more elaborate immune response in the vM1stop infected animals, which showed an increased presence of B cells mainly in the iBALT, an increase in APC and to lesser extent a increase in T cells.

At day 28 p.i. in the lung of vM1stop infected animals, the viral load did not significantly change in comparison to the observations at day 14 p.i. On the contrary, in vM1rev infected mice, at day 28 p.i. there was a large decrease in viral load of approximately a hundredfold when compared to the values on day 14 p.i. These findings suggest that in vM1stop infection, lytic replication is maintained for a longer period. In both infections, cells exhibiting latent replication were restricted to lymphocytes present in the iBALT. There was very little difference between the overall cellularity in the lung of animals infected with either virus. The most significant morphological difference was the presence of more frequent and pronounced iBALT in the lung of vM1stop infected mice. TNF-α and its binding to TNFR1 has been shown to be essential in secondary lymphoid follicle formation[113-115]. This suggests that the increase in the expression of TNF-α in the vM1stop infection might play a role in the more pronounced iBALT seen in infection with this virus. Furthermore, at day 14 p.i. in the vM1rev, there was still a mild infiltration by macrophages into the interstitium.

In summary, these findings indicate that in the presence of M1 there is greater lytic replication at day 14 p.i. but this subsides by day 28 p.i. M1 presence is not associated with latent replication in type II pneumocytes and macrophages as it is seen in the absence of M1. Furthermore, the presence of M1 is associated with decreased pathological changes in the lung such as infiltration by macrophages and less pronounced/frequent iBALT. The iBALT being more exuberant in the vM1stop infection is likely related to the increase in B cell priming by the macrophages which

are also more frequent at day 3 and 7 p.i. Furthermore, in the presence of M1, the infected cells, including macrophages, show less extensive degenerative changes. The degenerative changes seen in the macrophages in the vM1stop infection could be related to increased activation or metabolism that is reflected in the severe necrosis seen in the lung of the vM1stop animals. Furthermore the presence of M1 downregulates TNF-α and upregulates CCSP expression by airway epithelial cells. This cytokine expression profile favours an anti-inflammatory response and could explain the multifocal pattern of more severe pathogenesis seen in the absence of the M1 protein which is is seen mostly surrounding airways.

4.3 M1 influence on macrophages in the wood mouse infection

Considering the increase in macrophages in the absence of M1 expression, studies were performed to determine the mechanism of their activation. These included the qPCR assessment of transcript expression of cytokines and enzymes with known roles in macrophage activation and function. Lung sections from wood mice infected with vM1rev and vM1stop at day 7 p.i. were tested. Arginase I and iNOS were examined for relative expression. These enzymes are commonly used as indicators of classic versus alternative activation of macrophages[145-147, 332]. When macrophages are classically activated they express iNOS[145-147, 332]. On the other hand, alternatively activated macrophages (M2) express arginase I[145-147, 332].

In the vM1stop infection, arginase I expression was reduced by more than tenfold. This indicates M1 protein plays a role in an alternative activation of macrophages in MHV-68 infection of the wood mouse. Surprisingly there was little difference in the levels of arginase I expression by vM1rev and mock infected wood mice. This suggests that in wood mice the macrophage population resident in the lung exhibits an alternatively activated phenotype which is maintained following MHV-68 infection in the presence of the M1 protein.

The expression of iNOS showed little difference between viral infections, being mildly reduced in the vM1stop infected wood mouse. The iNOS reaction product is nitric oxide (NO) which exhibits cytotoxic properties[143, 145-147, 332]. The arginase I reaction products include proline, which is a known inducer of collagen production[145-147, 332]. Arginase I and iNOS compete for a common substrate, arginine[145-147, 332]. The cytokines produced by classically activated macrophages inhibit alternative macrophage

proliferation, and vice versa, through blockage of arginine metabolism at the translational level[145-148]. As mentioned previously, iNOS expression is increased in both vM1stop and vM1rev infections, being mildly increased in the vM1rev infection. This indicates that following the MHV-68 infection of wood mice there is a shift in macrophage activation into the classic activation route. If the expression profile was seen on its own, it would suggest that in the vM1stop infection there was a decrease in the overall activation of macrophages since there was a reduction in alternatively activated macrophages and no major change in classically activated ones. However, the morphological study of the lung from vM1stop infected wood mice indicated this is not the case. In the vM1stop infection, macrophages are more frequent and highly activated. iNOS is a persistently active enzyme[141] and in the vM1stop infection there is a decrease in the expression of the enzyme that competes for its substrate, arginase I. So it is safe to assume that in the vM1stop infection, iNOS will have higher substrate availability. The end result could be an increase in NO production despite no major change in iNOS expression. NO high-dose effects include vasodilation, disruption of the endothelial barrier and cytotoxicity[143]. The increase in NO could explain the augmented pathological changes observed in the lung of vM1stop infected mice. A possible interpretation of these results would be that M1 induced maintenance of alternatively activated macrophages is a step in the viral evasion to the immune system by decreasing NO induced cytotoxic effects on infected and neighbouring cells.

iNOS derived NO has been found to induce an increase in TNF-α expression[142]. TNF-α has on the other hand been implicated in the activation of IκB-NFκB complex phosphorylation resulting in the induction of iNOS expression[141, 333]. Both TNF-α and iNOS expression was increased in the vM1stop infection in comparison to the vM1rev infection. However, there was a lesser fold change in the increase in iNOS expression than that of the increase in TNF-α expression. This suggests that TNF-α is not a single activator of iNOS expression. The decrease in arginase expression in the vM1stop infection likely results in a increase in the availability of arginine for iNOS and could lead to the increased NO. Ultimately if NO is increased this could secondarily induce TNF-α expression.

Alternative activation of macrophages can be divided with respects to the source of their activation. M2a macrophages are the result of stimulation by Th2 cytokines (mainly IL-13 and IL-4)[145, 146]. M2b macrophages are induced by immune complexes, TLR and IL-1R agonists[145]. M2c macrophages are induced by IL-10, TGF-β and

glucocorticoids[145]. IL-10 is also the main cytokine released by alternatively activated macrophages[145]. In the current study, the expression of both IL-10 and TGF-β was seen to increase following MHV-68 infection of the wood mouse. There was little difference between the expression of TGF-β in the vM1stop and vM1rev infected wood mice. IL-10 is increased in vM1stop infected wood mice to a greater extent, being tenfold more in the vM1stop infected than in the vM1rev infected mice (Figure 3.45). Thus it is unlikely that changes in expression of IL-10 and TGF-β are related to the shift in the route of macrophage activation seen between the vM1stop and vM1rev infection in wood mice.

The increase in IL-10 in vM1stop infected animals is at odds with the decrease in IL-10 producing alternatively activated macrophages and thus indicates that the increase of IL-10 is due to secretion by another cell type. IL-10 is one of the main cytokines produced by B cells and Th2[138]. Considering that there is a decrease in alternatively activated macrophages in vM1stop infection, an increase in Th2 cells is unlikely to be responsible as this would result in activation of M2b macrophages. So, the IL-10 increase in the vM1stop infection is most probable due to secretion from B cells. This is further supported by the fact that at day 7 p.i., in the vM1stop infected animals there was a more frequent and better demarcated, B cell dominated iBALT. IL-10 is a known inducer of B cell maturation and/or survival. In the milieu of MHV-68 infection such role has been described to be associated with expression of the MHV-68 M2 protein[334]. NO has also been described as an inducer of IL-10 expression[142] and if increased in vM1stop infected wood mice could be related to the increase seen in IL-10. IL-10 is of major importance in epithelial cell maintenance. Other IL-10 effects include inhibition of pro-inflammatory cytokine expression including Th1 cytokines, leading to an immune response towards healing[136, 138].

TGF-β expression in mouse primary bronchiolar-alveolar cell lines (composed mostly of type II pneumocytes and fewer Clara cells) and pulmonary fibroblasts has been reported to be increased by TNF-α activation of the NF-κB pathway[125-128]. This TNF-α induced increase in TGF-β expression was also observed in RAW 624 cells (murine macrophage cell line) co-cultured with A549 cells (human lung adenocarcinoma cell line) and was related to an increased expression of TGF-β which led to the transformation of A549 cells from epithelial to a mesenchymal phenotype[128].

In this study there was little difference between expression of TGF-β in the vM1stop and vM1rev infected wood mice. This was accompanied by an increase in the

expression of TNF-α in the vM1stop infection. This suggests that the increase in TNF-α expression is not mediated by TGF-β in this case. Furthermore infection with either vM1stop or vM1rev was not associated with a mesenchymal differentiation of airway epithelial cells, a common change in pulmonary infections associated with increase in expression of TGF-β.

In the MHV-68 infection of laboratory mouse strains, IFN-γ is upregulated particularly in latent infection[98]. IFN-γ controls reactivation by interacting with the ORF50 promoters, encoding for RTA[101]. The IFN-γ effect on reactivation is specific to macrophage dominated and not B cell dominated cell populations[82]. During MHV-68 infection of $IFNR^{-/-}$ mice studies there was extensive fibrosis in the lung at 2 weeks p.i. and in mediastinal lymph nodes and spleen at 3 weeks p.i. [214-216]. The splenic fibrosis was caused by alternative activation of macrophages[209]. As mentioned previously, IL-10 expression was augmented in both vM1rev and vM1stop infection and this increase is likely related to the iBALT formation observed in this study. The formation of iBALT is a feature of MHV-68 infection in the wood mouse that is not seen in the BALB/c mouse[5]. Considering the inhibitory effect of IL-10 on expression of Th1 expressed cytokines, IL-10 increase in the infection of the wood mouse could explain the lack of change in expression of IFN-γ. An important role in the immune response induced by IFN-γ is the induction of expression of MHC Class I and II molecules[92, 97]. This taken together with the specificity effect of IFN-γ effect on macrophage cell populations and the findings in $IFNR^{-/-}$ mice could indicate that in the wood mouse, the lack of an IFN-γ increase allows the virus to replicate in macrophages. Furthermore, IFN-γ prevents to some extent macrophages from being classically activated, and thus possibly represents a viral mechanism to evade host recognition of viral antigens. Classical activation of macrophages occurs mostly upon stimulation by Th1 cytokines such as IFN-γ and α-α[145, 146]. Since in this study there was no evidence of an IFN-γ increase following infection with vM1stop or vM1rev virus (Figure 3.45), this cytokine is unlikely to have a role in the classical macrophage activation in the wood mouse infection. However in the vM1stop infection, in comparison to vM1rev and mock infected wood mice, there was a tenfold increase in TNF-α expression. The increase in expression of TNF-α occurred in airway epithelial cells, macrophages and type II pneumocytes. These findings suggest that this cytokine could be partly involved in or be a result of the macrophage classical activation in the vM1stop infected wood mice. A feature of

classically activated macrophages is enhanced expression of MHC Class I and II and complement factors which aid antigen recognition and phagocytosis[335, 336]. In classically activated macrophages there is also activation of IRF3 ultimately leading to IFN-β secretion[337]. IFN-β takes part in the host anti-viral response by inducing secretion of proteins which interfere with viral replication, protein synthesis and trafficking processes[51]. Thus the maintenance of alternatively activated macrophages in the presence of the M1 protein, allows MHV-68 to evade APC recognition and IFN-β mediated anti-viral immune response.

Weinheimer et al. suggested that the pathogenicity of viruses is not always correlated with the level of cytokine modulation, as is observed in the study of low pathogenicity H5NI and HPAIV-H5N1. They found that the low pathogenicity virus induced a greater increase of cytokines such as MIP1-α[62].

Infection and viral replication in MH-S cells, an alveolar macrophages cell line, and NIH3T3, a fibroblast cell line, was compared. MH-S and NIH3T3 cells lines are both derived from laboratory mouse strains. The studies showed evidence of active MHV-68 replication in both cell types. MH-S cells were less permissive to infection, requiring a higher multiplicity of infection (MOI) and longer incubation times. M1 presence or absence did not lead to a significant difference in lytic replication in either MH-S or NIH3T3 cells over a 72 h time course. M1 expression in vM1rev infected MH-S cells was quantified and seen to increase over the first 24 h and decrease thereafter. In vM1rev infected cells, during the first 24 h there was an increase in the expression of gp150 (a glycoprotein expressed during lytic replication) and an inversely proportional decrease in the expression of ORF73 (expressed during latency). This was observed together with a significant increase in viral titres. On the other hand in vM1stop infected cells, during the first 24 h, there was a decrease in the expression of gp150 (a glycoprotein expressed during lytic replication) and an inversely proportional increase in ORF 73 expression. This was seen together with no significant change in viral titre. Studies in laboratory mouse strains showed M1 controls reactivation from latency in a T-cell dependent manner[6-8]. The finding that the rise in M1 expression accompanies the rise in gp150 expression in this cell line, suggests M1 expression is driving MHV-68 lytic replication in macrophages. This is further supported by the fact that latently infected macrophages were identified in the vM1stop infected wood mice and not in vM1rev infected wood mice. It is not fully understood why some cells enter latency rather than the lytic cycle, however it is suspected that latency is due to failure in the

expression of IE genes, as happens in VZV[166]. This can be overcome when changes in the host cell occur (cell differentiation etc.), leading to lytic replication[150]. Both vM1stop and vM1rev infected MH-S cells showed an increase in RANTES expression within the first 24 hours, this was more pronounced in vM1stop infected cells. This increase was similar to the pattern of increase in expression of ORF73. RANTES (CCL5) is a potent chemeoattractant for T cells in particular for $CD8^+$ cells[338, 339]. RANTES expression can be induced by TNF-α and IFN-γ[340]. HSV infection of macrophage cell lines also leads to the increased expression in RANTES but this is driven by an immediate-early (IE) gene product, ICP10[341]. Contrary to this, the findings in this study suggest that during MHV-68 infection of the macrophages, increases in RANTES expression occur together with the expression of a latency associated transcript, ORF73.

In summary, evidence shows that in the wood mouse, macrophages are a site for MHV-68 lytic and latent viral replication, with the latter being enhanced in the absence of the M1 protein. The presence of M1 in the infection of wood mice leads to less intense macrophage infiltration likely related to M1 driven maintenance of macrophage alternative activation. Alternative activation, besides producing a lower pro-inflammatory response, also leads to decreased macrophage recognition of virally infected cells by reducing expression of MHC. Furthermore in laboratory mouse strain derived macrophages, the expression of M1 induces lytic replication but the absence of M1 induces latent replication. This latent replication is accompanied by an increase in RANTES expression.

4.4 M1 expression in the spleen

M1 expression was assessed by RNA-ISH in sections of the spleen from MHV-68 infected BALB/c and wood mice. The aim of this study was to determine in which cells M1 expression occurs. Comparing the different mice showed where there are similarities in the M1 expression pattern between an artificial and natural host. In both species, M1 expression in the spleen increased gradually until day 14 p.i. and was maintained at approximately at the same level on day 28 p.i. The viral load was highest in the wood mouse spleen at day 14 p.i., following infection with either vM1stop or vM1rev virus. When comparing M1 expression between BALB/c and wood mice, significant differences were seen at day 3 p.i., when expression was most intense in the

wood mouse. In both species M1 expression was seen in lymphocytes within follicles and subcapsularly. In the wood mouse, M1 expression was also seen in multinucleated cells in the red pulp. These multinucleated cells had morphologies consistent with megakaryocytes. This is the first time MHV-68 gene expression has been described in megakaryocytes. Megakaryocytes are precursors of platelets the main function of which is to seal areas of vascular damage. Interference with megakaryocytopoiesis can result in dysmegakaryocytopoiesis and thrombocytopaenia[342-346] and ultimately bleeding disorders. In the current study there was no evidence of coagulopathies within the mice examined. In HIV infection, platelets and megakaryocytes have been described as harbouring unaltered viral particles within the cytoplasm. This evidence suggests HIV viral entry occurs in megakaryocytes by endocytosis rather than fusion since the internalized virions retained the envelope. Infected platelets expressed a macrophage receptor (CD62) on their cellular membrane. It was hypothesised that the aim of megakaryocyte infection by HIV was to perform a protective role towards the virus[347].

4.5 M1 effect on the spleen of the wood mouse

The viral load in the spleen of wood mice infected with vM1stop and vM1rev virus was assessed by qPCR at day 3, 7, 14 and 28 p.i. It was highest at day 14 p.i coinciding with the time when splenomegaly was present and the time when secondary follicles were first observed. No statistically significant difference was seen between the vM1stop and vM1rev infection. Morphologically there were no extensive differences in the changes seen in the spleen following vM1rev and vM1stop infection. Unique to vM1stop infected wood mice megakaryocytes in the red pulp showed vacuolated cytoplasm. As mentioned previously megakaryocytes were shown to exhibit M1 expression. Furthermore latent replication was detected in megakaryocytes in both vM1stop and vM1rev infected wood mice. This indicates that the absence of M1 led to enhanced degeneration of megakaryocytes but did not impede latency establishment in these cells. vM1stop infected wood mice showed no signs of thrombocytopaenia, such as increased haemorrhages. This indicated that the degenerative changes in megakaryocytes were not sufficient to decrease the megakaryocyte population to a significant degree. Considering that there were no significant differences in the viral load observed with vM1stop or vM1rev infection, the protective role provided by megakaryocytes to HIV[347] is unlikely present in this case. The changes in vM1stop

infection and the expression of M1 in megakaryocytes indicate that M1 protects megakaryocytes from degenerative changes induced following viral entry and replication. Additionally, they suggest that M1 does not exert a major role in the virally induced changes to the spleen in the wood mouse. The spleen is the main site of MHV-68 latency establishment.

4.6 Conclusion

The expression of M1 in the BALB/c mouse is much reduced compared to the wood mouse. Furthermore M1 expression in laboratory mouse strain cell lines is also minimal. These observations indicate that the role of the M1 is more significant in the natural host. Differences between MHV-68 infection in both species include levels of IFN-γ expression. In BALB/c mice IFN-γ is increased following infection with MHV-68, however, in the current study neither vM1stop or vM1rev infection led to changes in the expression of IFN-γ. The lack of IFN-γ increase in the wood mouse infection possibly represents a viral mechanism to evade host recognition of viral antigens. In laboratory mouse strain studies the M1 protein has been indicated as a suppressor of reactivation following induction of IFN-γ production by $V\beta4^{+}CD8^{+}$ cells. Taking all of the above into consideration this IFN-γ mediated role of M1 is unlikely to occur in wood mouse infection. However studies into the reactivation process would have to be performed in the wood mouse to confirm this.

M1 is not essential for latency establishment or lytic replication since latently and lytically infected cells were detected in infected wood mice infected with vM1stop. In fact, when M1 expression was inpaired, at day 7 p.i. more cell types were seen to be latently infected including macrophages and type II pneumocytes. This was associated in the vM1stop infection with an increase in the frequency of iBALT, the main site of latent replication in the lung. At this time there was no significant difference in the viral load in the lung between the vM1stop and vM1rev infection. At a later timepoint, day 28 p.i., the viral load in the vM1stop when compared to the vM1rev infection was significantly higher indicating that lytic replication is maintained for longer in the absence of M1 expression. In the spleen however there were no significant differences with respect to cell types showing viral latent or lytic replication or in the viral load. These findings indicate that instead of controlling lytic replication, in the wood mouse M1 controls latency establishment. However this effect is restricted to the lungs since

the presence or absence of M1 does not affect significantly latency establishment in the spleen.

There was increased severity in pathological changes and increased macrophage infiltration following infection in the vM1stop infection at the early timepoints of infection, day 3 and 7 p.i. At day 7 p.i. this was seen together with a decrease in alternatively activated macrophages in the lung. Alternatively activated macrophages express arginase I which competes with iNOS for a common substrate, arginine. Thus the increased cytopathic effect could be related to an increase in NO production. The increased macrophage infiltration on the other hand is probably secondary to the increased cytopathic effect observed in vM1stop infection. This suggests that M1 abrogates cytopathic effects and/or the immune response ssociated with MHV-68 infection. Since there were no significant differences in the lytic replication at day 7 p.i. between the vM1stop and vM1rev infection this abrogation is probably not related to the viral replication itself but rather results from host produced substances such as cytokines. M1 expression was seen together with a significant decrease in the mainly anti-inflammatory cytokine IL-10, the mainly pro-inflammatory cytokines TNF-α and MIP1-α, and the growth factor HGF. IL-10 secretion is probably a result of B cell proliferation in the iBALT. TNF-α, expression was seen to be down regulated mainly in airway epithelial cells, a site where M1 is extensively expressed. In the airways there was also an increase in CCSP expression, an anti-inflammatory cytokine from Clara cells. The airways are interspaced between the site of entry, the nose and the site of acute replication, the lung and thus are likely essential for viral entry. This cytokine expression profile favours an anti-inflammatory response and could explain the milder pathogenesis seen in the presence of M1. These findings suggest that the main effect of M1 is the modulation of cytokine expression in order to elicit a less severe inflammatory response. This was not associated with a significant difference in viral replication at day 7 p.i., however, the extent of pathological changes could lead to changes in the behaviour of the host. Considering that this virus is transmitted via nasal route, viral spread will be enhanced if its host is not severely affected since it is less likely to have an effect in its natural behavior, including isolation from other animals.

4.7 Future work

The determination of the relative expression of cytokines and enzymes performed in this study enabled us to ascertain how infection by the vM1stop and vM1rev altered the expression profile in comparison to mock infected wood mice. However this was only performed on day 7 p.i. In order to fully evaluate the M1 effect on the modulation of cytokine expression, the timecourse analysed should be extended to ealier and later timepoints. Furthermore, these relative expression values did not allow the determination of the baseline levels for the expression of the different cytokines/enzymes in the wood mouse. Since the virus induced pathogenesis in the wood mouse is different to that seen in laboratory strains of mice, it is possible that there are differences between the immune system of these species including factors controlling the secretion of cytokines. This could explain the different effects of MHV-68 infection. In order to ascertain this, absolute quantification of the expression would be of benefit and enable further interpretation of the results obtained. Furthermore, apart from CCSP and TNF-α, the *in situ* expression and the presence of the fully formed cytokines/enzymes was not determined. Consequently it would be of interest to analyse these by RNA-ISH and immunohistology respectively in order to better understand the cause-effect mechanisms. These studies could be combined with techniques such as *in situ* chemokine binding assays[348].

The presence of NO should also be assessed in order to confirm or disprove the hypothesis that by maintaining the alternatively activated macrophages, M1 decreases the production of NO by iNOS and thus abrogates the virus induced pathogenesis.

Other studies to be considered would be the quantification of cell populations in the lung by fluorescence-activated cell sorting (FACS) coupled with histological examination. It is important to maintain the histological examination as the localization of the cell is fulcral to the understanding of the virally induced pathogenesis.

The main effects of M1 in the MHV-68 infection encountered during this study were seen in airway epithelial cells, macrophages, type I and type II pneumocytes in the lungs of infected wood mice. Considering that M1 was not seen highly expressed in the laboratory mice strain derived cell cultures, it would be of value to perform *in vitro* work on primary cell cultures obtained from non infected and infected wood mice. The benefit of using primary cell cultures would be to establish the direct cause-effect relationships since the environment is controlled. The establishment of these types of

cultures for primary airway epithelial cell cultures[349-351], macrophages[352] and pneumocytes[353] has been successful.

Also further studies investigating the potential neurotropism of MHV-68 possibly associated to the targeting of satellite cells of parabronchial ganglia, as seen in this study, should be investigated. The finding of M1 expression in satellite cells of parabronchial ganglia was an unexpected and suprising finding in this study and so the presence of these ganglia was not targetted during sampling and was not seen in all lung sections examined. Future work should include sampling aiming at including parabronchial ganglia in the lung sections examined and in all timepoints.

Another unexpected finding was the presence of M1 expression in megakaryocytes together with vaculation of megakaryocytes early in infection. However this was not accompanied by clear evidence of thrombocytopaenia or evidence of haemorrhagic disorders. A simple study that would allow to assess if M1 expression in megakaryocytes, the precursor of platelets, has an effect on their function, would be to carry out coagulation time studies.

Bibliography

1. **McGeoch, D.J., et al., *Molecular phylogeny and evolutionary timescale for the family of mammalian herpesviruses.* J Mol Biol, 1995. 247(3): p. 443-58.**
2. **David M. Knipe, P.M.H., ed. *Fields Virology.* Fields, ed. P.M.H. David M. Knipe, Diane E. Griffin, Malcom A. Martin, Robert A. Lamb, Bernard Roizman. Vol. 2nd. Lippincott Williams & Wilkins: Philadelphia2007. 3177.**
3. **Alcami, A. and S.A. Lira, *Modulation of chemokine activity by viruses.* Curr Opin Immunol, 2010. 22(4): p. 482-7.**
4. **Rajcani, J. and V. Durmanova, *Mechanisms of replication of alpha- and betaherpesviruses and their pathogenesis.* Bratisl Lek Listy, 2001. 102(11): p. 505-14.**
5. **Hughes, D.J., et al., *Pathogenesis of a model gammaherpesvirus in a natural host.* J Virol, 2010. 84(8): p. 3949-61.**
6. **Evans, A.G., et al., *A gammaherpesvirus-secreted activator of Vbeta4+ CD8+ T cells regulates chronic infection and immunopathology.* J Exp Med, 2008. 205(3): p. 669-84.**
7. **Clambey, E.T., H.W.t. Virgin, and S.H. Speck, *Disruption of the murine gammaherpesvirus 68 M1 open reading frame leads to enhanced reactivation from latency.* J Virol, 2000. 74(4): p. 1973-84.**
8. **Simas, J.P., et al., *Four tRNA-like sequences and a serpin homologue encoded by murine gammaherpesvirus 68 are dispensable for lytic replication in vitro and latency in vivo.* J Gen Virol, 1998. 79 (Pt 1): p. 149-53.**
9. **Hughes, D.J., et al., *Chemokine binding protein M3 of murine gammaherpesvirus 68 modulates the host response to infection in a natural host.* PLoS Pathog, 2011. 7(3): p. e1001321.**
10. **Koonin, E.V., T.G. Senkevich, and V.V. Dolja, *The ancient Virus World and evolution of cells.* Biol Direct, 2006. 1: p. 29.**
11. **Büchen-Osmond, D.C. *The Universal Virus database of the International Comittee on taxonomy of viruses.* 2008 [cited 2008 30.08.08]; http://www.ictvonline.org/ictvdbIntro.asp].**
12. **Rickinson, A.B.K., E, *Epstein-Barr Virus.* Fields' virology ed. D.M.K.P.M. Howley2007.**

13. **Russell, G.C., J.P. Stewart, and D.M. Haig, *Malignant catarrhal fever: a review.* Vet J, 2009. 179(3): p. 324-35.**

14. **Roizman, B. and D.M. Knipe, eds. *Herpes simplex virus and their replication.* 4th edition ed. Fields Virology, ed. D.M. Knipe and P.M. Howley. Vol. 2. Lippincott Williams & Wilkins: New York2001. 2399-2459.**

15. **Roizman, B. and P.E. Pellet, eds. *The herpesviridae: a brief introduction.* Fields Virology, ed. D.M. Knipe and P.M. Howley. Vol. 2. Lippincott Williams & Wilkins: New York2001.**

16. **Murphy, F.A., et al., eds. *Properties of herpesviridae.* Third ed. Veterinary Virology, Academic Press1999.**

17. **Spear, P.G. and R. Longnecker, *Herpesvirus entry: an update.* J Virol, 2003. 77(19): p. 10179-85.**

18. **Barton, E., P. Mandal, and S.H. Speck, *Pathogenesis and host control of gammaherpesviruses: lessons from the mouse.* Annu Rev Immunol, 2011. 29: p. 351-97.**

19. **Blasdell, K., et al., *The wood mouse is a natural host for Murid herpesvirus 4.* J Gen Virol, 2003. 84(Pt 1): p. 111-3.**

20. **Blaskovic, D., et al., *Isolation of five strains of herpesviruses from two species of free living small rodents.* Acta Virol, 1980. 24(6): p. 468.**

21. **zur Hausen, H., et al., *EBV DNA in biopsies of Burkitt tumours and anaplastic carcinomas of the nasopharynx.* Nature, 1970. 228(5276): p. 1056-8.**

22. **Bruce, A.G., et al., *High levels of retroperitoneal fibromatosis (RF)-associated herpesvirus in RF lesions in macaques are associated with ORF73 LANA expression in spindleoid tumour cells.* J Gen Virol, 2006. 87(Pt 12): p. 3529-38.**

23. **O'Connor, C.M. and D.H. Kedes, *Rhesus monkey rhadinovirus: a model for the study of KSHV.* Curr Top Microbiol Immunol, 2007. 312: p. 43-69.**

24. **Gulley, M.L., C.L. Chen, and N. Raab-Traub, *Epstein-Barr virus-related lymphomagenesis in a child with Wiskott-Aldrich syndrome.* Hematol Oncol, 1993. 11(3): p. 139-45.**

25. **Sunil-Chandra, N.P., et al., *Virological and pathological features of mice infected with murine gamma-herpesvirus 68.* J Gen Virol, 1992. 73 (Pt 9): p. 2347-56.**

26. **Usherwood, E.J., J.P. Stewart, and A.A. Nash, *Characterization of tumor cell lines derived from murine gammaherpesvirus-68-infected mice.* J Virol, 1996. 70(9): p. 6516-8.**

27. **Blaskovic, D., D. Stanekova, and J. Rajcani, *Experimental pathogenesis of murine herpesvirus in newborn mice.* Acta Virol, 1984. 28(3): p. 225-31.**

28. **Nash, A.A., et al., *Natural history of murine gamma-herpesvirus infection.* Philos Trans R Soc Lond B Biol Sci, 2001. 356(1408): p. 569-79.**

29. **Blackman, M.A. and E. Flano, *Persistent gamma-herpesvirus infections: what can we learn from an experimental mouse model?* J Exp Med, 2002. 195(7): p. F29-32.**

30. **Goldsby, R.A., *Immunology / Richard A. Goldsby ... [et al.]*: New York : W.H. Freeman, 2003.**

5th ed.2003.

31. **Hoebe, K., E. Janssen, and B. Beutler, *The interface between innate and adaptive immunity.* Nat Immunol, 2004. 5(10): p. 971-4.**

32. **Fox, J.G., *Immunology [electronic book] edited by James G. Fox ... [et al.].* Mouse in biomedical research: v. 4: Amsterdam : Elsevier, c2007.**

2nd ed.2007.

33. **Richard A. Goldsby, T.J.K., Barbara A. Osborne, ed. *Immunology.* Fourth ed. Kuby Immunology, ed. J. Kuby. Vol. 1. W. H. Freeman and company: New York1999.**

34. **Vermaelen, K. and R. Pauwels, *Pulmonary dendritic cells.* Am J Respir Crit Care Med, 2005. 172(5): p. 530-51.**

35. **Frasca, L., et al., *Interferon-gamma-treated renal tubular epithelial cells induce allospecific tolerance.* Kidney Int, 1998. 53(3): p. 679-89.**

36. **Holling, T.M., E. Schooten, and P.J. van Den Elsen, *Function and regulation of MHC class II molecules in T-lymphocytes: of mice and men.* Hum Immunol, 2004. 65(4): p. 282-90.**

37. **Snyder, P.W., *Diseases of immunity.* Pathologic Basis of Veterinary Disease, ed. M.D.Z. McGavin, J.F. Vol. 1. Mosby (Elsevier)2007.**

38. **Stevenson, P.G., *Immune evasion by gamma-herpesviruses.* Curr Opin Immunol, 2004. 16(4): p. 456-62.**

39. **Stevenson, P.G. and S. Efstathiou, *Immune mechanisms in murine gammaherpesvirus-68 infection.* Viral Immunol, 2005. 18(3): p. 445-56.**

40. **Stevenson, P.G., et al., *Inhibition of MHC class I-restricted antigen presentation by gamma 2-herpesviruses.* Proc Natl Acad Sci U S A, 2000. 97(15): p. 8455-60.**

41. **Boname, J.M. and P.G. Stevenson, *MHC class I ubiquitination by a viral PHD/LAP finger protein.* Immunity, 2001. 15(4): p. 627-36.**

42. **Boname, J.M., et al., *Viral degradation of the MHC class I peptide loading complex.* Immunity, 2004. 20(3): p. 305-17.**

43. **Boname, J.M., J.S. May, and P.G. Stevenson, *The murine gamma-herpesvirus-68 MK3 protein causes TAP degradation independent of MHC class I heavy chain degradation.* Eur J Immunol, 2005. 35(1): p. 171-9.**

44. **McNeilly, T.N., et al., *Role of alveolar macrophages in respiratory transmission of visna/maedi virus.* J Virol, 2008. 82(3): p. 1526-36.**

45. **Iwasaki, A. and R. Medzhitov, *Toll-like receptor control of the adaptive immune responses.* Nat Immunol, 2004. 5(10): p. 987-95.**

46. **Finberg, R.W. and E.A. Kurt-Jones, *Tolls: you pay them on the way in and on the way out!* J Infect Dis, 2007. 196(4): p. 497-8.**

47. **Hochreiter, R., et al., *Murine gammaherpesvirus-68 productively infects immature dendritic cells and blocks maturation.* J Gen Virol, 2007. 88(Pt 7): p. 1896-905.**

48. **Smith, C.M., et al., *Murine gammaherpesvirus-68 inhibits antigen presentation by dendritic cells.* PLoS ONE, 2007. 2(10): p. e1048.**

49. **Forster, R., et al., *CCR7 coordinates the primary immune response by establishing functional microenvironments in secondary lymphoid organs.* Cell, 1999. 99(1): p. 23-33.**

50. **MartIn-Fontecha, A., et al., *Regulation of dendritic cell migration to the draining lymph node: impact on T lymphocyte traffic and priming.* J Exp Med, 2003. 198(4): p. 615-21.**

51. **Vareille, M., et al., *The airway epithelium: soldier in the fight against respiratory viruses.* Clin Microbiol Rev, 2011. 24(1): p. 210-29.**

52. **Diamond, G., D. Legarda, and L.K. Ryan, *The innate immune response of the respiratory epithelium.* Immunol Rev, 2000. 173: p. 27-38.**

53. **Fokkens, W.J. and R.A. Scheeren, *Upper airway defence mechanisms.* Paediatr Respir Rev, 2000. 1(4): p. 336-41.**

54. **Knight, D.A. and S.T. Holgate, *The airway epithelium: structural and functional properties in health and disease.* Respirology, 2003. 8(4): p. 432-46.**

55. **Ioannidis, I., et al., *Plasticity and virus specificity of the airway epithelial cell immune response during respiratory virus infection.* J Virol, 2012. 86(10): p. 5422-36.**

56. **Takeuchi, O. and S. Akira, *Pattern recognition receptors and inflammation.* Cell, 2010. 140(6): p. 805-20.**

57. **Gitlin, L., et al., *Essential role of mda-5 in type I IFN responses to polyriboinosinic:polyribocytidylic acid and encephalomyocarditis picornavirus.* Proc Natl Acad Sci U S A, 2006. 103(22): p. 8459-64.**

58. **Kato, H., et al., *Differential roles of MDA5 and RIG-I helicases in the recognition of RNA viruses.* Nature, 2006. 441(7089): p. 101-5.**

59. **Kato, H., et al., *Cell type-specific involvement of RIG-I in antiviral response.* Immunity, 2005. 23(1): p. 19-28.**

60. **Shin, E.C., et al., *Virus-induced type I IFN stimulates generation of immunoproteasomes at the site of infection.* J Clin Invest, 2006. 116(11): p. 3006-14.**

61. **Kim, J.S., et al., *Stimulation of migration and wound repair of guinea-pig airway epithelial cells in response to epidermal growth factor.* Am J Respir Cell Mol Biol, 1998. 18(1): p. 66-74.**

62. **Weinheimer, V.K., et al., *Influenza A Viruses Target Type II Pneumocytes in the Human Lung.* J Infect Dis, 2012. 206(11): p. 1685-94.**

63. **Porter, A.G., *Flipping the safety catch of procaspase-3.* Nat Chem Biol, 2006. 2(10): p. 509-10.**

64. **Everett, H. and G. McFadden, *Apoptosis: an innate immune response to virus infection.* Trends Microbiol, 1999. 7(4): p. 160-5.**

65. **Cory, S., D.C. Huang, and J.M. Adams, *The Bcl-2 family: roles in cell survival and oncogenesis.* Oncogene, 2003. 22(53): p. 8590-607.**

66. **Kanduc, D., et al., *Cell death: apoptosis versus necrosis (review).* Int J Oncol, 2002. 21(1): p. 165-70.**

67. **Galluzzi, L., et al., *Molecular definitions of cell death subroutines: recommendations of the Nomenclature Committee on Cell Death 2012.* Cell Death Differ, 2012. 19(1): p. 107-20.**

68. **Saelens, X., et al., *Protein synthesis persists during necrotic cell death.* J Cell Biol, 2005. 168(4): p. 545-51.**

69. **Gonzalez, R.F., L. Allen, and L.G. Dobbs, *Rat alveolar type I cells proliferate, express OCT-4, and exhibit phenotypic plasticity in vitro.* Am J Physiol Lung Cell Mol Physiol, 2009. 297(6): p. L1045-55.**

70. **Banerjee, E.R. and W.R. Henderson, Jr., *Characterization of lung stem cell niches in a mouse model of bleomycin-induced fibrosis.* Stem Cell Res Ther, 2012. 3(3): p. 21.**

71. **Toews, G.B., *Cytokines and the lung.* Eur Respir J Suppl, 2001. 34: p. 3s-17s.**

72. **Moore, P.S., et al., *Molecular mimicry of human cytokine and cytokine response pathway genes by KSHV.* Science, 1996. 274(5293): p. 1739-44.**

73. **Neipel, F., et al., *Human herpesvirus 8 encodes a homolog of interleukin-6.* J Virol, 1997. 71(1): p. 839-42.**

74. **Baggiolini, M., *Chemokines and leukocyte traffic.* Nature, 1998. 392(6676): p. 565-8.**

75. **Sallusto, F. and M. Baggiolini, *Chemokines and leukocyte traffic.* Nat Immunol, 2008. 9(9): p. 949-52.**

76. **Webb, L.M., et al., *Binding to heparan sulfate or heparin enhances neutrophil responses to interleukin 8.* Proc Natl Acad Sci U S A, 1993. 90(15): p. 7158-62.**

77. **Luster, A.D., S.M. Greenberg, and P. Leder, *The IP-10 chemokine binds to a specific cell surface heparan sulfate site shared with platelet factor 4 and inhibits endothelial cell proliferation.* J Exp Med, 1995. 182(1): p. 219-31.**

78. **Middleton, J., et al., *Transcytosis and surface presentation of IL-8 by venular endothelial cells.* Cell, 1997. 91(3): p. 385-95.**

79. **Viejo-Borbolla, A., et al., *Enhancement of chemokine function as an immunomodulatory strategy employed by human herpesviruses.* PLoS Pathog, 2012. 8(2): p. e1002497.**

80. Alcami, A. and M. Saraiva, *Chemokine binding proteins encoded by pathogens.* Adv Exp Med Biol, 2009. 666: p. 167-79.

81. Alexander, J.M., et al., *Structural basis of chemokine sequestration by a herpesvirus decoy receptor.* Cell, 2002. 111(3): p. 343-56.

82. Steed, A., et al., *Gamma interferon blocks gammaherpesvirus reactivation from latency in a cell type-specific manner.* J Virol, 2007. 81(11): p. 6134-40.

83. Russo, J.J., et al., *Nucleotide sequence of the Kaposi sarcoma-associated herpesvirus (HHV8).* Proc Natl Acad Sci U S A, 1996. 93(25): p. 14862-7.

84. Cai, Q., et al., *Molecular biology of Kaposi's sarcoma-associated herpesvirus and related oncogenesis.* Adv Virus Res, 2010. 78: p. 87-142.

85. Nakano, K., et al., *Kaposi's sarcoma-associated herpesvirus (KSHV)-encoded vMIP-I and vMIP-II induce signal transduction and chemotaxis in monocytic cells.* Arch Virol, 2003. 148(5): p. 871-90.

86. Arvanitakis, L., et al., *Human herpesvirus KSHV encodes a constitutively active G-protein-coupled receptor linked to cell proliferation.* Nature, 1997. 385(6614): p. 347-50.

87. Takaoka, A., et al., *Integration of interferon-alpha/beta signalling to p53 responses in tumour suppression and antiviral defence.* Nature, 2003. 424(6948): p. 516-23.

88. Garcia, M.A., E.F. Meurs, and M. Esteban, *The dsRNA protein kinase PKR: virus and cell control.* Biochimie, 2007. 89(6-7): p. 799-811.

89. Samuel, C.E., *Antiviral actions of interferons.* Clin Microbiol Rev, 2001. 14(4): p. 778-809, table of contents.

90. Grant, D.J., H. Shi, and C.T. Teng, *Tissue and site-specific methylation correlates with expression of the mouse lactoferrin gene.* J Mol Endocrinol, 1999. 23(1): p. 45-55.

91. Gifford, J.L., H.N. Hunter, and H.J. Vogel, *Lactoferricin: a lactoferrin-derived peptide with antimicrobial, antiviral, antitumor and immunological properties.* Cell Mol Life Sci, 2005. 62(22): p. 2588-98.

92. Schroder, K., et al., *Interferon-gamma: an overview of signals, mechanisms and functions.* J Leukoc Biol, 2004. 75(2): p. 163-89.

93. Le Bon, A., et al., *Type i interferons potently enhance humoral immunity and can promote isotype switching by stimulating dendritic cells in vivo.* Immunity, 2001. 14(4): p. 461-70.

94. Tough, D.F., et al., *Stimulation of naive and memory T cells by cytokines.* Immunol Rev, 1999. 170: p. 39-47.

95. Waarts, B.L., et al., *Antiviral activity of human lactoferrin: inhibition of alphavirus interaction with heparan sulfate.* Virology, 2005. 333(2): p. 284-92.

96. Schneider, D., et al., *Increased cytokine response of rhinovirus-infected airway epithelial cells in chronic obstructive pulmonary disease.* Am J Respir Crit Care Med, 2010. 182(3): p. 332-40.

97. Goodbourn, S., L. Didcock, and R.E. Randall, *Interferons: cell signalling, immune modulation, antiviral response and virus countermeasures.* J Gen Virol, 2000. 81(Pt 10): p. 2341-64.

98. Barton, E.S., et al., *Herpesvirus latency confers symbiotic protection from bacterial infection.* Nature, 2007. 447(7142): p. 326-9.

99. Dal Canto, A.J., H.W.t. Virgin, and S.H. Speck, *Ongoing viral replication is required for gammaherpesvirus 68-induced vascular damage.* J Virol, 2000. 74(23): p. 11304-10.

100. Weck, K.E., et al., *Murine gamma-herpesvirus 68 causes severe large-vessel arteritis in mice lacking interferon-gamma responsiveness: a new model for virus-induced vascular disease.* Nat Med, 1997. 3(12): p. 1346-53.

101. Goodwin, M.M., et al., *Murine gammaherpesvirus 68 has evolved gamma interferon and stat1-repressible promoters for the lytic switch gene 50.* J Virol, 2010. 84(7): p. 3711-7.

102. Frankel, S.K., et al., *TNF-alpha sensitizes normal and fibrotic human lung fibroblasts to Fas-induced apoptosis.* Am J Respir Cell Mol Biol, 2006. 34(3): p. 293-304.

103. Matute-Bello, G., et al., *Soluble Fas ligand induces epithelial cell apoptosis in humans with acute lung injury (ARDS).* J Immunol, 1999. 163(4): p. 2217-25.

104. Matute-Bello, G., et al., *Fas (CD95) induces alveolar epithelial cell apoptosis in vivo: implications for acute pulmonary inflammation.* Am J Pathol, 2001. 158(1): p. 153-61.

105. Perrone, L.A., et al., *Mice lacking both TNF and IL-1 receptors exhibit reduced lung inflammation and delay in onset of death following infection with a highly virulent H5N1 virus.* J Infect Dis, 2010. 202(8): p. 1161-70.

106. Locksley, R.M., N. Killeen, and M.J. Lenardo, *The TNF and TNF receptor superfamilies: integrating mammalian biology.* Cell, 2001. 104(4): p. 487-501.

107. Pober, J.S., W. Min, and J.R. Bradley, *Mechanisms of endothelial dysfunction, injury, and death.* Annu Rev Pathol, 2009. 4: p. 71-95.

108. Barnes, P.J., *The cytokine network in asthma and chronic obstructive pulmonary disease.* J Clin Invest, 2008. 118(11): p. 3546-56.

109. Armstrong, D.J., *Anti-TNF alpha therapy, lipid profile and carotid intimal thickness.* Rheumatology (Oxford), 2007. 46(10): p. 1626; author reply 1626-7.

110. Chu, W.M., *Tumor necrosis factor.* Cancer Lett, 2013. 328(2): p. 222-5.

111. Carpentier, I., B. Coornaert, and R. Beyaert, *Function and regulation of tumor necrosis factor receptor type 2.* Curr Med Chem, 2004. 11(16): p. 2205-12.

112. Mazzon, E. and S. Cuzzocrea, *Role of TNF-alpha in lung tight junction alteration in mouse model of acute lung inflammation.* Respir Res, 2007. 8: p. 75.

113. Ruuls, S.R., et al., *Membrane-bound TNF supports secondary lymphoid organ structure but is subservient to secreted TNF in driving autoimmune inflammation.* Immunity, 2001. 15(4): p. 533-43.

114. Mebius, R.E., *Organogenesis of lymphoid tissues.* Nat Rev Immunol, 2003. 3(4): p. 292-303.

115. Nishikawa, S., et al., *Organogenesis of peripheral lymphoid organs.* Immunol Rev, 2003. 195: p. 72-80.

116. Zhang, L., et al., *Tumor necrosis factor receptor-2 signaling attenuates vein graft neointima formation by promoting endothelial recovery.* Arterioscler Thromb Vasc Biol, 2008. 28(2): p. 284-9.

117. Luo, D., et al., *Differential functions of tumor necrosis factor receptor 1 and 2 signaling in ischemia-mediated arteriogenesis and angiogenesis.* Am J Pathol, 2006. 169(5): p. 1886-98.

118. **Matute-Bello, G. and T.R. Martin,** ***Science review: apoptosis in acute lung injury.*** **Crit Care, 2003. 7(5): p. 355-8.**

119. **Hagimoto, N., et al.,** ***TGF-beta 1 as an enhancer of Fas-mediated apoptosis of lung epithelial cells.*** **J Immunol, 2002. 168(12): p. 6470-8.**

120. **Buckley, S., et al.,** ***TGF-beta signaling promotes survival and repair in rat alveolar epithelial type 2 cells during recovery after hyperoxic injury.*** **Am J Physiol Lung Cell Mol Physiol, 2008. 294(4): p. L739-48.**

121. **Teisanu, R.M., et al.,** ***Functional analysis of two distinct bronchiolar progenitors during lung injury and repair.*** **Am J Respir Cell Mol Biol, 2011. 44(6): p. 794-803.**

122. **Stoolman, J.S., et al.,** ***Latent infection by gammaherpesvirus stimulates profibrotic mediator release from multiple cell types.*** **Am J Physiol Lung Cell Mol Physiol, 2011. 300(2): p. L274-85.**

123. **Naik, P.K. and B.B. Moore,** ***Viral infection and aging as cofactors for the development of pulmonary fibrosis.*** **Expert Rev Respir Med, 2010. 4(6): p. 759-71.**

124. **Horowitz, J.C., et al.,** ***Plasminogen activation induced pericellular fibronectin proteolysis promotes fibroblast apoptosis.*** **Am J Respir Cell Mol Biol, 2008. 38(1): p. 78-87.**

125. **Warshamana, G.S., M. Corti, and A.R. Brody,** ***TNF-alpha, PDGF, and TGF-beta(1) expression by primary mouse bronchiolar-alveolar epithelial and mesenchymal cells: tnf-alpha induces TGF-beta(1).*** **Exp Mol Pathol, 2001. 71(1): p. 13-33.**

126. **Sullivan, D.E., et al.,** ***Tumor necrosis factor-alpha induces transforming growth factor-beta1 expression in lung fibroblasts through the extracellular signal-regulated kinase pathway.*** **Am J Respir Cell Mol Biol, 2005. 32(4): p. 342-9.**

127. **Sullivan, D.E., et al.,** ***TNF-alpha induces TGF-beta1 expression in lung fibroblasts at the transcriptional level via AP-1 activation.*** **J Cell Mol Med, 2009. 13(8B): p. 1866-76.**

128. **Kawata, M., et al.,** ***TGF-beta-induced epithelial-mesenchymal transition of A549 lung adenocarcinoma cells is enhanced by proinflammatory cytokines derived from RAW 264.7 macrophage cells.*** **J Biochem.**

129. **Gonzalez-Martin, A., et al.,** ***Maximal T cell-mediated antitumor responses rely upon CCR5 expression in both CD4(+) and CD8(+) T cells.*** **Cancer Res, 2011. 71(16): p. 5455-66.**

130. **Kroetz, D.N. and G.S. Deepe, Jr.,** ***An aberrant thymus in CCR5-/- mice is coupled with an enhanced adaptive immune response in fungal infection.*** **J Immunol, 2011. 186(10): p. 5949-55.**

131. **Oliveira, S.H., et al.,** ***Increased responsiveness of murine eosinophils to MIP-1beta (CCL4) and TCA-3 (CCL1) is mediated by their specific receptors, CCR5 and CCR8.*** **J Leukoc Biol, 2002. 71(6): p. 1019-25.**

132. **Tsunoda, I., et al.,** ***Distinct roles for IP-10/CXCL10 in three animal models, Theiler's virus infection, EAE, and MHV infection, for multiple sclerosis: implication of differing roles for IP-10.*** **Mult Scler, 2004. 10(1): p. 26-34.**

133. **Zhao, L., et al.,** ***The roles of chemokines in rabies virus infection: overexpression may not always be beneficial.*** **J Virol, 2009. 83(22): p. 11808-18.**

134. **Zhao, L., et al.,** ***Expression of MIP-1alpha (CCL3) by a recombinant rabies virus enhances its immunogenicity by inducing innate immunity and recruiting dendritic cells and B cells.*** **J Virol, 2010. 84(18): p. 9642-8.**

135. **Tregoning, J.S., et al.,** ***The chemokine MIP1alpha/CCL3 determines pathology in primary RSV infection by regulating the balance of T cell populations in the murine lung.*** **PLoS ONE, 2010. 5(2): p. e9381.**

136. **Filippi, C.M. and M.G. von Herrath,** ***IL-10 and the resolution of infections.*** **J Pathol, 2008. 214(2): p. 224-30.**

137. **Ouyang, W., et al.,** ***Regulation and functions of the IL-10 family of cytokines in inflammation and disease.*** **Annu Rev Immunol. 29: p. 71-109.**

138. **Trinchieri, G.,** ***Interleukin-10 production by effector T cells: Th1 cells show self control.*** **J Exp Med, 2007. 204(2): p. 239-43.**

139. **Manel, N., D. Unutmaz, and D.R. Littman,** ***The differentiation of human T(H)-17 cells requires transforming growth factor-beta and induction of the nuclear receptor RORgammat.*** **Nat Immunol, 2008. 9(6): p. 641-9.**

140. **O'Garra, A. and P. Vieira,** ***T(H)1 cells control themselves by producing interleukin-10.*** **Nat Rev Immunol, 2007. 7(6): p. 425-8.**

141. **Hewett, J.A. and S.J. Hewett,** ***Induction of nitric oxide synthase-2 expression and measurement of nitric oxide production in enriched primary cortical astrocyte cultures.*** **Methods Mol Biol, 2012. 814: p. 251-63.**

142. **Kobayashi, Y.,** ***The regulatory role of nitric oxide in proinflammatory cytokine expression during the induction and resolution of inflammation.*** **J Leukoc Biol, 2010. 88(6): p. 1157-62.**

143. **Adler, H., et al.,** ***Suppression of herpes simplex virus type 1 (HSV-1)-induced pneumonia in mice by inhibition of inducible nitric oxide synthase (iNOS, NOS2).*** **J Exp Med, 1997. 185(9): p. 1533-40.**

144. **Uetani, K., et al.,** ***Central role of double-stranded RNA-activated protein kinase in microbial induction of nitric oxide synthase.*** **J Immunol, 2000. 165(2): p. 988-96.**

145. **Martinez, F.O., L. Helming, and S. Gordon,** ***Alternative activation of macrophages: an immunologic functional perspective.*** **Annu Rev Immunol, 2009. 27: p. 451-83.**

146. **Classen, A., J. Lloberas, and A. Celada,** ***Macrophage activation: classical versus alternative.*** **Methods Mol Biol, 2009. 531: p. 29-43.**

147. **Byers, D.E. and M.J. Holtzman,** ***Alternatively activated macrophages as cause or effect in airway disease.*** **Am J Respir Cell Mol Biol, 2010. 43(1): p. 1-4.**

148. **Byers, D.E. and M.J. Holtzman,** ***Alternatively activated macrophages and airway disease.*** **Chest, 2011. 140(3): p. 768-74.**

149. **Pellet, P.E.R., B.,** ***The family herpesviridae: a brief introduction.*** **Fields Virology, ed. D.M.H. Knipe, P.M. Vol. 2. New York: Lippincott Williams & Wilkins2007.**

150. **Claude Fauquet, M.A.M., J. Maniloff, U. Desselberger, L.A. Ball (editors),** ***VIRUS TAXONOMY: VIIIth Report of the International Committee on Taxonomy of Viruses*** **E.A. Press, Editor.2005.**

151. **Serwer, P., et al.,** ***Improved isolation of undersampled bacteriophages: finding of distant terminase genes.*** **Virology, 2004. 329(2): p. 412-24.**

152. **Brown, J.C.M., M. A. & Homa, F.L.,** ***Packaging DNA into herpesvirus capsids. In structure Function Relantionships of Human Pathogenic Viruses,*** **ed. A.H.E. Bogner, New York: Kluwer Academic/Plenum2002.**

153. **Fossum, E., et al., *Evolutionarily conserved herpesviral protein interaction networks.* PLoS Pathog, 2009. 5(9): p. e1000570.**

154. **Hughes, D.J., *Pathogenesis of Murid Herpesvirus Type 4 in its Natural Host, Apodemus Sylvaticus*, University of Liverpool: Liverpool.2006.**

155. **Bortz, E., et al., *Identification of proteins associated with murine gammaherpesvirus 68 virions.* J Virol, 2003. 77(24): p. 13425-32.**

156. **Dai, W., et al., *Unique structures in a tumor herpesvirus revealed by cryo-electron tomography and microscopy.* J Struct Biol, 2008. 161(3): p. 428-38.**

157. **Wang, S., et al., *In vitro cytokine release from rat type II pneumocytes and alveolar macrophages following exposure to JP-8 jet fuel in co-culture.* Toxicology, 2002. 173(3): p. 211-9.**

158. **Cohrs, R.J. and D.H. Gilden, *Human herpesvirus latency.* Brain Pathol, 2001. 11(4): p. 465-74.**

159. **Morita, S.Y., et al., *Evaluation for concomitant thyroid nodules and primary hyperparathyroidism in patients undergoing parathyroidectomy or thyroidectomy.* Surgery, 2008. 144(6): p. 862-7.**

160. **Fields, *Fields virology.* 5 th ed. Fields virology, ed. D.M.K. Bernard N. Fields, Peter M. Howley associate editors, Robert M. Chanock ... [et al.] Vol. 2. Philadelphia: Lippincott Williams & Wilkins, a Wolters Kluwer Business2007.**

161. **Roizman, B.K., D. M., *Herpes simplex virus.* 4th edition ed. Field's Virology, ed. D.M.H. Knipe, P.M. Vol. 2. New York: Lippincott Williams & Wilkins2007. 2502-2601.**

162. **McGeoch, D.J., F.J. Rixon, and A.J. Davison, *Topics in herpesvirus genomics and evolution.* Virus Res, 2006. 117(1): p. 90-104.**

163. **Virgin, H.W.t., et al., *Complete sequence and genomic analysis of murine gammaherpesvirus 68.* J Virol, 1997. 71(8): p. 5894-904.**

164. **Stewart, J.P.H., D.; L Roaden & B. Ebrahimi, *Molecular pathogenesis of virus infection: sixty-fourth Symposium of the Society for General Microbiology,* , ed. A.A.N.R.E.R. P. Digard: Cambridge University Press2005.**

165. **Barozzi, P., et al., *B cells and herpesviruses: a model of lymphoproliferation.* Autoimmun Rev, 2007. 7(2): p. 132-6.**

166. **Sinclair, J. and P. Sissons, *Latency and reactivation of human cytomegalovirus.* J Gen Virol, 2006. 87(Pt 7): p. 1763-79.**

167. **Hu, J., A.C. Garber, and R. Renne, *The latency-associated nuclear antigen of Kaposi's sarcoma-associated herpesvirus supports latent DNA replication in dividing cells.* J Virol, 2002. 76(22): p. 11677-87.**

168. **Ballestas, M.E. and K.M. Kaye, *Kaposi's sarcoma-associated herpesvirus latency-associated nuclear antigen 1 mediates episome persistence through cis-acting terminal repeat (TR) sequence and specifically binds TR DNA.* J Virol, 2001. 75(7): p. 3250-8.**

169. **Cotter, M.A., 2nd and E.S. Robertson, *The latency-associated nuclear antigen tethers the Kaposi's sarcoma-associated herpesvirus genome to host chromosomes in body cavity-based lymphoma cells.* Virology, 1999. 264(2): p. 254-64.**

170. **Habison, A.C., et al., *Murine gammaherpesvirus 68 LANA acts on terminal repeat DNA to mediate episome persistence.* J Virol, 2012. 86(21): p. 11863-76.**

171. **Forrest, J.C., et al., *ORF73-null murine gammaherpesvirus 68 reveals roles for mLANA and p53 in virus replication.* J Virol, 2007. 81(21): p. 11957-71.**

172. **Kusewitt, D.F.R., L. J., *Neoplasia and tumor biology.* Pathologic Basis of Veterinary Disease, ed. M.D.Z. McGavin, J.F. Vol. 1. Mosby (Elsevier)2007.**

173. **Casavant, N.C., et al., *Potential role for p53 in the permissive life cycle of human cytomegalovirus.* J Virol, 2006. 80(17): p. 8390-401.**

174. **Radkov, S.A., P. Kellam, and C. Boshoff, *The latent nuclear antigen of Kaposi sarcoma-associated herpesvirus targets the retinoblastoma-E2F pathway and with the oncogene Hras transforms primary rat cells.* Nat Med, 2000. 6(10): p. 1121-7.**

175. **Fujimuro, M., et al., *A novel viral mechanism for dysregulation of beta-catenin in Kaposi's sarcoma-associated herpesvirus latency.* Nat Med, 2003. 9(3): p. 300-6.**

176. **Cai, Q.L., et al., *EC5S ubiquitin complex is recruited by KSHV latent antigen LANA for degradation of the VHL and p53 tumor suppressors.* PLoS Pathog, 2006. 2(10): p. e116.**

177. **Friborg, J., Jr., et al., *p53 inhibition by the LANA protein of KSHV protects against cell death.* Nature, 1999. 402(6764): p. 889-94.**

178. **Liu, J., et al., *The Kaposi's sarcoma-associated herpesvirus LANA protein stabilizes and activates c-Myc.* J Virol, 2007. 81(19): p. 10451-9.**

179. **Lan, K., et al., *Kaposi's sarcoma-associated herpesvirus-encoded latency-associated nuclear antigen inhibits lytic replication by targeting Rta: a potential mechanism for virus-mediated control of latency.* J Virol, 2004. 78(12): p. 6585-94.**

180. **Gradoville, L., et al., *Kaposi's sarcoma-associated herpesvirus open reading frame 50/Rta protein activates the entire viral lytic cycle in the HH-B2 primary effusion lymphoma cell line.* J Virol, 2000. 74(13): p. 6207-12.**

181. **Lukac, D.M., et al., *Reactivation of Kaposi's sarcoma-associated herpesvirus infection from latency by expression of the ORF 50 transactivator, a homolog of the EBV R protein.* Virology, 1998. 252(2): p. 304-12.**

182. **Lan, K., et al., *Induction of Kaposi's sarcoma-associated herpesvirus latency-associated nuclear antigen by the lytic transactivator RTA: a novel mechanism for establishment of latency.* J Virol, 2005. 79(12): p. 7453-65.**

183. **Martinez-Guzman, D., et al., *Transcription program of murine gammaherpesvirus 68.* J Virol, 2003. 77(19): p. 10488-503.**

184. **Pavlova, I., C.Y. Lin, and S.H. Speck, *Murine gammaherpesvirus 68 Rta-dependent activation of the gene 57 promoter.* Virology, 2005. 333(1): p. 169-79.**

185. **Chevallier-Greco, A., et al., *Both Epstein-Barr virus (EBV)-encoded trans-acting factors, EB1 and EB2, are required to activate transcription from an EBV early promoter.* EMBO J, 1986. 5(12): p. 3243-9.**

186. **Cox, M.A., J. Leahy, and J.M. Hardwick, *An enhancer within the divergent promoter of Epstein-Barr virus responds synergistically to the R and Z transactivators.* J Virol, 1990. 64(1): p. 313-21.**

187. **Staudt, M.R. and D.P. Dittmer, *The Rta/Orf50 transactivator proteins of the gamma-herpesviridae.* Curr Top Microbiol Immunol, 2007. 312: p. 71-100.**

188. **Wu, T.T., et al., *Function of Rta is essential for lytic replication of murine gammaherpesvirus 68.* J Virol, 2001. 75(19): p. 9262-73.**

189. **Feederle, R., et al., *The Epstein-Barr virus lytic program is controlled by the co-operative functions of two transactivators.* EMBO J, 2000. 19(12): p. 3080-9.**

190. **Kuppers, R., *B cells under influence: transformation of B cells by Epstein-Barr virus.* Nat Rev Immunol, 2003. 3(10): p. 801-12.**

191. **Boshoff, C. and R. Weiss, *AIDS-related malignancies.* Nat Rev Cancer, 2002. 2(5): p. 373-82.**

192. **Young, L.S. and A.B. Rickinson, *Epstein-Barr virus: 40 years on.* Nat Rev Cancer, 2004. 4(10): p. 757-68.**

193. **Schulz, T.F., *Kaposi's sarcoma-associated herpesvirus (human herpesvirus-8).* J Gen Virol, 1998. 79 (Pt 7): p. 1573-91.**

194. **Arvanitakis, L., et al., *Establishment and characterization of a primary effusion (body cavity-based) lymphoma cell line (BC-3) harboring kaposi's sarcoma-associated herpesvirus (KSHV/HHV-8) in the absence of Epstein-Barr virus.* Blood, 1996. 88(7): p. 2648-54.**

195. **Carbone, A., et al., *Establishment of HHV-8-positive and HHV-8-negative lymphoma cell lines from primary lymphomatous effusions.* Int J Cancer, 1997. 73(4): p. 562-9.**

196. **Gaidano, G., et al., *Molecular characterization of HHV-8 positive primary effusion lymphoma reveals pathogenetic and histogenetic features of the disease.* J Clin Virol, 2000. 16(3): p. 215-24.**

197. **Gaidano, G., et al., *Microsatellite instability in KSHV/HHV-8 positive body-cavity-based lymphoma.* Hum Pathol, 1997. 28(6): p. 748-50.**

198. **Gaidano, G., et al., *Human herpesvirus type-8 (HHV-8) in haematopoietic neoplasia.* Leuk Lymphoma, 1997. 24(3-4): p. 257-66.**

199. **Graham, C., et al., *Kaposi's sarcoma-associated herpesvirus oncoprotein K13 protects against B cell receptor induced growth arrest and apoptosis through NF-kappaB activation.* J Virol, 2012.**

200. **Jung, J.U., et al., *Herpesvirus saimiri as a model for gammaherpesvirus oncogenesis.* Semin Cancer Biol, 1999. 9(3): p. 231-9.**

201. **Fickenscher, H. and B. Fleckenstein, *Herpesvirus saimiri.* Philos Trans R Soc Lond B Biol Sci, 2001. 356(1408): p. 545-67.**

202. Kim, Y., et al., *Activation of the STAT6 transcription factor in Jurkat T-cells by the herpesvirus saimiri Tip protein.* J Gen Virol, 2012. 93(Pt 2): p. 330-40.

203. Hebenstreit, D., et al., *Signaling mechanisms, interaction partners, and target genes of STAT6.* Cytokine Growth Factor Rev, 2006. 17(3): p. 173-88.

204. Akimoto, T., et al., *Abrogation of bronchial eosinophilic inflammation and airway hyperreactivity in signal transducers and activators of transcription (STAT)6-deficient mice.* J Exp Med, 1998. 187(9): p. 1537-42.

205. Behr, J., *Evidence-based treatment strategies in idiopathic pulmonary fibrosis.* Eur Respir Rev, 2013. 22(128): p. 163-8.

206. King, T.E., Jr., A. Pardo, and M. Selman, *Idiopathic pulmonary fibrosis.* Lancet, 2011. 378(9807): p. 1949-61.

207. Raghu, G., et al., *An official ATS/ERS/JRS/ALAT statement: idiopathic pulmonary fibrosis: evidence-based guidelines for diagnosis and management.* Am J Respir Crit Care Med, 2011. 183(6): p. 788-824.

208. Calabrese, F., et al., *Herpes virus infection is associated with vascular remodeling and pulmonary hypertension in idiopathic pulmonary fibrosis.* PLoS ONE, 2013. 8(2): p. e55715.

209. Gangadharan, B., et al., *Murine gammaherpesvirus-induced fibrosis is associated with the development of alternatively activated macrophages.* J Leukoc Biol, 2008. 84(1): p. 50-8.

210. Krug, L.T., et al., *Inhibition of NF-kappaB signaling reduces virus load and gammaherpesvirus-induced pulmonary fibrosis.* Am J Pathol, 2010. 177(2): p. 608-21.

211. Soare, T., et al., *Equine multinodular pulmonary fibrosis in horses in the UK.* Vet Rec, 2011. 169(12): p. 313.

212. Williams, K.J., et al., *Equine multinodular pulmonary fibrosis: a newly recognized herpesvirus-associated fibrotic lung disease.* Vet Pathol, 2007. 44(6): p. 849-62.

213. Farkas, L., et al., *VEGF ameliorates pulmonary hypertension through inhibition of endothelial apoptosis in experimental lung fibrosis in rats.* J Clin Invest, 2009. 119(5): p. 1298-311.

214. **Dutia, B.M., et al., *Pathological changes in the spleens of gamma interferon receptor-deficient mice infected with murine gammaherpesvirus: a role for CD8 T cells.* J Virol, 1997. 71(6): p. 4278-83.**

215. **Dutia, B.M., et al., *Identification of a region of the virus genome involved in murine gammaherpesvirus 68-induced splenic pathology.* J Gen Virol, 2004. 85(Pt 6): p. 1393-400.**

216. **Ebrahimi, B., et al., *Murine gammaherpesvirus-68 infection causes multi-organ fibrosis and alters leukocyte trafficking in interferon-gamma receptor knockout mice.* Am J Pathol, 2001. 158(6): p. 2117-25.**

217. **Weinberg, A., et al., *Dual infections of the central nervous system with Epstein-Barr virus.* J Infect Dis, 2005. 191(2): p. 234-7.**

218. **Turkulov, V., N. Madle-Samardzija, and S. Brkic, *[Meningoencephalitis as the only manifestation of Epstein-Barr virus infection].* Med Pregl, 1999. 52(9-10): p. 391-3.**

219. **Mathew, A.G. and Y. Parvez, *Fulminant epstein barr virus encephalitis.* Indian Pediatr, 2013. 50(4): p. 418-9.**

220. **Gheuens, S., et al., *A game of viral hide and seek: Miliary PML masquerading as EBV encephalitis in an HIV patient.* Clin Neurol Neurosurg, 2013.**

221. **Freymuth, F., et al., *[Meningoencephalitis, expression of Epstein-Barr virus primary infection in a patient with renal transplantation. Value of the search of the viral genome by PCR].* Presse Med, 1994. 23(28): p. 1314, 1316.**

222. **Dagan, R. and E. Shahak, *Prolonged meningoencephalitis due to Epstein-Barr virus with favorable outcome in a young infant.* Infection, 1993. 21(6): p. 400-2.**

223. **Chan, P.K., et al., *Survey for the presence and distribution of human herpesvirus 8 in healthy brain.* J Clin Microbiol, 2000. 38(7): p. 2772-3.**

224. **Karatas, H., et al., *Investigation of HSV-1, HSV-2, CMV, HHV-6 and HHV-8 DNA by real-time PCR in surgical resection materials of epilepsy patients with mesial temporal lobe sclerosis.* J Neurol Sci, 2008. 264(1-2): p. 151-6.**

225. Corbellino, M., et al., *Restricted tissue distribution of extralesional Kaposi's sarcoma-associated herpesvirus-like DNA sequences in AIDS patients with Kaposi's sarcoma.* AIDS Res Hum Retroviruses, 1996. 12(8): p. 651-7.

226. Koguchi, Y., et al., *[Fulminant cerebello-brainstem encephalitis with polyradiculitis following probable Epstein-Barr virus infection].* Rinsho Shinkeigaku, 1996. 36(11): p. 1225-8.

227. Cho, H.J., et al., *Age-dependent pathogenesis of murine gammaherpesvirus 68 infection of the central nervous system.* Mol Cells, 2009. 27(1): p. 105-11.

228. Bossolasco, S., et al., *Ganciclovir is associated with low or undetectable Epstein-Barr virus DNA load in cerebrospinal fluid of patients with HIV-related primary central nervous system lymphoma.* Clin Infect Dis, 2006. 42(4): p. e21-5.

229. Doja, A., et al., *Pediatric Epstein-Barr Virus-Associated Encephalitis: 10-Year Review.* J Child Neurol, 2006. 21(5): p. 385-391.

230. Terry, L.A., et al., *Murine gammaherpesvirus-68 infection of and persistence in the central nervous system.* J Gen Virol, 2000. 81(Pt 11): p. 2635-43.

231. Hausler, M., et al., *Murine gammaherpesvirus-68 infection of mice: A new model for human cerebral Epstein-Barr virus infection.* Ann Neurol, 2005. 57(4): p. 600-3.

232. Kang, H.R., et al., *Persistent infection of a gammaherpesvirus in the central nervous system.* Virology, 2012. 423(1): p. 23-9.

233. Gill, M.B., et al., *A gamma-herpesvirus glycoprotein complex manipulates actin to promote viral spread.* PLoS ONE, 2008. 3(3): p. e1808.

234. Shukla, D. and P.G. Spear, *Herpesviruses and heparan sulfate: an intimate relationship in aid of viral entry.* J Clin Invest, 2001. 108(4): p. 503-10.

235. Ryckman, B.J., et al., *Human cytomegalovirus entry into epithelial and endothelial cells depends on genes UL128 to UL150 and occurs by endocytosis and low-pH fusion.* J Virol, 2006. 80(2): p. 710-22.

236. Compton, T., R.R. Nepomuceno, and D.M. Nowlin, *Human cytomegalovirus penetrates host cells by pH-independent fusion at the cell surface.* Virology, 1992. 191(1): p. 387-95.

237. Gillet, L. and P.G. Stevenson, *Antibody evasion by the N terminus of murid herpesvirus-4 glycoprotein B.* EMBO J, 2007. 26(24): p. 5131-42.

238. Gillet, L., et al., *Murine gammaherpesvirus-68 glycoprotein B presents a difficult neutralization target to monoclonal antibodies derived from infected mice.* J Gen Virol, 2006. 87(Pt 12): p. 3515-27.

239. Wu, L., C.M. Borza, and L.M. Hutt-Fletcher, *Mutations of Epstein-Barr virus gH that are differentially able to support fusion with B cells or epithelial cells.* J Virol, 2005. 79(17): p. 10923-30.

240. Gillet, L., S. Colaco, and P.G. Stevenson, *The Murid Herpesvirus-4 gL regulates an entry-associated conformation change in gH.* PLoS ONE, 2008. 3(7): p. e2811.

241. Avitabile, E., C. Forghieri, and G. Campadelli-Fiume, *Complexes between herpes simplex virus glycoproteins gD, gB, and gH detected in cells by complementation of split enhanced green fluorescent protein.* J Virol, 2007. 81(20): p. 11532-7.

242. Atanasiu, D., et al., *Bimolecular complementation reveals that glycoproteins gB and gH/gL of herpes simplex virus interact with each other during cell fusion.* Proc Natl Acad Sci U S A, 2007. 104(47): p. 18718-23.

243. Borza, C.M. and L.M. Hutt-Fletcher, *Alternate replication in B cells and epithelial cells switches tropism of Epstein-Barr virus.* Nat Med, 2002. 8(6): p. 594-9.

244. Mettenleiter, T.C., B.G. Klupp, and H. Granzow, *Herpesvirus assembly: a tale of two membranes.* Curr Opin Microbiol, 2006. 9(4): p. 423-9.

245. Kalejta, R.F., *Tegument proteins of human cytomegalovirus.* Microbiol Mol Biol Rev, 2008. 72(2): p. 249-65, table of contents.

246. Batterson, W. and B. Roizman, *Characterization of the herpes simplex virion-associated factor responsible for the induction of alpha genes.* J Virol, 1983. 46(2): p. 371-7.

247. Bechtel, J.T., R.C. Winant, and D. Ganem, *Host and viral proteins in the virion of Kaposi's sarcoma-associated herpesvirus.* J Virol, 2005. 79(8): p. 4952-64.

248. Krishnan, H.H., et al., *Concurrent expression of latent and a limited number of lytic genes with immune modulation and antiapoptotic function by Kaposi's sarcoma-associated herpesvirus early during infection of primary endothelial and fibroblast cells and subsequent decline of lytic gene expression.* J Virol, 2004. 78(7): p. 3601-20.

249. Zhu, F.X., et al., *Virion proteins of Kaposi's sarcoma-associated herpesvirus.* J Virol, 2005. 79(2): p. 800-11.

250. Smith, G.A. and L.W. Enquist, *Break ins and break outs: viral interactions with the cytoskeleton of Mammalian cells.* Annu Rev Cell Dev Biol, 2002. 18: p. 135-61.

251. Dohner, K., C.H. Nagel, and B. Sodeik, *Viral stop-and-go along microtubules: taking a ride with dynein and kinesins.* Trends Microbiol, 2005. 13(7): p. 320-7.

252. Kliche, S., et al., *Signaling by human herpesvirus 8 kaposin A through direct membrane recruitment of cytohesin-1.* Mol Cell, 2001. 7(4): p. 833-43.

253. Muralidhar, S., et al., *Identification of kaposin (open reading frame K12) as a human herpesvirus 8 (Kaposi's sarcoma-associated herpesvirus) transforming gene.* J Virol, 1998. 72(6): p. 4980-8.

254. Mettenleiter, T.C. and T. Minson, *Egress of alphaherpesviruses.* J Virol, 2006. 80(3): p. 1610-1; author reply 1611-2.

255. Mettenleiter, T.C., *Intriguing interplay between viral proteins during herpesvirus assembly or: the herpesvirus assembly puzzle.* Vet Microbiol, 2006. 113(3-4): p. 163-9.

256. Weck, K.E., et al., *Mature B cells are required for acute splenic infection, but not for establishment of latency, by murine gammaherpesvirus 68.* J Virol, 1996. 70(10): p. 6775-80.

257. Raslova, H., et al., *Susceptibility of mouse mammary glands to murine gammaherpesvirus 72 (MHV-72) infection: evidence of MHV-72 transmission via breast milk.* Microb Pathog, 2001. 31(2): p. 47-58.

258. Francois, S., et al., *Illumination of murine gammaherpesvirus-68 cycle reveals a sexual transmission route from females to males in laboratory mice.* PLoS Pathog, 2013. 9(4): p. e1003292.

259. Mora, A.L., et al., *Activation of alveolar macrophages via the alternative pathway in herpesvirus-induced lung fibrosis.* Am J Respir Cell Mol Biol, 2006. 35(4): p. 466-73.

260. Tarakanova, V.L., et al., *Murine gammaherpesvirus 68 infection is associated with lymphoproliferative disease and lymphoma in BALB beta2 microglobulin-deficient mice.* J Virol, 2005. 79(23): p. 14668-79.

261. Tarakanova, V.L., et al., *Murine gammaherpesvirus 68 genes both induce and suppress lymphoproliferative disease.* J Virol, 2008. 82(2): p. 1034-9.

262. Jacoby, M.A., H.W.t. Virgin, and S.H. Speck, *Disruption of the M2 gene of murine gammaherpesvirus 68 alters splenic latency following intranasal, but not intraperitoneal, inoculation.* J Virol, 2002. 76(4): p. 1790-801.

263. Milho, R., et al., *In vivo imaging of murid herpesvirus-4 infection.* J Gen Virol, 2009. 90(Pt 1): p. 21-32.

264. Gillet, L., H. Adler, and P.G. Stevenson, *Glycosaminoglycan interactions in murine gammaherpesvirus-68 infection.* PLoS ONE, 2007. 2(4): p. e347.

265. de Lima, B.D., J.S. May, and P.G. Stevenson, *Murine gammaherpesvirus 68 lacking gp150 shows defective virion release but establishes normal latency in vivo.* J Virol, 2004. 78(10): p. 5103-12.

266. Gill, M.B., et al., *Murine gammaherpesvirus-68 glycoprotein H-glycoprotein L complex is a major target for neutralizing monoclonal antibodies.* J Gen Virol, 2006. 87(Pt 6): p. 1465-75.

267. Gillet, L., S. Colaco, and P.G. Stevenson, *Glycoprotein B switches conformation during murid herpesvirus 4 entry.* J Gen Virol, 2008. 89(Pt 6): p. 1352-63.

268. Ehtisham, S., N.P. Sunil-Chandra, and A.A. Nash, *Pathogenesis of murine gammaherpesvirus infection in mice deficient in CD4 and CD8 T cells.* J Virol, 1993. 67(9): p. 5247-52.

269. Bowden, R.J., et al., *Murine gammaherpesvirus 68 encodes tRNA-like sequences which are expressed during latency.* J Gen Virol, 1997. 78 (Pt 7): p. 1675-87.

270. Flano, E., et al., *Latent murine gamma-herpesvirus infection is established in activated B cells, dendritic cells, and macrophages.* J Immunol, 2000. 165(2): p. 1074-81.

271. Caton, A.J., et al., *Activation and negative selection of functionally distinct subsets of antibody-secreting cells by influenza hemagglutinin as a viral and a neo-self antigen.* J Exp Med, 1996. 183(1): p. 13-26.

272. Flano, E., et al., *Gamma-herpesvirus latency is preferentially maintained in splenic germinal center and memory B cells.* J Exp Med, 2002. 196(10): p. 1363-72.

273. Kim, I.J., et al., *Maintenance of long term gamma-herpesvirus B cell latency is dependent on CD40-mediated development of memory B cells.* J Immunol, 2003. 171(2): p. 886-92.

274. Weck, K.E., et al., *Macrophages are the major reservoir of latent murine gammaherpesvirus 68 in peritoneal cells.* J Virol, 1999. 73(4): p. 3273-83.

275. Willer, D.O. and S.H. Speck, *Long-term latent murine Gammaherpesvirus 68 infection is preferentially found within the surface immunoglobulin D-negative subset of splenic B cells in vivo.* J Virol, 2003. 77(15): p. 8310-21.

276. Usherwood, E.J., et al., *Murine gammaherpesvirus-induced splenomegaly: a critical role for CD4 T cells.* J Gen Virol, 1996. 77 (Pt 4): p. 627-30.

277. Tripp, R.A., et al., *Pathogenesis of an infectious mononucleosis-like disease induced by a murine gamma-herpesvirus: role for a viral superantigen?* J Exp Med, 1997. 185(9): p. 1641-50.

278. Simas, J.P. and S. Efstathiou, *Murine gammaherpesvirus 68: a model for the study of gammaherpesvirus pathogenesis.* Trends Microbiol, 1998. 6(7): p. 276-82.

279. Davis, D.A., et al., *Hypoxia induces lytic replication of Kaposi sarcoma-associated herpesvirus.* Blood, 2001. 97(10): p. 3244-50.

280. Cesarman, E., et al., *Kaposi's sarcoma-associated herpesvirus-like DNA sequences in AIDS-related body-cavity-based lymphomas.* N Engl J Med, 1995. 332(18): p. 1186-91.

281. Deng, H., A. Young, and R. Sun, *Auto-activation of the rta gene of human herpesvirus-8/Kaposi's sarcoma-associated herpesvirus.* J Gen Virol, 2000. 81(Pt 12): p. 3043-8.

282. Lu, F., L. Day, and P.M. Lieberman, *Kaposi's sarcoma-associated herpesvirus virion-induced transcription activation of the ORF50 immediate-early promoter.* J Virol, 2005. 79(20): p. 13180-5.

283. Miller, G., et al., *Antibodies to butyrate-inducible antigens of Kaposi's sarcoma-associated herpesvirus in patients with HIV-1 infection.* N Engl J Med, 1996. 334(20): p. 1292-7.

284. Gargano, L.M., J.C. Forrest, and S.H. Speck, *Signaling through Toll-like receptors induces murine gammaherpesvirus 68 reactivation in vivo.* J Virol, 2009. 83(3): p. 1474-82.

285. Gregory, S.M., et al., *Toll-like receptor signaling controls reactivation of KSHV from latency.* Proc Natl Acad Sci U S A, 2009. 106(28): p. 11725-30.

286. Wilson, S.J., et al., *X box binding protein XBP-1s transactivates the Kaposi's sarcoma-associated herpesvirus (KSHV) ORF50 promoter, linking plasma cell differentiation to KSHV reactivation from latency.* J Virol, 2007. 81(24): p. 13578-86.

287. Willer, D.O. and S.H. Speck, *Establishment and maintenance of long-term murine gammaherpesvirus 68 latency in B cells in the absence of CD40.* J Virol, 2005. 79(5): p. 2891-9.

288. Flano, E., et al., *Early establishment of gamma-herpesvirus latency: implications for immune control.* J Immunol, 2005. 174(8): p. 4972-8.

289. Sunil-Chandra, N.P., S. Efstathiou, and A.A. Nash, *Murine gammaherpesvirus 68 establishes a latent infection in mouse B lymphocytes in vivo.* J Gen Virol, 1992. 73 (Pt 12): p. 3275-9.

290. Tibbetts, S.A., et al., *Immune control of the number and reactivation phenotype of cells latently infected with a gammaherpesvirus.* J Virol, 2002. 76(14): p. 7125-32.

291. Obar, J.J., et al., *Gammaherpesvirus persistence alters key CD8 T-cell memory characteristics and enhances antiviral protection.* J Virol, 2006. 80(17): p. 8303-15.

292. Capello, D., D. Rossi, and G. Gaidano, *Post-transplant lymphoproliferative disorders: molecular basis of disease histogenesis and pathogenesis.* Hematol Oncol, 2005. 23(2): p. 61-7.

293. Ehlers, B., et al., *Identification of novel rodent herpesviruses, including the first gammaherpesvirus of Mus musculus.* J Virol, 2007. 81(15): p. 8091-100.

294. Vuillemenot, B.R., J.F. Rodriguez, and G.W. Hoyle, *Lymphoid tissue and emphysema in the lungs of transgenic mice inducibly expressing tumor necrosis factor-alpha.* Am J Respir Cell Mol Biol, 2004. 30(4): p. 438-48.

295. van Berkel, V., et al., *Identification and initial characterization of the murine gammaherpesvirus 68 gene M3, encoding an abundantly secreted protein.* J Virol, 1999. 73(5): p. 4524-9.

296. Simas, J.P., et al., *Analysis of murine gammaherpesvirus-68 transcription during lytic and latent infection.* J Gen Virol, 1999. 80 (Pt 1): p. 75-82.

297. **Krug, L.T., et al.,** ***The absence of M1 leads to increased establishment of murine gammaherpesvirus 68 latency in IgD-negative B cells.*** **J Virol, 2013. 87(6): p. 3597-604.**

298. **Locksley, R.M., et al.,** ***Murine cutaneous leishmaniasis: susceptibility correlates with differential expansion of helper T-cell subsets.*** **Ann Inst Pasteur Immunol, 1987. 138(5): p. 744-9.**

299. **Mills, C.D., et al.,** ***M-1/M-2 macrophages and the Th1/Th2 paradigm.*** **J Immunol, 2000. 164(12): p. 6166-73.**

300. **Maxwell, M.J., et al.,** ***Genetic segregation of inflammatory lung disease and autoimmune disease severity in SHIP-1-/- mice.*** **J Immunol, 2011. 186(12): p. 7164-75.**

301. **Watanabe, H., et al.,** ***Innate immune response in Th1- and Th2-dominant mouse strains.*** **Shock, 2004. 22(5): p. 460-6.**

302. **Macpherson, I. and M. Stoker,** ***Polyoma transformation of hamster cell clones--an investigation of genetic factors affecting cell competence.*** **Virology, 1962. 16: p. 147-51.**

303. **Muller, U., et al.,** ***Functional role of type I and type II interferons in antiviral defense.*** **Science, 1994. 264(5167): p. 1918-21.**

304. **Bojan, F., A.R. Kinsella, and M. Fox,** ***Effect of tumor promoter 12-O-tetradecanoylphorbol-13-acetate on recovery of methotrexate-, N-(phosphonacetyl)-L-aspartate-, and cadmium-resistant colony-forming mouse and hamster cells.*** **Cancer Res, 1983. 43(11): p. 5217-21.**

305. **Mbawuike, I.N. and H.B. Herscowitz,** ***MH-S, a murine alveolar macrophage cell line: morphological, cytochemical, and functional characteristics.*** **J Leukoc Biol, 1989. 46(2): p. 119-27.**

306. **Fowler, P., et al.,** ***ORF73 of murine herpesvirus-68 is critical for the establishment and maintenance of latency.*** **J Gen Virol, 2003. 84(Pt 12): p. 3405-16.**

307. **Duffy, C., et al.,** ***Characterization of a UL49-null mutant: VP22 of herpes simplex virus type 1 facilitates viral spread in cultured cells and the mouse cornea.*** **J Virol, 2006. 80(17): p. 8664-75.**

308. **Bennett, M., et al.,** ***Cowpox in British voles and mice.*** **J Comp Pathol, 1997. 116(1): p. 35-44.**

309. **Feore, S.M., et al., *The effect of cowpox virus infection on fecundity in bank voles and wood mice.* Proc Biol Sci, 1997. 264(1387): p. 1457-61.**

310. **Kipar, A., et al., *Comparative examination of cats with feline leukemia virus-associated enteritis and other relevant forms of feline enteritis.* Vet Pathol, 2001. 38(4): p. 359-71.**

311. **Yoshida, H., et al., *Lethal anemia caused by interferon-beta produced in mouse embryos carrying undigested DNA.* Nat Immunol, 2005. 6(1): p. 49-56.**

312. **Friberg, I.M., et al., *Temporal anomalies in immunological gene expression in a time series of wild mice: signature of an epidemic?* PLoS ONE, 2011. 6(5): p. e20070.**

313. **Ishibe, T., et al., *Reduced acetaminophen-induced liver injury in mice by genetic disruption of IL-1 receptor antagonist.* Lab Invest, 2009. 89(1): p. 68-79.**

314. **Fukuda, S., et al., *Genomic organization of the genes for human and mouse CC chemokine LEC.* DNA Cell Biol, 1999. 18(4): p. 275-83.**

315. **Hoffman, L.M., et al., *Central nervous system chemokine expression during Theiler's virus-induced demyelinating disease.* J Neurovirol, 1999. 5(6): p. 635-42.**

316. **Pfaffl, M.W., *A new mathematical model for relative quantification in real-time RT-PCR.* Nucleic Acids Res, 2001. 29(9): p. e45.**

317. **Kipar, A., et al., *Morphologic features and development of granulomatous vasculitis in feline infectious peritonitis.* Vet Pathol, 2005. 42(3): p. 321-30.**

318. **Becker, S.D., et al., *Serological survey of virus infection among wild house mice (Mus domesticus) in the UK.* Lab Anim, 2007. 41(2): p. 229-38.**

319. **Lobo, N., et al., *Ultrastructural Analysis of the Reactivation of the Murid Herpesvirus 4, Strain 68 (MHV-68) in a Latently-Infected B Cell Line.* Microscopy and Microanalysis, 2008. 14(S2): p. 2.**

320. **Tugizov, S.M., J.W. Berline, and J.M. Palefsky, *Epstein-Barr virus infection of polarized tongue and nasopharyngeal epithelial cells.* Nat Med, 2003. 9(3): p. 307-14.**

321. **Matute, H., F. Arcediano, and R.R. Miller, *Test question modulates cue competition between causes and between effects.* J Exp Psychol Learn Mem Cogn, 1996. 22(1): p. 182-96.**

322. **Harrod, K.S. and R.J. Jaramillo, *Pseudomonas aeruginosa and tumor necrosis factor-alpha attenuate Clara cell secretory protein promoter function.* Am J Respir Cell Mol Biol, 2002. 26(2): p. 216-23.**

323. **Leeming, G.H., *Alterations in the expression of CCSP and SPLUNC1 in the respiratory tract following viral infection of murine models*, University of Liverpool 2010.**

324. **Harrod, K.S., et al., *Clara cell secretory protein decreases lung inflammation after acute virus infection.* Am J Physiol, 1998. 275(5 Pt 1): p. L924-30.**

325. **Wang, S.Z., et al., *Clara cell secretory protein modulates lung inflammatory and immune responses to respiratory syncytial virus infection.* J Immunol, 2003. 171(2): p. 1051-60.**

326. **Message, S.D. and S.L. Johnston, *Host defense function of the airway epithelium in health and disease: clinical background.* J Leukoc Biol, 2004. 75(1): p. 5-17.**

327. **Schildgen, O., et al., *Human bocavirus: passenger or pathogen in acute respiratory tract infections?* Clin Microbiol Rev, 2008. 21(2): p. 291-304, table of contents.**

328. **Reichelt, M., L. Zerboni, and A.M. Arvin, *Mechanisms of varicella-zoster virus neuropathogenesis in human dorsal root ganglia.* J Virol, 2008. 82(8): p. 3971-83.**

329. **Ma, W., et al., *2009 pandemic H1N1 influenza virus causes disease and upregulation of genes related to inflammatory and immune responses, cell death, and lipid metabolism in pigs.* J Virol, 2011. 85(22): p. 11626-37.**

330. **Domachowske, J.B., C.A. Bonville, and H.F. Rosenberg, *Gene expression in epithelial cells in response to pneumovirus infection.* Respir Res, 2001. 2(4): p. 225-33.**

331. **Wang, S., et al., *Influenza virus-cytokine-protease cycle in the pathogenesis of vascular hyperpermeability in severe influenza.* J Infect Dis, 2010. 202(7): p. 991-1001.**

332. **Chaussabel, D., et al., *Unique gene expression profiles of human macrophages and dendritic cells to phylogenetically distinct parasites.* Blood, 2003. 102(2): p. 672-81.**

333. Aktan, F., *iNOS-mediated nitric oxide production and its regulation.* Life Sci, 2004. 75(6): p. 639-53.

334. Siegel, A.M., J.H. Herskowitz, and S.H. Speck, *The MHV68 M2 protein drives IL-10 dependent B cell proliferation and differentiation.* PLoS Pathog, 2008. 4(4): p. e1000039.

335. Vilarino, A., et al., *[Rectocolonic plasty using mechanical stapler as a surgical solution in complications of megacolon].* Cir Pediatr, 1995. 8(4): p. 139-41.

336. Miguel-Garcia, A., et al., *Circulating Ki67 positive lymphocytes in multiple myeloma and benign monoclonal gammopathy.* J Clin Pathol, 1995. 48(9): p. 835-9.

337. Farahat, N., et al., *Quantitative flow cytometry can distinguish between normal and leukaemic B-cell precursors.* Br J Haematol, 1995. 91(3): p. 640-6.

338. Crawford, A., et al., *A Role for the Chemokine RANTES in Regulating CD8 T Cell Responses during Chronic Viral Infection.* PLoS Pathog, 2011. 7(7): p. e1002098.

339. Culley, F.J., et al., *Role of CCL5 (RANTES) in viral lung disease.* J Virol, 2006. 80(16): p. 8151-7.

340. Lee, A.H., J.H. Hong, and Y.S. Seo, *Tumour necrosis factor-alpha and interferon-gamma synergistically activate the RANTES promoter through nuclear factor kappaB and interferon regulatory factor 1 (IRF-1) transcription factors.* Biochem J, 2000. 350 Pt 1: p. 131-8.

341. Melchjorsen, J., et al., *Herpes simplex virus selectively induces expression of the CC chemokine RANTES/CCL5 in macrophages through a mechanism dependent on PKR and ICP0.* J Virol, 2002. 76(6): p. 2780-8.

342. Battinelli, E.M., J.H. Hartwig, and J.E. Italiano, Jr., *Delivering new insight into the biology of megakaryopoiesis and thrombopoiesis.* Curr Opin Hematol, 2007. 14(5): p. 419-26.

343. Kaushansky, K., *Historical review: megakaryopoiesis and thrombopoiesis.* Blood, 2008. 111(3): p. 981-6.

344. Matsumura, I. and Y. Kanakura, *Molecular control of megakaryopoiesis and thrombopoiesis.* Int J Hematol, 2002. 75(5): p. 473-83.

345. **Oda, A. and Y. Ikeda,** ***[Regulation of megakaryopoiesis and thrombopoiesis by thrombopoietin].*** **Rinsho Byori, 1998. 46(5): p. 430-4.**

346. **Montenegro-Medina, Y.M., et al.,** ***[Roll of antibodies antiplatelets in viral infection: a systematic review of literature].*** **Biomedica, 2011. 31(1): p. 35-43.**

347. **Flaujac, C., S. Boukour, and E. Cramer-Borde,** ***Platelets and viruses: an ambivalent relationship.*** **Cell Mol Life Sci, 2010. 67(4): p. 545-56.**

348. **Rot, A.,** ***In situ binding assay for studying chemokine interactions with endothelial cells.*** **J Immunol Methods, 2003. 273(1-2): p. 63-71.**

349. **Brockman-Schneider, R.A., et al.,** ***Serial culture of murine primary airway epithelial cells and ex vivo replication of human rhinoviruses.*** **J Immunol Methods, 2008. 339(2): p. 264-9.**

350. **You, Y., et al.,** ***Growth and differentiation of mouse tracheal epithelial cells: selection of a proliferative population.*** **Am J Physiol Lung Cell Mol Physiol, 2002. 283(6): p. L1315-21.**

351. **Davidson, D.J., et al.,** ***A primary culture model of differentiated murine tracheal epithelium.*** **Am J Physiol Lung Cell Mol Physiol, 2000. 279(4): p. L766-78.**

352. **Garn, H., et al.,** ***Shift toward an alternatively activated macrophage response in lungs of NO2-exposed rats.*** **Am J Respir Cell Mol Biol, 2003. 28(3): p. 386-96.**

353. **Chen, J., et al.,** ***Isolation of highly pure alveolar epithelial type I and type II cells from rat lungs.*** **Lab Invest, 2004. 84(6): p. 727-35.**

5. APPENDICES

Appendix 1

harlan™

Health Monitoring Report

Test Date	Species	Submitter	Area	Profile
02 December 10	Mouse	University of Liverpool	8735	51M(S)

Viruses	Positive/Tested	Test Method
Minute virus of mice	0/1	Bead
Mouse hepatitis virus	0/1	Bead
Mouse parvovirus	0/1	Bead
Mouse rotavirus (EDIM)	0/1	Bead
Pneumonia virus of mice	0/1	Bead
Sendai virus	0/1	Bead
Theiler's murine encephalomyelitis virus	0/1	Bead
Bacteria, Mycoplasma and Fungi	**Positive/Tested**	**Test Method**
Clostridium piliforme	0/1	Bead
Mycoplasma spp	0/1	Bead

Figure 5.1 Example of health monitoring report provided by Harlan.

Appendix 2

ELSEVIER LICENSE
TERMS AND CONDITIONS

Jan 22, 2013

This is a License Agreement between rita papoula-pereira ("You") and Elsevier ("Elsevier") provided by Copyright Clearance Center ("CCC"). The license consists of your order details, the terms and conditions provided by Elsevier, and the payment terms and conditions.

All payments must be made in full to CCC. For payment instructions, please see information listed at the bottom of this form.

Supplier	Elsevier Limited The Boulevard,Langford Lane Kidlington,Oxford,OX5 1GB,UK
Registered Company Number	1982084
Customer name	rita papoula-pereira
Customer address	The School of Veterinary Science, Liverpool, L3 5RP
License number	3074141016939
License date	Jan 22, 2013
Licensed content publisher	Elsevier
Licensed content publication	Cell
Licensed content title	Structural Basis of Chemokine Sequestration by a Herpesvirus Decoy Receptor
Licensed content author	Jennifer M. Alexander,Christopher A. Nelson,Victor van Berkel,Elaine K. Lau,Joey M. Studts,Tom J. Brett,Samuel H. Speck,Tracy M. Handel,Herbert W. Virgin,Daved H. Fremont
Licensed content date	1 November 2002
Licensed content volume number	111
Licensed content issue number	3
Number of pages	14
Start Page	343
End Page	356
Type of Use	reuse in a thesis/dissertation
Portion	figures/tables/illustrations
Number of figures/tables/illustrations	1
Format	both print and electronic
Are you the author of this Elsevier article?	No
Will you be translating?	No
Order reference number	
Title of your	Studies into the influence of the M1 protein in MHV68 infection

Figure 5.2 License agreement for use of Figure 1.8. M3, M1 and M4 sequence alignment.

Appendix 3

Figure 5.3 License agreement for use of Figure 1.4 Alignment of HVS, MHV-68, KSHV and EBV genomes.